A Study of Magnetohydrodynamic Flow and Heat Transfer Along a Smooth Surface

A

Thesis submitted for the award of the degree of

DOCTOR OF PHILOSOPHY

By

Prashu

(901611009)

Under the Guidance of

Dr. Raj Nandkeolyar

(Assistant Professor, NIT Jamshedpur)

&

Dr. Vivek Sangwan

(Assistant Professor, TIET Patiala)

School of Mathematics

THAPAR INSTITUTE OF ENGINEERING AND TECHNOLOGY
PATIALA - 147004, INDIA

August, 2021

Certificate

I hereby certify that the work which is being presented in the thesis entitled "**A Study of Magnetohydrodynamic Flow and Heat Transfer Along a Smooth Surface**" in partial fulfillment of the requirements for the award of degree of **Doctor of Philosophy** and submitted in School of Mathematics, Thapar Institute of Engineering and Technology, Patiala, is an authentic record of my own work carried out during the period **25 July, 2016 to August 31, 2021** under the supervision of **Dr. Raj Nandkeolyar**, Assistant Professor, Department of Mathematics, National Institute of Technology Jamshedpur, Jamshedpur and **Dr. Vivek Sangwan**, Assistant Professor, School of Mathematics, Thapar Institute of Engineering and Technology, Patiala.

Prashu

(Prashu)

(901611009)

Date:

August 31, 2021

This is certified that the above statement made by the candidate is correct and true to the best of my knowledge.

Date:

August 31, 2021

Dr. Raj Nandkeolyar

Supervisor

Dr. Vivek Sangwan

Co-Supervisor

Acknowledgements

First and foremost, praises and thanks to the **God**, the Almighty, for His showers of blessings throughout my thesis work to complete the thesis successfully. He has given me the power to believe in myself and pursue my dreams.

I would like to express my deep sense of respect and sincere gratitude to my esteemed supervisor, **Dr. Raj Nankeolyar**, Assistant Professor, Department of Mathematics, NIT Jamshedpur for his excellent guidance, sympathetic attitude, constant encouragement, logical suggestions, moral support all through the pursuance of this work. I learnt a lot from him, which I am sure will be useful in different stages of my life. More importantly, I would like to thank for the patience he has shown in carefully reading and commenting on the manuscripts, and countless revisions of this dissertation. I am highly privileged to have got an opportunity to work with such a wonderful personality. I could not have imagined having a better advisor and mentor for my Ph.D. study. This thesis would not happen to be possible without his support. He has been a steady influence throughout my Ph.D. career, he has oriented and supported me with promptness and care, and have always been patient and encouraging in times of new ideas and difficulties. I am deeply beholden to him from the inner core of my heart.

I wish to express my sincere thanks to my Co-supervisor **Dr. Vivek Sangwan**, Assistant Professor, School of Mathematics, Thapar Institute of Engineering and Technology, Patiala for his guidance, constant support and insightful comments during the entire journey of my Ph.D. tenure. I really appreciate him for always being so supportive.

I would also like to extend my sincere thanks to the doctoral committee members **Dr. A. K. Lal**, **Dr. M. K. Sharma**, **Dr. Ajay Kumar**, **Dr. Kavita**, and **Dr. Jolly Puri** for their insightful comments, suggestions and encouragement during my Ph.D. journey. Also, I am highly grateful to **Dr. Amit Kumar**, **Dr. Navdeep Kailey**, **Dr. Satish Sharma** and all the faculty members and administrative staff of School of Mathematics, TIET, Patiala who have contributed directly or indirectly to this work.

Words can not express how grateful I am to my parents, **Rinkal Bansal** and **Harish Bansal**, for their love, prayers, caring and sacrifices for educating and preparing me for my future. My special thanks goes to my husband, **Rajat Mittal**, for his love, encouragement, support and being with me in every situation of my journey. I express my thanks to my brother, **Akshay Bansal**, and all the family members for their support and valuable prayers.

It gives me great pleasure in acknowledging the love of my close friends **Mandeep Kaur Saggi**, **Nikita Madaan**, **Prab Simrat Kaur**, **Jagroop Kaur**, **Deepika Sharma**,

Rajinder kaur, **Shahid Bhatt** and all the lab-mates, hostlers who have been always there for me and motivating me. I feel blessed to have all of you in my life and for all the moments we have fun together.

At last, I would like to pay my warmest tribute to my glorious and esteemed institute, **Thapar Institute of Engineering and Technology**, Patiala.

Prashu

Prashu

Abstract

The present thesis entitled "***A Study of Magnetohydrodynamic Flow and Heat Transfer Along a Smooth Surface***" is devoted towards the numerical investigation of the hydromagnetic flow and heat transfer of a viscous incompressible electrically conducting fluid along a stretching surface under the considering different aspects and conditions. The thesis is divided into seven chapters in which Chapter 1 is introductory. Chapter 2 presents the study of the magnetohydrodynamic boundary layer three-dimensional transient flow of a Casson fluid along a stretching surface. The effects of Hall current and nonlinear radiation are taken into account. The model discussed in Chapter 2 is extended in Chapter 3 including the presence of Darcy porous medium and convective heat transfer at the surface. In Chapter 3, a numerical analysis is presented to investigate the effects of Hall current and radiative heat transfer on the unsteady three-dimensional magnetohydrodynamic flow of a Casson fluid flowing over a stretching surface with convective boundary conditions in a porous medium. Chapter 4 is devoted to investigating the two-dimensional transient two-phase flow of a couple-stress dusty fluid along a porous surface in the presence of a magnetic field. Moreover, the heat transfer phenomenon is investigated under heat source/sink and viscous dissipation effects. An entropy generation analysis is carried out in Chapter 5 on the hydromagnetic three-dimensional stagnation point flow of a Casson fluid along a stretching surface under the effects of viscous dissipation, Hall current, and radiation. Chapter 6 deals with the study of the magnetohydrodynamic two-dimensional flow of a viscous fluid along a curved stretching sheet in a non-Darcy porous medium under the influence of thermal radiation. The physical models of the different problems considered in the thesis include nonlinear radiative heat transfer, non-uniform heat generation/absorption, convective heating, Hall current, and viscous dissipation effects. In order to investigate the effects of the pertinent flow parameters, at first, the mathematical model is developed in terms of nonlinear coupled partial differential equations and suitable boundary conditions. The governing nonlinear partial differential equations modeling the problem's flow and heat transfer phenomenon are transformed to a similar form using a suitable similarity transformation. The nonlinear ordinary differential equations resulting from the transformation are treated with the spectral-based method, namely the spectral quasi-linearization method (SQLM), and Matlab's in-built boundary value problem solver bvp4c. The effects of several physical parameters such as radiation, heat generation/absorption, porosity, magnetic field, unsteadiness, Hall current, etc., on the flow and heat transfer are discussed using graphs and tables. The flow-field and the associated momentum and thermal boundary layers are found to be significantly affected by

these parameters. The crucial findings and the future scope of the present thesis are discussed in Chapter 7. The work presented in the thesis has several practical implications in the fluid engineering problems and technological fields.

Contents

List of Figures

List of Tables

Dedicated to My Parents

Chapter 1

Introduction

1.1 Magnetohydrodynamics and its applications

Matter is made up of molecules or atoms and are present in two states, namely solids and fluids. Any state of matter that can flow and assumes the shape of container is a fluid. Magnetohydrodynamic flow is concerned with the motion of viscous and electrically conducting fluids which are flowing under the influence of magnetic field and the discipline, to investigate such flows, is called "Magnetohydrodynamics" or MHD. The word "Magnetohydrodynamics" consists of three terms, the first one is *magneto* which refers to the magnetic field, *hydro* is for fluid (liquid or gas), and the last term *dynamics* directs to the motion of a body by forces. Mainly, it is a theoretical framework underlying a system which deals with the interrelationship between the flow of electrically conducting fluids such as salt water or ionized gases and the magnetic field. The fluid should be electrically conductive when it is flowing under some electromagnetic field. The leading principle of MHD says that an induced electric current appears, due to the flow of electrically conducting fluid experiencing an external magnetic field. This induced current produces an another magnetic field (namely induced magnetic field), which disturbs the original one. Moreover, when induced current experiences the magnetic effects, an electromagnetic force (namely Lorentz force) appear which influences the fluid flow.

The basic principles of Magnetohydrodynamics are derived from three important disciplines of physics, namely fluid dynamics, thermodynamics and electrodynamics. When a fluid moves in such a manner that there occurs relative movements among the fluid particles, then fluid is said to be flowing and the discipline which deals with the flows of fluids is known as Fluid dynamics. As the fluid dynamics, the continuum hypothesis

is generally considered in Magnetohydrodynamics and fluid is assumed to be as continuously distributed. Thermodynamics relates to the study of inter-conversion between heat energy and any other form of energy, processes involving heat, work, entropy and the direction in which heat flows. A study of mutual interaction between flowing charged particles and the produced forces due to presence of the electrical and magnetic field is known as Electrodynamics. Hence composition of these three branches give occurrence to *Magnetohydrodynamics*. It was Hannes Alfven who discovered the phenomenon of Magnetohydrodynamics and was rewarded with the nobel prize in 1970. In the study of Magnetohydrodynamics or MHD flow, generally fluid is considered as incompressible and the other fluid's other characteristics (viscosity, electrical and thermal conductivity) remain same. However, the study of such type of fluids (ionized gases or plasmas) which are assumed to be compressible and their other properties are not considered as constant comes under the word "Magnetogasdynamics", or MGD.

MHD is a center of attraction of many of the researchers today because of its extensive applications in many fields they can get applied to. Geophysics applications suggests the magnetism of the Earth and the other planets. The outer core of the earth is extremely hot and contains huge amount of liquid metals such as iron, nickel and flow of liquid iron gives occurrence to the magnetism of the earth. The fact that a compass is always pointed towards the direction of north is the evidence that there is a magnetic field all around us due to the earth. Also the concept of magnetohydrodynamics is applied quite well in the distinct fields of astrophysics such as solar structures, stars, galaxies and the space between them. A high amount of plasma exist in these structures and the magnetism effect on these galactic structures may be seen in the form of dark spots, cool spots and bright spots (sun spots). The concept of MHD works as a intermediate medium to make several devices of engineering and technology fields such as MHD power generators, submarines and meters. MHD power generator is an equipment which is used to generate electricity directly from the thermal energy by flowing a electrically conducting gas (plasmas) in the existence of some magnetic field. MHD power generator offers us more capability of high temperature, great survivability and less loss of energy caused by thermodynamic conversion. Due to this, MHD power generators are considered superior in comparison to regular generators. Propulsion systems of underwater vehicles such as MHD submarines work also on the basic principles of MHD. When the sea water experiences some electric current and magnetic field, a lorentz force is generated which gives a push to the submarines and offers high speed, more carrying capacity , low resistance, and no surface disturbances. Due to this MHD submarines are more advanced as compared to surface ships and are preferred for transporting cargos. Moreover, to measure the speed of ships in the oceans, MHD flow meters are used. For the use of these types of equipments, fluid must be electrically conducting such as water

including ions. MHD deals with the process of sustaining the plasmas for thermonuclear fusion reactions. High forces are required to confine the plasmas away from the walls as the plasma can not be sustained by the solid walls. In stars, galaxies these forces are present in the form of gravity naturally. But in laboratories, to examine the characteristics and behavior of plasma, scientists use high magnetic field to contain the plasma with in a device namely Tokamak.

1.2 Basic Terminology

- **Stress**
  It is described as force per unit area which has two components, normal force component and tangential force components which built up two stresses i.e. normal stress and shear stress respectively. Generally, shear stress is denoted as τ. Deformation of fluid due to the shear stress is known as shear strain.

- **Fluid**
  Fluid is that substance (liquid/gases) which under goes on continuous deformation after the experience of some shear stress. In solids, stress is proportional to strain, but in fluids, stress is proportional to strain rate.

- **Viscosity**
  Viscosity is that characteristic of any liquid or gas which resists the relative movement between their adjacent layers. It exists in the form of either fluid friction or internal friction and the force which retards the fluid flow is known as viscous force. According to Newton's law of viscosity, the shear stress τ between adjacent fluid layers is directly proportional to the velocity gradient $\frac{du}{dy}$, i.e $\tau \propto \frac{du}{dy} \Rightarrow \tau = \mu \frac{du}{dy}$, where μ is constant of proportionality and called coefficient of viscosity. Those fluids which obey Newton's law of viscosity, are known as Newtonian fluids and which do not, are called non-Newtonian fluids. The fluids like water, air, mercury, kerosene all are Newtonian fluids while paints, sauces, coal tar, honey and polymer solutions etc are non-Newtonian fluids.

- **Density**
  The density of a matter is defined as mass per unit volume i.e. $\rho = \frac{m}{V}$. A Greek letter ρ is used to denote the density, where m is for mass and V denotes the volume. With the help of density, the substructure of the matter can be revealed. For example density of a solid is greater that density of gas as the molecules in gas are separated by more empty spaces compared to the solid ones.

- **Specific Heat Capacity**
  Specific heat capacity of a substance is the amount of heat absorbed to change the temperature of unit mass of it by one unit. It is denoted as c_p.

- **Thermal Conductivity**
  Thermal conductivity (K) is a characteristic of a substance which signifies its ability to transfer heat and is computed as $K = \frac{Ql}{A\delta T}$, where Q is amount of heat transfer, l is displacement between two isothermal planes, and $\delta T$is difference in temperature.

- **Types of fluid flow**

  - **Steady and Unsteady Flow**
    In steady flow, the characteristics of fluid like velocity, pressure, density remain same with respect to time. On the other hand in unsteady flows these fluid characteristics vary with time.

  - **Laminar and Turbulent flow**
    When the fluid is flowing in a well defined straight streamline path, then such flows are known as laminar flow. In this case, velocity may have distinct magnitudes at distinct positions, but the directions of velocity remains parallel. On the other hand, in turbulent flows, fluid follows irregular paths and may flow in zig-zag pattern which creates turbulence in the flow and leads to the high energy loses.

  - **Compressible and Incompressible Flow**
    Those fluids which have uniform density throughout come under the category of incompressible fluids such as liquids. But in the case of compressible fluids such as gases, the density of the fluid can change anytime.

  - **Rotational and Irrotational Flow**
    When the fluid is flowing along some path-lines as well as rotate about its own axis with some angular velocity then such flow is called rotational, otherwise it is said to be irrotational flow.

1.3 Governing Equations

The fundamental equations governing the MHD flow of the viscous, incompressible, electrically conducting fluids are the combination of electrodynamics and hydrodynamics equations. The basic laws and equations which are used in different chapters of the present thesis are presented below

- Equation of continuity: This is based on the principle of conservation of mass is given by

$$\frac{\partial \rho}{\partial t} + \nabla.(\rho \vec{q}) = 0. \tag{1.1}$$

For an incompressible fluid, the Eq. (1.1) reduces to

$$\frac{\partial u}{\partial x} + \frac{\partial v}{\partial y} + \frac{\partial w}{\partial z} = 0 \tag{1.2}$$

where $\vec{q}$ is the velocity vector, u , v , w present the velocity components along the x , y , z axes, respectively, and ρ denotes the density of fluid.

- Equation of motion: The equation governing the motion of a viscous fluid including the influence of Lorentz force can be stated as

$$\frac{\partial \vec{q}}{\partial t} + (\vec{q} \cdot \nabla)\, \vec{q} = -\frac{1}{\rho}\nabla p + \varphi + \frac{1}{\rho}\nabla.\vec{\tau} + \frac{1}{\rho}\left(\vec{J} \times \vec{B}\right), \tag{1.3}$$

where t is time, p is pressure, φ is body force, $\vec{J}$ is electric current density vector and $\vec{B}$ is magnetic induction vector, and $\vec{\tau}$ is the stress tensor depending on the constitutive relationship of the fluid.

- Energy equation: This equation presents the conservation to total energy of the system, and is given by

$$\rho c_p \left[\frac{\partial T}{\partial t} + (\vec{q}.\nabla)\, T\right] = k\nabla^2 T + \psi + \mu\Phi + \frac{J^2}{\sigma}, \tag{1.4}$$

where T is taken as fluid's temperature, k is fluid's thermal conductivity, ψ is used for including the terms of heat source/sink or thermal radiation effects, c_p denotes the specific heat at constant pressure and Φ is the for viscous dissipation term.

- Maxwell's relations: In order to incorporate the Lorentz force term, Maxwell's relations are used. These are stated as

$$\nabla \times \vec{B} \;=\; \mu_m \vec{J}\,, \tag{1.5}$$

$$\nabla \times \vec{E} \;=\; -\frac{\partial \vec{B}}{\partial t}\,, \tag{1.6}$$

$$\nabla.\vec{B} \;=\; 0\,, \tag{1.7}$$

where μ_m denotes the fluid's magnetic permeability.

Also, the constitutive field relations defining the relation between two physical quantities, under the consideration of magnetic field, is given by

$$\vec{B} = \mu_m \vec{H}, \tag{1.8}$$

where $\vec{H}$ is the magnetic field.

- Ohm's law: This law says that the current (I) moving along the conductor is directly proportional to the volatage (V)/(potential difference across it's two ends) i.e. $I = \frac{V}{R}$,where R is a proportionality constant, called electric resistance. This is used in vector form which represent the relationship between current density $\vec{J}$, electrical conductivity σ and electric field $\vec{E}$ i.e. $\vec{J} = \sigma\vec{E}$. In order to incorporate the magnetic field effect in the flow field, the modified Ohm's law including induced current, can be written as

$$\vec{J} \;=\; \sigma\left[\vec{E} \;+\; \left(\vec{q}\times\vec{B}\right)\right]. \tag{1.9}$$

- Hall Current: When an electric current flows in the direction of an electric field $\vec{E}$ and in the existence of a magnetic field $\vec{B}$ acting perpendicular to the electric field, an electromagnetic force $\vec{J}\times\vec{B}$, arises, which results the charged particles to flow in another direction. This is called as Hall effect and the resulting electrical current density $\vec{J}_{Hall}$ is known as Hall current. Mathematically, it is expressed as

$$\vec{J}_{Hall} = \frac{\sigma(\vec{J}\times\vec{B})}{n_e e},$$

where n_e, e denote the electron number density and charge of the electron, respectively.

1.4 Heat Transfer Process

Heat is a form of energy that gets transferred from a substance at a high temperature to a substance at a lower temperature i.e. temperature determines the thermal state of a body whether it can give or receive heat. Heat Transfer is a process in which thermal energy gets exchanged between distinct systems. This process may occur in three modes which are mentioned below:

1. Conduction: The mode in which heat transfer process occurs in solids where different atoms have different temperature, transferring the thermal energy from a hot

particle to its physically contacted cold particle without any movement between the particles.

2. Convection: In convection mode, heat transfer process occurs due to actual movement of heated substance (usually fluid).

3. Radiation: In radiation mode, the process of heat transfer between different bodies takes place due to electromagnetic waves/rays. There is no requirement of any intermediate medium/phisical contact to transfer the heat. The perfect example of this mode is heat of sun that reaches the earth.

The Stefan-Boltzmann law states that, " the emissive power E_b of a black body is directly proportional to fourth power of its absolute temperature" i.e.

$$E_b \propto T^4.$$

If there is different temperatures at the surface, the the heat flux equals to the net radiation flow. With the help of Rosseland approximation, the radiative heat flux q_r is given by

$$q_r = -\frac{4\sigma}{3k^*}\frac{\partial T^4}{\partial y},$$

where σ and k^* denote Stephan-Boltzmann constant and the mean absorption coefficient.

1.5 Literature Survey

The fluid flow problems considered in the present thesis mainly involve the flow of a viscous fluid along a stretching surface under the effect of a magnetic field, considering several aspects. In this section, an attempt has been made to discuss a brief literature relevant to the problems considered in the thesis.

The boundary layer concept derived its name from the great German professor Ludwig Prandtl at the beginning of the 1900s. Even though general fluid flow equations existed for many years, the solutions of these equations could not describe the effects of the flow field properly. To overcome this problem, Prandtl was the first who suggests dividing the whole fluid flow into two parts, namely boundary layer region and outside the boundary layer region. He observed a change in values of inertia and viscous force from a region very near to the surface to a region far from the surface. His excellent work was published in 1904 at Heidelberg, the third international congress of mathematicians entitled "On

the motion of a fluid of very small viscosity". Thus with the help of the boundary layer concept, the effects of the flow field can be analyzed properly. Then inspired by Prandtl's theory, numerous researchers made different inventions on it with new aspects. It was the Sakiadis [1] who initially examined the boundary layer theory of fluid flow towards a moving surface with uniform speed. He analyzed the behavior of both laminar and irregular flow in the boundary layer region. In recent decades, the theory of boundary layer flow of fluid along a sheet was extended by many researchers with considering distinct aspects and conditions such as stretching surface and shrinking surface. In the aspect of stretching surface, Crane [2] was the first who extended Sakiadis's theory and introduced the boundary layer two-dimensional fluid flow towards a linearly stretching surface. The boundary layer flow of viscous, incompressible fluid towards a stretching surface attracts the most interest of numerous researchers ascribable to its extensive applications in the industrial and technology fields such as metallurgical, petrochemical, and material processing. Erickson et al. [3] discussed the boundary layer flow of viscous incompressible fluid for heat and mass transfer along a plate with suction and blowing parameters. Dutta et al. [4] did an analysis on temperature field for two-dimensional boundary layer fluid flow toward a stretching surface with uniform heat flux. Patil et al. [5] formulated a 2-D mixed convection flow model towards the semi-infinite power-law stretching surface and solved it numerically using a finite difference approach. Maleki et al. [6] analyzed the influence of heat source/sink parameters for the boundary layer two-dimensional flow of nanofluid along a moving plate under the consideration of viscous dissipation. They used Runge-Kutta-Fehlberg's fourth-fifth order approach to solve the governing equations. Some literature regarding boundary layer flow can be seen through ([7],[8],[9] ,[10],[11] ,[12], [13], [14], [15]).

Fluid has two crucial properties, stretching rate, and cooling rate; both play a crucial role for a better outcome. During the manufacturing process, rapid changes in these two properties of fluid diminishes the quality of the product. To control these fluid properties and to avoid solidification, some external magnetic field is required. Therefore the demand for modern technology has raised the interest in Magnetohydrodynamics (MHD). The phenomenon of MHD was originated in the first half of the twentieth century. At present, the existence of MHD is possible due to the pioneering work of various researchers. The fundamentals of MHD were derived by Hartman [16], and Hartman and Lazarus [17]. After 1950, this phenomenon evolved expeditiously and attracted numerous researchers due to its various real-life applications. The famous scientist Hannes Alfvén [18] contributed greatly to developing the concept of Magnetohydrodynamics in the area of plasma physics. For this, he was awarded the Nobel prize in 1970. Initially, the flow of hydromagnetic fluid towards a stretching surface was discussed by Pavlov [19]. Kumaran et al. [20] investigated the flow model of hydromagnetic fluid along a

quadratically stretching surface and solved the governing model for the exact solution. Mahanthesh et al. [21] analyzed the 3-D MHD nanofluid flow towards a bidirectional nonlinear stretching surface in the existence of radiation and dissipation effects. He obtained numerical solutions by using an efficient technique, the shooting method. Jusoh et al. [22] discussed the flow and heat transfer of viscous incompressible nanofluid along a bidirectional exponential permeable stretching surface under the consideration of viscous dissipation and magnetic field. He has computed the dual solutions as well as done the stability analysis in his paper. The combined impacts of heat source/sink and thermal radiation on 3-D MHD Jeffrey fluid flow along a stretching surface were analyzed by Gireesha et al. [23]. Some recent studies regarding the flow of hydromagnetic fluid can be seen through ([24],[25],[26],[27], [28]).

While studying the flow of hydromagnetic fluid, the concept of the Hall current/Hall effect takes an important place as it arises under the consideration of some external magnetic field. It was the great American physicist Edwin Hall [29] who introduced the concept of the Hall effect in 1879. Even though the concept of Hall current was introduced in 1879, it took several years to get established properly. The principle of Hall effect describes the charging behavior when it is subject to electric and magnetic fields and is widely used in modern technology equipment such as magnetometers, wheel speed sensors, positional sensors, switches, MHD power generators. Also, it is used to cool nuclear reactors, large metallic plates, and MHD pumps in the industry. Thus, these applications have intensified the interest of researches in the study of Hall current. Gupta [30] investigated a boundary layer MHD fluid flow under the consideration of Hall current towards a porous surface. Hayat et al. [31] analyzed the behavior of Hall parameter for the MHD flow of second-grade fluid and heat transfer towards a permeable surface. The combined study of Hall current and heat source/sink effects on laminar flow of hydromagnetic fluid with mass diffusion was done by Saleem and Aziz [32]. Motsa and Shateyi [33] formulated a model for both Hall and ion-slip currents on magnetohydrodynamic fluid flow through a porous medium and solved it by using an efficient technique successive linearization method. [34],[35],[36], [37], [38] present some discussions regarding fluid flow in the existence of Hall current with distinct aspects.

All the studies mentioned above are time-independent (steady-state), but to examine the flow configuration more realistically, the study of time-dependent (unsteady state) fluid flow is necessary. All the flows which vary at a particular point with time come under the category of unsteady flows. Initially, the boundary layer theory was established only for time-independent laminar flows, But soon it was realized that in real life, all flow problems, artificial and natural flows, depending on time. Some excellent pioneering research on unsteady fluid flow can be seen through ([39],[40],[41],[42],[43],[44], [45]). There is a great contribution of Wang [46] to formulate a flow configuration for unsteady

fluid flow passing a stretching sheet. He used similarity transformations to convert the time-dependent Navier-Stokes equations into ODEs. Elbashbeshy and Bazid [47] analyzed the behavior of unsteady parameters on the flow of hydromagnetic fluid and heat transfer towards a stretching surface. He concluded that the thickness of momentum and thermal boundary layers diminishes with increasing values of the unsteady parameter. Also, Ishak et al. [48] examine the characteristics of heat transfer for boundary layer time-dependent fluid flow along a vertical stretching surface. Aziz [49] solved the transient boundary layer fluid flow for similarity solutions in the existence of radiation. Pal [50] analyzed the effects of Hall current and radiation on MHD unsteady fluid flow towards a porous surface. Recently, Megahed et al. [51] have examined the transient boundary layer MHD fluid flow and heat transfer along the stretching surface, assuming that there is a change in viscosity and thermal conductivity with respect to temperature. They solved the proposed model using the shooting method. Matta [52] have analyzed the influences of a chemical reaction and thermal radiation on time-dependent free convection flow of viscous incompressible hydromagnetic fluid along a permeable surface by solving the flow configuration with the finite element method. Stability analysis on the unsteady flow of Maxwell nanofluid along a shrinking porous surface has been done by Khan et al. [53]. They have concluded that shrinking and suction at the permeable surface causes multiple solutions of the governing system of equations. Bhandari [54] has examined the viscous incompressible transient fluid flow of ferrofluid passing through a cylinder in the existence of 10 kilo-ampere per meter magnetic field and concluded that velocity profile falls in the existence of magnetic field. Vemula et al. [55] examined the influences of heat source and magnetic field on time-dependent hybrid nanofluid towards a plate.

Since fluids have multiple properties, it is essential to examine the fluid flow problems via formulating models with various combinations. In research, the aspect of Non-newtonian fluids is prominent due to its wide range of real-life applications. The fluid that does not follow Newton's law of viscosity comes under the category of non-Newtonian fluids. Paint, condensed milk, chocolate flows, ink, Mayonnaise, sauces, lubricant, jelly all are examples of non-Newtonian fluids. To avoid the complexities of such fluids, these are categorized into different flow configurations such as micropolar, Casson, Maxwell, power-law, etc. Among all of these models, Casson fluid model is one of the essential models that specify yield stress characteristics. It was Casson who introduced Casson fluid model in 1995. The said model is based on the interaction of solid and liquid states. It acts as solid when the yield stresses are dominant on shear stress; otherwise, it starts flowing. Chocolate flows, Jelly, Blood flow, are all examples of Casson fluid flow. This phenomenon attracts many researchers due to its applications in various fields such as biophysics, industries, engineering, rheology, cancer therapy. El Dabe and

Salwa [56] did a theoretical analysis to investigate the time-dependent, incompressible, electrically conducting Casson fluid flow between two co-axial cylinders in the presence of the radial magnetic field. Initially, to establish properly, Casson fluid phenomena took many years. With the chemical reactions and suction effects, the flow of heat and mass transfer of viscous, electrically conducting, hydromagnetic, non-Newtonian fluid was investigated by Shehzad et al.[57]. Tufail et al. [58] formulated a flow configuration for viscous incompressible hydromagnetic Non-Newtonian fluid along a permeable surface with heat generation/absorption effects. Nandy [59] examined the influences of partial velocity- slip parameter on viscous hydromagnetic Casson fluid flowing over a stretching surface and obtained the solutions which are analytic about the stagnation point. More significant studies related to said model are ([60], [61], [62], [63], [64],[65],[66]). Recently, Awais et al. [67] have explored the influences of heat and mass transfer on viscous electrically conduction hydromagnetic Casson fluid flowing through permeable medium along a shrinking wall in the existence of heat source/sink effects. Salahuddin et al. [68] have examined the thermophysical properties and internal energy change on 3-D time-independent fluid flow of viscoelastic fluid with convective boundary conditions. For the study of the chemical reactions, they assumed the existence of activation energy in the flow field. The combined effects of thermal radiation and heat source/sink parameters on 2-D mixed convection Brownian motion of Casson fluid towards an infinite plate have been studied by Mittal and Patel [69]. They applied some external magnetic field, and flow was assumed to be flowing through a porous medium.

As said earlier, there is a considerable variety of Non-Newtonian fluids; that is why all the fluid models cannot be studied using a single constitutive relation between shear stress and shear strain. In some cases, the stress tensor is not symmetrical; hence the features of such fluids cannot be studied by viscous fluid theory. There is a generalization of viscous fluid known as couple stress fluid, such as liquid crystals, blood, and synthetic liquids. By adding random solid substances into the fluid suspended to a viscous medium, some forces are induced due to substances which direct in the opposite direction of present force; the combination of these two opposite forces leads to a couple-force which causes the couple stress in fluid. Initially, it was the great American mechanical engineer Stokes [70] who introduced the couple-stress fluid flow model. To study the concept of couple stress fluid, he worked on a series of boundary layer flows. Later, various researchers extended his theory with different aspects. Hayat et al. [71] analyzed the effects of chemical reactions on a 3-D boundary layer transient fluid flow for a couple-stress fluid towards a stretching surface. Ramzan et al. [72] observed the influences of Joule heating and viscous dissipation of 3-D couple stress fluid flow in the existence of some magnetic field. A boundary layer two-dimensional transient flow of a nano-polymer hydromagnetic fluid towards a stretching surface was examined by Kumar et al. [73].

Recently, Narayana et al. [74] made a physical model to examine the effect of heat source and chemical reactions on 3-D boundary layer flow of couple-stress nanofluid towards a stretching surface considering the Brownian motion and thermophoresis force. A heat transfer analysis has been done to analyze the impacts of thermal radiation parameter on a time-dependent 3-D boundary layer fluid flow of couple stress nanofluid flowing over a bidirectional oscillatory stretching surface by Aziz et al. [75]. Also, they have included magnetic field and mixed convection in the flow field. Ali et al. [76] et al. made a model for three-dimensional flow of couple stress fluid with convective boundary conditions and solved it numerically by using HAM efficient technique. Narayana et al. [77] have done a analysis foe the 3-D flow of a couple-Stress Casson Nanofluid along a stretching surface in the existence of radiation.

The above-mentioned research studies are restricted to the study of the fluid flow phase only. However, to solve some technical issues such as cement production, paint spraying, wastewater treatment, and blood rheology, one must formulate and examine two-phase flow models. In these flow models, some solid spherical substances are added to the fluid, and the resulting mixed fluid is known as dusty fluid. Fir this, the study of the flow field is divided into two phases- the fluid phase and the dust phase. It was the Saffman [78] who pioneered the study of particles in the viscous fluid. He attained the equations for the two-phase flow of dusty gas by assuming that the dust substances are uniformly distributed in the gas. Due to the extensive demand of solving technical issues, numerous researchers worked on two-phase dusty fluid considering different aspects. Vajravelu and Nayfeh [79] formulated a flow configuration for two-phase dusty fluid flow flowing over a stretching surface in the existence of a magnetic field and uniform suction. The influence of heat source/sink parameters for boundary layer two-phase fluid flow towards a stretching surface was analyzed by Gireesha et al. [80]. A mathematical analysis was done by Turkyilmazoglu [81] on hydromagnetic two-phase dusty fluid past a porous surface. Kumar et al. [82] examined the effect of thermal radiation on two-phase dusty hyperbolic tangent fluid passing on a stretching surface under the a magnetic field. Abbas [83] discussed the combined impacts of porosity and slip parameters for boundary layer two-phase MHD flow of dusty fluid flowing along a stretching surface. With variable thermal conductivity and convective boundary, a transient boundary layer flow model for hyperbolic tangent fluid was formulated by Bibi et al. [84]. Ali et al.[85] have done a mathematical analysis on time-dependent hydromagnetic two-phase dusty fluid flow between the parallel plates with the consideration of heat and mass source. Mahanthesh et al. [86] have investigated the two-phase boundary layer flow of nanofluid along a vertical surface with the consideration of quadratic thermal convection and quadratic thermal radiation effects, and the governing equations are solved by finite difference method. Bilal et al. [87] have examined the heat transfer process of free

convection Couette flow of a dusty fluid along a rotating surface. The study of MHD two-phase flow and heat transfer of dusty Casson fluid towards a stretching surface with Cattaneo-Christov heat flux model has been done by Gireesha et al. [88]. Wain et al. [89] examined the two-phase fluid flow of hybrid nanofluid passing over a stretching surface in the existence of a magnetic field.

All the above-mentioned studies of heat transfer are just restricted to the first law of thermodynamics, which is associates with the quantity of energy, not with the quality of energy. In this law, heat (low-grade energy) and work (high-grade energy) both are the same. However, as the concept of heat transfer is widespread in all fields such as engineering, industries, and technical equipments, it demands understanding the difference between heat and work. Heat relates to that molecule that is not in order when energy flows in a system or from one system to another; some disorganization occurs, which diminishes the quality of the working system, and this process is known as entropy. Besides, work relates to the molecule flowing in well-order, leading to raising the working system's quality. Despite Numerous flow configurations that have been discussed above for examine the flow and heat transfer of distict fluids along various surfaces, it is still required to study the entropy generation and its minimization during the heat transfer process. Bejan [90, 91] was the first who introduced the concept of entropy generation in thermal engineering. Later, numerous researchers have contributed to examining the entropy generation within various flow configurations having different properties. Rashidi et al. [92] performed an entropy generation analysis for investigating stagnation point flow towards a permeable surface under the heat source/sink impacts. Khan et al. [93] carried out an entropy generation analysis for boundary layer flow of viscous fluid passing a stretching surface, including the frictional and Joule heating terms. To study the entropy generation, Aziz and Afify [94] formulated a flow configuration for MHD Casson fluid flowing in the existence of Hall current. He summarized that the high values of magnetic parameter raise the entropy generation in the system, besides it reduces with a large value of Hall current. Hassan [95] investigated boundary layer MHD fluid flow of couple stress fluid passing through a permeable channel. Aldi et al. [96] have formulated a mixed convection flow model for Eyring-Powell nanofluid and have done an analysis of entropy generation and minimization on the governing flow configuration. The influence of the non-darcy medium on boundary layer flow of viscous incompressible fluid which contains micropolar water-based tio2 nanomaterial has been observed by Zaib et al. [97] along with mixed convection entropy generation aspects. Siddabasappa et al. [98] have done an entropy generation analysis on the flow of hydrmagnetic couple stress fluid flowing through a vertical channel.

Most of the research mentioned earlier is based on flat stretching surfaces, and the governing models are formulated using a cartesian coordinate system. However, only

cartesian coordinate-based flow models are not enough to solve the issues in industrial and engineering fields. Considering this, numerous researchers contributed in formulating relevant models based on different coordinate systems such as polar coordinate system, curvilinear coordinate system, spherical coordinate system, and cylindrical coordinate system. Among these, models based on curvilinear coordinate system are one of the most relevant ones widely used in stretching forming machines with curving jaws, technical equipment and manufacturing processes. It was the Sajid et al. [99] who introduced a curvature in a flat surface and pioneered a flow model based on the curvilinear coordinate system. Sajid et al. [100] examined the flow of micropolar fluid towards a curvilinear stretching surface. They observed that pressure can not be ignored in the case of curved surfaces, unlike flat surfaces. Also, they concluded that the drag force is low as compared with flat surfaces. Later various researchers followed this theory and extended it considering different aspects. An analysis was done on fluid flow, and heat transfer of hydromagnetic fluid towards a curved stretching surface by Abbas et al. [101]. Rosca and Pop [102] did relevant research on time-dependent fluid flow flowing passing permeable curved stretching surface. The simultaneous effects of heat generation/absorption and radiation parameters were analyzed by Abbas et al. [103] on boundary layer flow of nanofluid passing a curved surface. Hayat et al. [104] examined the chemical reactions on convective flow of viscous fluid towards a curved surface under magnetic field and thermal radiation effects. Imtiaz et al. [105] formulated a model to investigate the convective flow of ferrofluid flowing over a curved stretching surface in the existence of homogeneous-heterogeneous reactions. Shabbir et al. [106] formulated a flow configuration of micropolar fluid past a curved surface. The study of homogeneous and heterogeneous reactions for a convective flow of viscous fluid towards a nonlinear stretching surface was done by Saif et al. [107]. Nadeem et al. [108] analyzed to inspect the boundary layer flow of hybrid nanofluid flowing over a curved surface.

The research of fluid flow through a porous medium is the relevant concepts for the researchers because of its extensive applications such as drying of wood, catalytic reactors, heat exchanger design, groundwater system, petroleum resources. The earliest mentioned research of porous media is just restricted to the classical Darcy's law. This law is applicable only when the inertia and boundary features are considered at a low flow rate. It is not sufficient for those flow models which have the assumptions of nonuniform porosity and high-velocity conditions. Later, a modified model was established by Forchheimer [109]. He incorporated a square velocity term in the momentum equation, which handles the nonuniform porosity condition in the flow field. This phenomenon took many years to establish properly. In 1946, Muskat [110] examined Forchheimer's theory and called that square velocity term as Forchheimer term. Later the modified

model was inspected by various researchers with distinct aspects. Saddeek [111] examined the mixed convection Darcy- Forchheimer flow of viscous fluid passing through a porous media under the viscous dissipation and thermophoresis effects. Hayat et al. [112] presented a study to investigate homogeneous-heterogeneous reactions on the flow of viscoelastic fluids flowing over a linearly stretching sheet. Also, they incorporate Cattaneo-Christov heat flux with variable thermal conductivity in the flow field. An analysis of three-dimensional boundary layer flow of nanofluid with the consideration of Forchheimer term and convective boundary conditions was done by Muhammad et al. [113]. They analyzed that the values of Skin-friction coefficients rise for the Forchheimer parameter, whereas the local Nusselt number falls with increasing the Forchheimer parameter. Do et al. [114] formulated a model of transient flow of nanofluid with Navier's slip condition and solved it via using an efficient numerical scheme is spectral relaxation method. Recently, Hayat et al. [115] have worked on the Entropy generation minimization concept for boundary layer flow of nanofluid flowing through a porous media passing a curved stretching surface. Also, they incorporate partial slip conditions and Forchheimer term in the flow field. The most recent studies on Darcy-Forchheimer flow are examined through([116], [117],[118],[119],[120],[121],[122],[123],[124],[125],[126]).

1.6 Solution Methodology

The mathematical models of present study are obtained as a set of coupled non-linear partial differential equations subject to suitable boundary conditions, which are non-dimensionalized using suitable non-dimensional variables and solved numerically using a suitable numerical technique. As the non-dimensionalized equations are highly non-linear the solution of the equations are carried out using spectral method based numerical techniques due to the robustness and fast convergence of these methods. In particular, spectral method based quasi-linearization method and the in-built matlab solver bvp4c are used to obtain the solution the governing equations and carry out a parametric study of the considered model. Below we present a brief discussion of the Spectral Quasi-Linearization Method (SQLM) and the in-built matlab solver bvp4c.

1.7 Spectral Quasi-linearisation Method

The quasi-linearisation method is an efficient numerical approach which is used for linearizing the highly nonlinear ordinary and partial differential equations. It follows the idea of Newton's method and linearize various differential equations by using one term

Taylor series about the previous approximation of the solution. Consider a following example to demonstrate the QLM iterative scheme.

$$\phi\left[\, c(x)\ ,\ c'(x)\ ,\ c''(x)\ ,\ldots,\ c^{(n)}(x)\ \right] = 0,\ \ x \in [a,b], \tag{1.10}$$

with boundary conditions

$$H_{a,k}[\, c(a), c'(a), c''(a), \ldots, c^{(n-1)(a)}] \ = \ 0,\ \ k \ = \ 1\,2\ \ldots, m, \tag{1.11}$$

$$H_{b,k}[\, c(b), c'(b), c''(b), \ldots, c^{(n-1)(b)}] \ = \ 0,\ \ k \ = \ m+1, m+2, \ldots, n. \tag{1.12}$$

In QLM approach, it is considered that there exist a small difference between the value of approximated solution at the current iteration $c_{r+1}(x)$ and the value of approximated solution at previous iteration (denoted by $c_r(x)$). The difference between the derivatives at the subsequent iteration levels, $c_{r+1}^{(p)} - c_r^{(p)}$, is also assumed to be small. Expanding (1.10) using one term Taylor series gives

$$\begin{aligned}\phi[c, c', c'', \ldots c^{(n)}] \ \approx \ \phi[c_r, c_r', c_r'', \ldots c_r^{(n)}] + (c - c_r, c' - c_r', c'' - c_r'', \ldots, c^{(n)} - c_r^{(n)}) \\ .\nabla\phi\left[c_r, c_r', c_r'', \ldots, c_r^{(n)}\right] = 0,\end{aligned} \tag{1.13}$$

where ∇ is a vector of partial derivatives defined as

$$\nabla = \left\{ \tfrac{\partial}{\partial c}, \tfrac{\partial}{\partial c'}, \tfrac{\partial}{\partial c''}, \ldots \tfrac{\partial}{\partial c^{(n)}} \right\}. \tag{1.14}$$

Using the notation $c \ = \ c^{(0)}, c' \ = \ c^{(1)}, c'' \ = \ c^{(2)}, c''' \ = \ c^{(3)}$, etc, we can write equation (1.13) as

$$\begin{aligned}\phi\left[c_r, c_r', c_r'', \ldots, c_r^{(n)}(x)\right] + \left(c^{(0)} - c_r^{(0)}\right) \frac{\partial\phi}{\partial c^{(0)}}\left[c_r, c_r', c_r'', \ldots c_r^{(n)}\right] + \left(c^{(1)} - c_r^{(1)}\right) \\ \frac{\partial\phi}{\partial c^{(1)}}\left[c_r, c_r', c_r'', \ldots c_r^{(n)}\right] + \left(c^{(2)} - c_r^{(2)}\right) \frac{\partial\phi}{\partial c^{(2)}}\left[c_r, c_r', c_r'', \ldots c_r^{(n)}\right] + \ldots + \\ \left(c^{(n)} - c_r^{(n)}\right) \frac{\partial\phi}{\partial c^{(n)}}\left[c_r, c_r', c_r'', \ldots c_r^{(n)}\right] = 0.\end{aligned} \tag{1.15}$$

The above equation can be written in compact form as

$$\phi\left[c_r(x), c_r'(x), c_r''(x), \ldots, c_r^{(n)(x)}\right] + \sum_{p=0}^{n} \frac{\partial \phi}{\partial c^{(p)}} \left[c_r(x), c_r'(x), \ldots, c_r^{(n)(x)}\right] \left(c^{(p)}(x) - c_r^{(p)}(x)\right) = 0. \tag{1.16}$$

To keep track of the solution after several iterations, we use the label c_{r+1} to donate the approximation after $(r+1)$ iterations. Thus, determining the approximate solution at the $(r+1)$ level of iteration as the solution of the linear equation

$$\phi\left[c_r(x), c_r'(x), c_r''(x), \ldots, c_r^{(n)(x)}\right] + \sum_{p=0}^{n} \frac{\partial \phi}{\partial c^{(p)}} \left[c_r(x), c_r'(x), \ldots, c_r^{(n)(x)}\right] \left(c^{(p)}(x) - c_r^{(p)}(x)\right) = 0, \tag{1.17}$$

with linearized boundary conditions

$$H_{a,k}\left[c_r(a), c_r'(a), \ldots, c_r^{(n-1)}(a)\right] + \sum_{p=0}^{n-1} \frac{\partial H_{a,k}}{\partial c^(p)} \left[c_r(a), c_r'(a), \ldots, c_r^{(n-1)}(a)\right] \left(c_{r+1}^{(p)}(a) - c_r^{(p)}(a)\right) = 0, \tag{1.18}$$

for $k = 1, 2, \ldots, m$ and

$$H_{b,k}\left[c_r(b), c_r'(b), \ldots, c_r^{(n-1)}(b)\right] + \sum_{p=0}^{n-1} \frac{\partial H_{b,k}}{\partial c^(p)} \left[c_r(b), c_r'(b), \ldots, c_r^{(n-1)}(b)\right] \left(c_{r+1}^{(p)}(b) - c_r^{(p)}(b)\right) = 0, \tag{1.19}$$

for $k = m+1, \ldots, n$.
Rewrite the equations (1.17) − (1.19) in the following form

$$a_{n,r}(x)c_{r+1}^{(n)}(x) + a_{n-1,r}(x)c_{r+1}^{(n-1)}(x) + \ldots + a_{1,r}(x)c_{r+1}'(x) + a_{0,r}(x)c_{r+1}(x) = R_r(x), \tag{1.20}$$

$$\alpha_{n-1,k}c_{r+1}^{(n-1)}(a) + \alpha_{n-2,k}c_{r+1}^{(n-2)}(a) + \ldots + \alpha_{1,k}c_{r+1}'(a) + \alpha_{0,k}c_{r+1}(a) = R_{a,k}, \tag{1.21}$$

$$\beta_{n-1,k}c_{r+1}^{(n-1)}(b) + \beta_{n-2,k}c_{r+1}^{(n-2)}(b) + \ldots + \beta_{1,k}c_{r+1}'(b) + \beta_{0,k}c_{r+1}(b) = R_{b,k}, \tag{1.22}$$

where

$$a_{p,r}(x) = \frac{\partial \phi}{\partial c^{(p)}} \left[c_r(x), c_r'(x), \ldots, c_r^{(n)}(x) \right], \; p = 0, 1, 2, \ldots, n,$$

$$R_r(x) = \sum_{p=0}^{n} \frac{\partial \phi}{\partial c^{(p)}} \left[c_r(x), c_r'(x), \ldots, c_r^{(n)}(x) \right] c_r^{(p)}(x) - \phi \left[c_r(x), c_r'(x), \ldots, c_r^{(n)}(x) \right],$$

$$\alpha_{p,k} = \frac{\partial H_{a,k}}{\partial c^{(p)}} \left[c_r(a), c_r'(a), \ldots, c_r^{(p)(a)} \right], p = 0, 1, \ldots, n-1, \; k = 1, 2, \ldots, m,$$

$$\beta_{p,k} = \frac{\partial H_{b,k}}{\partial c^{(p)}} \left[c_r(b), c_r'(b), \ldots, c_r^{(p)(b)} \right], p = 0, 1, \ldots, n-1, k = m+1, m+2, \ldots, n,$$

$$R_{a,k} = \sum_{p=0}^{n-1} \frac{\partial H_{a,k}}{\partial c^{(p)}} \left[c_r(a), c_r'(a), \ldots, c_r^{(n-1)}(a) \right] c_r^{(p)}(a) - H_{a,k} \left[c_r(a), c_r'(a), \ldots, c_r^{(n-1)}(a) \right],$$

$$for \; k = 1, 2, \ldots, m,$$

$$R_{b,k} = \sum_{p=0}^{n-1} \frac{\partial H_{b,k}}{\partial c^{(p)}} \left[c_r(b), c_r'(b), \ldots, c_r^{(n-1)}(b) \right] c_r^{(p)}(b) - H_{b,k} \left[c_r(b), c_r'(b), \ldots, c_r^{(n-1)}(b) \right],$$

$$for \; k = m+1, m+2, \ldots, n.$$

Then the linearized equations (1.20)-(1.22) obtained from QLM scheme are solved by applying Chebyshev spectral collocation approch. As this approach can apply in the domain [-1,1], So it is required to convert the original domain $[a, b]$ into [-1,1] by using a linear mapping $x = (b - a)(\zeta + 1)/2$. Basically, in spectral methods, a differentiation matrix D is introduced for approximate the derivatives of unknown variables.
To illustrate the process of spectral methods, approximate the derivatives of the function $\phi(\zeta)$ with respect to ζ. For approximate the function at the mesh points $\zeta_0, \zeta_1, \ldots, \zeta_{N-1}$, ζ_N, it is convenient to form a mesh by defining mesh points ζ_j $(j = 0, 1, \ldots, N)$ as

$$\zeta_j = \cos \tfrac{\pi j}{N}, \quad j = 0, 1, 2, \ldots, N \tag{1.23}$$

The above mesh points are called Chebyshev-Gauss-Lobatto points. The values of the function $\phi(\zeta)$ at the mesh points are denoted as $\phi_k = \phi(\zeta_k)$. Approximating the function

using Lagrange interpolation polynomials as

$$\phi(\zeta) \approx P_N(\zeta) = \sum_{k=0}^{N} \phi_k L_k(\zeta). \tag{1.24}$$

where L_k are the Lagrange interpolation polynomials,

$$L_k(\zeta_j) = \begin{pmatrix} 0 & if j \neq k \\ 1 & if j = k \end{pmatrix}.$$

Differentiate the interpolating function and obtained approximate derivative of the function $\phi(\zeta)$ as

$$\phi'(\zeta) = \sum_{k=0}^{N} \phi_k L'_k(\zeta) \tag{1.25}$$

Computing (1.25) at the mesh points ζ_j gives

$$\phi'(\zeta_j) = \sum_{k=0}^{N} \phi_k L'_k(\zeta_j) = \sum_{k=0}^{N} D_{jk}\phi_k, \quad j = 0, 1, 2, \ldots, N, \tag{1.26}$$

where $D_{jk} = L'_k(\zeta_j)$. Equation (1.26) can be written as

$$\begin{pmatrix} \phi'(\zeta_0) \\ \phi'(\zeta_1) \\ \phi'(\zeta_2) \\ \vdots \\ \phi'(\zeta_{N-1}) \\ \phi'(\zeta_N) \end{pmatrix} = \begin{pmatrix} D_{0,0} & D_{0,1} & D_{0,2} & \cdots & D_{0,N-1} & D_{0,N} \\ D_{1,0} & D_{1,1} & D_{1,2} & \cdots & D_{1,N-1} & D_{1,N} \\ D_{2,0} & D_{2,1} & D_{2,2} & \cdots & D_{2,N-1} & D_{2,N} \\ \vdots & \vdots & \vdots & \vdots & \vdots & \vdots \\ D_{N-1,0} & D_{N-1,1} & D_{N-1,2} & \cdots & D_{N-1,N-1} & D_{N-1,N} \\ D_{N,0} & D_{N,1} & D_{N,2} & \cdots & D_{N,N-1} & D_{N,N} \end{pmatrix} \begin{pmatrix} \phi(\zeta_0) \\ \phi(\zeta_1) \\ \phi(\zeta_2) \\ \vdots \\ \phi(\zeta_{N-1}) \\ \phi(\zeta_N) \end{pmatrix}.$$

Rewrite the above equation in compact form as

$$\mathbf{\Phi'} \approx D\mathbf{\Phi}, \tag{1.27}$$

where $\mathbf{\Phi'} = [\phi'(\zeta_0), \phi'(\zeta_1), \ldots, \phi'(\zeta_N)]^T, \mathbf{\Phi} = [\phi(\zeta_0), \phi(\zeta_1), \ldots, \phi(\zeta_N)]^T$. The entries of D are D_{jk} for $j, k = 0, 1, 2, \ldots N$.

Also, for computing higher order derivatives, product the matrix D as below

$$\mathbf{\Phi''} \approx D^2\mathbf{\Phi},\ \mathbf{\Phi'''} \approx D^3\mathbf{\Phi}, \text{ etc.}$$

The size of D depends upon N, for $N = 1$, we have $N + 1 = 2$ mesh points $\zeta_0 = 1, \zeta_1 = -1$. So

$$P_1(\zeta) = \frac{1}{2}(1 + \zeta)\phi_0 + \frac{1}{2}(1 - \zeta)\phi_1,\ \phi'(\zeta) \approx \frac{1}{2}\phi_0 + \frac{1}{2}\phi_1. \tag{1.28}$$

In matrix-vector form, it is written as $\begin{pmatrix} \phi'(\zeta_0) \\ \phi'(\zeta_1) \end{pmatrix} = \begin{pmatrix} \frac{1}{2} & -\frac{1}{2} \\ \frac{1}{2} & -\frac{1}{2} \end{pmatrix} \begin{pmatrix} \phi(\zeta_0) \\ \phi(\zeta_1) \end{pmatrix}$.
For $N = 2$, there is $N + 1 = 3$ interpolation points obtained as $\zeta_0 = 1, \zeta_1 = 0, \zeta_2 = -1$,

$$P_2(\zeta) = \frac{1}{2}\zeta(\zeta+1)\phi_0 + (1+\zeta)(1-\zeta)\phi_1 + \frac{1}{2}\zeta(\zeta-1)\phi_2, \tag{1.29}$$

$$\phi'(\zeta) \approx \left(\zeta + \frac{1}{2}\right)\phi_0 - 2\zeta\phi_1 + \left(\zeta - \frac{1}{2}\right)\phi_2. \tag{1.30}$$

Evaluating at the collocation points provides

$$\zeta_0 = 1, \;\; \phi'(\zeta_0) = \frac{3}{2}\phi_0 - 2\phi_1 + \frac{1}{2}\phi_2, \tag{1.31}$$

$$\zeta_1 = 0, \;\; \phi'(\zeta_1) = \frac{1}{2}\phi_0 - \frac{1}{2}\phi_2, \tag{1.32}$$

$$\zeta_3 = -1, \;\; \phi'(\zeta_2) = -\frac{1}{2}\phi_0 + 2\phi_1 - \frac{3}{2}\phi_2, \tag{1.33}$$

which can be obtained in matrix form as below
$\begin{pmatrix} \phi'(\zeta_0) \\ \phi'(\zeta_1) \\ \phi'(\zeta_2) \end{pmatrix} \begin{pmatrix} \frac{3}{2} & -2 & \frac{1}{2} \\ \frac{1}{2} & 0 & -\frac{1}{2} \\ -\frac{1}{2} & 2 & -\frac{3}{2} \end{pmatrix} \begin{pmatrix} \phi(\zeta_0) \\ \phi(\zeta_1) \\ \phi(\zeta_2) \end{pmatrix}$.
When $N = 3$, with collocation points $\zeta_0 = 1, \zeta_1 = \frac{1}{2}, \zeta_3 = -\frac{1}{2}, \zeta_4 = -1$,
$\begin{pmatrix} \phi'(\zeta_0) \\ \phi'(\zeta_1) \\ \phi'(\zeta_2) \\ \phi'(\zeta_3) \end{pmatrix} = \begin{pmatrix} \frac{19}{6} & -4 & \frac{4}{3} & -\frac{1}{2} \\ 1 & -\frac{1}{3} & -1 & \frac{1}{3} \\ -\frac{1}{3} & 1 & \frac{1}{3} & -1 \\ \frac{1}{2} & -\frac{4}{3} & 4 & -\frac{19}{6} \end{pmatrix} \begin{pmatrix} \phi(\zeta_0) \\ \phi(\zeta_1) \\ \phi(\zeta_2) \\ \phi(\zeta_3) \end{pmatrix}$.
In general, for each $N > 1$,the entries of the spectral differentiation matrix D of size $(N+1) \times (N+1)$ are

$$D_{jk} = \frac{z_j}{z_k}\frac{(-1)^{j+k}}{\zeta_j - \zeta_k} \quad j \neq k;\; j,\; k = 0,\; 1, \ldots, N, \tag{1.34}$$

$$D_{kk} = -\frac{\zeta_k}{2(1-\zeta_k^2)} \quad k \;=\; 1,\; 2, \ldots, N-1, \tag{1.35}$$

$$D_{0}0 = \frac{2N^2+1}{6} = -D_{NN}, \tag{1.36}$$

with $z_k = \begin{pmatrix} 2 & k = 0, N \\ 1 & -1 \leq k \leq N-1 \end{pmatrix}$.

To illustrate the implementation of the SQLM, we consider the Jeffery-Hamel equation given by

$$c''' + 2\alpha Re cc' + 4\alpha^2 c' \;\; = \;\; 0, \tag{1.37}$$

subject to the boundary conditions

$$c(0) = 1,\ c'(0) = 0,\ c(1) = 0, \tag{1.38}$$

where Re is the Reynolds number and α is a constant. Rewrite the above equation as

$$F[x, c(x), c'(x), c''(x), c'''(x)] = c''' + 2\alpha Recc' + 4\alpha^2 c' = 0,\ \ x \in [0, 1], \tag{1.39}$$

with boundary conditions

$$\begin{aligned} G_{0,1}[c(0), c'(0), c''(0)] &= c(0) - 1, & (1.40)\\ G_{0,2}[c(0), c'(0), c''(0)] &= c'(0), & (1.41)\\ G_{1,1}[c(1), c'(1), c''(1)] &= c(1). & (1.42) \end{aligned}$$

Thus, the QLM scheme becomes

$$a_{0,r}(x)c'''_{r+1}(x) + a_{1,r}(x)c''_{r+1}(x) + a_{2,r}(x)c'_{r+1}(x) + a_{3,r}(x)c_{r+1} = R_r(x), \tag{1.43}$$

$$\begin{aligned} \alpha_{0,1}c''_{r+1}(0) + \alpha_{1,1}c'_{r+1}(0) + \alpha_{2,1}c_{r+1}(0) &= R_{0,1},\\ \alpha_{0,2}c''_{r+1}(0) + \alpha_{1,2}c'_{r+1}(0) + \alpha_{2,2}c_{r+1}(0) &= R_{0,2},\\ \beta_{0,1}c''_{r+1}(1) + \beta_{1,1}c'_{r+1}(1) + \beta_{2,1}c_{r+1}(1) &= R_{1,1}, \end{aligned}$$

where

$$\begin{aligned} a_{0,r}(x) &= \frac{\partial F}{\partial c'''}[x,\ c_r(x),\ c'_r(x),\ c''_r(x),\ c'''_r(x)] = 1,\\ a_{1,r}(x) &= \frac{\partial F}{\partial c''}[x,\ c_r(x),\ c'_r(x),\ c''_r(x),\ c'''_r(x)] = 0,\\ a_{2,r}(x) &= \frac{\partial F}{\partial c'}[x,\ c_r(x),\ c'_r(x),\ c''_r(x),\ c'''_r(x)] = 2\alpha Rec_r + 4\alpha^2,\\ a_{3,r}(x) &= \frac{\partial F}{\partial c}[x,\ c_r(x),\ c'_r(x),\ c''_r(x),\ c'''_r(x)] = 2\alpha Rec'_r,\\ R_r(x) &= \sum_{p=0}^{3} \frac{\partial F}{\partial c^{(p)}}[x, c_r(x), c'_r(x), c''_r(x), c'''_r(x)]c_r^{(p)}(x) - F\left[x, c_r(x), c'_r(x), \ldots, c_r^{(n)}(x)\right],\\ &= 2\alpha Rec_r c'_r. \end{aligned}$$

Similarly, it can be shown that the boundary conditions $(1.40) - (1.42)$ become

$$c_{r+1}(0) = 1,\ \ c'_{r+1}(0) = 0,\ \ c_{r+1}(1) = 0.$$

Applying spectral collocation on (1.43) gives

$$\mathbf{AC}_{r+1} \quad = \quad R_r,$$

where $A = D^3 + a_{2,r}D + a_{3,r}$,
$\mathbf{C} = [c(x_0), c(x_1), \ldots, c(x_N)]^T, R_r = [R_r(x_0), R_r(x_1), \ldots, R_r(x_N)]^T$,
and $a_{p,r}$ are diagonal matrices of $[a_{p,r}(x_0), a_{p,r}(x_1), \ldots, a_{p,r}(x_N)]$.
The boundary conditions become

$$c_{r+1}(x_N) = 1, \ \sum_{k=0}^{N} D_{N,k}c_k = 0, \ \ c(x_0) = 0. \tag{1.44}$$

The boundary conditions (1.44) are imposed on the first, second from last and last row of (1.44) as shown below,

$$\begin{pmatrix} 1 & 0 & \cdots & 0 & 0 \\ A_{1,0} & A_{1,1} & \cdots & A_{1,N-1} & A_{1,N} \\ A_{2,0} & A_{2,1} & \cdots & A_{2,N-1} & A_{2,N} \\ \vdots & \vdots & \vdots & \vdots & \vdots \\ A_{N-2,0} & A_{N-2,1} & \cdots & A_{N-2,N-1} & A_{N-2,N} \\ D_{N,0} & D_{N,1} & \cdots & D_{N,N-1} & D_{N,N} \\ 0 & 0 & \cdots & 0 & 1 \end{pmatrix} \begin{pmatrix} c(x_0) \\ c(x_1) \\ c(x_2) \\ \vdots \\ c(x_{N-2}) \\ c(x_{N-1}) \\ c(x_N) \end{pmatrix} = \begin{pmatrix} 0 \\ R_r(x_1) \\ R_r(x_2) \\ \vdots \\ R_r(x_{N-2}) \\ 0 \\ 1 \end{pmatrix}.$$

Thus starting from a suitable initial approximation $c_0(x)$, the approximate solution $c(x)$ can be obtained iteratively by solving equation for $r = 1, 2, 3, \ldots$.

$$\begin{pmatrix} c_{r+1}(x_0) \\ c_{r+1}(x_1) \\ c_{r+1}(x_2) \\ \vdots \\ c_{r+1}(x_{N-2}) \\ c_{r+1}(x_{N-1}) \\ c_{r+1}(x_N) \end{pmatrix} = \begin{pmatrix} 1 & 0 & \cdots & 0 & 0 \\ A_{1,0} & A_{1,1} & \cdots & A_{1,N-1} & A_{1,N} \\ A_{2,0} & A_{2,1} & \cdots & A_{2,N-1} & A_{2,N} \\ \vdots & \vdots & \vdots & \vdots & \vdots \\ A_{N-2,0} & A_{N-2,1} & \cdots & A_{N-2,N-1} & A_{N-2,N} \\ D_{N,0} & D_{N,1} & \cdots & D_{N,N-1} & D_{N,N} \\ 0 & 0 & \cdots & 0 & 1 \end{pmatrix}^{-1} \begin{pmatrix} 0 \\ R_r(x_1) \\ R_r(x_2) \\ \vdots \\ R_r(x_{N-2}) \\ 0 \\ 1 \end{pmatrix}.$$

1.8 BVP4C

In Matlab software there is an in-built solver namely bvp4c is used to solve highly nonlinear system of differential equations together with the given boundary conditions. Also the obtained results can be plotted and compared by graphs and tables. The algorithm of bvp4c solver is written as follows:
Consider a differential equation

$$\phi\left[\ c(x)\ ,\ c'(x)\ ,\ c''(x)\ ,\ldots,\ c^{(n)}(x)\ \right]=0,\ \ x\in[a,b], \tag{1.45}$$

with boundary conditions

$$H_{a,k}[\ c(a)\ ,\ c'(a)\ ,\ c''(a)\ ,\ldots,\ c^{(n-1)(a)}\ ]\ =\ 0\ ,k=1\ ,2,\ldots,m, \tag{1.46}$$

$$H_{b,k}[\ c(b)\ ,\ c'(b)\ ,\ c''(b)\ ,\ldots,\ c^{(n-1)(b)}\ ]\ =\ 0\ ,k=m+1,m+2,\ldots,n, \tag{1.47}$$

where ϕ is non-linear operator of $c(x)$ and its n derivatives, $H_{a,k}, H_{b,k}$ are non linear functions of $c(x)$ its $n-1$ derivatives at $x=a$ and $x=b$.

Step1 Convert the nonlinear differential equation into a system of first order differential equations. Use the following substitutions for getting it.
$c=v_1(x),\ c'=v_2(x),\ c''=v_3(x),\ c'''=v_4(x),\ \ldots,\ c^{(n-2)}=v_{n-1}(x),\ c^{(n-1)}=v_n(x).$
Thus the system of first order differential equation is given as $;v_1'=v_2(x),\ v_2'=v_3(x),\ v_3'=v_4(x),\ \ldots,\ v_{n-1}'=v_n(x),$ and $v_n'=\psi(v_1,v_2,\ldots,v_n)$.

Step2 Code the governing system of first order differential equation in Matlab software by using in-built solver namely bvp4c. For this make a function as follows, which can be used by bvp4c solver

$$\text{function } \tfrac{dy}{dx}=ode(x,c),$$

$$\frac{dy}{dx}=\begin{cases} v(2)\\ v(3)\\ v(4)\\ \vdots\\ v(n)\\ \psi\left(v(1),v(2),\ldots,v(n)\right). \end{cases} \tag{1.48}$$

Step3 Also for code the boundary conditions, It is required to make a function as follows

$$\text{function } res=bcs(va,vb),$$

$$res=\begin{cases} H_k[\ va(1)\ ,va(2)\ ,\ldots\ ,va(n)] & k\ =\ 1\ ,\ 2\ ,\ldots,\ m\\ H_k[\ vb(1)\ ,vb(2)\ ,\ldots\ ,vb(n)] & k\ =\ m+1\ ,m+2\ ,\ldots,\ n \end{cases} \tag{1.49}$$

Step3 For starting the iterative scheme, there is a need of initial guess say *solinitial* for each $v(1), v(2), \ldots, v(n)$. For this, we choose initial guess as it satisfies the boundary conditions and for the remaining ones, it takes the values randomly (generally 0.5). Also we set the values of unknown parameters occurs in the given differential equation.

Step4 The final step is to use bvp4c solver along with the above generated functions, print and plot the governing solution . For this use the command as below

$$sol = bvp4c(@ode, @bcs, solinitial). \tag{1.50}$$

1.9 Thesis Contribution

Motivated from the above mentioned research work the aim of the present thesis is to investigate the boundary layer magnetohydrodynamic flow of viscous incompressible electrically conducting fluid and heat transfer along the stretching surface under the existence of different conditions and aspects such as Hall current, viscous dissipation, couple stress, thermal radiation, heat sorce/sink effects, two-phase fluid flow, entropy generation, porous stretching surface, and many more. Also it is observed that the combined study of considered parameters in the present thesis in various combinations has not been examined yet. For this, different flow models are formulated in the form of set of coupled partial differential equations subject to some boundary conditions. Further some relevant transformations are used to convert the governing PDEs into set of coupled ordinary differential equations. In order to obtain the solutions of the differential equations, some efficient numerical techniques are used and are implemented in Matlab software. The obtained solutions are present in the form of graphs and figures of velocity and temperature profiles with respect to governing parameters such as magnetic field parameter, unsteadiness parameter, couple stress parameter, Casson parameter, radiation parameter and many more. Moreover the numerical values of essential physical quantities such as Nusselt number and skin friction coefficients are computed and presented in the form of tables to analyze the effects of distinct parameters of flow field. Also for the validation of solutions, residue analysis is done and presented by using graphs and tables. The fluid flow models which are formulated in this thesis may find applications in modern engineering problems which are working under some magnetic field.

1.10 Objectives of the study

The aim of the present research work leading to Ph.D. degree is to investigate the flow of a viscous, incompressible and electrically conducting fluid in the presence of a magnetic field over a smooth surface under different conditions. The proposed work is to provide a theoretical insight into such flows. The objectives are:

1. To study the hydromagnetic flow of a viscous, incompressible, and electrically conducting fluid over a smooth surface in the presence of heat generation/absorption.
2. To investigate the hydromagnetic boundary layer flow and heat transfer of a viscous, incompressible, and electrically conducting fluid over a stretching surface in the presence of thermal radiation.
3. To study the flow and heat transfer behavior due to the flow of a viscous and incompressible fluid over a curved surface permeated with an external magnetic field.

1.11 Outline of the thesis

The work of present thesis is divided into seven chapters. A brief outline of the chapters presented in the thesis is given below

Chapter-1 is the introductory chapter of the thesis in which a brief background of magnetohydrodynamics, the fundamental laws and equations required to study the magnetohydrodynamic flow and heat transfer along a smooth surface is presented. Objectives of the proposed research work is clearly stated, and the methodology used for solving the problems discussed in the thesis is provided in brief. An ample number of relevant literatures is provided in the literature review section of this chapter.

Chapter-2 is presented to perform a numerical treatment of the transient three dimensional MHD flow of a Casson fluid considering the influences of Hall current and thermal radiation. In this work, the three dimensional flow of a Casson fluid induced due to the linear stretching of a sheet is investigated. The flow field is permeated with a time-dependent magnetic field acting perpendicular to the direction of stretching of the sheet. The heat transfer phenomenon includes the influence of non-linear thermal radiation. The flow model is represented by time-dependent partial differential equations which are highly non-linear. Suitable transformations are used to convert the governing PDEs into ODEs. Then, a spectral method, namely (SQLM), is used to solve the

resulting ODEs. To study the influences of different significant parameters on the profiles of velocity field and temperature field, a detailed analysis is taken. Moreover, it is concluded that velocity profiles are increased for larger values of Hall current parameter and skin friction coefficient, in the primary direction, is reduced for higher values of Hall current parameter. This works is published in the form of a research paper in the **Results in Physics** [Result in Physics, Vol. 11, pp. 966-974 (2018)].

In **Chapter-3**, a numerical investigation of the Hall current and radiative heat transfer effects on the unsteady magnetohydrodynamic three-dimensional Casson fluid flow over a stretching surface in a porous medium is performed. The problem discussed in Chapter-2 is extended to include the presence of Darcy porous medium and convective heat transfer at the surface. The mathematical model of the problem is presented in the form of a set of non-linear partial differential equations along with suitable boundary conditions. These equations are transformed to a set of non-linear ordinary differential equations using suitable similarity transformations which are later dealt with the efficient Spectral quasi-linearization method (SQLM) to obtain the numerical solution of the considered model. A parametric study involving the emerging physical parameters is performed to analyse the effects of relevant flow parameters on the fluid velocity, fluid temperature, and the coefficients of skin-friction and heat transfer at the surface. It is found that the momentum boundary layers, in both the directions, get thicker whereas the thermal boundary layer becomes thinner with increasing Hall current. Moreover, it is concluded that fluid velocities in both the directions rise for higher values of the permeability of the medium and convective heating from the surface and the radiation give increment to the fluid temperature within the boundary layer region, and as a result, the heat transfer at the surface also observes a rise. This works is published in the form of a research paper in the **Journal of Porous Media**[Journal of Porous Media, Vol. 24 (6), pp. 15-30 (2021)]. **Chapter-2** and **Chapter-3** contribute to fulfilling the **Objective-2** as listed earlier.

The study in **Chapter-4** is chosen in such a way as to satisfy the **Objective-1**. In this chapter, the transient magnetohydrodynamic flow of a couple-stress dusty fluid over a stretching surface is investigated considering the impacts of viscous-dissipation and non-uniform heat generation/absorption.The fluid flow is assumed to be taking along a porous sheet. The two-phase flow configuration is used to develop the mathematical model in terms of non-linear PDEs subject to the suitable boundary conditions. The mathematical model is then transformed to ODEs model using suitable transformations. Subsequently, the governing equations are solved numerically using SQLM. The effects of emerging parameters on both the fluid-phase and dustphaseare shownusing graphs. Further, the influence of important parameters on the skin-friction coefficient and Nusselt number are analyzed through table. It is concluded that both the fluid and dust

phases temperature profiles rise with an increment in the value of magnetic field. Fluid velocities for both the phases reduce with increased values of the suction. The skin-friction in the x direction decreases with increased values of the suction parameter. The rate of heat transfer at the surface is higher with the higher value of the suction parameter.An increment in the value of Pr decreases the thermal diffusivity. Due to this, there is a fall in temperature distributions and thermal boundary layer thickness. The work presented in this chapter is presented accepted for publication in the **AIP Conference Proceedings**.

Chapter-5 of the thesis is devoted to study the entropy generation in the three-dimensional stagnation point flow of a Casson fluid along a stretching sheet with radiative and dissipative heat transfer. The fluid flow is permeated with a time-depended magnetic field and the influence of Hall current is also considered. The resulting mathematical model is again treated with similarity transformations to transform the model involving non-linear ordinary differential equations. The spectral method based quasi-linearization technique (SQLM) is used to obtain the numerical solution for the fluid velocity and fluid temperature, as well as the coefficients of skin-friction and heat transfer. These results are presented in graphs and table and discussed for varying values of the parameters. In order to estimate coefficients of skin-friction and heat transfer, a statistical approach, namely regression analysis is also used. From the parametric analysis, it is concluded that the velocity distribution diminishes with increasing values of unsteadiness parameter and Casson parameter. The Bejan number is reduced for higher values of magnetic field parameter. On the other hand, entropy generation is increased for higher values of magnetic field parameter. The work presented in this chapter has been communicated to the **Journal of Applied Fluid Mechanics** for possible publication.

The flow geometry in all the previous chapters were associatedwith flat stretching surface and the mathematical modelling used cartesian coordinate system. In **Chapter-6**, an investigation of the transient magnetohydrodynamic flow of a viscous fluid over a curved stretching surface in a non-Darcy porous medium is performed considering the influence of thermal radiation. The governing non-linear PDEs, after transformation were dealt with MATLAB's in-built solved "bvp4c". The numerical results are presented in the form of tables and graphs and a parametric analysis is performed to understand the behaviour of different emerging flow parameters on the fluid flow and heat transfer. It is concluded that a large value of radius of curvature leads to rise in the fluid velocity distribution, whereas the fluid velocity falls for large values of porosity parameter and Forchheimer parameter. The work presented in this chapter fulfill the **Objective-3**, and has been communicated to the **Pramana**.

In **Chapter-7**, the summary and conclusions drawn from the previous chapters is presented. A brief overview of the future scope is also stated.

Chapter 2

A Numerical Treatment of Unsteady Three-Dimensional Hydromagnetic Flow of a Casson Fluid with Hall and Radiation Effects

2.1 Introduction

The role of boundary layer flow along a stretching surface finds remarkable applications in engineering and industrial processes. In the steel industry, for a better outcome in the manufacturing process, the primary fluid features, such as stretching rate and cooling rate of liquid, are essential. Since rapid stretching destroys the characteristics of the final product due to sudden solidification, hence managing the stretching rate is very important. Boundary layer flow over stretching sheets also has applications in glass production, crude oil refinement, and paper production. It was Crane [2] who first presented the boundary layer theory for an incompressible liquid along a two-dimensional linearly stretching surface. Following this, various researchers, such as Elbashbeshy [44] and Mahapatra and Gupta [45], examined the flows along a stretching surface, in the

Contents of this chapter has been published in Result in Physics [Prashu, R. Nandkeolyar, A numerical treatment of unsteady three-dimensional hydromagnetic flow of a Casson fluid with Hall and radiation effects, Results in Physics, Vol. 11, 966-974 (2018)]

existence of many significant parameters. Makinde and Aziz [14] examined the boundary layer flow of viscous nanofluid flowing a linear stretching sheet having convective boundary conditions.

The flow of an electrically conducting fluid under the influence of a magnetic field is encountered in many engineering devices, such as in MHD propulsion system driven submarines, geothermal heat source pumps, and MHD generators. The application of a magnetic field produces a resistive force in the flow field which acts as a stabilizing agent to the flow and delays the boundary layer separation. In heat transfer processes, the desired properties of the final product can be obtained by controlling the rate of cooling. In order to control the cooling rate, the flow field is subjected to an externally applied magnetic field. Therefore, the study of magnetohydrodynamic (MHD) fluid flow has attracted numerous researchers because of its vast applications in multiple areas such as in power generation, MHD submarines, solar flares etc. Pavlov [19] was the first who investigated the hydromagnetic fluid flow towards a stretching surface. Takhar et al. [127] studied the boundary layer flow and heat transfer over a rotating stretching sheet considering the effect of an externally applied magnetic field. Al-Mudhaf and Chamkha [128] discussed the thermosolutal Marangoni convection in steady laminar boundary layer flow along a vertical permeable surface in the presence of a magnetic field, chemical reaction and heat generation/absorbption. Magyari and Chamkha [129] studied the thermosolutal Marangoni boundary layer flow under the influence of an external magnetic field. The exact solution of MHD boundary layer flow is obtained by Kumaran et al. [20]. They examined the hydromagnetic flow over a quadratically stretching sheet. Rashidi et al. [130] presented the second law of thermodynamics analysis of the boundary layer nanofluid flow over a rotating porous disk in the presence of a magnetic field. The influence of a variable magnetic field on the forced convection heat transfer in a ferrofluid filled semi-annulus lid was investigated by Sheikholeslami et al. [131]. Contributions on the topic of magnetohydrodynamic flow of a viscous and electrically conducting fluid under different conditions are also due to Chamkha and Khaled [132], Khedr et al. [133], and Chamkha et al. [134].

The investigations mentioned above are all associated with steady-state models describing the fluid flow. However, to investigate the flow properties of more realistic problems, it becomes essential to examine the models which are time-dependent. Wang [46] made the first attempt to analyze the unsteady-state problem. By using a particular type of similarity transformation, he transformed the governing partial differential equations into ordinary differential equations in similar form. Takhar et al. [135] considered the induced magnetic field effects on the unsteady boundary layer MHD flow of a viscous incompressible and electrically conducting fluid over an impulsively started semi-infinite plate. The effect of the magnetic Prandtl number was found to be prominent on the

fluid velocity along the length of the flat plate. Takhar et al. [136] also investigated the transient mixed convective flow of a viscous incompressible and electrically conducting fluid over a rotating cone in the presence of a magnetic field. Elbashbeshy and Bazid [47] analyzed the impact of heat transfer on hydromagnetic liquid flow towards a time-dependent stretching surface. They inferred that, as the unsteadiness parameter increases, both the momentum and thermal boundary layer thicknesses decrease. The heat transfer properties of the unsteady boundary layer flow problem over a vertical stretching surface was analyzed by Ishak et al. [48]. The unsteady laminar flow of an electrically conducting fluid in the presence of a magnetic field and heat generation absorption effects considering different aspects and geometry were investigated by Chamkha and Al-Mudhaf [137], and Chamkha and Ahmed [138].

The effect of radiative heat transfer on the flow of a viscous incompressible fluid appears due to the presence of temperature differences between the surrounding and the ambient fluid. Radiative heat transfer also affects the penultimate product that is to be produced. Several authors have considered the influence of radiative heat transfer effects on the boundary layer flow of a Newtonian fluid under different conditions. Chamkha [139] studied the magnetohydrodynamic natural convective heat and mass transfer boundary layer flow of a truncated cone in the presence of radiative heat transfer. Aziz [49] obtained the similarity solutions for the boundary layer problem in the presence of a radiative heat transfer. Rashidi et al. [140] presented the Homotopy analysis based solutions to the boundary layer flow of a micropolar fluid in a porous medium considering the effects of radiative heat transfer. The combined effects of Hall current and radiative heat transfer for the time-dependent hydromagnetic fluid flow along a porous surface was analyzed by Pal [50]. Chamkha et al. [141] considered the thermal radiation effects on the chemically reactive MHD natural convection flow from a heated vertical plate including the Joule dissipations. Seth et al. [142] investigated the radiative heat transfer influence on the natural convective MHD fluid flow past an accelerated moving vertical plate. They also included the effect of ramped wall temperature and porous medium in their study. The heat transfer characteristics in the boundary layer flow of a water-based nanofluid over a stretching sheet under the influence of an external magnetic field and radiative heat transfer were considered by Rashidi et al. [143]. In this paper, the authors used the volume fraction model to incorporate the presence of nanoparticle in the flow field. Seth et al. [144] also studied the thermal radiation influence on the two-dimensional hydromagnetic boundary layer flow along an exponentially stretching sheet including the effects of viscous and Joule dissipations. Bhatti and Rashidi [145] presented a numerical analysis of the similarity solution of the combined effects of thermo-diffusion and thermal radiation on the Williamson nanofluid over a porous stretching surface. Seth and Mishra [146] analyzed the unsteady boundary layer flow of a nanofluid along a

nonlinearly stretching sheet with Navier's slip and radiative heat transfer using Galerkin finite element technique.

It is well known that the flow field, in case of an electrically conducting fluid flow under the influence of a magnetic field, experiences the induction of a secondary flow due to the Hall effect which arise as a result of a strong magnetic field or if the density of the fluid is low. The Hall effect has several implications in determining the flow features within the flow field. As a result of this, several authors have theoretically examined the effects of Hall current on the magnetohydrodynamic flow of a viscous, incompressible, and electrically conducting fluid. Gupta [30] examined the influence of Hall current for the hydromagnetic liquid along a permeable surface. Chamkha [34] studied the influence of Hall current on the hydromagnetic natural convective flow of viscous and electrically conducting fluid flow in a stratified porous medium. Takhar et al. [147] presented the non-similar solutions for the boundary layer flow of an electrically conducting fluid over a moving surface in the presence of a magnetic field and the effects of Hall current. Hayat et al. [31] investigated the influence of heat transfer and Hall current in a rotating second-grade fluid flow toward a permeable surface. The combined influence of Hall current and mass diffusion on laminar flow of a hydromagnetic heat generating/absorbing fluid was studied by Saleem and Aziz [32]. Seth et al. [148, 149] presented the exact results of the unsteady hydromagnetic natural convective heat and mass transfer flow in a porous medium considering the effects of Hall current, heat absorption, and thermal radiation. In these studies, authors also included the influence of the Coriolis force. It was found in [149] that the rate of heat transfer increased with increasing heat absorption and thermal radiation whereas the Hall current reduced the primary shear stress and increased the shear stress in the secondary direction. The effects of Hall current and heat absorption on a natural convection flow induced due to an accelerated plate in the presence of chemical reaction was studied by Hussain et al. [150].

As a single model cannot describe all the properties of fluids, therefore it becomes essential to study the flow problems over stretching surfaces through various combinations. In literature, the phenomena of non-Newtonian fluids take much attention due to its vast range of applications. In 1995, Casson introduced a fluid flow model associated with the flow of non-Newtonian liquids. Amongst all non-Newtonian liquid models, the Casson liquid model is one of the most important models which reveals the properties of yield stresses. A Casson liquid model is based on the interaction of solid and liquid phases. When the yield stresses are more significant than shear stresses, the Casson fluid acts like a solid. On the other hand, when yield stresses are less than the shear stresses, it starts moving. Chilly sauce, honey, jelly, condensed milk, blood are some of the examples of Casson liquid. The Casson fluid flow model also derives its application

in cancer therapy. Eldabe and Salwa [56] first studied the Casson fluid flow between two co-axial cylinders. It took many years to take full advantage of this phenomena. Shehzad et al.[57] examined the heat and mass transfer in hydromagnetic Non-Newtonian liquid flow by considering the chemical reaction and suction effects. Tufail et al. [58] analyzed the heat source/sink impacts on magnetohydrodynamic fluid flow and heat transfer towards a porous stretching surface. The partial velocity-slip effects in MHD Casson liquid flow along a stretching surface is investigated by Nandy [59]. He obtained the solutions which are analytic about the stagnation point. Mukhopadhyay [60] studied the heat transfer phenomenon in MHD Casson liquid flow along a stretching sheet. The flow and heat transfer of a Casson liquid due to an exponentially stretching permeable surface is studied by Vajravelu et al.[61]. Mukhopadhyay and Vajravelu [62] examined the unsteady-state problem for Casson liquid toward a porous surface. The theoretical investigation of entropy generation in the steady laminar flow of a Casson nanofluid including the effects of velocity-slip and convective boundary conditions was performed by Abolbashari et al. [151]. It was found that the entropy generation increases with a decrease in Casson parameter. Ashraf et al. [65] investigated the mixed convection flow of a Casson liquid in the presence of Hall effect along a stretching surface. Butt et al. [63] examined the three-dimensional problem of Casson fluid flow along an unsteady stretching surface. Khan et al. [64] investigated the homogeneous-heterogeneous reactions for Casson liquid flow. The effects of viscous and Ohmic dissipations on the unsteady MHD flow of a Casson fluid over a horizontal stretching sheet in a non-Darcy porous medium was considered by Seth et al. [152]. The Casson parameter was found to enhance the free surface velocity.

The combined effects of Hall current and radiative heat transfer on the time-dependent three-dimensional hydromagnetic Casson liquid flow over a stretching surface is not investigated by any researcher. Therefore, through this study, we aim to analyze the unsteady three-dimensional hydromagnetic Casson fluid flow along a stretching surface assuming the effect of Hall current and radiative heat transfer. The fluid flow model framed in the form of a set of coupled partial differential equations which are highly nonlinear and time-dependent. Similarity transformations are utilized to obtain a set of nonlinear coupled ordinary differential equations in similarity form. Further, a numerical approach namely spectral quasi-linearization method (SQLM) is applied to solve the similar form of governing highly nonlinear ordinary differential equations. A detailed parametric analysis is carried out to examine the influences of several significant parameters such as Casson liquid parameter, Hall current parameter, magnetic parameter, unsteadiness parameter, radiation parameter on the profiles' of the velocity field and temperature field. The behavior of emerging quantities of engineering interest such as

skin friction coefficient and the Nusselt number is also discussed. The fluid flow problem presented in the paper finds applications in silicon suspensions, blood flow, polymer engineering, and printing industry.

2.2 Mathematical Formulation

We consider the unsteady three-dimensional flow of a Casson fluid along a linearly stretching surface in the presence of radiative heat transfer and an external magnetic field. In Fig. 2.1, We assume the surface to be along the plane $y = 0$ and the liquid to be confined in the region $y \geq 0$. The surface of the sheet is stretched in x - direction only with a time-dependent velocity $u = u_w(x, t)$. The fluid is viscous and electrically conducting and the externally applied time-dependent magnetic field $B(t)$ is acting along y - direction, which is normal to the surface of the sheet. The intensity of the applied magnetic is strong enough to produce an effective Hall current in the flow-field. The magnetic Reynolds number of the fluid is small so that the induced magnetic fields are negligible in comparison to the applied one.

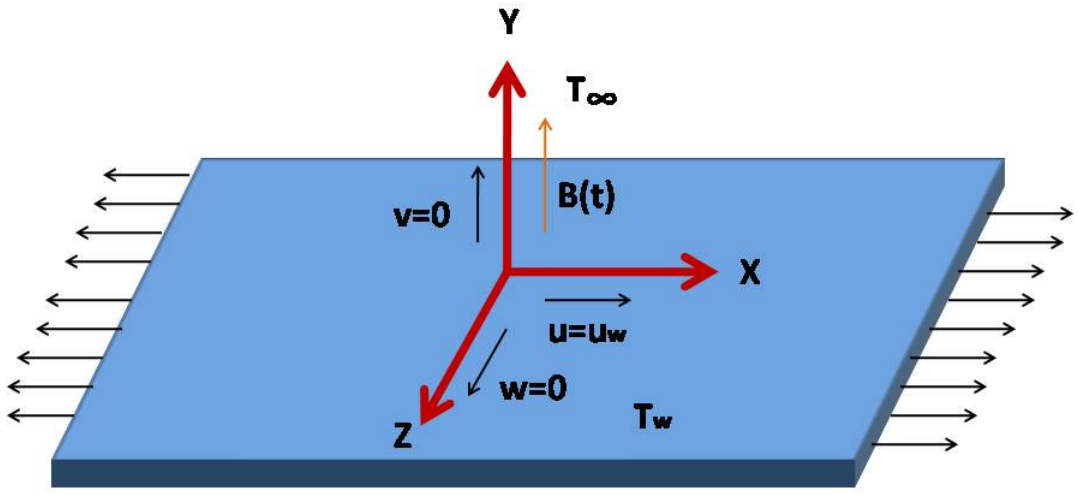

FIGURE 2.1: Model of the problem

Following the above assumptions, the equations governing the conservation of mass, momentum, and energy transfer, are written as

$$\frac{\partial u}{\partial x}+\frac{\partial v}{\partial y}+\frac{\partial w}{\partial z}=0, \tag{2.1}$$

$$\frac{\partial u}{\partial t}+u\frac{\partial u}{\partial x}+v\frac{\partial u}{\partial y}+w\frac{\partial u}{\partial z}=\nu\Big(1+\frac{1}{\beta}\Big)\frac{\partial^2 u}{\partial y^2}-\frac{\sigma B^2(t)}{\rho(1+m^2)}(u+mw), \tag{2.2}$$

$$\frac{\partial w}{\partial t}+u\frac{\partial w}{\partial x}+v\frac{\partial w}{\partial y}+w\frac{\partial w}{\partial z}=\nu\Big(1+\frac{1}{\beta}\Big)\frac{\partial^2 w}{\partial y^2}+\frac{\sigma B^2(t)}{\rho(1+m^2)}(mu-w), \tag{2.3}$$

$$\frac{\partial T}{\partial t}+u\frac{\partial T}{\partial x}+v\frac{\partial T}{\partial y}+w\frac{\partial T}{\partial z}=\alpha_m\frac{\partial^2 T}{\partial y^2}-\frac{1}{\rho c_p}\frac{\partial q_r}{\partial y}, \tag{2.4}$$

where components of velocity in x , y , and z directions are represented as u, v, and w, respectively, t is taken as time, β is the Casson liquid parameter, σ is electrical conductivity, ρ is density of the liquid, ν is the liquid's kinematic viscosity, m is Hall current parameter, T is the temperature within the boundary layer, $\alpha_m=\frac{k}{\rho c_p}$ represents the liquid's thermal diffusivity. Here, k denotes the thermal conductivity of the fluid, and c_p be the specific heat capacity of the fluid at constant pressure. The radiative heat flux is denoted by q_r.

For applying Rosseland approximation, the media should be optically dense media in which radiation can travel only for a short distance before scattering. Some literature on Rosseland approximation for Casson fluid can be seen through ([153],[154], [155],[156], [157]). Since in the present study, we are assuming the fluid to be an optically thick Casson fluid which emits/absorbs radiation and does not allow it to scatter, the radiative heat flux vector is computed using the Rosseland Approximation and is defined as

$$q_r=-\frac{4\sigma^*}{3\alpha^*}\frac{\partial T^4}{\partial y}, \tag{2.5}$$

where σ^* is Stefan-Boltzmann constant and α^* be the coefficient of Rosseland mean absorption. Following Pantokratoras and Fang [158] and Cortell [159], the value of q_r is further simplified as

$$q_r=-\frac{16\sigma^*}{3\alpha^*}T^3\frac{\partial T}{\partial y}. \tag{2.6}$$

The energy equation (2.4), on using (2.6), reduce to

$$\frac{\partial T}{\partial t}+u\frac{\partial T}{\partial x}+v\frac{\partial T}{\partial y}+w\frac{\partial T}{\partial z}=\frac{\partial}{\partial y}\Big(\Big(\alpha_m+\frac{16\sigma^*T^3}{3\alpha^*\rho c_p}\Big)\frac{\partial T}{\partial y}\Big). \tag{2.7}$$

The associated boundary conditions for the flow problem are

$$\text{At } y = 0: \ u = u_w, \ v = 0, \ w = 0, \ T = T_w; \tag{2.8}$$

$$\text{As } y \to \infty: \ u \to 0, \ w \to 0, \ T \to T_\infty; \tag{2.9}$$

where u_w is the stretching velocity of the sheet in x - direction. It is assumed that the wall stretching velocity $u_w(x,t) = \frac{ax}{1-\gamma t}$, and the time-dependent magnetic field $B(t) = B_0(1-\gamma t)^{-1/2}$, where a and γ are constants. We now define the following set of transformations ([160],[161]) to transform the governing equations into similarity form

$$u = \frac{ax}{(1-\gamma t)} f'(\eta), \ v = -\sqrt{\frac{a\nu}{(1-\gamma t)}} f(\eta), \ w = \frac{ax}{(1-\gamma t)} g(\eta), \tag{2.10}$$

$$\theta(\eta) = \frac{T - T_\infty}{T_w - T_\infty}; \ \eta = y\sqrt{\frac{a}{\nu(1-\gamma t)}}, \tag{2.11}$$

where η is the similarity variable. On using the transformations defined in (2.10) and (2.11), the conservation of mass equation (2.1) is satisfied automatically, and the Eqs. (2.2), (2.3), and (2.7), respectively, yield us

$$\Big(1 + \frac{1}{\beta}\Big) f''' + ff'' - (f')^2 - A(f' + \frac{\eta}{2} f'') - \frac{M}{(1+m^2)}(f' + mg) = 0, \tag{2.12}$$

$$\Big(1 + \frac{1}{\beta}\Big) g'' - gf' + fg' - A(g + \frac{\eta}{2} g') + \frac{M}{(1+m^2)}(mf' - g) = 0, \tag{2.13}$$

$$\Big(1 + \frac{4}{3N_r}(1 + (tr-1)\theta)^3\Big)\theta'' - PrA\frac{\eta}{2}\theta' + Prf\theta' + \frac{4}{N_r}(tr-1)(1 + (tr-1)\theta)^2\theta'^2 = 0. \tag{2.14}$$

Here a prime ($'$) denotes derivative with respect to η. The non-dimensional parameters used in Eqs. (2.12)-(2.16) are defined as

$$A = \frac{\gamma}{a}, \ M = \frac{\sigma B_0^2}{\rho a}, \ N_r = \frac{k\alpha^*}{4\sigma^* T_\infty^3}, \ Pr = \frac{\nu}{\alpha_m}, \ tr = \frac{T_w}{T_\infty},$$

where $A, M, N_r, Pr, \ tr$ are, respectively, the unsteadiness parameter, magnetic strength parameter, radiation parameter, Prandtl number, and the temperature ratio parameter. One must note that the radiation parameter N_r is inversely proportional to the thermal radiation effect and thus the case $N_r \to \infty$ indicates the fluid flow without radiative heat transfer.

The boundary conditions (2.8) and (2.9), on using the transformations (2.10) and (2.11), reduce to

$$\text{At } \eta = 0: \ f' = 1, \ f = 0, \ g = 0, \ \theta = 1; \tag{2.15}$$

$$\text{As } \eta \to \infty: \ f' \to 0, \ g \to 0, \ \theta \to 0. \tag{2.16}$$

Apart from the velocity and temperature fields, the important physical quantities of engineering interest are the friction coefficients along x and z directions, and the local Nusselt number. These are denoted in the text as C_{fx}, C_{fz}, and Nu_x, respectively, and are defined as

$$C_{fx} = \frac{\tau_{wx}}{\rho u_w^2}, \quad C_{fz} = \frac{\tau_{wz}}{\rho u_w^2}, \quad Nu_x = \frac{x q_w}{k(T_w - T_\infty)}, \tag{2.17}$$

where the shear-stress components τ_{wx}, τ_{wz}, and the rate of heat transfer at the surface q_w, are defined as

$$\tau_{wx} = \mu\Big(1 + \frac{1}{\beta}\Big)\Big(\frac{\partial u}{\partial y}\Big)_{y=0}, \quad \tau_{wz} = \mu\Big(1 + \frac{1}{\beta}\Big)\Big(\frac{\partial w}{\partial y}\Big)_{y=0}, \quad q_w = \Big(-k\Big(\frac{\partial T}{\partial y}\Big) + q_r\Big)_{y=0}. \tag{2.18}$$

Therefore, the values of C_{fx}, C_{fz}, and Nu_x, respectively, are given by

$$C_{fx} Re_x^{1/2} = \Big(1 + \frac{1}{\beta}\Big) f''(0), \; C_{fz} Re_x^{1/2} = \Big(1 + \frac{1}{\beta}\Big) g'(0); \tag{2.19}$$

$$Re_x^{-1/2} Nu_x = -\Big[1 + \frac{4}{3N_r}(1 + (tr - 1)\theta(0))^3\Big]\theta'(0), \tag{2.20}$$

where q_r is the radiative heat flux and $Re_x = \frac{x u_w}{\nu}$ is the local Reynolds number.

2.3 Numerical Solution

The mathematical model of the physical problem, described by the nonlinear ordinary differential equations (2.12)-(2.14) and boundary conditions prescribed in equations (2.15) and (2.16), is numerically solved using spectral quasi-linearization method (SQLM). The method utilizes a one-term Taylor series approximation to linearize the nonlinear equations (2.12)-(2.14). The iteration scheme then follows from the linearized equations as

$$a_{11}^{(3)} f'''_{r+1} + a_{11}^{(2)} f''_{r+1} + a_{11}^{(1)} f'_{r+1} + a_{11}^{(0)} f_{r+1} + a_{12}^{(0)} g_{r+1} = R_1 \tag{2.21}$$

$$a_{22}^{(2)} g''_{r+1} + a_{22}^{(1)} g'_{r+1} + a_{22}^{(0)} g_{r+1} + a_{21}^{(1)} f'_{r+1} + a_{21}^{(0)} f_{r+1} = R_2 \tag{2.22}$$

$$a_{33}^{(2)} \theta''_{r+1} + a_{33}^{(1)} \theta'_{r+1} + a_{33}^{(0)} \theta_{r+1} + a_{31}^{(0)} f_{r+1} = R_3 \tag{2.23}$$

where

$$a_{11}^{(3)} = (1+\frac{1}{\beta});\ a_{11}^{(2)} = f_r - A\frac{\eta}{2};\ a_{11}^{(1)} = -2f_r' - A - \frac{M}{1+m^2};\ a_{11}^{(0)} = f_r'';\ a_{12}^{(0)} = -\frac{Mm}{1+m^2};$$
$$R_1 = f_r f_r'' - (f_r')^2;\ a_{22}^{(2)} = (1+\frac{1}{\beta});\ a_{22}^{(1)} = f_r - A\frac{\eta}{2};\ a_{22}^{(0)} = -f_r' - A - \frac{M}{1+m^2};$$
$$a_{21}^{(1)} = -g_r + \frac{Mm}{1+m^2};\ a_{21}^{(0)} = g_r';\ R_2 = -g_r f_r' + g_r' f_r;\ a_{33}^{(2)} = \frac{4}{3N_r}(1+(tr-1)\theta_r)^3 + 1;$$
$$a_{33}^{(1)} = -APr\frac{\eta}{2} + Prf_r + \frac{8(tr-1)}{N_r}(1+(tr-1)\theta_r)^2\theta_r';$$
$$a_{33}^{(0)} = \frac{4(tr-1)}{N_r}(1+(tr-1)\theta_r)^2\theta_r'' + \frac{8(tr-1)^2}{N_r}(1+(tr-1)\theta_r)(\theta_r')^2;$$
$$R_3 = \frac{N_r Prf_r\theta_r' + 4(tr-1)(1+(tr-1)\theta_r)(\theta_r(1+(tr-1)\theta_r)\theta_r'' + (3(tr-1)\theta_r+1)(\theta_r')^2)}{N_r}.$$

The boundary conditions for the above iteration scheme are obtained as

$$\text{At } \eta = 0: \ f_{r+1}' = 1; f_{r+1} = 0;\ g_{r+1} = 0;\ \theta_{r+1} = 1 \tag{2.24}$$
$$\text{As } \eta \to \infty: \ f_{r+1}' \to 0;\ g_{r+1} \to 0;\ \theta_{r+1} \to 0. \tag{2.25}$$

The initial approximations, required to start the iterative scheme, are chosen to be convenient functions that satisfy the boundary conditions as

$$f_0 = 1 - e^{-\eta};\ g_0 = 0;\ \theta_0 = e^{-\eta}.$$

The linearized Eqs. (2.21)-(2.23) are then treated with the well-known Chebyshev pseudo-spectral collocation method. The computational domain $[0,\ \infty)$ is transformed to $[-1,\ 1]$ by using the transformation $\eta = L(\xi+1)/2$. This transformation is required to utilize the so-called Gauss-Lobatto points to discretize the computational domain. The main idea is to introduce a differentiation matrix, known as Chebyshev differentiation matrix, to approximate the derivatives of the unknown functions at the grid points. At the end of the process, one arrives at the matrix equation given as

$$\begin{pmatrix} A_{11} & A_{12} & A_{13} \\ A_{21} & A_{22} & A_{23} \\ A_{31} & A_{32} & A_{33} \end{pmatrix} \begin{pmatrix} f_{r+1} \\ g_{r+1} \\ \theta_{r+1} \end{pmatrix} = \begin{pmatrix} R_1 \\ R_2 \\ R_3 \end{pmatrix}$$

where each A_{ij} is of order $(N+1)\times(N+1)$. $f_{r+1}, g_{r+1}, \theta_{r+1}, R_1, R_2$, and R_3, are each of order $(N+1)\times 1$.

2.4 Residual Analysis

Equations (2.12)-(2.14) are highly nonlinear and couple ordinary differential equations. Hence, to trust the approximate solution of the boundary value problem consisting of these equations and the boundary conditions (2.15)-(2.16), it becomes necessary to perform a validation of the results. The approximate results are validated using a residual analysis of Eqs. (2.12)-(2.14), taking 150 collocation points, and the residuals of $f(\eta)$, $g(\eta)$, and θ are presented in Fig. 2.2.

It is evident from the residuals obtained for these quantities that the corresponding residuals go down to become less than 10^{-5} in mere 10 iterations which validates the results produced by the spectral quasilinearization mthod (SQLM). It must be noted that the spectral quasilinearization method or in general the spectral methods are closely related with finite element methods. The spectral methods differ with the later in the sense that it uses basis functions that are non-zero in the whole domain, and has the so-called exponential order of convergence as a result of which less computational time is needed by the system to produce entirely accurate and usable results. This is also evident from the present residual analysis where only 10 iterations and 150 collocation points are sufficient to guarantee a sufficiently small residual. However, these methods produce not-so-good results for complex geometry problems and discontinuous coefficients.

2.5 Results and Discussion

A numerical study of the unsteady hydromagnetic three-dimensional nonlinear radiative flow of a Casson fluid along a stretching surface including the effect of Hall current is investigated. The fluid flow model is represented by a set of time and space dependent coupled partial differential equations which are highly nonlinear. Similarity transformations are utilized to obtain a set of similar ordinary differential equations from these equations which were then treated with a numerical approach namely spectral quasilinearization method (SQLM) to solve the differential equations. The numerical results showing the impact of pertinent flow parameters, such as the Casson liquid parameter β, magnetic strength parameter M, and Hall current parameter m on the velocity and temperature field are depicted in Figs. 2.3-2.5 while the effects of radiation parameter N_r, Prandtl number Pr, and the temperature ratio parameter tr on the temperature profiles is depicted in Figs. 2.7-2.9. To investigate the implications of non-dimensional parameters on the skin-friction coefficients and local Nusselt number, the numerical values of C_{fx} and C_{fz}, and Nu_x for different values of the parameters are presented in Table 2.1. For computational purpose the default parameter values are taken as

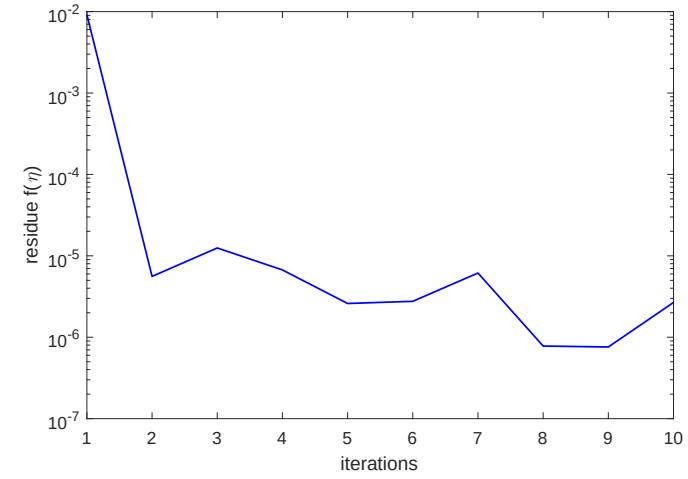

(a)

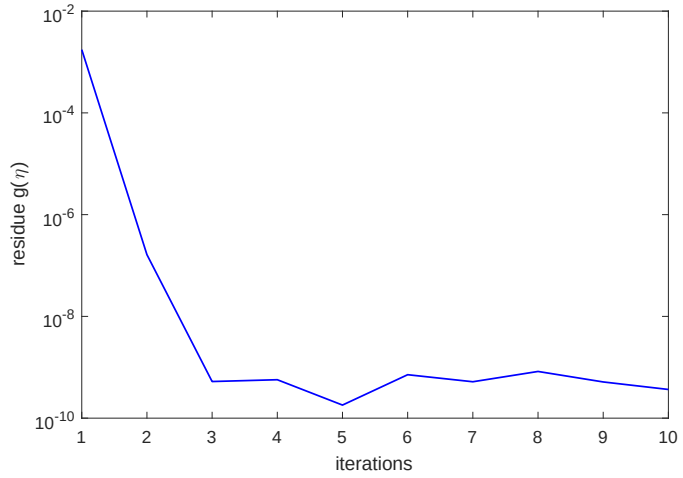

(b)

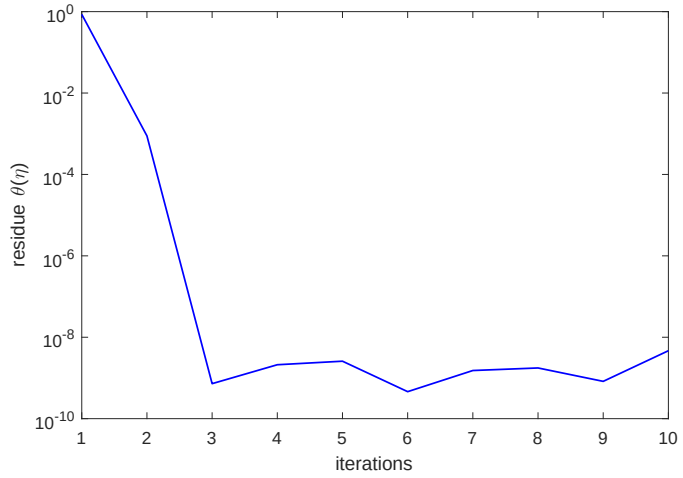

(c)

FIGURE 2.2: Residuals of (a) $f(\eta)$, (b) $g(\eta)$, and (c) $\theta(\eta)$

$A = 0.1,\ M = 6, m = 0.1,\ \beta = 0.3,\ N_r = 2,\ Pr = 10,\ tr = 1$. Since, we know that the Casson parameter $\beta \to \infty$ indicates the case of Newtonian fluid and the remaining values of β indicates the case of Casson fluid. Also, if $\beta = 0$ then the term $\left(1 + \frac{1}{\beta}\right) \to \infty$ and the momentum equations gives divergent results. Therefore, $\beta > 0$ values are enough to analyze the physical behavior of a Casson fluid. Also, the Prandtl number gives the ratio of heat that is transferred by fluid momentum to the heat that can be transferred by thermal diffusion. Since, we are considering $Pr > 1$, i.e heat transfer is more favorable to occur by fluid momentum rather than by the fluid conduction. Also, the investigation deals with the flow of a Casson liquid, and for liquids, generally Pr=10. Moreover, the values of remaining emerging parameters such as $M,\ m,\ A,\ N_r$ are indicating towards the scale of presence of that respective effect in the flow field.

The influence of Casson parameter β and magnetic parameter M on the profiles of fluid velocity in x and z-directions, and on the profiles of temperature are shown graphically in Figs. 2.3 and 2.4, respectively. It is evident from these figures that on increasing the values of both Casson parameter β and magnetic field parameter M the fluid flow in x-direction $f'(\eta)$ decreases within the boundary layer region. The Casson parameter β measures the yield stress and when it becomes large, the fluid behaves as a Newtonian fluid. The increase in the yield stress causes a stabilization effect. The effect of the applied magnetic field is to introduce a resistive force within the flow-field, and it is, for this reason, the fluid velocity $f'(\eta)$ in x-direction gets decelerated with an increase in the magnetic parameter M. From both the figures it is analyzed that, inside the boundary layer region near the stretching surface, the profile of secondary velocity $g(\eta)$ firstly get accelerated and then change its behaviour by getting decelerated on increasing the values of β and M. As we are assuming that there is no fluid flow in z direction at the sheet i.e. g(0)=0. Therefore the secondary velocity curve $g(\eta)$ starts from 0 and then gets increasing near to the stretching surface due to the existence of the Hall current which actuates a cross flow i.e. a flow in z direction which causes the flow to be three dimensional in the boundary layer region. But after attaining a peak, as we go far from the stretching surface it starts decreasing to free stream. It happens because higher values of Casson parameter β increase the plastic dynamic viscosity which diminishes the yield stress and, as $\beta \to \infty$ fluid starts behaving as Newtonian fluid, and velocity of the fluid gets reduced. Also, for the case of higher values of magnetic parameter M offers stronger Lorentz force which opposes fluid motion and reduce the velocity of the fluid. Fluid temperature $\theta(\eta)$ increases with increasing both Casson parameter β and magnetic parameter M.

The utilization of the magnetic field B_0 on the flow of an electrically conducting fluid produces Hall current, and the influence of this current is depicted graphically in Fig. 2.5. The strength of Hall current is estimated using the Hall current parameter m,

whose impact on the velocity and temperature profiles is exhibited in this figure. The Hall current is found not to have a significant effect on the fluid velocity in x-direction $f'(\eta)$. However, one must note that there is a marginal increase in $f'(\eta)$ with increasing values of m. The fluid velocity in z-direction $g(\eta)$ increases significantly with an increase in Hall current. On the other hand, the fluid temperature $\theta(\eta)$ is found to behave as a decreasing function of the Hall current parameter m.

The effects of unsteadiness parameter A on the velocity profiles and fluid temperature can be seen in Fig. 2.6. It resembles from the figures presented in Fig. 2.6 that the unsteadiness parameter A has a marginal effect on the velocity profiles in x and z directions and fluid temperature, but this marginal impact is to reduce the thickness of momentum boundary layers. However, the thermal boundary layer thickens with increasing values of unsteadiness parameter A.

The influences of radiative parameter N_r, Prandtl number Pr, and the temperature ratio parameter tr on the fluid temperature within the boundary layer region are presented in Figs. 2.7, 2.8, and 2.9, respectively. It is important to notice that the impact of radiation is inversely proportional to the radiative parameter N_r, i.e. an increase in N_r correspond to a decrease in radiation and vice-versa. The radiative parameter N_r is found to be diminishing the fluid temperature within the boundary layer region (see Fig. 2.7) which is equivalent to say that the fluid temperature rises with an increase in thermal radiation. From Fig. 2.8 we observe that fluids with larger Prandtl number Pr has a comparatively lesser fluid temperature within the boundary layer region. Prandtl number Pr is the ratio of viscous diffusion to thermal diffusion which indicates that the higher viscous diffusion rate leads to a lesser fluid temperature while a greater thermal diffusion enhances the fluid temperature within the boundary layer region. The temperature ratio parameter tr estimates the ratio of fluid temperature at the surface to the fluid temperature beyond the boundary layer region, and it is observed from Fig. 2.9 that the fluid temperature is inversely affected by the temperature ratio parameter and gets decreased with increasing values of this parameter.

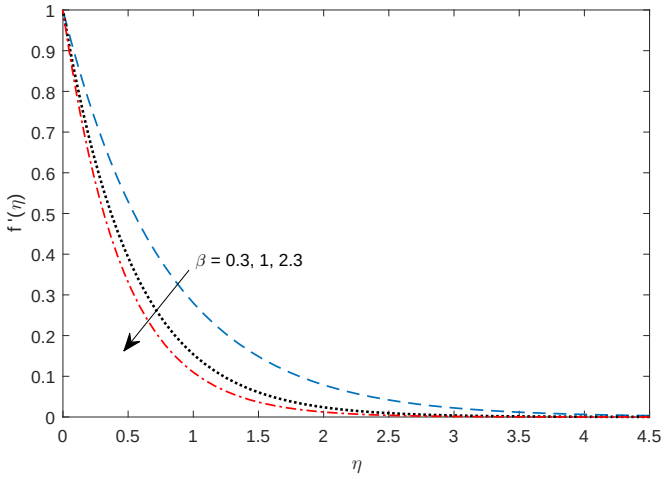

(a)

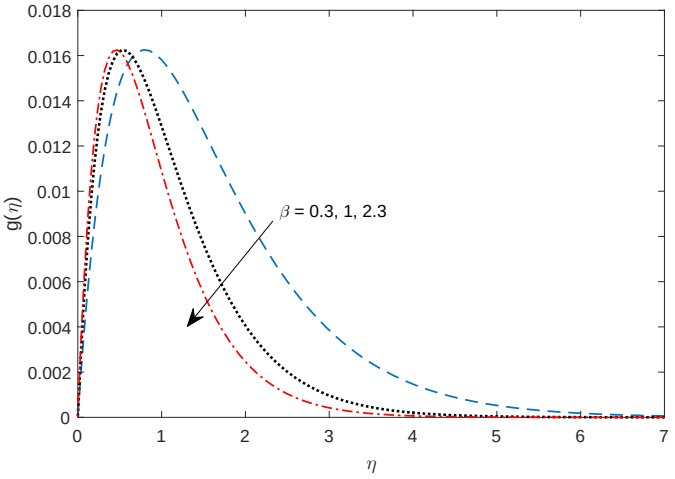

(b)

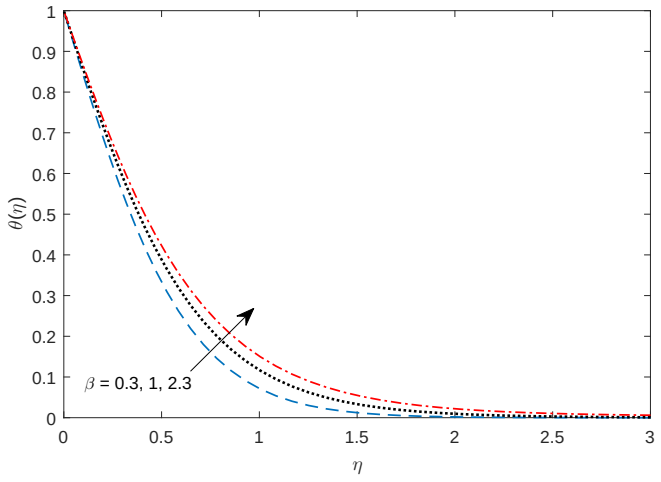

(c)

FIGURE 2.3: Effect of Casson parameter β on (a) f', (b) g, and (c) θ when $A = 0.1$, $M = 6, m = 0.1$, $N_r = 2$, $Pr = 10$, and $tr = 1$.

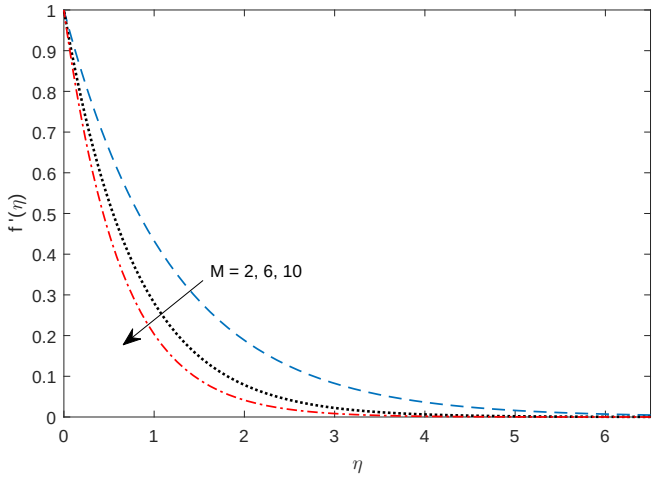

(a)

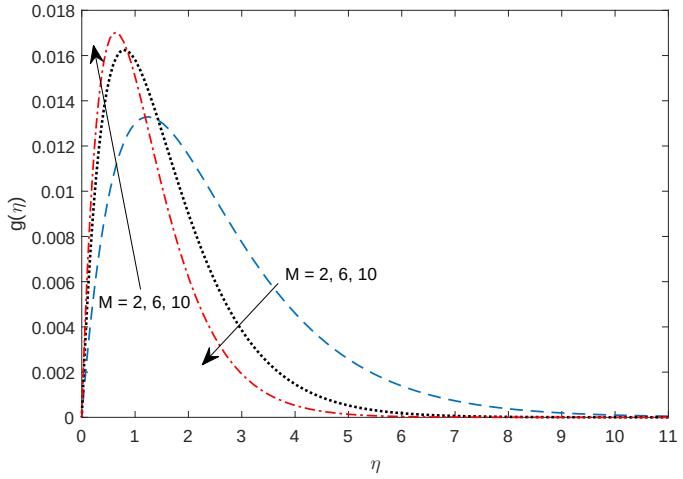

(b)

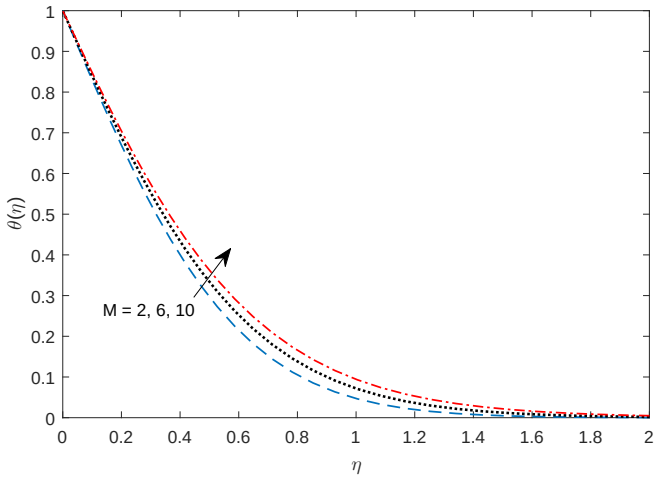

(c)

FIGURE 2.4: Effect of magnetic parameter M on (a) f', (b) g, and (c) θ when $A = 0.1,\ \beta = 0.3, m = 0.1,\ N_r = 2,\ Pr = 10$, and $tr = 1$.

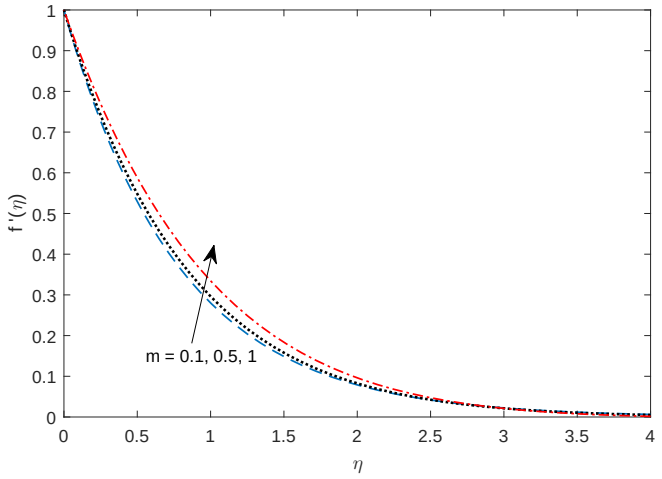

(a)

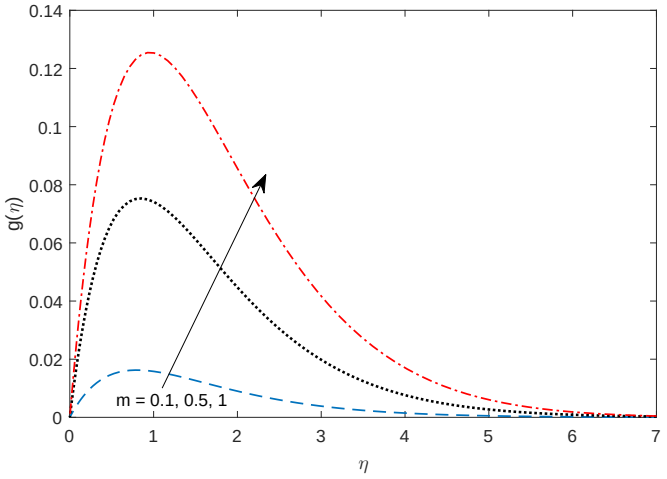

(b)

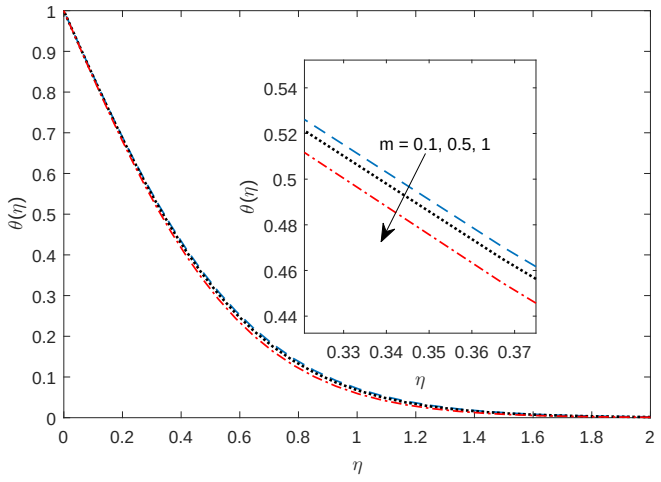

(c)

FIGURE 2.5: Effect of Hall current parameter m on (a) f', (b) g, and (c) θ when $A = 0.1,\ \beta = 0.3, M = 6,\ N_r = 2,\ Pr = 10$, and $tr = 1$.

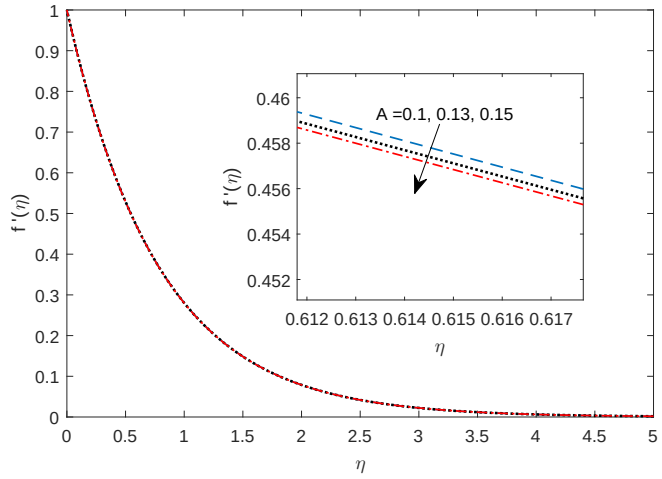

(a)

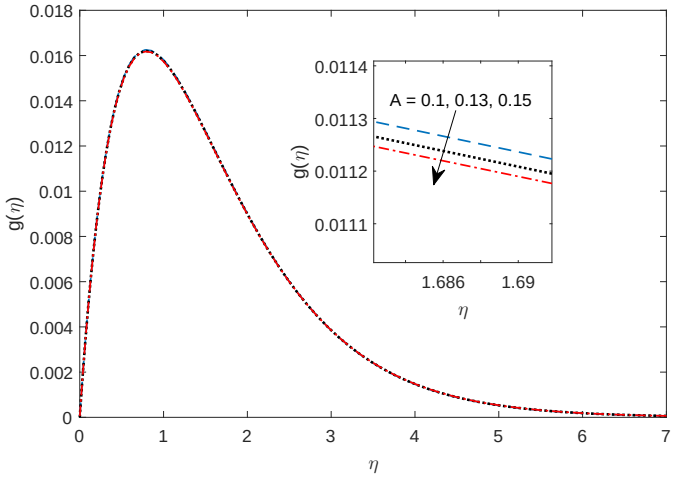

(b)

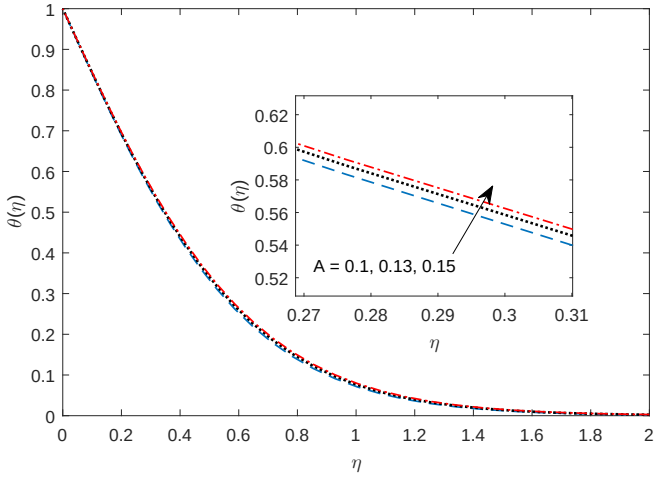

(c)

FIGURE 2.6: Effect of unsteadiness parameter A on (a) f', (b) g, and (c) θ when $m = 0.1,\ \beta = 0.3, M = 6,\ N_r = 2,\ Pr = 10$, and $tr = 1$.

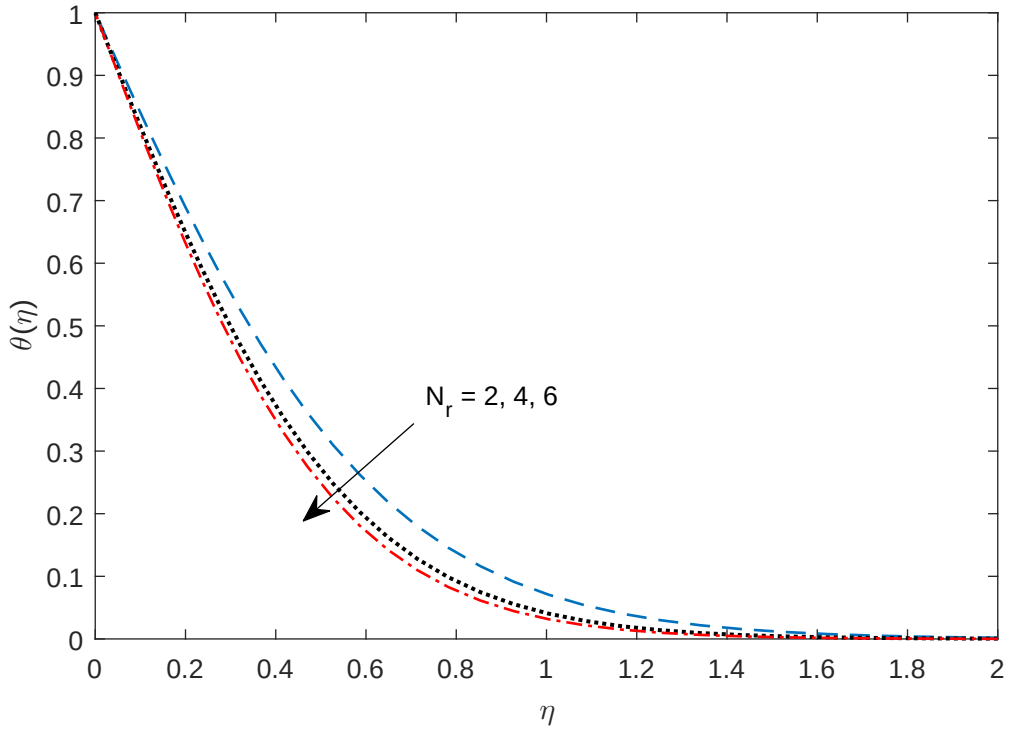

FIGURE 2.7: Effect of radiation parameter N_r on θ when $A = 0.1,\ \beta = 0.3, M = 6,\ m = 0.1,\ Pr = 10$, and $tr = 1$.

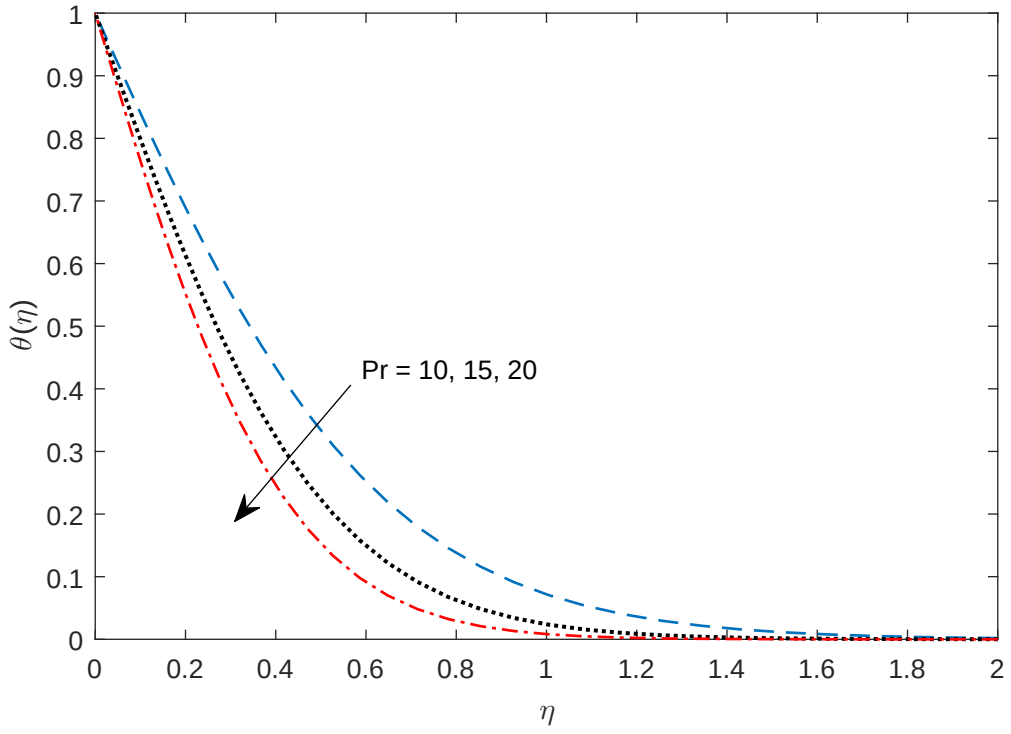

FIGURE 2.8: Effect of Prandtl number Pr on θ when $A = 0.1,\ \beta = 0.3, M = 6,\ m = 0.1,\ N_r = 2$, and $tr = 1$.

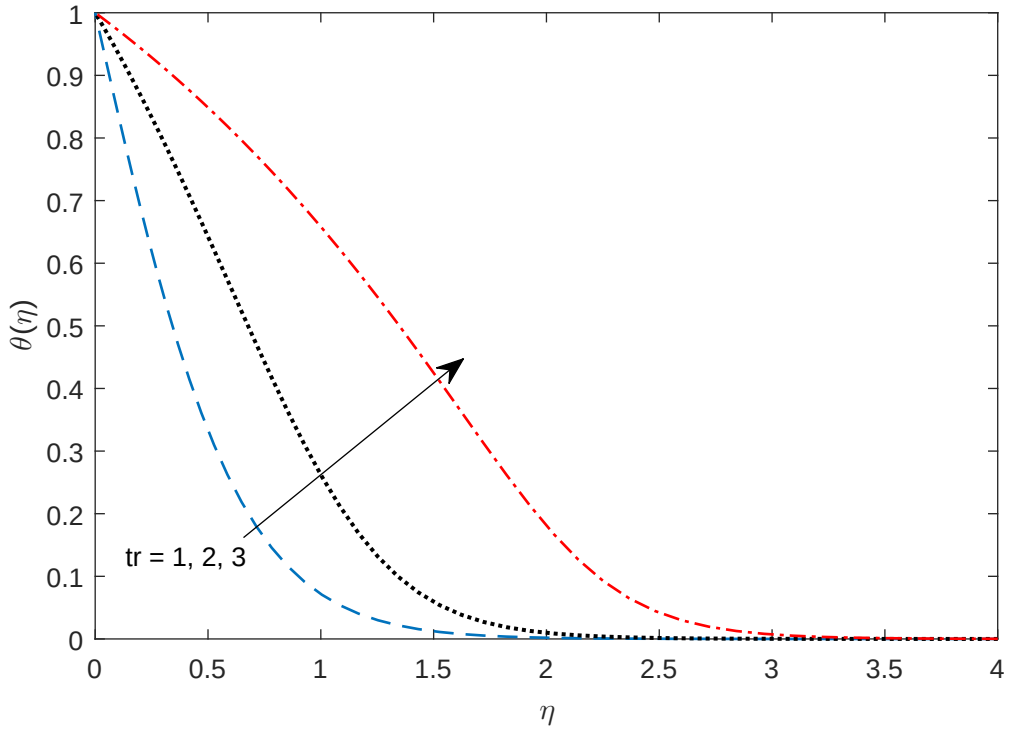

FIGURE 2.9: Effect of temperature ratio parameter tr on θ when $A = 0.1,\ \beta = 0.3, M = 6,\ m = 0.1,\ N_r = 2$, and $Pr = 10$.

The numerically computed values of coefficients of skin-friction C_{fx} and C_{fz}, and coefficient of heat transfer at the surface known as Nusselt number Nu_x, are tabulated in Table 2.1. It is noticed from Table 2.1 that the implication of the applied magnetic field (measured with a variation in M) is to increase the coefficients of skin-friction in x and z-directions, whereas the impact of Casson parameter β is to decrease the coefficients of skin-friction in both the directions. The skin-friction coefficient in x-direction decreases while the skin-friction in z-direction increases due to the presence of Hall effects into the flow-field. There is a marginal increase in C_{fx} and a marginal decrease in C_{fz} with increasing unsteadiness parameter A. It is also noted from Table 2.1 that the effect of Hall current m, Prandtl number Pr, and temperature ratio parameter tr is to increase the rate of heat transfer from the surface whereas the effects of magnetic field, unsteadiness in the flow-field, and Casson parameter is to reduce the rate of heat transfer at the surface. As the radiation parameter N_r is inversely proportional to the radiation effect, it is inferred that the rate of heat transfer is improved with an increase in radiative heat transfer.

TABLE 2.1: Influence of different parameters on skin-friction coefficients (C_{fx} and C_{fz}) and Nusselt number Nu_x.

M	m	A	N_r	tr	β	Pr	$-C_{fx}Re^{1/2}$	$C_{fz}Re^{1/2}$	$Re^{-1/2}Nu_x$
6	0.1	0.1	2	1	0.3	10	5.51874456	0.23905696	2.68073953.
2							3.63997437	0.12517671	2.85395341
8							6.24973648	0.27988605	2.61197510
	0.1						5.51874456	0.23905696	2.68073953.
	0.5						5.15310039	1.03810463	2.70970177
	1						4.47154368	1.50968576	2.76677553.
		0.1					5.51874456	0.23905696	2.68073953
		0.13					5.52749427	0.23866458	2.64303470
		0.15					5.53332180	0.23840377	2.61732067
			2				5.51874456	0.23905696	2.68073953
			4				5.51874456	0.23905696	2.44614512
			6				5.51874456	0.23905696	2.35862695
				1			5.51874456	0.23905696	2.68073953
				2			5.51874456	0.23905696	3.86324873
				3			5.51874456	0.23905696	5.08255834
					0.3		5.51874456	0.23905696	2.68073953
					1		3.74924863	0.16240722	2.43305224
					2.3		3.17557443	0.13755722	2.28286739
						10	5.51874456	0.23905696	2.68073953
						15	5.51874456	0.23905696	3.39809230
						20	5.51874456	0.23905696	4.00188854

2.6 Conclusions

The present research work modeled the unsteady three-dimensional hydromagnetic Casson fluid flow along a stretching sheet in the presence of Hall current and radiative heat transfer neglecting the influence of the induced magnetic field. The nonlinear partial differential equations governing the fluid flow were subjected to similarity transformations to obtain a set of similar ordinary differential equations and are then solved numerically. The essential findings of the study are summarized below.

1. The momentum boundary layer in x direction gets thinner with increasing magnetic field, yield stress, and unsteadiness in the flow-field. A resultant increase in

the shear-stress along x direction take place with increasing magnetic field and unsteadiness. However, with increasing yield stress the shear-stress along x direction is found to get decreased.

2. The fluid velocity in z direction increases near the surface of the sheet and then decreases away from the surface with the increasing yield stress and magnetic field, and as a result, the skin-friction z direction is increased with increasing magnetic field and reduced with increasing yield stress.

3. Hall current effect is to increase the velocity profiles and to reduce the fluid temperature within the boundary layer region. However, this effect of Hall current, on the fluid velocity in x-direction and fluid temperature, are not so prominent. Hall current decreases the skin-friction coefficient in x-direction whereas it increases the coefficient of skin-friction in z-direction and rate of heat transfer at the surface.

4. The thermal radiation has increasing effects on thermal boundary layer thickness and heat transfer at the surface.

Chapter 3

A Numerical Investigation of Hall and Radiation Effects on MHD Three-Dimensional Casson Fluid Flow in a Porous Medium

3.1 Introduction

Boundary layer flow of a viscous fluid finds applications in many engineering processes,such as in paper production, glass production, and steel production. In steel production, a better outcome in the manufacturing process is achieved by controlling the cooling rate of the liquid and the stretching rate of the sheet. The rapid stretching of the sheet may finally affect the penultimate quality of the product. As a result, the theoretical study of the flow of a viscous fluid over a stretching surface was investigated by several researchers such as ([2], [44], [45], [5]). It is well known that the implication of presence of a magnetic field in the flow of a viscous incompressible electrically conducting fluid results in the production of a resistive force in the flow field which acts as a stabilizing agent to the flow and delays the boundary layer separation. The boundary layer flow of a viscous and electrically conducting fluid in the presence of a magnetic field is encountered in several engineering devices, such as, in geothermal heat sources

Contents of this chapter has been published in Journal of Porous Media [Prashu, R. Nandkeolyar, Ali J. Chamkha, A numerical investigation of Hall and radiation effects on MHD three-dimensional Casson fluid flow in a porous medium, Journal of Porous Media, Vol. 24, 15-30 (2021)]

pump, MHD generator, MHD flow meter, and MHD propulsion system. In heat transfer processes, the desired properties of the final product can be obtained by controlling the rate of cooling. In order to control the cooling rate, the flow field is also subjected to an externally applied magnetic field. For these reasons, the magnetohydrodynamic flow of a viscous fluid was studied by several researchers. Nandkeolyar et. al [162, 163] investigated the homogeneous and heterogeneous reaction effects on the flow of a viscous nanofluid along the stretching sheet in the presence of an external magnetic field under different conditions. Another relevant studies regarding boundary layer flow of hydromagnetic fluid can be seen through ([19], [20], [130], [131])

When the strength of the externally applied magnetic field is strong and or the density of the electrically conducting working fluid is low, the effect of Hall current become significant which induces a flow in the secondary direction. Even though, the Hall effect phenomenon was discovered by Edwin Herbert Hall in 1879, it took several years for the researchers to feel the impetus towards the study of Hall current effects on hydromagnetic flows. Gupta [30] was perhaps the first to investigate the influence of Hall current on the magnetohydrodynamic fluid flow along a porous surface. Reddy and Bathaiah [164] discussed the problem involving the effects of Hall current on the steady flow of a viscous incompressible and electrically conducting fluid in the presence of a magnetic field. Saleem and Aziz [32] studied the combined influence of Hall current and mass diffusion on laminar flow of a hydromagnetic heat generating/absorbing fluid. Seth et. al [165] considered the effects of Hall current on the Hartmann flow of a viscous and incompressible fluid under the influence of an inclined magnetic field. Sarkar et al.[166] further investigated the effects of Hall current on the hydromagnetic rotating flow of an electrically conducting fluid within a parallel plate channel. The influence of Hall current on the hydromagnetic boundary layer flow of an electrically conducting fluid over a variable thickness stretching sheet was investigated by Prasad et. al [167]. It was observed by Prasad et. al [167] that the presence of Hall current has significant effect on the flow and heat transfer within the boundary layer region and the Hall current induces a cross flow in the flow-field. These investigations mostly deal with steady state aspect of the problem and assume the fluid properties to be independent of time. However, to study the flow characteristics of real-life problems, it is essential to investigate the models which are transient. Some significant literature regarding unsteady boundary layer fluid flow can be examined through ([46], [47], [48], [34], [31], [32], [150]).

The effect of radiative heat transfer on the flow of a viscous incompressible fluid appears due to the presence of temperature differences between the surrounding and the ambient fluid. Radiative heat transfer also affects the penultimate product that is to be produced. Several authors have considered the influence of radiative heat transfer effects on the boundary layer flow of a Newtonian fluid under different conditions. Aziz [49]

obtained the similarity solutions for the unsteady boundary layer flow in the presence of a radiative heat transfer. The combined effects of Hall current and radiative heat transfer for the time-dependent hydromagnetic fluid flow along a porous surface was analyzed by Pal [50]. Ram et. al ([168],[169]) and Singh et. al [170] have extensively studied the related problems on unsteady heat and mass transfer problems in MHD radiating/reacting fluids flow past a moving vertical porous plate in the presence of source/ sink. In this parametric study of boundary layer flow, they have considered an ordinary viscous fluid under the application of uniform transverse/cosinusoidally magnetic field. Seth et. al ([148],[149]) obtained the exact results of the Hall effects on the transient hydromagnetic natural convective heat and mass transfer flow in a porous medium including effects of heat absorption and thermal radiation. In these studies, authors also included the influence of the Coriolis force. It was found in the study of Seth et al. [149] that the rate of heat transfer is increased with increasing heat absorption and thermal radiation, whereas the Hall current reduced the primary shear stress and increased the shear stress in the secondary direction.

The study of the magnetohydrodynamic flow of a Newtonian fluid through a porous medium has attracted the attention of many researchers due to its applications in the optimization of solidification processes of metals and metal alloys. Rashad et al. [171] presented a numerical simulation to discuss the effect of thermal radiation, permeability of the medium, and chemical reaction on the flow of a viscous fluid in a square enclosure. The steady mixed convective boundary layer flow of a viscous nanofluid about a solid sphere with convective heating at the surface in the presence of thermal radiation and Darcy porous medium was investigated by EL-Kabeir et. al [172]. Nabwey et. al [173] presented Lie group analysis to study the implications of thermal radiation, chemical reaction and velocity slip on the unsteady heat and mass transfer in a laminar flow of a viscous and incompressible fluid along a horizontal stretching surface embedded in porous medium. Mallikarjuna et. al [174] investigated the effects of thermal radiation and transpiration on the flow and heat transfer in a non-Darcy convective flow of a viscous fluid flow adjacent to a rotating vertical cone. Joshi et al. ([175],[176]) have also carried numerical investigations about porosity effects of Magnetic Nanofluids over a moving/stationary stretchable disk. Some relevent contribution on the magnetohydrodynamic flow of a Newtonian fluid in a porous medium under different conditions are also due to Makinde et. al [177], Sekhar et. al [178], and Sheikholeslami and Abelman [179].

Unlike the Newtonian fluids, the rheological properties of non-Newtonian fluids cannot be described by a single model, and hence researchers have developed different models to study the flow behaviour of different types of non-Newtonian fluids. One such type of non-Newtonian fluid model is the Casson fluid model which is based on the yield stresses.

The Casson fluid model includes the interaction of solid and liquid phases. When the yield stresses are more significant than shear stresses, the Casson fluid acts like a solid. On the other hand, when yield stresses are less than the shear stresses, the fluid starts moving. Examples of liquids following the Casson fluid model in our day to day life are chilly sauce, honey, jelly, and condensed milk. Casson fluid model also finds applications in drug delivery during Cancer therapy as the flow of blood within the artery can be treated as a Casson fluid flow. Keeping in view the important applications of this model, several researchers investigated the flow and heat transfer properties in a Casson fluid flow. [56] was the first to study the Casson fluid flow between two co-axial cylinders. However, it took many years before many researchers conducted the theoretical study Casson fluid flow under different conditions and configuration. The mixed convective boundary layer Casson fluid flow about a solid sphere including the effects of chemical reaction was studied by EL-Kabeir et. al [180]. Kumar et. al [15] have done an entropy generation analysis for the boundary layer flow of Casson nanofluid with activation energy. More relevant studies of Casson fluid flow problem can be investigated through ([57], [58], [59], [60], [61], [62], [65], [63], [64], [181]).

To the best of authors knowledge, no one has studied the simultaneous effects of Hall current and nonlinear Rosseland thermal radiation on the transient three-dimensional flow of a viscous and incompressible Casson fluid in a fluid saturated porous medium along a convectively heated stretching surface. Keeping in view this in mind, our aim through this article is to numerically investigate a time-dependent model for the three dimensional hydromagnetic Casson fluid flow along a stretching surface embedded in a porous medium considering the combined effects of Hall current, nonlinear radiation, and convective heating at the surface. The mathematical model describing the physics of the problem is in the form of a set of nonlinear partial differential equations along with suitable boundary conditions. The governing nonlinear partial differential equations are reduced to a set of nonlinear ordinary differential equations using a suitable similarity transformation. To obtain the numerical solutions of the non-dimensionalized coupled nonlinear differential equations, an efficient technique, namely the spectral quasi-linearization method, is employed. The effects of several parameters on the flow and heat transfer characteristics are studied with the help of suitable graphs and tables.

3.2 The Mathematical Model

Let us consider a transient three-dimensional flow of a Casson fluid along a convectively heated stretching sheet embedded in a fluid-saturated porous medium under the influence of an applied magnetic field. The stretching surface is assumed to be in the plane

$y = 0$, and the Casson fluid is confined in the region $y \geq 0$. The fluid flow in the region $y \geq 0$ is induced due the linear stretching of the sheet along x - axis with a velocity $u = u_w(x, t)$. The fluid flow is permeated with an externally applied magnetic field $B(t)$ acting in y - direction, see Fig. 3.1. In addition to these, the following assumptions are made:

1. The density of the fluid is low and or the strength of the magnetic field is high so that the effects of Hall current become significant.
2. The magnetic Reynolds number of the fluid is small so that the effect of induced magnetic field is neglected in comparison to the applied one.
3. The fluid is optically thick, and a nonlinear Rosseland diffusion approximation is employed to study the effects of radiative heat transfer.
4. The Casson fluid is flowing in a saturated porous medium.

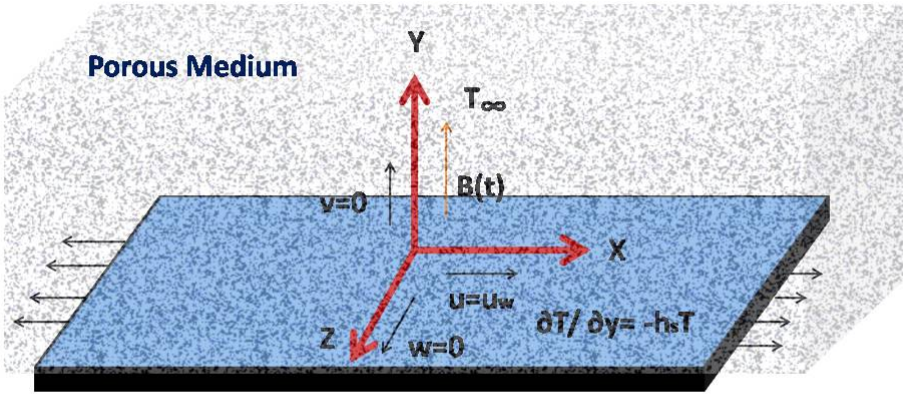

FIGURE 3.1: Model of the problem

Under the above assumptions, and using the Rosseland approximation, the equations governing the flow, and heat transfer in the unsteady three-dimensional magnetohydrodynamic flow of a Casson fluid along a stretching sheet within a fluid-saturated porous

medium in the presence of Hall current, and nonlinear radiative heat transfer, are

$$\frac{\partial u}{\partial x}+\frac{\partial v}{\partial y}+\frac{\partial w}{\partial z}=0, \tag{3.1}$$

$$\frac{\partial u}{\partial t}+u\frac{\partial u}{\partial x}+v\frac{\partial u}{\partial y}+w\frac{\partial u}{\partial z}=\nu\Big(1+\frac{1}{\beta}\Big)\frac{\partial^2 u}{\partial y^2}-\frac{\sigma B^2(t)}{\rho(1+m^2)}(u+mw)-\frac{\mu_e}{\rho K}u, \tag{3.2}$$

$$\frac{\partial w}{\partial t}+u\frac{\partial w}{\partial x}+v\frac{\partial w}{\partial y}+w\frac{\partial w}{\partial z}=\nu\Big(1+\frac{1}{\beta}\Big)\frac{\partial^2 w}{\partial y^2}+\frac{\sigma B^2(t)}{\rho(1+m^2)}(mu-w)-\frac{\mu_e}{\rho K}w, \tag{3.3}$$

$$\frac{\partial T}{\partial t}+u\frac{\partial T}{\partial x}+v\frac{\partial T}{\partial y}+w\frac{\partial T}{\partial z}=\frac{\partial}{\partial y}\Big(\Big(\alpha_m+\frac{16\sigma^* T^3}{3\alpha^*\rho c_p}\Big)\frac{\partial T}{\partial y}\Big), \tag{3.4}$$

where the components of velocity in the x, y, and z directions are represented as u, v, and w, respectively, t is taken as time, β is the Casson liquid parameter, μ_e denotes the effective viscosity of the fluid, K is the permeability of the porous medium, σ is electrical conductivity of the fluid, ρ is density of the fluid, $\nu=\mu/\rho$ is the liquid's kinematic viscosity, m is Hall current parameter, $\alpha_m=\frac{k}{\rho c_p}$ represents the liquid's thermal diffusivity. The Stefan-Boltzmann constant and coefficient of Rosseland mean absorption are denoted as σ^* and α^*, respectively, c_p is specific heat capacitance at constant pressure, and T is the temperature within the boundary layer.

The appropriate boundary conditions for the physical problem are

$$\text{At } y=0:\ u=u_w,\ v=0,\ w=0,\ \frac{\partial T}{\partial y}=-h_s T\ ; \tag{3.5}$$

$$\text{As } y\to\infty:\ u\to 0,\ w\to 0,\ T\to T_\infty, \tag{3.6}$$

where h_s is the convective heat transfer coefficient. In the present problem the stretching velocity is assumed as $u_w(x,t)=\frac{ax}{1-\gamma t}$ and the time-dependent magnetic field is taken as $B(t)=B_0(1-\gamma t)^{-1/2}$, where a and γ are constants and B_0 is the strength of the magnetic field.

We now choose a transformation of the form

$$u=\frac{ax}{(1-\gamma t)}f'(\eta),\ v=-\sqrt{\frac{a\nu}{(1-\gamma t)}}f(\eta),\ w=\frac{ax}{(1-\gamma t)}g(\eta), \tag{3.7}$$

$$\theta(\eta)=\frac{T-T_\infty}{T_\infty},\ \eta=y\sqrt{\frac{a}{\nu(1-\gamma t)}}, \tag{3.8}$$

so that the equation of continuity (3.1) is automatically satisfied and the Eqs. (3.2)-(3.4), reduce to

$$\Big(1+\frac{1}{\beta}\Big)f'''+ff''-(f')^2-A(f'+\frac{\eta}{2}f'')-\frac{M}{(1+m^2)}(f'+mg)-\lambda f'=0, \tag{3.9}$$

$$\Big(1+\frac{1}{\beta}\Big)g''-gf'+fg'-A(g+\frac{\eta}{2}g')+\frac{M}{(1+m^2)}(mf'-g)-\lambda g=0, \tag{3.10}$$

$$\Big(1+\frac{4}{3N_r}(1+\theta)^3\Big)\theta''-PrA\frac{\eta}{2}\theta'+Prf\theta'+\frac{4}{N_r}(1+\theta)^2\theta'^2=0. \tag{3.11}$$

The boundary conditions (3.7) and (3.8) reduce to

$$\text{At } \eta=0: \ f'=1, f=0, \ g=0, \ \theta'=-C\ (1+\theta)\ ; \tag{3.12}$$

$$\text{As } \eta\to\infty: \ f'\to 0, \ g\to 0, \ \theta\to 0, \tag{3.13}$$

where η is the dimensionless similarity variable and the primes denote derivative with respect to η. The non-dimensional parameters used above are defined as

$$A=\frac{\gamma}{a}, \ M=\frac{\sigma B_0^2}{\rho a}, \ N_r=\frac{k\alpha^*}{4\sigma^* T_\infty^3}, \ Pr=\frac{\nu}{\alpha_m}, \ \lambda=\frac{\mu_e}{\rho K}\frac{Re_x}{Re_k^2}, \ \ C=-h_s\sqrt{\frac{\nu(1-ct)}{a}},$$

where A, M, N_r, Pr, λ, and C are, respectively, the unsteadiness parameter, magnetic field parameter, radiation parameter, Prandtl number, local porosity parameter, and the convective heating parameter.

Apart from the velocity and temperature fields, the important physical quantities of engineering interest are the friction coefficients along x and z directions, and the local Nusselt number. These are denoted in the text as C_{fx}, C_{fz}, and Nu_x, respectively, and are defined as

$$C_{fx}=\frac{\tau_{wx}}{\rho u_w^2}, \ \ C_{fz}=\frac{\tau_{wz}}{\rho u_w^2}, \ \ Nu_x=\frac{xq_w}{k(T-T_\infty)}, \tag{3.14}$$

where the shear-stress components τ_{wx}, τ_{wz}, and the rate of heat transfer at the surface q_w, are defined as

$$\tau_{wx}=\mu\Big(1+\frac{1}{\beta}\Big)\Big(\frac{\partial u}{\partial y}\Big)_{y=0}, \ \ \tau_{wz}=\mu\Big(1+\frac{1}{\beta}\Big)\Big(\frac{\partial w}{\partial y}\Big)_{y=0}, \ \ q_w=\Big(-k\Big(\frac{\partial T}{\partial y}\Big)+q_r\Big)_{y=0}. \tag{3.15}$$

Therefore, the values of C_{fx}, C_{fz}, and Nu_x, respectively, are given by

$$C_{fx}Re_x^{1/2}=\Big(1+\frac{1}{\beta}\Big)f''(0), \ C_{fz}Re_x^{1/2}=\Big(1+\frac{1}{\beta}\Big)g'(0); \tag{3.16}$$

$$Re_x^{-1/2}Nu_x=C\Big[1+\frac{4}{3N_r}(1+\theta(0))^3\Big]\Big(1+\frac{1}{\theta(0)}\Big), \tag{3.17}$$

where q_r is the radiative heat flux and $Re_x=\frac{xu_w}{\nu}$ is the local Reynolds number.

3.3 Numerical Solution

The governing non-dimensionalized nonlinear ordinary differential equations (3.9)-(3.11) are solved using an efficient numerical technique known as spectral quasi-linearization method (SQLM). SQLM follows the idea of linearizing the nonlinear differential equations using linear Taylor series approximation. In the framework of SQLM, we obtain the linearized iteration scheme as

$$a_{11}^{(3)} f'''_{r+1} + a_{11}^{(2)} f''_{r+1} + a_{11}^{(1)} f'_{r+1} + a_{11}^{(0)} f_{r+1} + a_{12}^{(0)} g_{r+1} = R_1, \tag{3.18}$$

$$a_{22}^{(2)} g''_{r+1} + a_{22}^{(1)} g'_{r+1} + a_{22}^{(0)} g_{r+1} + a_{21}^{(1)} f'_{r+1} + a_{21}^{(0)} f_{r+1} = R_2, \tag{3.19}$$

$$a_{33}^{(2)} \theta''_{r+1} + a_{33}^{(1)} \theta'_{r+1} + a_{33}^{(0)} \theta_{r+1} + a_{31}^{(0)} f_{r+1} = R_3, \tag{3.20}$$

where

$$a_{11}^{(3)} = (1 + \frac{1}{\beta}),\ a_{11}^{(2)} = f_r - A\frac{\eta}{2},\ a_{11}^{(1)} = -2f'_r - A - \frac{M}{1+m^2} - \lambda,\ a_{11}^{(0)} = f''_r,$$

$$R_1 = f_r f''_r - (f'_r)^2,\ a_{22}^{(2)} = (1 + \frac{1}{\beta}),\ a_{22}^{(1)} = f_r - A\frac{\eta}{2},\ a_{22}^{(0)} = -f'_r - A - \frac{M}{1+m^2} - \lambda,$$

$$a_{21}^{(1)} = -g_r + \frac{Mm}{1+m^2},\ a_{21}^{(0)} = g'_r,\ R_2 = -g_r f'_r + g'_r f_r,\ a_{33}^{(2)} = \frac{4}{3N_r}(1+\theta_r)^3 + 1,$$

$$a_{33}^{(1)} = -APr\frac{\eta}{2} + Prf_r + \frac{8}{N_r}(1+\theta_r)^2\theta'_r,\ a_{33}^{(0)} = \frac{4}{N_r}(1+\theta_r)^2\theta''_r + \frac{8}{N_r}(1+\theta_r)(\theta'_r)^2,$$

$$R_3 = \frac{N_r Pr f_r \theta'_r + 4(1+\theta_r)(\theta_r(1+\theta_r)\theta''_r + (3\theta_r+1)(\theta'_r)^2)}{N_r},\ a_{12}^{(0)} = -\frac{Mm}{1+m^2}.$$

The corresponding boundary conditions for the iteration scheme are

$$\text{At } \eta = 0:\ f'_{r+1} = 1, f_{r+1} = 0,\ g_{r+1} = 0,\ \theta'_{r+1} = -C(1+\theta_{r+1}), \tag{3.21}$$

$$\text{As } \eta \to \infty:\ f'_{r+1} \to 0,\ g_{r+1} \to 0,\ \theta_{r+1} \to 0. \tag{3.22}$$

The above iteration scheme requires initial approximations to start-with which are chosen to be convenient functions satisfying the boundary conditions as

$$f_0 = 1 - e^{-\eta},\ h_0 = 0,\ \theta_0 = \left(\frac{C}{1-C}\right)e^{-\eta}.$$

The Chebyshev pseudo-spectral collocation method is used to solve the linearized equations (3.18)-(3.20). The domain of the physical problem $[0,\ \infty)$ is approximated with $[0,\ L]$, where L is used to invoke the boundary conditions at ∞. The computational domain $[0,\ L]$ is then transformed to $[-1,\ 1]$ by using the transformation $\eta = L(\xi+1)/2$ so that the Gauss-Lobatto points can be used to discretize the computational domain. The derivatives of the unknown functions at the grid points, in the linearized equations,

are approximated with the Chebyshev differentiation matrix. The application of the Chebyshev pseudo-spectral collocation method yield us

$$\begin{pmatrix} A_{11} & A_{12} & A_{13} \\ A_{21} & A_{22} & A_{23} \\ A_{31} & A_{32} & A_{33} \end{pmatrix} \begin{pmatrix} f_{r+1} \\ g_{r+1} \\ \theta_{r+1} \end{pmatrix} = \begin{pmatrix} R_1 \\ R_2 \\ R_3 \end{pmatrix}$$

where each A_{ij} is of order $(N+1)\times(N+1)$. $f_{r+1}, g_{r+1}, \theta_{r+1}, R_1, R_2$, and R_3, are vectors of order $(N+1)\times 1$.

3.4 Results and Discussion

The present article numerically investigates the flow and heat transfer characteristics due to the unsteady three-dimensional hydromagnetic flow of a Casson fluid along a stretching sheet in a fluid-saturated porous medium. The primary purpose of the work is to highlight the combined effects of Hall current, the porosity of the medium, nonlinear thermal radiation, and convective heating of the surface on the fluid flow and heat transfer. In an attempt to fulfill the primary objective, suitable similarity transformations are used to reduce the governing nonlinear partial differential equations to a set of coupled nonlinear ordinary differential equations. Several pertinent non-dimensional parameters appear in the nonlinear coupled ordinary differential equations, such as, magnetic parameter M, Hall current parameter m, Casson fluid parameter β, porosity parameter λ, unsteadiness parameter A, Prandtl number Pr, and convective parameter C. To investigate the effect of these parameters, Eqs. (3.9)-(3.11) are solved using SQLM, and the profiles of fluid velocities $f'(\eta)$ and $g(\eta)$, and fluid temperature $\theta(\eta)$ are presented in Figs. 3.2-3.6. The numerical values of coefficients of skin-friction C_{fx}, C_{fz}, and coefficient of heat transfer, formally known as Nusselt number Nu_x, are tabulated in Table 3.1.

Figure 3.2 presents the effect of the magnetic parameter M and the Hall current parameter m on the fluid velocity in the x direction $f'(\eta)$, fluid velocity in the z direction $g(\eta)$, and the fluid temperature $\theta(\eta)$ within the boundary layer region. The magnetic parameter M measures the strength of the Lorentz force that appears in the flow field due to the presence of the external magnetic field while the Hall current parameter m measures effect of Hall current which appears in the flow field due to the presence of a strong magnetic field and/or if the density of the fluid is low. Figure 3.2 shows that the Lorentz force appearing due to the magnetic field acts as a resistive force in the flow field, and it decelerates the fluid flow in the x direction throughout the boundary layer region. The fluid flow in z direction gets accelerated but only in a region near to the

stretching surface, whereas it gets decelerated afterward before attaining the free-stream velocity. The implication of the Hall current in the flow field is to accelerate the fluid velocities in both the directions. However, the noted impact is significant on the fluid velocity in z direction. The magnetic field generated Lorentz force, and the Hall current has opposite effects on the fluid temperature. The fluid temperature is found to be an increasing function of the magnetic field parameter whereas a decreasing function of the Hall current parameter. As we can see from the figures, the primary and secondary velocities increase for rising values of Hall parameter. This happens because the Hall current usually reduces the strength of the Lorentz force which resist the fluid motion in x direction. Also, Hall current actuates a cross flow by giving a force in z direction. Therefore, the resistive force gets reduced by increasing Hall current in flow field. This reduced resistive force is the main reason for decreasing temperature, which results in thinning the thermal boundary layer.

The influence of Casson fluid parameter β and the porosity parameter λ on the fluid velocities in x and z directions, and on the fluid temperature is shown in Figure 3.3. One must note that the Casson parameter β measures the yield stress and the fluid behave as a Newtonian fluid as $\beta \to \infty$. Also, the porosity parameter λ is inversely proportional to the permeability of the medium, i.e., smaller the value of λ higher is the permeability of the medium. It resembles from the figure that the fluid velocity in x direction decreases with increasing values of λ, and this shows that the velocity is higher in mediums with higher permeability. The fluid velocity in x direction decreases with increasing Casson parameter β. Therefore, it follows that the fluid velocity in a Casson fluid is higher than that of a Newtonian fluid. Also it is analyzed that, inside the boundary layer region near the stretching surface, the profiles of secondary velocity $g(\eta)$ firstly get accelerated and then change its behaviour by getting decelerated on increasing the values of β and λ. As we are assuming that there is no fluid flow in z direction at the sheet i.e. $g(0) = 0$. Therefore, the secondary velocity curve $g(\eta)$ starts from 0 and then gets increasing near the stretching surface due to the existence of Hall current which actuates a cross flow i.e. a flow in z direction which causes the flow to be three-dimensional in the boundary layer region. But after attaining a peak, as we go far from the stretching surface it starts decreasing to free stream. It happens because higher values of Casson parameter β increase the plastic dynamic viscosity which diminishes the yield stress and, as $\beta \to \infty$ fluid starts behaving as Newtonian fluid, and velocity of the fluid gets reduced. Also, the porosity parameter λ is inversely proportional to the permeability of the medium, i.e., smaller the value of λ higher is the permeability of the medium. Permeability offers to the ability of a porous medium to let fluid flow through it. Hence, rising the porosity parameter means reducing the number of pores in the porous medium, which generates

resistance in the flow path due to the relation of porosity parameter with frictional force and substantial drag force caused reduction in the velocity field. The fluid temperature, within the boundary layer region, rises with an increase in either λ and β, which imply that the temperature of the fluid is higher in case of a Newtonian fluid and lesser in a medium with higher permeability.

The unsteadiness parameter A measures the transient behavior of the flow and heat transfer and the flow-field becomes steady when $A = 0$.Figure 3.4 captures the implications of increasing unsteadiness parameters on the fluid velocity in the x direction $f'(\eta)$, fluid velocity in the z direction $g(\eta)$, and fluid temperature $\theta(\eta)$. From the observed results, it is clear that the fluid velocity in both the directions gets decelerated with increasing unsteadiness in the flow field whereas the fluid temperature experiences a rise in case of a transient flow. These effects on the fluid velocities and heat transfer, however, are not that significant.

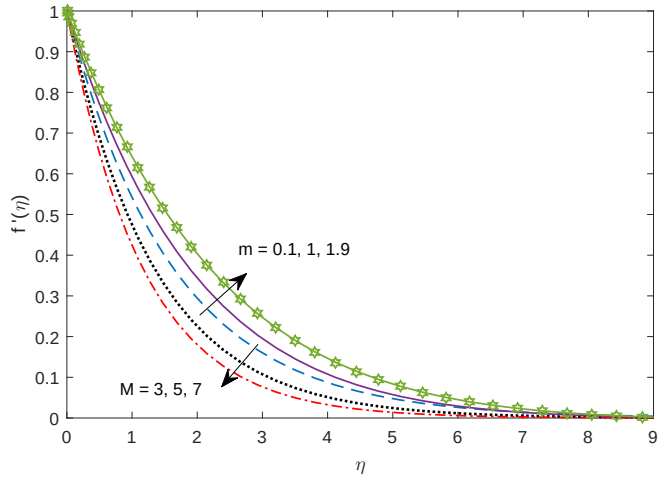

(a)

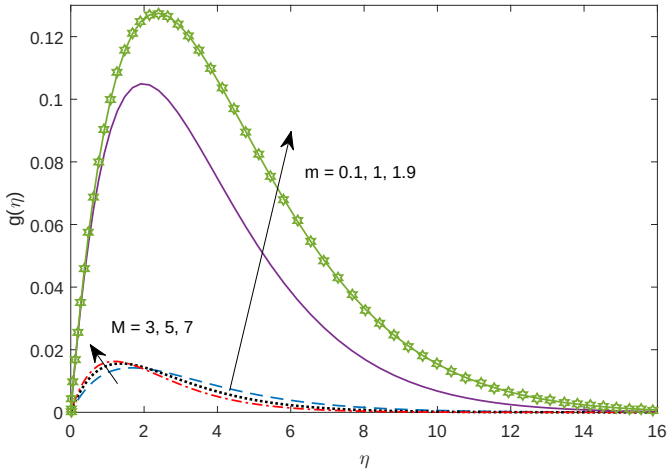

(b)

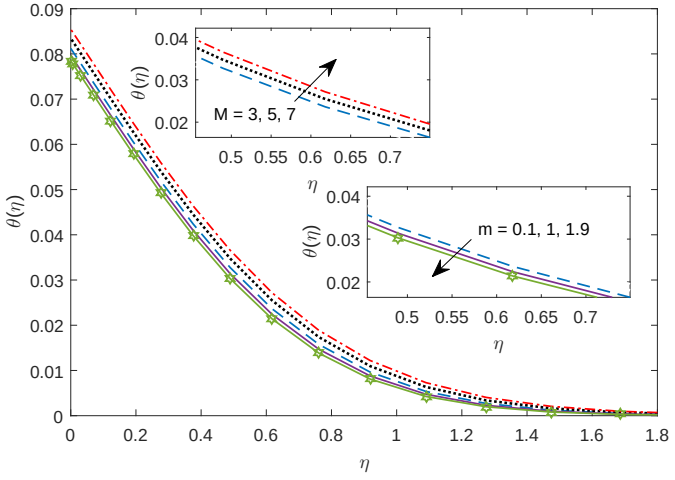

(c)

FIGURE 3.2: Effect of magnetic parameter M and Hall current parameter m on (a) f', (b) g, and (c) θ when $A = 0.1,\ \lambda = 0.1,\ \beta = 0.1,\ N_r = 1,\ Pr = 10,\ C = 0.1$.

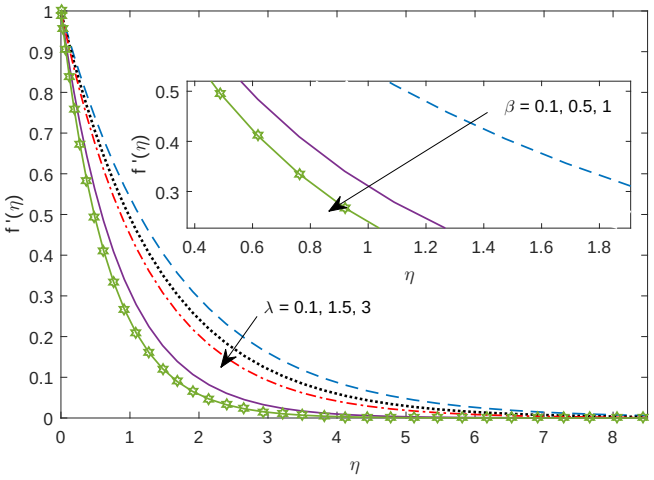

(a)

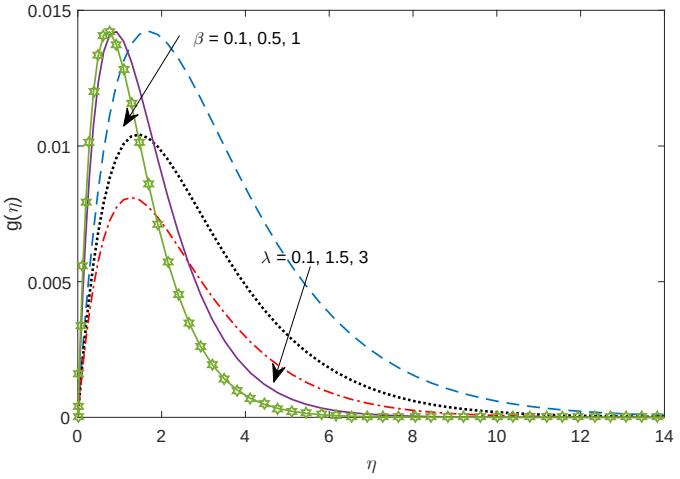

(b)

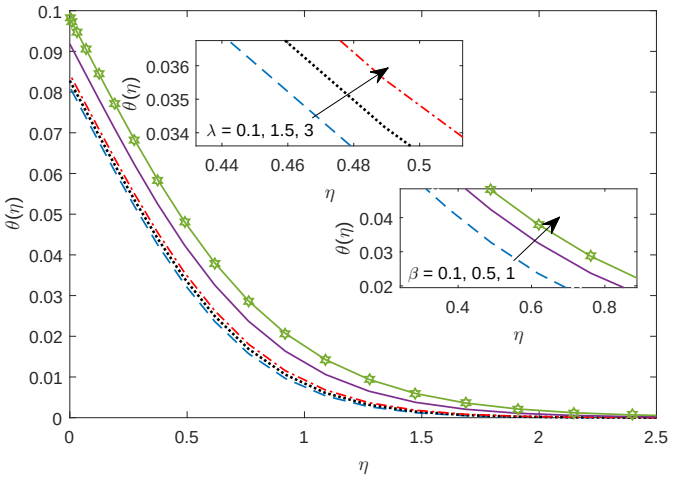

(c)

FIGURE 3.3: Effect of Casson parameter β and porosity parameter λ on (a) f', (b) g, and (c) θ when $A = 0.1,\ m = 0.1,\ M = 3,\ N_r = 1,\ Pr = 10,\ C = 0.1$.

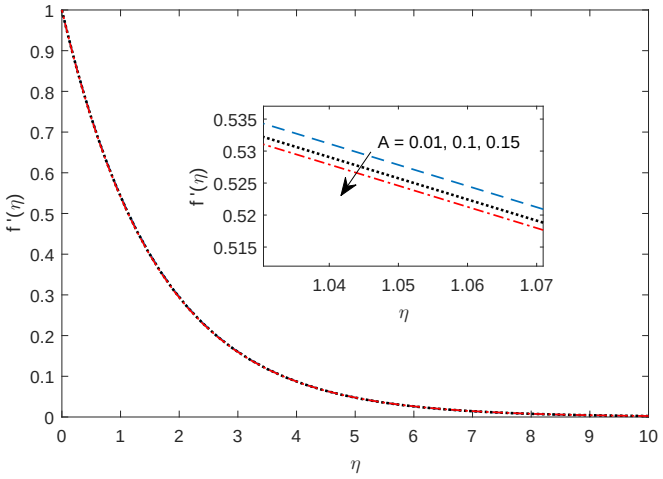

(a)

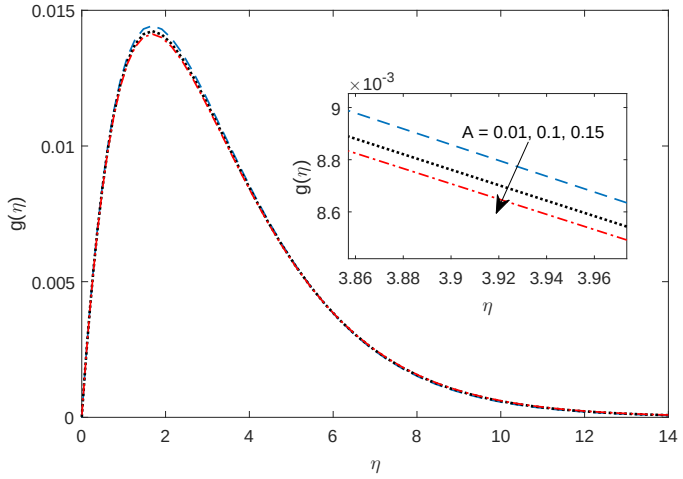

(b)

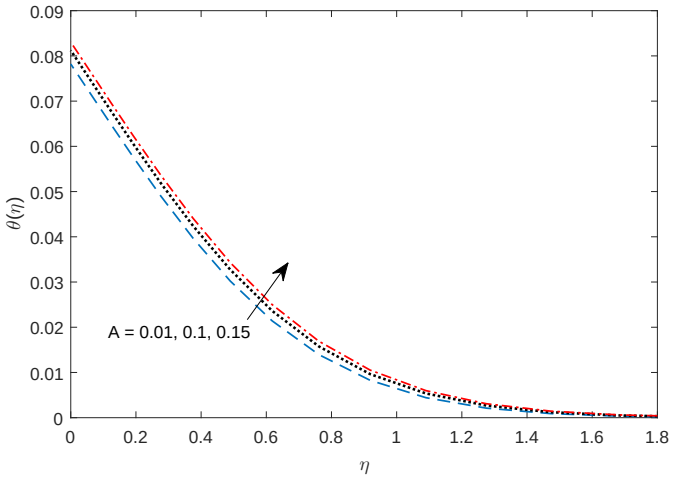

(c)

FIGURE 3.4: Effect of unsteadiness parameter A on (a) f', (b) g, and (c) θ when $m = 0.1,\ \lambda = 0.1,\ \beta = 0.1,\ N_r = 1,\ Pr = 10,\ M = 3.$

Figure 3.5 captures the variations in fluid temperature $\theta(\eta)$ with increasing values of the N_r and Pr. The radiation parameter N_r measures the effect of radiative heat transfer on the fluid temperature and is inversely proportional to the radiation effect. Therefore, increasing values of N_r correspond to decreasing radiative heat transfer effect and vice versa. From this figure, one may note that the fluid temperature $\theta(\eta)$ falls with increasing values of N_r, which shows that the radiative heat transfer tends to increase the fluid temperature within the boundary layer region. The radiation contributes to the thermal energy of the system which forces the fluid temperature to rise in the flow-field. The Prandtl number Pr is the ratio of viscous diffusivity to thermal diffusivity, and an increase in Prandtl number lead to a decrease in the thermal diffusivity of the fluid. Figure 3.5 shows that the fluid temperature is a decreasing function of the Prandtl number of the fluid, which implies that the increasing thermal diffusivity leads to higher fluid temperature. The convective heating parameter C signifies the impact of convective heating at the surface. Behavior of fluid temperature with increasing values of the convective parameter is presented in figure 3.6 and it follows that the temperature of the fluid, within the boundary layer region, rises with the increase in the convective heating at the surface. This increase in temperature happens as a result of heat transfer that takes place from the surface to the fluid lying in the boundary layer region.

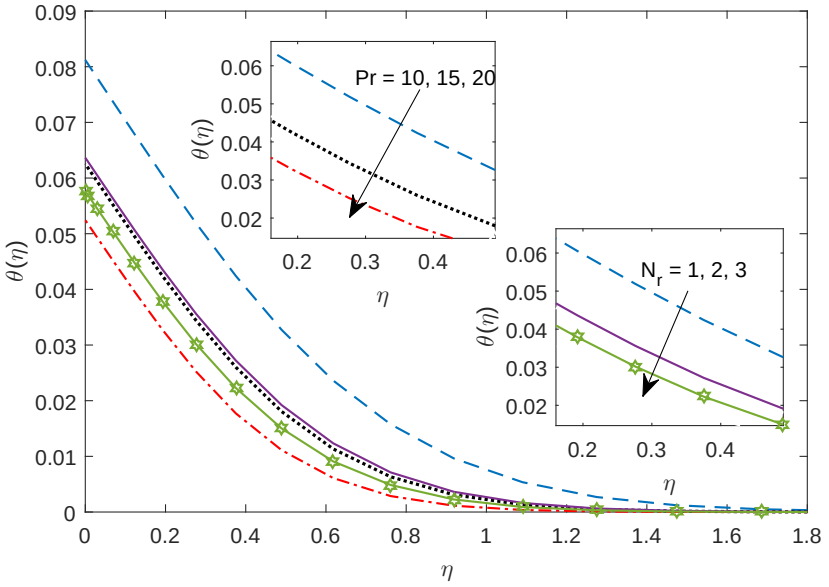

FIGURE 3.5: Effect of radiation parameter N_r and Prandtl number Pr on θ when $m = 0.1,\ \lambda = 0.1,\ \beta = 0.1,\ A = 0.1,\ C = 0.1,\ M = 3.$

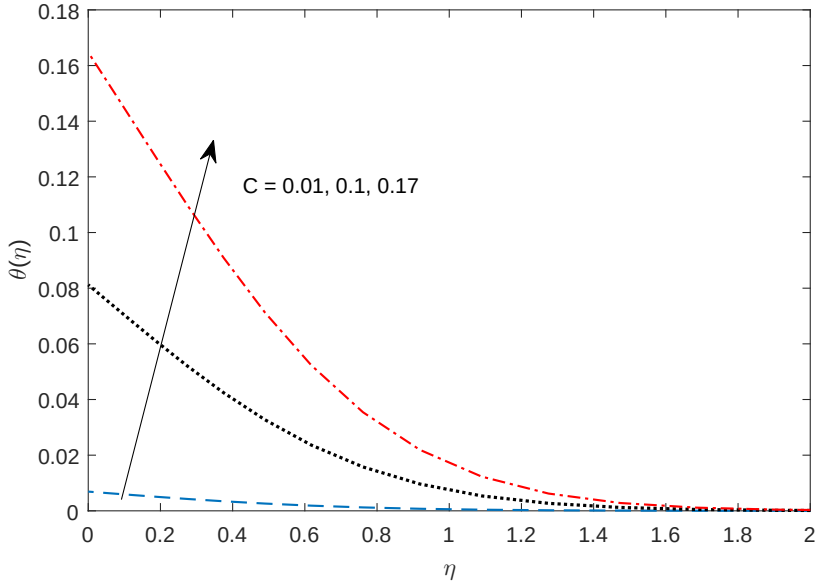

FIGURE 3.6: Effect of convective parameter C on θ when $m = 0.1,\ \lambda = 0.1,\ \beta = 0.1,\ A = 0.1,\ Pr = 10,\ N_r = 1,\ M = 3.$

The effects of pertinent flow parameters, viz. the magnetic parameter M, Hall current parameter m, unsteadiness parameter A, Casson fluid parameter β, and porosity parameter λ on the skin-friction coefficients C_{fx} and C_{fz}, and on the coefficient of heat transfer at the surface Nu_x is presented in Table 3.1. The coefficient of skin-friction in the x direction C_{fx} increases with increasing values of the magnetic parameter, unsteadiness parameter, and porosity parameter whereas it decreases upon increasing the Hall current parameter and the Casson fluid parameter. Thus, the skin-friction in the x direction increases with the increasing strength of the Lorentz force and the unsteadiness in the flow field whereas the Hall current tends to reduce it. A Newtonian fluid has lesser skin-friction C_{fx} as compared to a Casson fluid. The skin-friction is higher in the case of a lesser permeable medium. It follows from Table 3.1 that the coefficient of skin-friction in the z direction C_{fz} increases with increasing effects of the Lorentz force, Hall current, and the permeability of the medium while it decreases with the increase in the unsteadiness in the flow field. The coefficient of heat transfer at the surface Nu_x decreases with increase permeability of the medium. Since the porosity parameter λ is inversely proportional to the permeability of the medium, i.e., smaller the value of λ higher is the permeability of the medium. Permeability offers to the ability of a porous medium to let fluid flow through it. Hence, rising the porosity parameter means reducing the number of pores in the porous medium, which generates resistance in the flow path. Due to the relation of porosity parameter with frictional forces and substantial drag force, a reduction in the velocity field and as well as enhancement in the temperature field is seen. Therefore, these resistive forces are the main reason for affecting the rate

of heat transfer at the surface. Also the coefficient of heat transfer at the surface Nu_x decreases with increase in the strength of the magnetic field, unsteadiness, and Casson parameter whereas it increases with the increase in the Hall current. Since the heat transfer coefficient decreases with increasing values of the Casson parameter, it follows that the heat transfer from the surface is higher in the case of Casson liquids than in the case the Newtonian fluids. Table 3.1 also reflects the influence of the radiation parameter N_r, convective heating parameter C, and the Prandtl number Pr. Following the tabulated values, it is clear that the heat transfer at the surface increases with increasing values of the thermal radiation, convective heating, and the Prandtl number.

TABLE 3.1: Influence of different parameters on skin-friction coefficients and Nusselt number.

M	m	A	N_r	C	β	Pr	λ	$-C_{fx}Re_x^{1/2}$	$C_{fz}Re_x^{1/2}$	$Re_x^{-1/2}Nu_x$
3	0.1	0.1	1	0.1	0.1	10	0.1	6.75668869	0.25242903	3.57521555
5								8.21533482	0.34099012	3.50034797
7								9.45142273	0.41197207	3.43616354
	0.1							6.75668869	0.25242903	3.57521555
	1							5.65134497	1.55455540	3.62835138
	1.9							4.76295267	1.56554520	3.67298301
		0.01						6.70234056	0.25460189	3.68312501
		0.1						6.75668869	0.25242903	3.57521555
		0.15						6.78675232	0.25123802	3.51317283
			1					6.75668869	0.25242903	3.57521555
			2					6.75668869	0.25242903	3.01147937
			3					6.75668869	0.25242903	2.79957595
				0.01				6.75668869	0.25242903	3.44113263
				0.1				6.75668869	0.25242903	3.57521555
				0.17				6.75668869	0.25242903	3.73455556
					0.1			6.75668869	0.25242903	3.57521555
					0.5			3.52856559	0.13182676	3.25256053
					1			2.88106174	0.10763610	3.09495642
						10		6.75668869	0.25242903	3.57521555
						15		6.75668869	0.25242903	4.41622642
						20		6.75668869	0.25242903	5.12636593
							0.1	6.75668869	0.25242903	3.57521555
							1.5	7.81266622	0.21582339	3.52117747
							3	8.80504026	0.19016116	3.46994702

3.5 Conclusions

The combined effects of the Hall current, nonlinear Rosseland thermal radiation, the permeability of the porous medium, and the convective heating at the surface in the unsteady three-dimensional flow of a Casson fluid along a stretching surface are investigated numerically using the Spectral quasi-linearization method (SQLM). The crucial findings of the study are

1. The effect of Lorentz force in the flow field is to resist the fluid flow in x direction whereas the fluid velocity in z direction increases near the surface, and then decreases away from the surface, within the boundary layer region. The temperature of the fluid experiences an enhancement with the increase in the strength of Lorentz force.

2. The effect of Hall current arising in the flow field is to the accelerate the fluid velocities in both the directions. The coefficient of skin-friction in the x direction decreases while the coefficient of skin-friction in the z direction increases with increasing Hall current. The Hall current tends to reduce the temperature of the fluid within the boundary layer region which results in an increase in the rate of heat transfer at the surface.

3. Fluid velocities in both the directions increase with increasing permeability of the medium. The skin-friction in the x direction decreases with increased permeability of the medium, whereas the skin-friction in z direction increases with the increase in the permeability. The rate of heat transfer at the surface is higher in mediums with higher permeability. This increase in the rate of heat transfer contributes in enhancing the fluid temperature.

4. The convective heating from the surface and thermal radiation tend to rise the fluid temperature within the boundary layer region, and as a result, an increment in the heat transfer rate may also be observed.

Chapter 4

Non-uniform Heat Generation/Absorption and Dissipation Effects on the Unsteady MHD Flow of a Couple-Stress Dusty Fluid along a Porous Sheet

4.1 Introduction

Investigating the fluid flow confined in the boundary layer region along a stretching surface is essential because numerous modern engineering and industrial domain equipment depend on the theory of the boundary layers. The pioneering work of Crane [2] originated the study of boundary layer flow of a viscous fluid along a stretching surface in two dimensions. Later, this work was extended by Elbashbeshy [44] and Mahapatra and Gupta [45] considering the influence of heat transfer. Recently, Maleki et al. [6] examined the combined impacts of heat source/sink and viscous dissipation on the flow

Contents of this chapter has been accepted for publication in AIP Conference Proceedings [Prashu, R. Nandkeolyar, V. Sangwan, Numerical Simulation of Non-uniform Heat Generation and Dissipation Effects on the Unsteady MHD Flow of a Couple-Stress Dusty Fluid, AIP Conference Proceedings (Accepted)]

of pseudo-plastic fluid along a moving porous surface. In order to obtain quality-product in manufacturing processes, it is crucial that the essential characteristics of the fluid be maintained. Stretching and cooling rates are fundamental properties of the fluid, and a sudden change in these properties demolishes the product quality. These properties of the fluid can be regulated using an externally applied magnetic field. Because of this, the study of magnetohydrodynamic fluid flow attracted many researchers. The investigation of the flow of hydromagnetic fluid flowing over a stretching sheet is done by Pavlov [19]. The analytical study to inspect the mathematical model for the hydromagnetic fluid flow along a quadratically stretching sheet was carried out by Kumaran et al. [20]. Jusoh et al. [22] discussed the flow and heat transfer of a viscous incompressible nanofluid along a bidirectional exponential permeable shrinking/stretching surface considering the influences of viscous dissipation and magnetic field. They presented the dual solutions together with the stability analysis in their work.

The research studies cited above deal with the problems in steady-state. The time-dependent problems are also found to be of great interest by researchers, which enabled them to understand more real properties of the flow problem. Wang [46] was the first who started the study of unsteady problems. He introduced the time-dependent similarity transformations to convert the PDEs into ODEs. To analyze the influence of heat transfer, Elbashbeshy and Bazid [47] discussed the unsteady problem for electrically conducting fluid considering the magnetic field effect. Ishak et al. [48] discussed the unsteady hydromagnetic fluid flow along a vertical surface. Similarity solutions for the time-dependent model were obtained by Aziz [49]. Pal [50] analyzed the combined influence of Hall current and radiation on the unsteady hydromagnetic fluid flow towards a porous surface.

Researchers find much attention in investigating the flow of couple stress fluids due to their application in several engineering problems. There are different types of mathematical models in literature dealing with different types of non-Newtonian fluids. It is impossible to specify the association of stress to the shear strain of all the non-Newtonian fluids by a single constitutive relationship. In addition to this, the stress tensor of a couple-stress fluid is not symmetrical. The notion of couple stress fluid is a generalization of viscous fluids. The concept comes into the picture due to the mixing of randomly oriented solid particles to the fluid, which results in forces present in the fluid to oppose the forces generated by additives. These opposite forces produce a couple force, and a couple-stress is induced in the fluid. Liquid crystals, synthetic liquids, blood all fall in the category of couple stress liquids. In 1966, Stokes[70] initiated the study of the fluid flow model concerned with the couple-stress fluids. He solved a series of problems to examine the influence of couple-stresses and measured the various material constants. Hayat et al. [71] presented a three-dimensional time-dependent model for

the flow of a couple-stress fluid along a stretching surface. His study also included the chemical reaction and mass transfer effects. The collective influences of viscous dissipation and Joule heating on the three-dimensional MHD flow of a couple-stress fluid were investigated by Ramzan et al. [72]. An analytical solution of the time-dependent mixed convective couple-stress nanofluid flow along a stretching surface was obtained by Khan et al. [93]. Moreover, Kumar et al. [73] considered the two-dimensional unsteady flow of hydromagnetic nano-polymer fluid flowing over a stretching sheet.

The studies mentioned above are all limited to the analysis of the flow of the fluid phase only. The phenomenon of the two-phase fluid flow, in which rigid spherical particles are present in a fluid, concerns researchers for its varied application in cement production, paint spraying, wastewater treatment, blood rheology, and presence of dust in gas cooling systems, etc. Saffman [78] was the first to investigate the significance of the presence of dust particles in the flow of a viscous fluid. He derived the equations for the laminar flow of dusty gas, assuming the dust particles to be equally distributed in the gas. Vajravelu and Nayfeh [79] investigated the two-phase dusty fluid flow past a stretching surface in the presence of the magnetic field and uniform suction. The impact of non-uniform heat generation/absorption on the two-phase flow of a dusty fluid along a stretching sheet was examined by Gireesha et al. [80]. Turkyilmazoglu [81] carried out a mathematical analysis for the hydromagnetic two-phase dusty fluid flowing over a shrinking/stretching permeable surface. Considering the influence of radiation, Kumar et al. [82] discussed the MHD two-phase flow of a dusty tangent hyperbolic fluid along a stretching surface. The simultaneous effects of slip and porosity for the two-phase hydromagnetic dusty fluid over a porous stretching sheet were examined by Abbas [83]. Bibi et al. [84] investigated the time-dependent solid-particle flow of a tangent hyperbolic fluid with variable thermal conductivity and convective boundary conditions. Some of the most recent studies involving two-phase flow are due to ([88], [85], [86], [87]).

It can be seen easily from the research works cited above that many researchers studied the flow of different non-Newtonian fluids under different conditions. Also, the study of dusty fluid flow is of significant importance due to application of such models in the purification of crude oil, etc. The present chapter intends to examine the time-dependent MHD flow of a couple-stress dusty fluid along a permeable stretching surface, considering the impacts of heat generation/absorption and viscous dissipation. The mathematical modeling of the problem consists of highly nonlinear partial differential equations and suitable boundary conditions. The mathematical model is then transformed to the similarity form invoking appropriate transformations, dealing with the effective spectral quasilinearization method to obtain the numerical solution. A detailed parametric examination of significant physical quantities, such as the fluid velocities for both the fluid

and dust phases, temperature distributions for both the phases, skin-friction, and heat transfer coefficients, has been performed.

4.2 Mathematical Modelling

A time-dependent hydromagnetic two-phase flow of dusty couple-stress fluid along a stretching surface is considered. The stretching surface is permeable and is supposed to be located in the plane $y = 0$. The surface if the sheet is stretched in x direction with velocity $u = u_w(x, t)$. A magnetic field $B(t) = B_0(1 - at)^{-1/2}$, which is dependent on time, is applied normal to the stretching surface, see Fig. 4.1. It is presumed that the magnetic Reynolds number small enough so that the induced magnetic field is ignored. The dust particles are considered to have a spherical shape and to be constant during the whole flow in size and number density. The effects of viscous dissipation, and heat generation/absorption are also taken into account in the present study. Under these

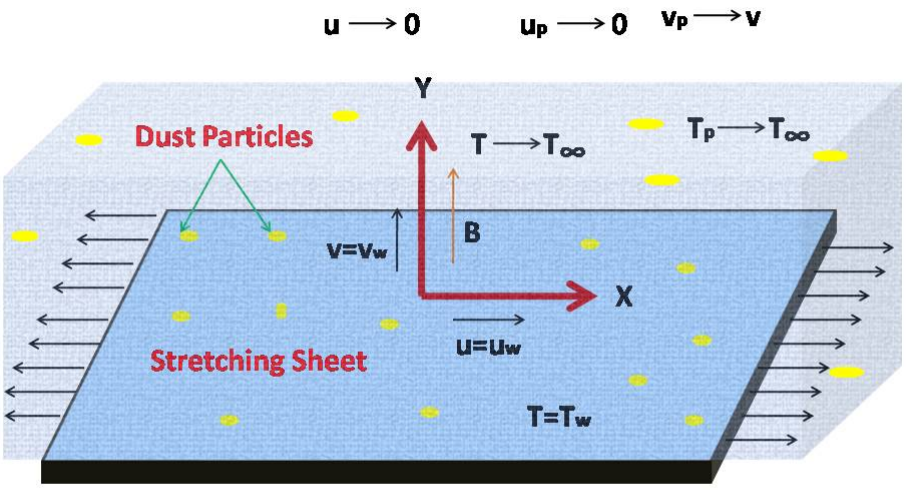

FIGURE 4.1: Model of the problem

assumptions, the mathematical model governing the flow and heat transfer for the two-phase flow of a dusty fluid is given by

$$\frac{\partial u}{\partial x}+\frac{\partial v}{\partial y}=0, \tag{4.1}$$

$$\frac{\partial u}{\partial t}+u\frac{\partial u}{\partial x}+v\frac{\partial u}{\partial y}=\frac{\mu}{\rho}\frac{\partial^2 u}{\partial y^2}-\frac{n_0}{\rho}\frac{\partial^4 u}{\partial y^4}+\frac{KN}{\rho}(u_p-u)-\frac{\sigma B^2(t)}{\rho}u, \tag{4.2}$$

$$\frac{\partial u_p}{\partial x}+\frac{\partial v_p}{\partial y}=0, \tag{4.3}$$

$$\frac{\partial u_p}{\partial t}+u_p\frac{\partial u_p}{\partial x}+v_p\frac{\partial u_p}{\partial y}=\frac{K}{m}(u-u_p), \tag{4.4}$$

$$\rho c_p\left(\frac{\partial T}{\partial t}+u\frac{\partial T}{\partial x}+v\frac{\partial T}{\partial y}\right)=k\frac{\partial^2 T}{\partial y^2}+\frac{\rho_p c_m}{\tau_T}(T_p-T)+\frac{\rho_p}{\tau_v}(u_p-u)^2 + \mu\left(\frac{\partial u}{\partial y}\right)^2+n_0\left(\frac{\partial^2 u}{\partial y^2}\right)^2+q''', \tag{4.5}$$

$$\rho_p c_m\left(\frac{\partial T_p}{\partial t}+u_p\frac{\partial T_p}{\partial x}+v_p\frac{\partial T_p}{\partial y}\right)=-\frac{\rho_p c_m}{\tau_T}(T_p-T), \tag{4.6}$$

where t is time, (u,v) and (u_p,v_p) represent the fluid and dust particle phase velocity components along the x-axis and y-axis respectively. The particle phase relaxation time and the number of dust particles per unit volume are denoted as $\tau_v=\frac{m}{K}$ and N, respectively. m represents the particle mass concentration. ρ and ρ_p denotes the fluid and particle densities. T is fluid temperature, and μ is the fluid viscosity coefficient. K the Stoke's resistance co-efficient (for spherical particles of radius r is $6\pi r\mu$), T_p is temperature of the dust particle. c_p and c_m are specific heats of the fluid and dust particles respectively, k is thermal conductivity and q''' is the of heat source (>0) or sink (<0) coefficient. τ_T denotes the thermal equilibrium time.

The boundary conditions for the above model

$$\text{at } y=0:\ u=u_w(x,t),\ v=v_w(x,t),\ \frac{\partial^2 u}{\partial y^2}=0,\ T=T_w(x,t)\ ; \tag{4.7}$$

$$\text{as } y\to\infty:\ u\to 0,\ u_p\to 0,\ v_p\to v,\ \frac{\partial u}{\partial y}\to 0,\ T\to T_\infty,\ T_p\to T_\infty, \tag{4.8}$$

where $u_w=\frac{cx}{1-at}$ is the stretching velocity of the sheet, a and c are positive constants, $v_w=-\frac{v_0}{\sqrt{(1-at)}}$ is suction velocity, v_0 is positive constant, $T_w-T_\infty=T_0\frac{cx^2}{\nu(1-at)^2}$, T_0 is reference temperature.

In order to convert the above model into similarity form the following transformations are defined

$$u=\frac{cx}{(1-at)}f'(\eta),\ v=-\sqrt{\frac{c\nu}{(1-at)}}f(\eta),\ u_p=\frac{cx}{(1-at)}F'(\eta),\ v_p=-\sqrt{\frac{c\nu}{(1-at)}}F(\eta),$$
$$\theta(\eta)=\frac{T-T_\infty}{T_w-T_\infty};\ \theta_p(\eta)=\frac{T_p-T_\infty}{T_w-T_\infty};\ \eta=y\sqrt{\frac{c}{\nu(1-at)}}.$$

The heat souce/sink term is taken to be

$$q''' = \frac{ku_w}{x\nu}[A^*(T_w - T_\infty)f' + B^*(T - T_\infty)], \tag{4.9}$$

where A^* is coefficient of space-dependent heat generation/absorption and B^* is coefficient of temperature-dependent heat generation/absorption.

In view of the above, the reduced model is given by

$$Sf^v - f''' - ff'' + (f')^2 + \alpha(f' + \frac{\eta}{2}f'') - l\beta(F' - f') + Mf' = 0, \tag{4.10}$$

$$FF'' - (F')^2 + \beta(f' - F') - \alpha(F' + \frac{\eta}{2}F'') = 0, \tag{4.11}$$

$$\theta'' + Pr(f\theta' - 2f'\theta) + l\gamma Pr\beta_T(\theta_p - \theta) - \alpha Pr\left(2\theta + \frac{\eta}{2}\theta'\right) + l\beta PrEc(F' - f')^2$$
$$+ EcPr\left[(f'')^2 + S(f''')^2\right] + (A^*f' + B^*\theta) = 0, \tag{4.12}$$

$$- F\theta_p' + 2F'\theta_p + \frac{\alpha}{2}(4\theta_p + \eta\theta_p') + \beta_T(\theta_p - \theta) = 0, \tag{4.13}$$

subject to the following boundary conditions

$$\text{at } \eta = 0: \ f' = 1, f = f_0, \ f''' = 0, \ \theta = 1 \ ; \tag{4.14}$$

$$\text{as } \eta \to \infty: \ f' \to 0, \ f'' \to 0, \ F - f \to 0, \ F' \to 0, \ \theta \to 0, \ \theta_p \to 0, \tag{4.15}$$

where $l = \frac{\rho_p}{\rho}$ denotes the mass concentration of dust particles (or particle loading parameter) with $\rho_p = mN$ as the particle phase density, $\beta = \frac{1}{c\tau_v}(1 - at)$ is the fluid particle interaction parameter for velocity, $M = \frac{\sigma B_0^2}{\rho c}$ is the magnetic field parameter, $f_0 = \frac{v_0}{\sqrt{c\nu}}$ is suction parameter, $\alpha = \frac{a}{c}$ unsteadiness parameter, $S = \frac{n_0 U_w}{\rho x\nu^2}$ is the couple-stress parameter, $Pr = \frac{\mu C_p}{k}$ is the Prandtl number, $\gamma = \frac{c_m}{c_p}$ is the specific heat parameter, $\beta_T = \frac{1}{c\tau_T}(1 - at)$ is the local fluid-interaction parameter for temperature, and $Ec = \frac{U_w^2}{c_p(T_w - T_\infty)}$ is the Eckert number.

The essential physical quantities, friction coefficient along x direction and the local Nusselt number are represented as C_{fx} and Nu_x, respectively, and are defined as

$$C_{fx} = \frac{\tau_{wx}}{\rho u_w^2}, \quad Nu_x = \frac{xq_w}{k(T_w - T_\infty)}, \tag{4.16}$$

where

$$\tau_{wx} = \mu\left(\frac{\partial u}{\partial y} - \frac{n_0}{\rho}\frac{\partial^3 u}{\partial y^3}\right)_{y=0}, \quad q_w = \left(-k\frac{\partial T}{\partial y}\right)_{y=0}. \tag{4.17}$$

Therefore, the values of C_{fx}, and Nu_x, respectively, are given by

$$C_{fx}Re_x^{1/2} = f''(0) - Sf''''(0),\ Re_x^{-1/2}Nu_x = -\theta'(0); \tag{4.18}$$

$$\tag{4.19}$$

where $Re_x = \frac{xu_w}{\nu}$ is the local Reynolds number.

4.3 Numerical Solution

The solution of reduced non-dimensionalized mathematical model in similarity form is obtained using a numerical method known as the spectral quasi-linearization method (SQLM). SQLM follows the idea of linearizing the nonlinear differential equations using linear Taylor series approximation. Following the algorithm of SQLM, we obtain the linearized iteration scheme as

$$a_{11}^{(5)}f''''_{r+1} + a_{11}^{(3)}f'''_{r+1} + a_{11}^{(2)}f''_{r+1} + a_{11}^{(1)}f'_{r+1} + a_{11}^{(0)}f_{r+1} + a_{12}^{(1)}F'_{r+1} = R_1, \tag{4.20}$$

$$a_{22}^{(2)}F''_{r+1} + a_{22}^{(1)}F'_{r+1} + a_{22}^{(0)}F_{r+1} + a_{21}^{(1)}f'_{r+1} = R_2, \tag{4.21}$$

$$a_{31}^{(3)}f'''_{r+1} + a_{31}^{(2)}f''_{r+1} + a_{31}^{(1)}f'_{r+1} + a_{31}^{(0)}f_{r+1} + a_{33}^{(2)}\theta''_{r+1} + a_{33}^{(1)}\theta'_{r+1} + a_{33}^{(0)}\theta_{r+1} + a_{34}^{(0)}\theta_{p_{r+1}} = R_3, \tag{4.22}$$

$$a_{42}^{(1)}F'_{r+1} + a_{42}^{(0)}F_{r+1} + a_{43}^{(0)}\theta_{r+1} + a_{44}^{(1)}\theta'_{p_{r+1}} + a_{44}^{(0)}\theta_{p_{r+1}} = R_4, \tag{4.23}$$

where

$a_{11}^{(5)} = S,\ a_{11}^{(3)} = -1,\ a_{11}^{(2)} = -f_r + \alpha\frac{\eta}{2},\ a_{11}^{(1)} = 2f'_r + \alpha + M + l\beta,\ a_{11}^{(0)} = -f''_r,\ a_{12}^{(1)} = -l\beta,$

$R_1 = -f_r f''_r + (f'_r)^2,\ a_{22}^{(2)} = \frac{\alpha\eta}{2} - F_r,\ a_{22}^{(1)} = \alpha + \beta + 2F'_r,\ a_{22}^{(0)} = -F''_r,$

$a_{21}^{(1)} = -\beta,\ R_2 = (F'_r)^2 - F_r F''_r,\ a_{33}^{(2)} = 1,$

$a_{33}^{(1)} = -\alpha Pr\frac{\eta}{2} + Prf_r,\ a_{33}^{(0)} = -2Pr\alpha + B^* - \beta_T\gamma lPr - 2Prf'_r,$

$a_{31}^{(3)} = 2EcPrSf'''_r,\ a_{31}^{(2)} = 2EcPrf''_r,\ a_{31}^{(1)} = A^* - 2\beta EclPr(F'_r - f'_r) - 2Pr\theta_r,$

$a_{31}^{(0)} = Pr\theta_r,\ a_{34}^{(0)} = \beta_t\gamma lPr,$

$R_3 = Pr(-2\beta Ecl f'_r F'_r + \beta Ecl(f'_r)^2 + \beta Ecl(F'_r)^2 + EcS(f'''_r)^2 + Ec(f''_r)^2 - 2\theta_r f'_r + f_r\theta'_r)$

$a_{42}^{(1)} = 2\theta_{p_r},\ a_{42}^{(0)} = -\theta'_{p_r},\ a_{43}^{(0)} = -\beta_T,\ a_{44}^{(1)} = \frac{a\eta}{2} - F_r,$

$a_{44}^{(0)} = 2\alpha + \beta_T + 3F'_r,\ R_4 = 2\theta_{p_r}F'_r - F_r\theta'_{p_r}.$

The boundary conditions for the iterative scheme are

$$\text{at } \eta = 0: \ f'_{r+1} = 1, f_{r+1} = f_0, \ f'''_{r+1} = 0, \ \theta_{r+1} = 1 \ ; \tag{4.24}$$

$$\text{as } \eta \to \infty: \ f'_{r+1} \to 0, \ f''_{r+1} \to 0, \ F_{r+1} - f_{r+1} \to 0, \ F'_{r+1} \to 0, \ \theta_{r+1} \to 0, \ \theta_{p_{r+1}} \to 0. \tag{4.25}$$

The above iteration scheme requires initial approximations to start-with which functions are considered to fulfill the boundary conditions as

$$f_{00} = -\frac{8}{6}e^{-\eta} + \frac{1}{6}e^{-2\eta} + f_0 + \frac{7}{6}, \ F_{00} = f_0 + \frac{7}{6}, \ \theta_{00} = e^{-\eta}, \ \theta_{p_{00}} = e^{-\eta}.$$

To obtain the numerical solutions the linearized equations (4.20)-(4.23) are subsequently dealt with the Chebyshev pseudo-spectral collocation method. The domain of the physical problem $[0, \ \infty)$ is approximated with $[0, L]$. The computational domain $[0, L]$ is then converted to $[-1, \ 1]$. Using $\eta = L\frac{(\xi+1)}{2}$ so that the Gauss-Lobattor points can be utilized. The values of the functions' derivatives are approximated at the nodes using the Chebyshev differentiation matrix. The application of the Chebyshev pseudo-spectral collocation method finally yield us

$$\begin{pmatrix} \hat{A}_{11} & \hat{A}_{12} & \hat{A}_{13} & \hat{A}_{14} \\ \hat{A}_{21} & \hat{A}_{22} & \hat{A}_{23} & \hat{A}_{24} \\ \hat{A}_{31} & \hat{A}_{32} & \hat{A}_{33} & \hat{A}_{34} \\ \hat{A}_{41} & \hat{A}_{42} & \hat{A}_{43} & \hat{A}_{44} \end{pmatrix} \begin{pmatrix} f_{r+1} \\ F_{r+1} \\ \theta_{r+1} \\ \theta_{p_{r+1}} \end{pmatrix} = \begin{pmatrix} R_1 \\ R_2 \\ R_3 \\ R_4 \end{pmatrix},$$

where each $\hat{A}_{ij}$ is of order $(\hat{N}+1) \times (\hat{N}+1)$, $f_{r+1}, F_{r+1}, \theta_{r+1}, \theta_{p_r+1}, R_1, R_2, R_3$, and R_4, are vectors of order $(\hat{N}+1) \times 1$.

4.4 Validation & Residual analysis

It is to be noted that the reduced similar equations (4.10)-(4.13) are coupled and highly nonlinear. Therefore, it becomes essential to validate the outcomes to trust the approximate solution obtained using SQLM framework. In order to arrive at a conclusion that the numerical technique used in the present work and the numerical computations are error-free, two important methodologies are used. Firstly, a comparison of the $-f''(0)$ values obtained for some particular values of parameters setting $f_0 = 2$ is made with the values obtained by Turkyilmazoglu [81]. This comparison is presented in Table 4.1 from which it is clearly visible that our results are in excellent agreement with the results of Turkyilmazoglu [81].

TABLE 4.1: Comparative values of $-f''(0)$. Present results are in parentheses.

	$l = 0.2$ $\beta = 0.02$	$l = 0.2$ $\beta = 0.5$	$l = 1$ $\beta = 0.02$	$l = 1$ $\beta = 0.5$
$M = 3$	3.23696(3.23695984)	3.25694(3.25693616)	3.24052(3.24052375)	3.33868(3.33868078)
$M = 5$	3.64651(3.64650531)	3.66352(3.66351940)	3.64952(3.64951919)	3.73352(3.73351790)

Secondly, in order to be sure of the fact that the generated iteration scheme converge, a residual analysis is also carried out. The solutions which are calculated by the spectral quasilinearization method (SQLM) are verified using a residual analysis of (4.10)-(4.13). The residuals of velocity and temperature profiles are presented in Figs. 4.2 and 4.3. Using 70 collocation points and 20 iterations. Figs. 4.2 and 4.3 illustrate that the residuals are reduced to $< 10^{-5}$ in just 20 iterations. Hence, the obtained results are trustworthy.

4.5 Results and Discussion

We now analyze the behavior of different physical quantities, such as fluid fluid and dust phase velocities, temperature of fluid and dust phases, coefficient of heat transfer, and Nusselt number emerging in the time-dependent hydromagnetic flow of a couple-stress dusty fluid along a permeable stretching surface. The impacts of permeability of the surface (f_0), fluid-particle interaction (β), magnetic field (M), unsteadiness parameter (α), couple-stress parameter (S), mass concentration of the dust particles (l), local fluid-interaction parameter (β_T), Eckert number (Ec), Prandtl number (Pr), and space and temperature dependent heat generation/absorption coefficients (A^*) and (B^*), respectively are analyzed in this section. To examine the influence of these parameters, the velocity profiles and temperature profiles are presented in Fig. 4.4-4.15 while the numerical values of Cf_x and Nu_x are shown in Table 4.2. For numerical computations, default values of the non-dimensional parameter are taken to be $\alpha = 0.01,\ \beta = 1,\ f_0 = 1,\ l = 1,\ M = 3,\ S = 0.01,\ A^* = 0.3,\ B^* = 0.3,\ \beta_T = 0.5,\ Ec = 0.2,\ \gamma = 0.1,\ Pr = 1.$

The impacts of α on the velocity and temperature profiles of both the phases are presented in Fig. 4.4. The parameter α is measuring the influence of unsteadiness on the model. It is easy to see that the velocity distributions for both phases decrease for rising values of the unsteadiness parameter. The fluid and dust phase temperature profiles fall with increasing values of α. Physically, it seems that the cooling rate is high for higher values of α, i.e., for the time-dependent flows. The thermal and momentum boundary layers for both cases get thicker here.

The effects of β, the fluid-particle interaction parameter, on the velocity and temperature fields of both the phases are shown graphically in Fig. 4.5. It is visible that larger values of β lead to a decrease in $f'(\eta)$, i.e., the fluid velocity profile. This happens as a result of the increased frictional forces due to higher fluid-particle interaction. Apart from this, larger values of β cause an increase in the dust phase's velocity profile $F'(\eta)$. Both the temperature fields, $\theta(\eta)$ and $\theta_p(\eta)$, are found to be increasing with increasing fluid-particle interaction measure with an increase in β. It is due to the fact that the increase in β increases the interaction time between the fluid and dust particles, and hence higher the value of β longer the fluid stays in contact with the dust particles causing an increase in the fluid temperature.

The impact of suction parameter f_0 on the velocity and temperature distributions for both the fluid and dust phases is visible in Fig. 4.6. It is noticed that increasing the suction parameter f_0 decreases the velocity distributions for the fluid and dust phases. Similar behavior is found in temperature profiles where both the temperature distributions begin to fall monotonically with increasing suction velocity from the sheet's surface. Also, we can observe that the fluid phase temperature $\theta(\eta)$ is higher than the dust phase temperature $\theta_p(\eta)$ in the boundary layer region. This implies a transfer of heat from the fluid phase to the dust phase, and hence dust particles can be utilized as cooling agents in the boundary layer flow of a couple-stress fluid.

The influence of mass concentration of the dust particles is measured by the parameter l, and this effect is visible through Fig. 4.7. Figure 4.7 depicts that the profiles of $f'(\eta)$ and $F'(\eta)$ get decreased for increasing values of l. Similarly, the fluid and dust phase temperature fall for increasing values of dust concentration l. However, near the surface, the temperature of fluid phase $\theta(\eta)$ increase for increasing the mass concentration of dust particles l. This behavior is due to the higher thermal energy of the dust particles due to collisions near the surface where the fluid experiences more viscous forces. Therefore, it is apparent that the momentum and thermal boundary layers get thinner with increasing dust particles in the fluid.

Fig. 4.8 displays the behavior of velocity and temperature profiles for the fluid and dust phases due to the variations in the values of the magnetic parameter M. The influence of the presence of the Lorentz force in the flow field arising due to the magnetic field $B(t)$ can be seen through the varying value of the magnetic parameter M. It is observed that the curves of velocity profiles $f'(\eta)$ and $F'(\eta)$ fall for increment in the values of M. Besides this, enhancement in both temperature fields is observed for rising values of M. The reason behind this is the increment in Lorentz force which occurs due to increasing M. Thus, it follows that the resistive force appearing in the flow field due to the presence of a magnetic field tends to retard the fluid and dust phase velocities, while

the resulting force enhances the fluid and dust phase temperatures within the boundary layer.

The behavior of velocity profiles and temperature distributions for the fluid and dust phases, with respect to the varying values of the couple-stress parameter S, is presented in Fig. 4.9. It is analyzed that, near to the surface, an increment in couple stress parameter S increases the velocity for both the phases whereas, away from the surface, the velocity profiles decrease with increment in the S. Since the fluid's viscosity increases with increasing couple-stress in the fluid, the fluid and dust velocities get reduced. Temperatures in both cases fall with increasing the couple stress parameter. It is also easy to see that the fluid temperature $\theta(\eta)$ is higher than the dust phase temperature $\theta_p(\eta)$.

The impact of space-dependent and temperature-dependent heat generation/absorption on the temperature profiles of fluid and dust phases $\theta(\eta)$ and $\theta_p(\eta)$ is investigated with the help of the parameters A^* and B^* and are presented in Fig. 4.10 and 4.11, respectively. From Fig. 4.10, it is clear that the thermal energy in the boundary layer increases with increasing $A^*(> 0)$ (heat generation) and decreases with increasing $A^*(< 0)$ (heat absorption). The thermal energy thus generated/absorbed results in the temperature profiles for both the fluid and dust phases to rise with enhancement in heat generation and fall with increment in heat absorption. Similarly, 4.11 represents that energy is generated for increasing values of $B^*(> 0)$ which results in the rise in temperature, whereas energy is absorbed for increasing values of $B^*(< 0)$ which results in the fall in temperature within the boundary layer.

Figures 4.12- 4.14 represent the distributions of both the fluid and dust temperature fields for varying values of local fluid-interaction parameter β_T, Eckert number Ec, and specific heat parameter γ, respectively. It is visible from these figures that the fluid temperature $\theta(\eta)$ falls for an increment in the values of the local fluid-interaction parameter for temperature β_T and specific heat parameter γ. Besides, the temperature rises for growing values of Ec. Due to the consideration of the dissipative term in the energy equation, the temperature field is experiencing the influence of viscous forces, and the resistive frictional force contributes to the rise of the fluid and dust phase temperatures. With an increase in the value of the local fluid-interaction parameter, the interaction between the fluid and dust particles with respect to the distribution of temperature increases. As a result, the temperature of the dust phase decreases. The temperature of the dust phase gets increased with an increase in the specific heat parameter.

Fig. 4.15 represents the impact of varying values of Pr on $\theta(\eta)$ and $\theta_p(\eta)$ curves. It is observed that a rise in the value of Pr decreases the thermal diffusivity, which causes a fall in the temperature fields and the thermal boundary layer gets thinner. We

know that Pr is the proportion of viscous diffusion to thermal diffusion, and hence it is concluded that the high value of viscous diffusion tends to reduce the fluid temperature. In contrast, a lower value of thermal diffusion causes a fall in the fluid temperature within the boundary layer area.

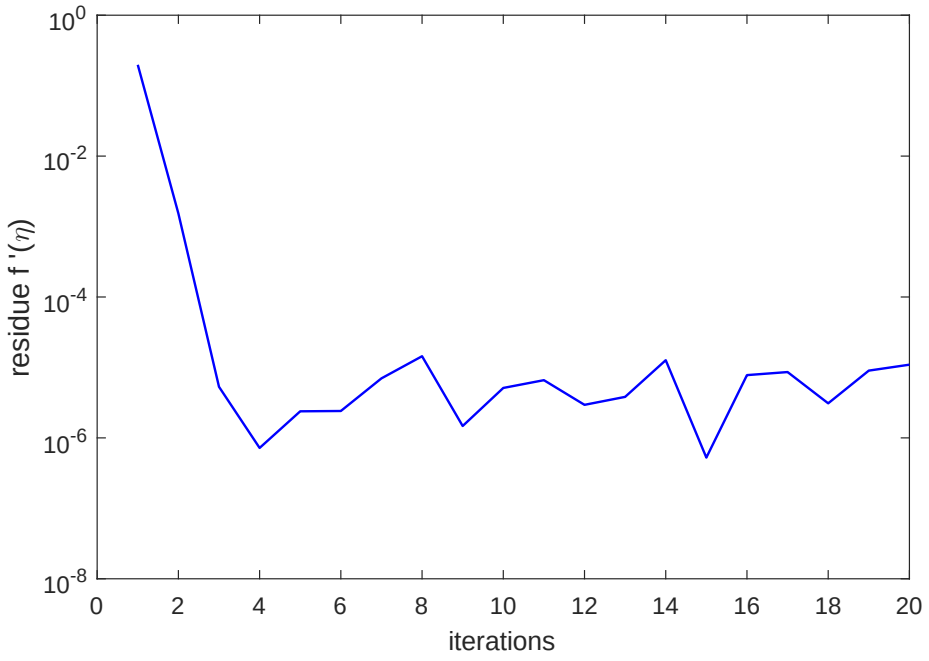

(a)

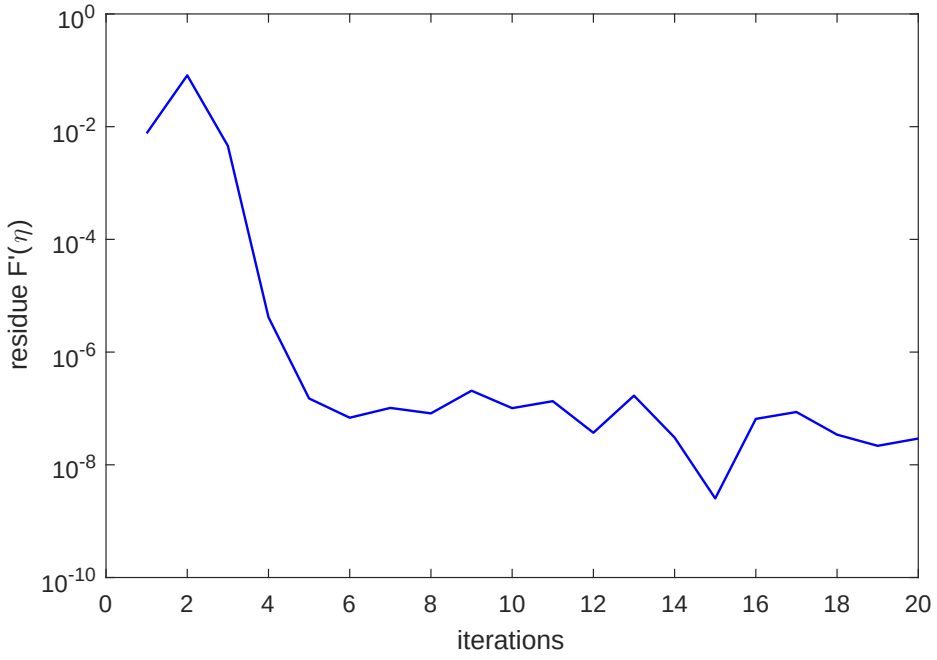

(b)

FIGURE 4.2: Residuals in $f'(\eta)$ and $F'(\eta)$

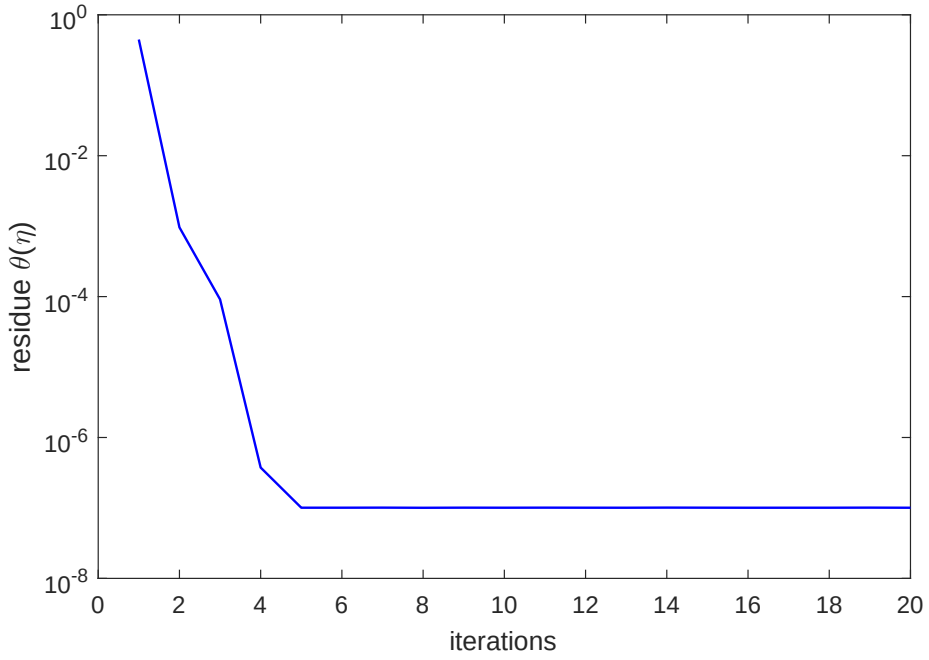

(a)

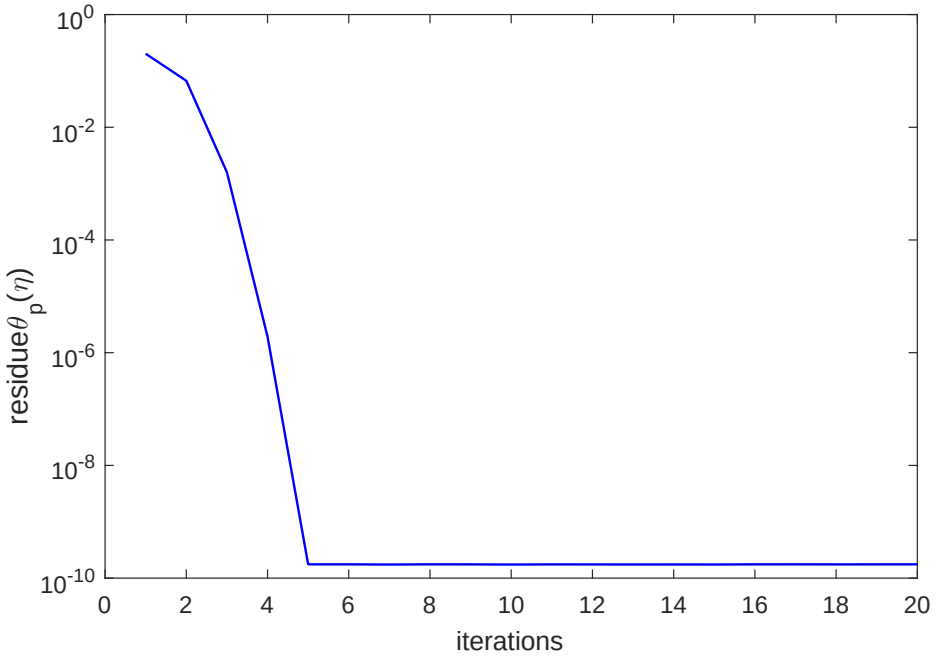

(b)

FIGURE 4.3: Residuals in $\theta(\eta)$ and $\theta_p(\eta)$

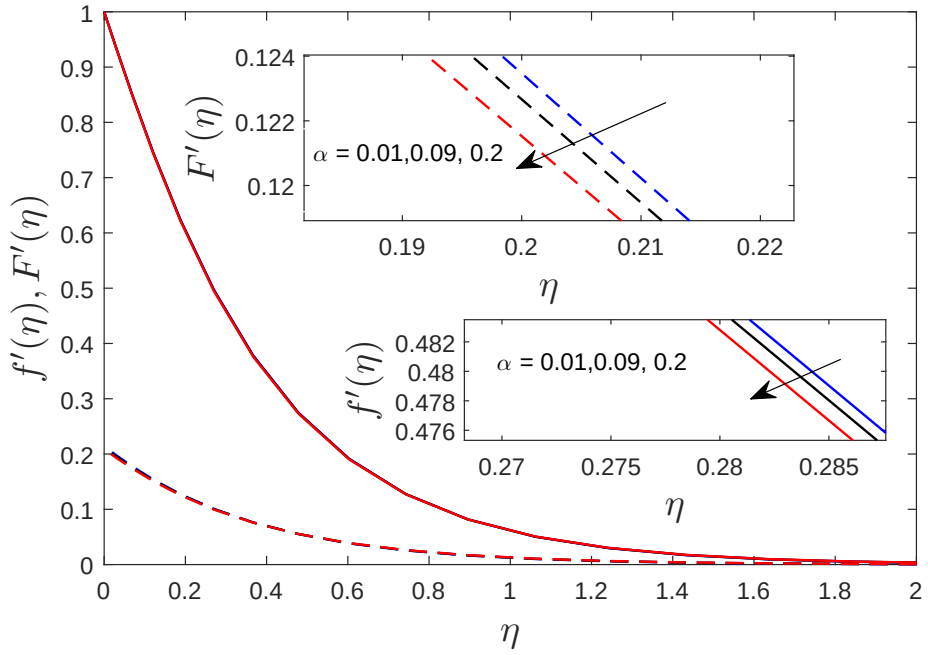

(a)

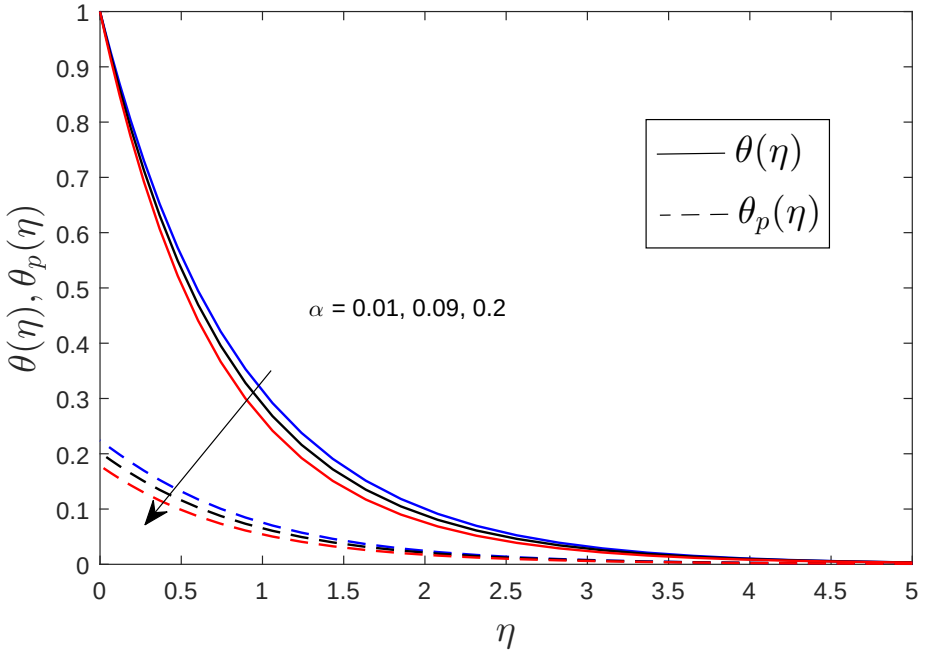

(b)

FIGURE 4.4: Profiles of (a) $f'(\eta)$ and $F'(\eta)$, (b) $\theta(\eta)$ and $\theta_p(\eta)$ for varying values of α when $\beta = 1,\ f_0 = 1,\ l = 1,\ M = 3,\ S = 0.01,\ A^* = 0.3,\ B^* = 0.3,\ \beta_T = 0.5,\ Ec = 0.2,\ \gamma = 0.1,\ Pr = 1$

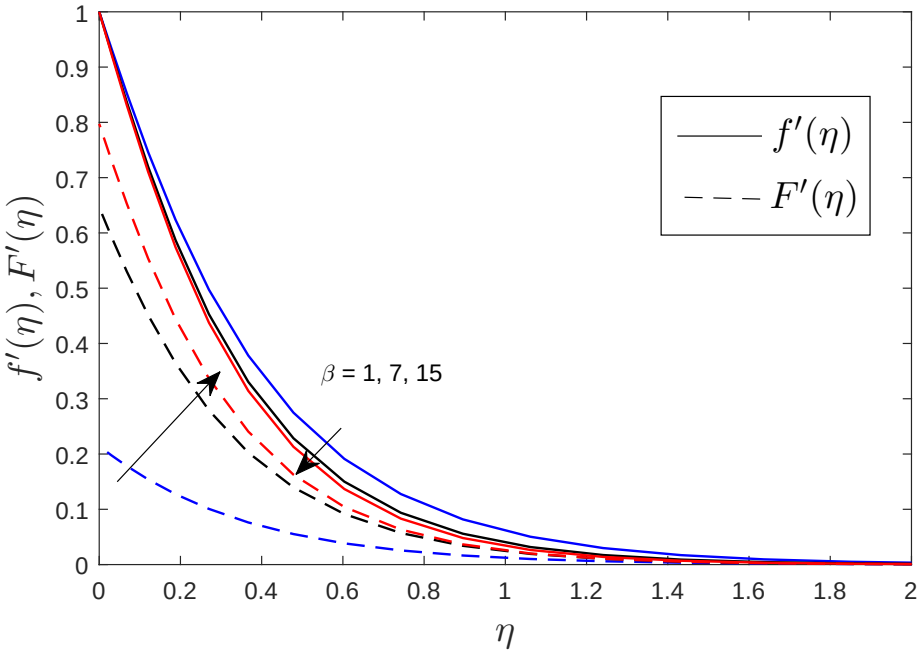

(a)

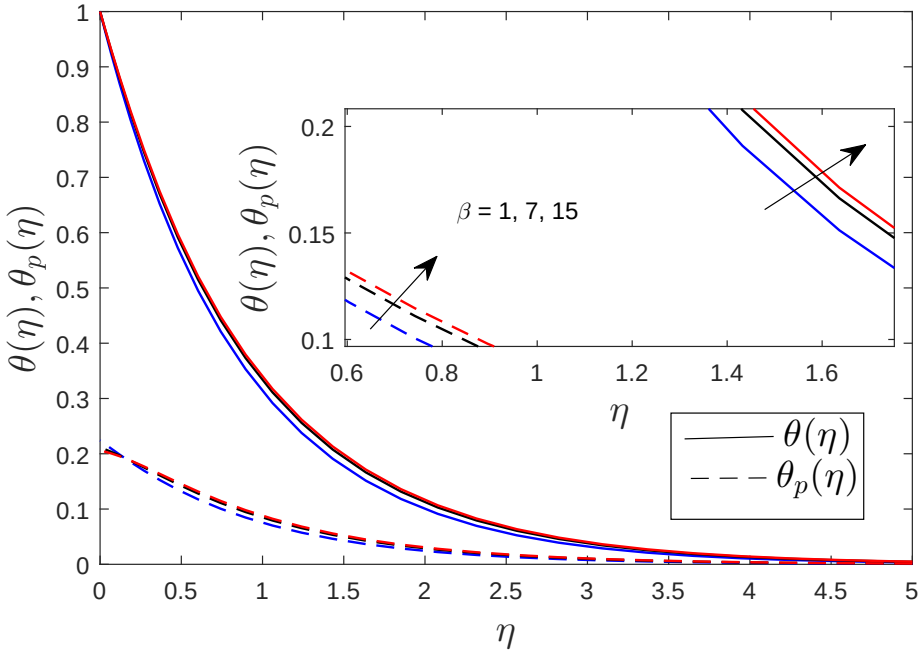

(b)

FIGURE 4.5: Profiles of (a) $f'(\eta)$ and $F'(\eta)$, (b) $\theta(\eta)$ and $\theta_p(\eta)$, varying values of β when $\alpha = 0.01$, $f_0 = 1$, $l = 1$, $M = 3$, $S = 0.01$, $A^* = 0.3$, $B^* = 0.3$, $\beta_T = 0.5$, $Ec = 0.2$, $\gamma = 0.1$, $Pr = 1$

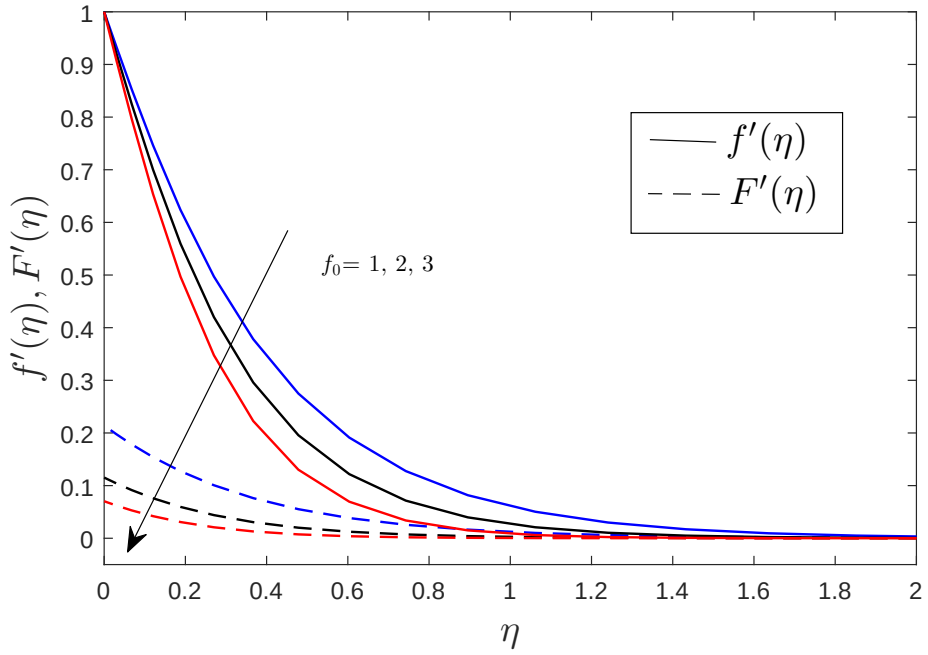

(a)

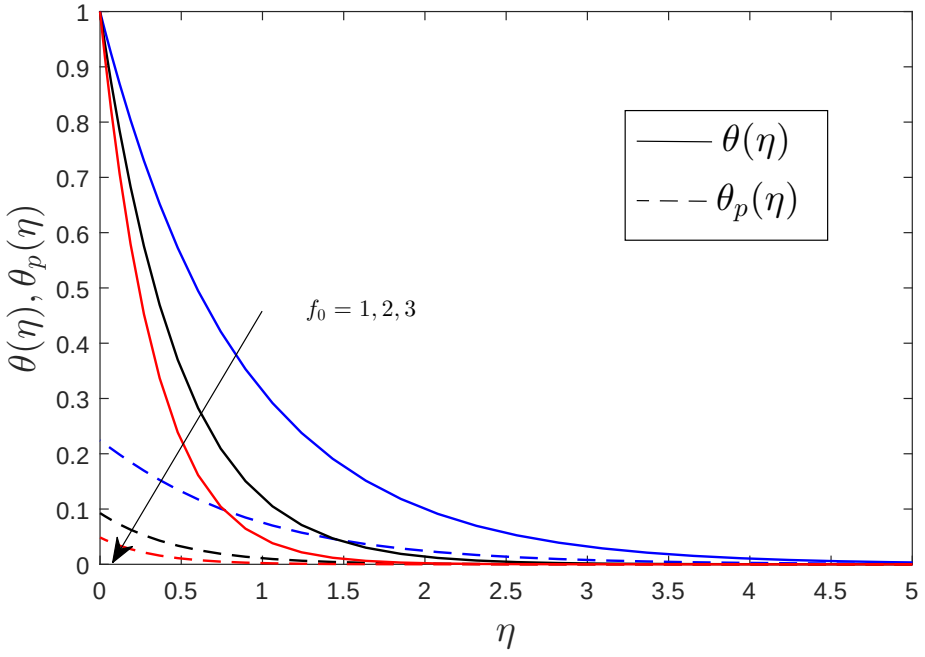

(b)

FIGURE 4.6: Profiles of (a) $f'(\eta)$ and $F'(\eta)$, (b) $\theta(\eta)$ and $\theta_p(\eta)$, varying values of f_0 when $\alpha = 0.01,\ \beta = 1,\ l = 1,\ M = 3,\ S = 0.01,\ A^* = 0.3,\ B^* = 0.3,\ \beta_T = 0.5,\ Ec = 0.2,\ \gamma = 0.1,\ Pr = 1$

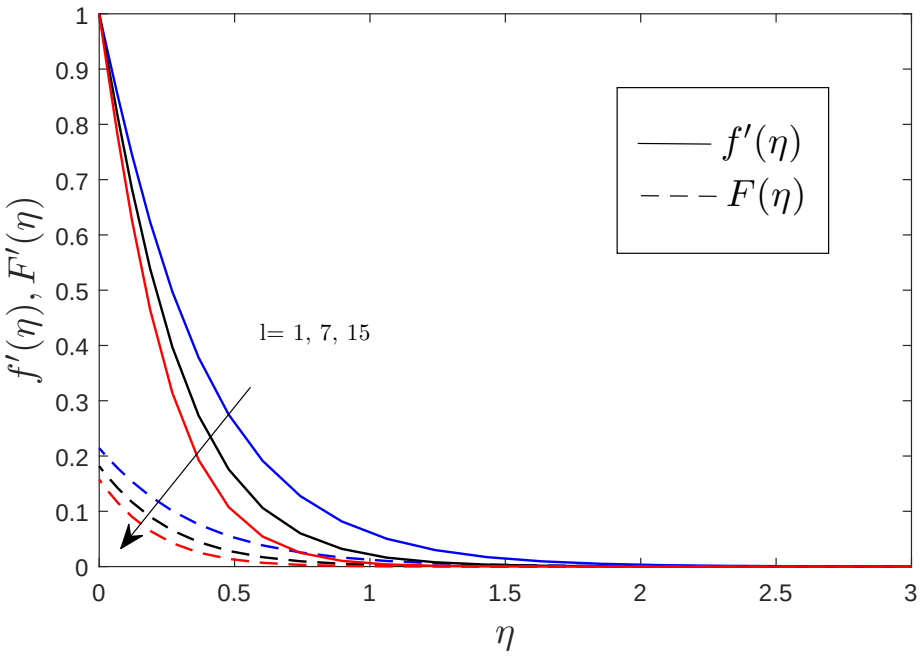

(a)

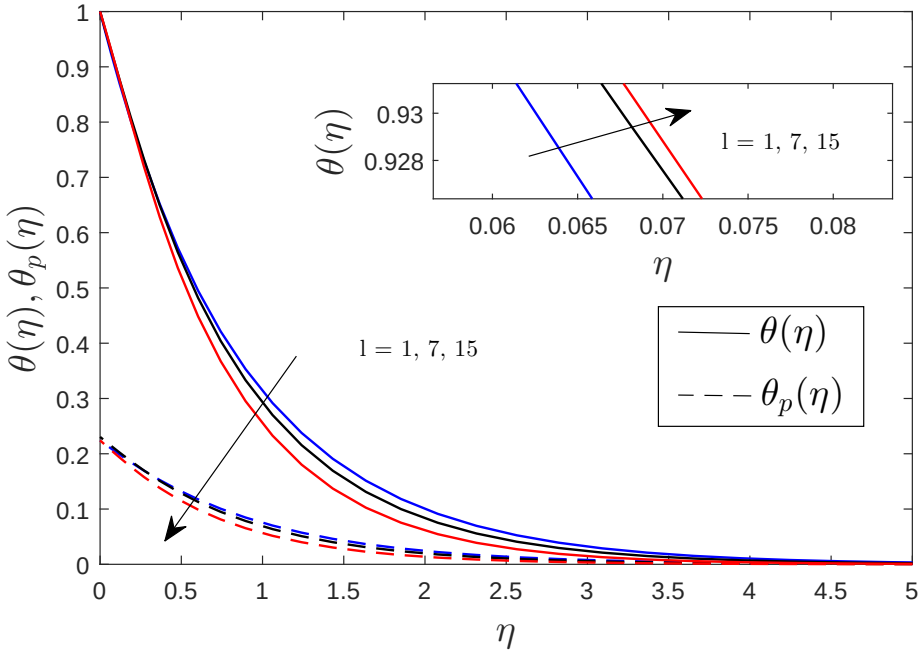

(b)

FIGURE 4.7: Profiles of (a) $f'(\eta)$ and $F'(\eta)$, (b) $\theta(\eta)$ and $\theta_p(\eta)$ for varying values of l when $\alpha = 0.01$, $f_0 = 1$, $\beta = 1$, $M = 3$, $S = 0.01$, $A^* = 0.3$, $B^* = 0.3$, $\beta_T = 0.5$, $Ec = 0.2$, $\gamma = 0.1$, $Pr = 1$

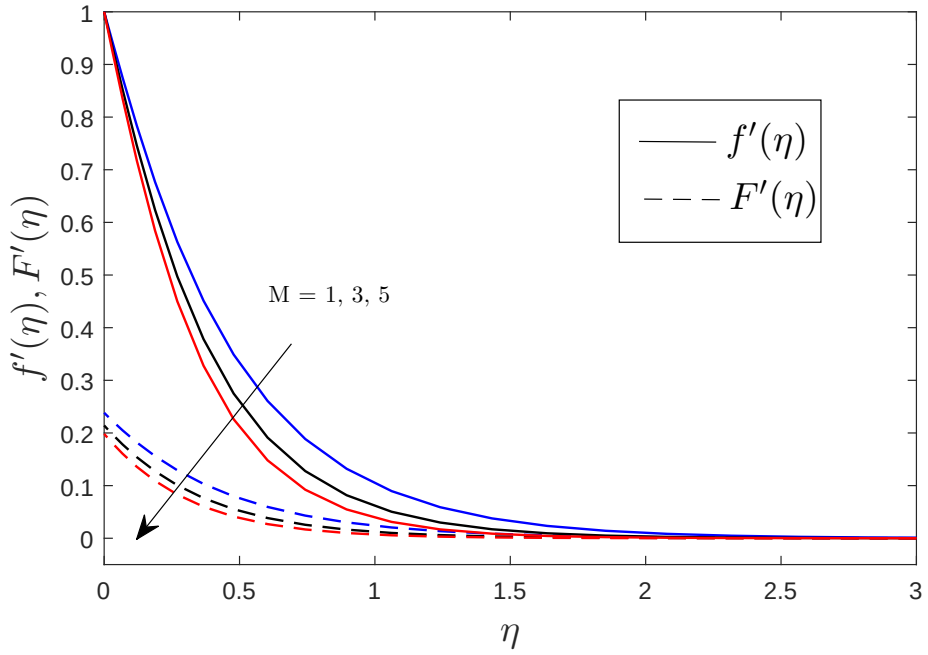

(a)

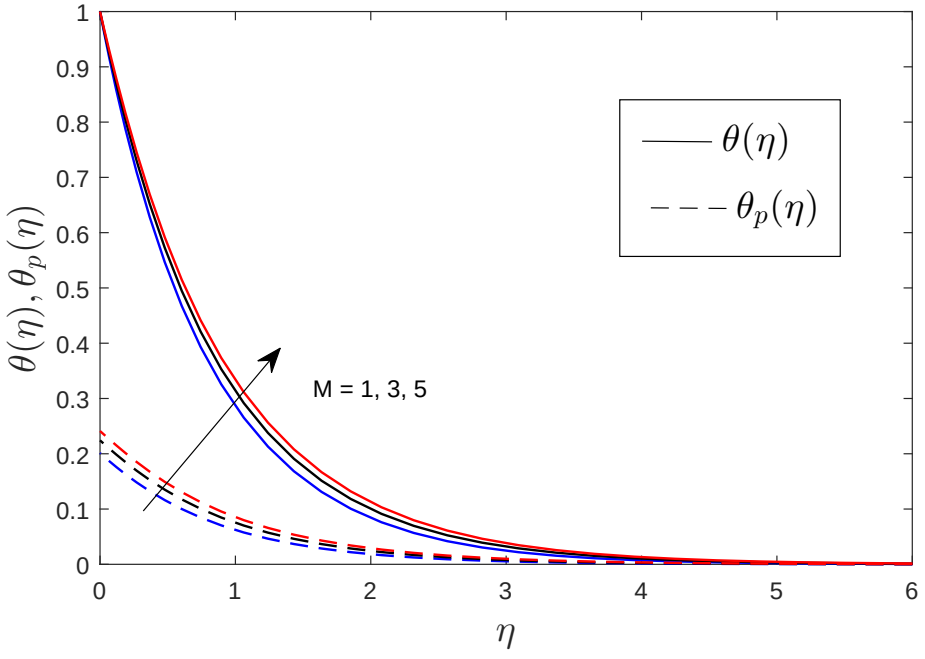

(b)

FIGURE 4.8: Profiles of (a) $f'(\eta)$ and $F'(\eta)$, (b) $\theta(\eta)$ and $\theta_p(\eta)$, varying values of M when $\alpha = 0.01,\ f_0 = 1,\ l = 1,\ \beta = 1,\ S = 0.01,\ A^* = 0.3,\ B^* = 0.3,\ \beta_T = 0.5,\ Ec = 0.2,\ \gamma = 0.1,\ Pr = 1$

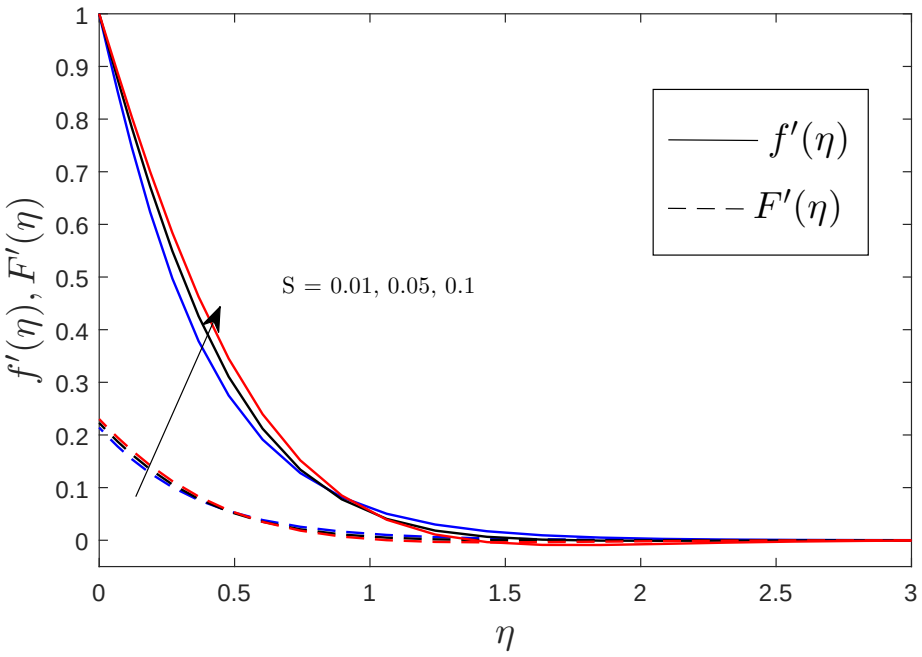

(a)

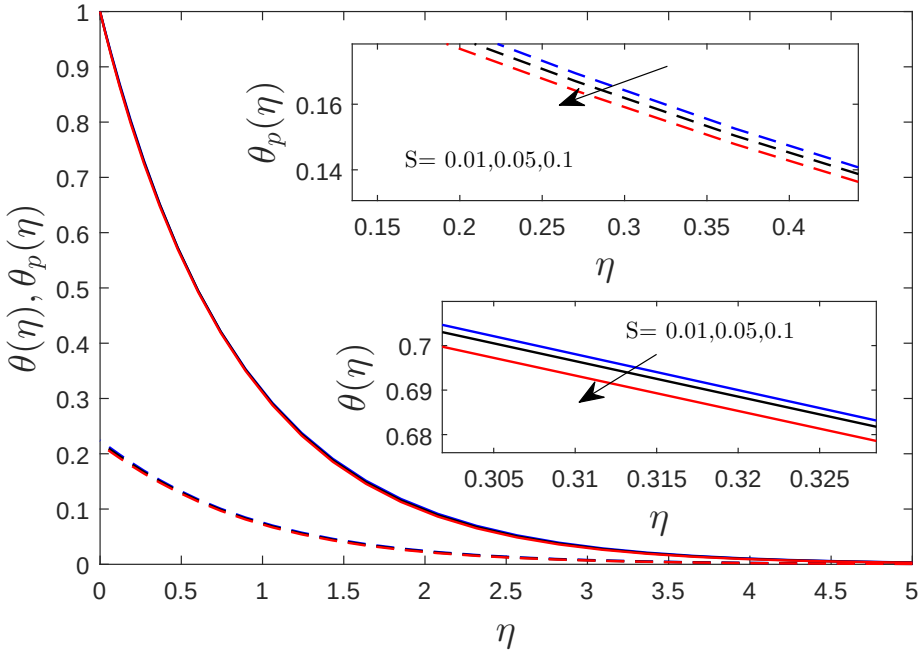

(b)

FIGURE 4.9: Profiles of (a) $f'(\eta)$ and $F'(\eta)$, (b) $\theta(\eta)$ and $\theta_p(\eta)$, varying values of S when $\alpha = 0.01,\ f_0 = 1,\ l = 1,\ M = 3,\ \beta = 1,\ A^* = 0.3,\ B^* = 0.3,\ \beta_T = 0.5,\ Ec = 0.2,\ \gamma = 0.1,\ Pr = 1$

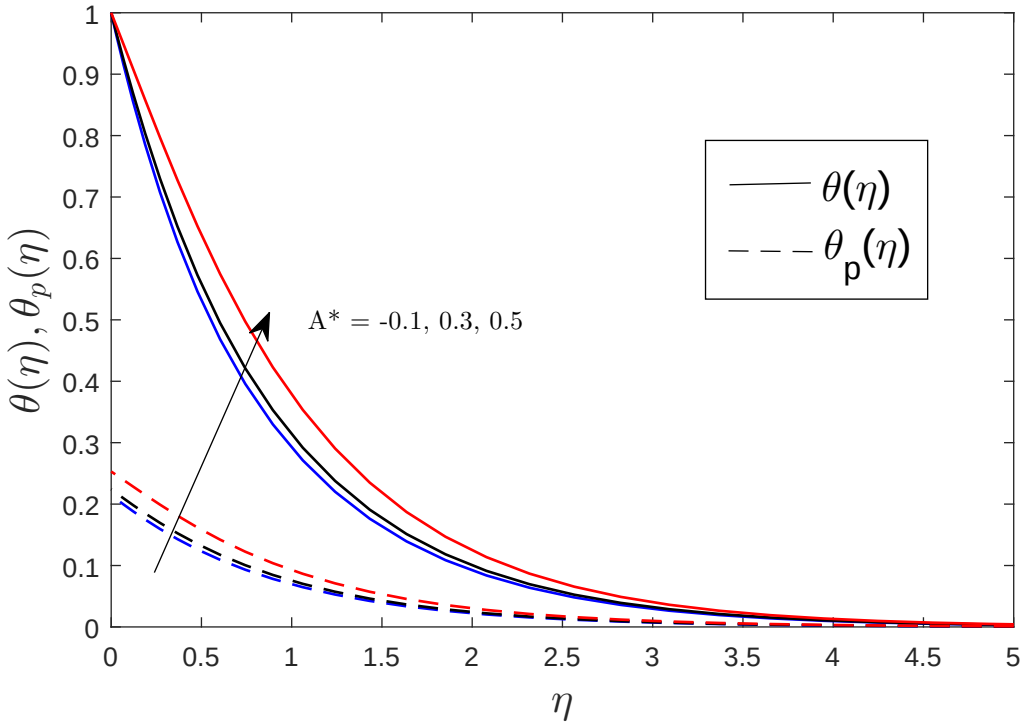

FIGURE 4.10: Profiles of $\theta(\eta)$ and $\theta_p(\eta)$ for varying values of A^* when $\alpha = 0.01,\ f_0 = 1,\ l = 1,\ M = 3,\ S = 0.01,\ \beta = 1,\ B^* = 0.3,\ \beta_T = 0.5,\ Ec = 0.2,\ \gamma = 0.1,\ Pr = 1$

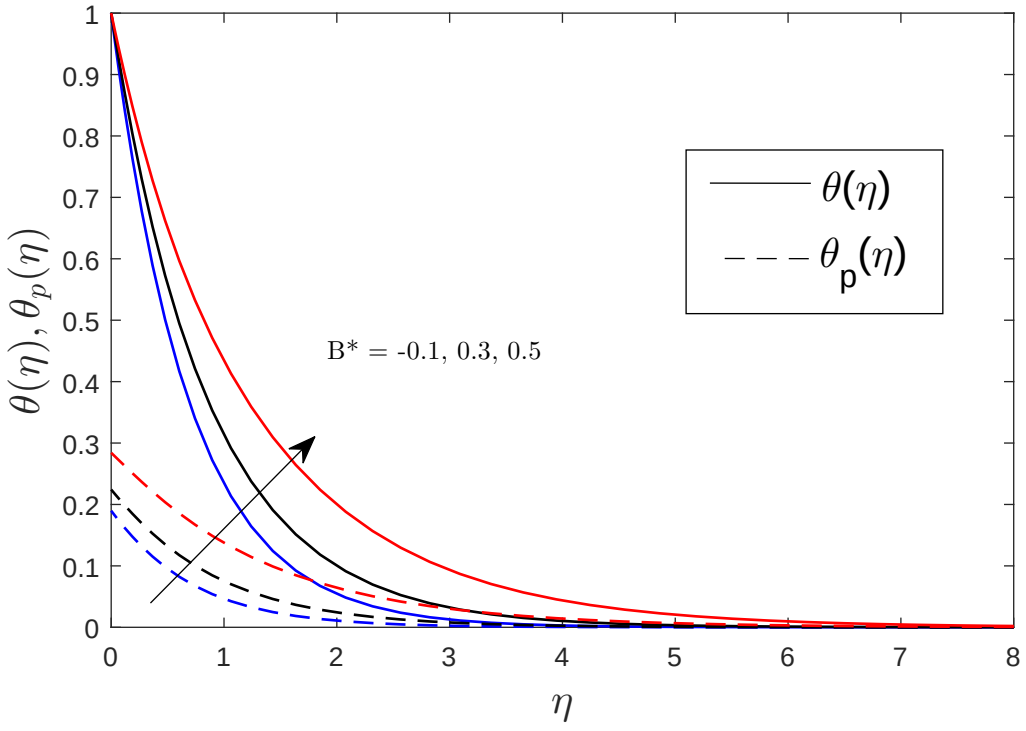

FIGURE 4.11: Profiles of $\theta(\eta)$ and $\theta_p(\eta)$, varying values of B^* when $\alpha = 0.01,\ f_0 = 1,\ l = 1,\ M = 3,\ S = 0.01,\ A^* = 0.3,\ \beta = 1,\ \beta_T = 0.5,\ Ec = 0.2,\ \gamma = 0.1,\ Pr = 1$

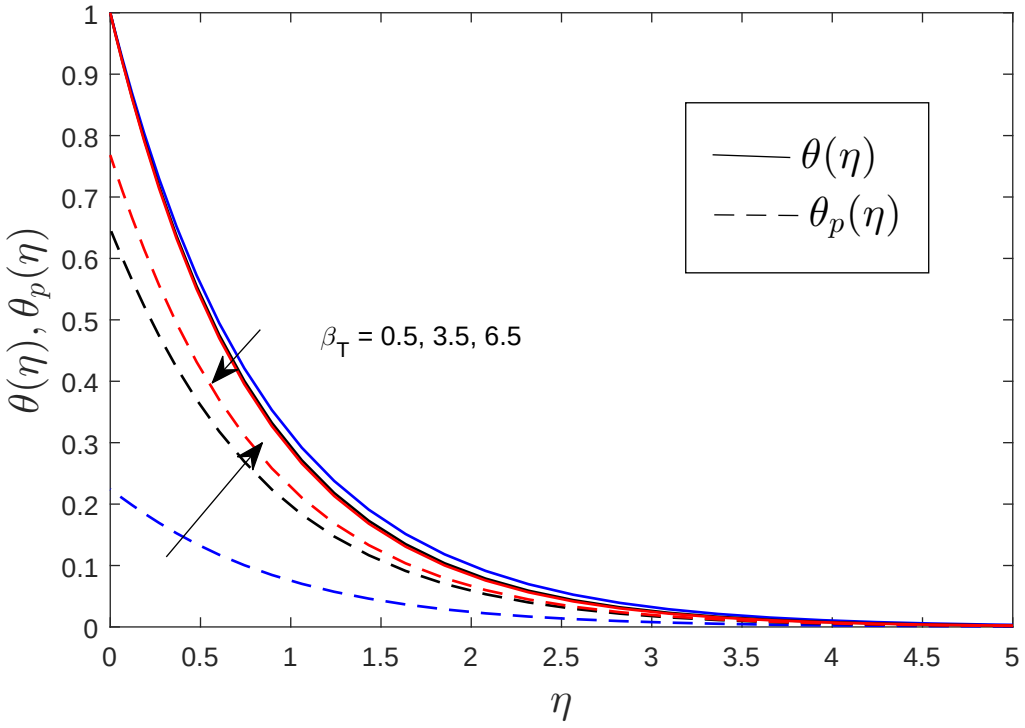

FIGURE 4.12: Profiles of $\theta(\eta)$ and $\theta_p(\eta)$, varying values of β_T when $\alpha = 0.01,\ f_0 = 1,\ l = 1,\ M = 3,\ S = 0.01,\ A^* = 0.3,\ B^* = 0.3,\ \beta = 1,\ Ec = 0.2,\ \gamma = 0.1,\ Pr = 1$

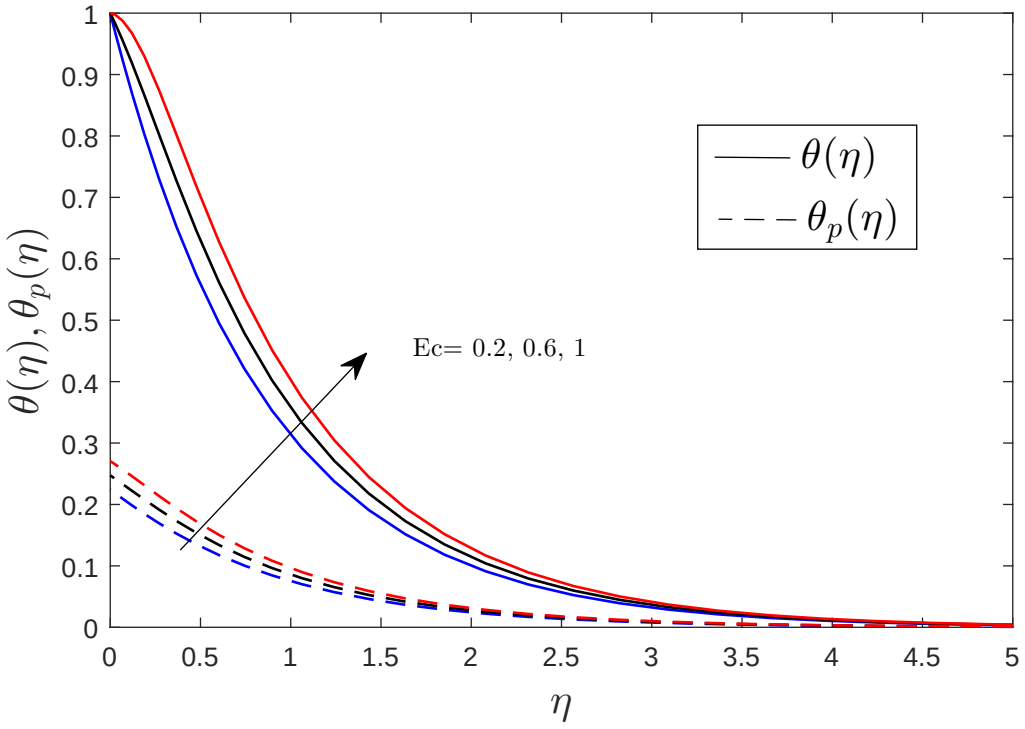

FIGURE 4.13: profiles of $\theta(\eta)$ and $\theta_p(\eta)$, varying values of Ec when $\alpha = 0.01,\ f_0 = 1,\ l = 1,\ M = 3,\ S = 0.01,\ A^* = 0.3,\ B^* = 0.3,\ \beta_T = 0.5,\ \beta = 1,\ \gamma = 0.1,\ Pr = 1$

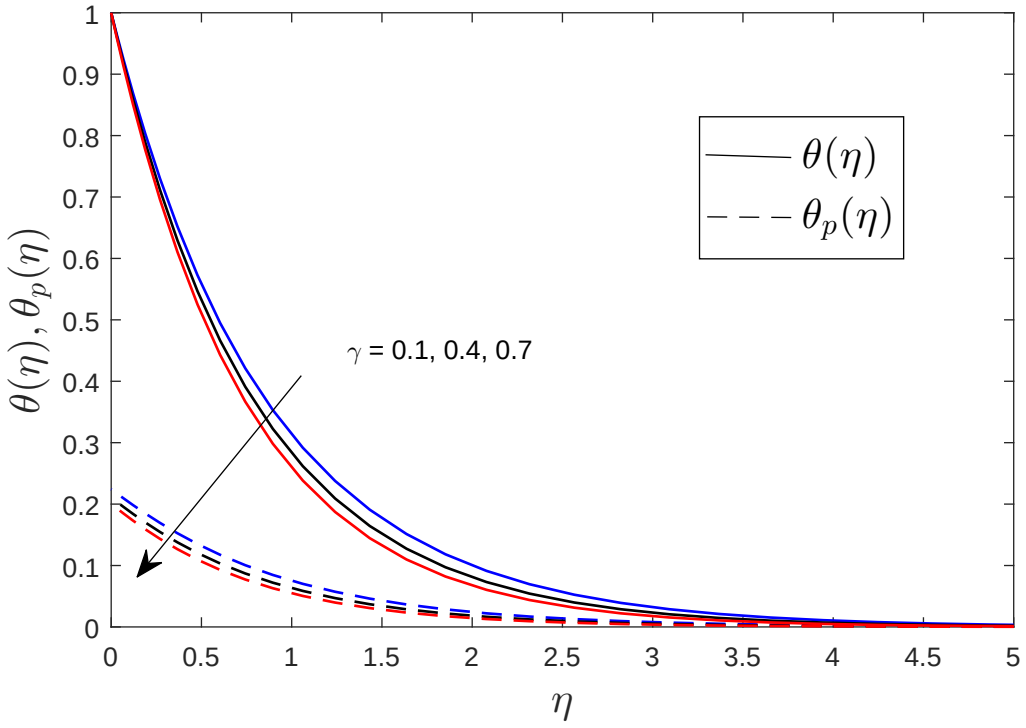

FIGURE 4.14: Profiles of $\theta(\eta)$ and $\theta_p(\eta)$, varying values of γ when $\alpha = 0.01$, $f_0 = 1$, $l = 1$, $M = 3$, $S = 0.01$, $A^* = 0.3$, $B^* = 0.3$, $\beta_T = 0.5$, $Ec = 0.2$, $\beta = 1$, $Pr = 1$

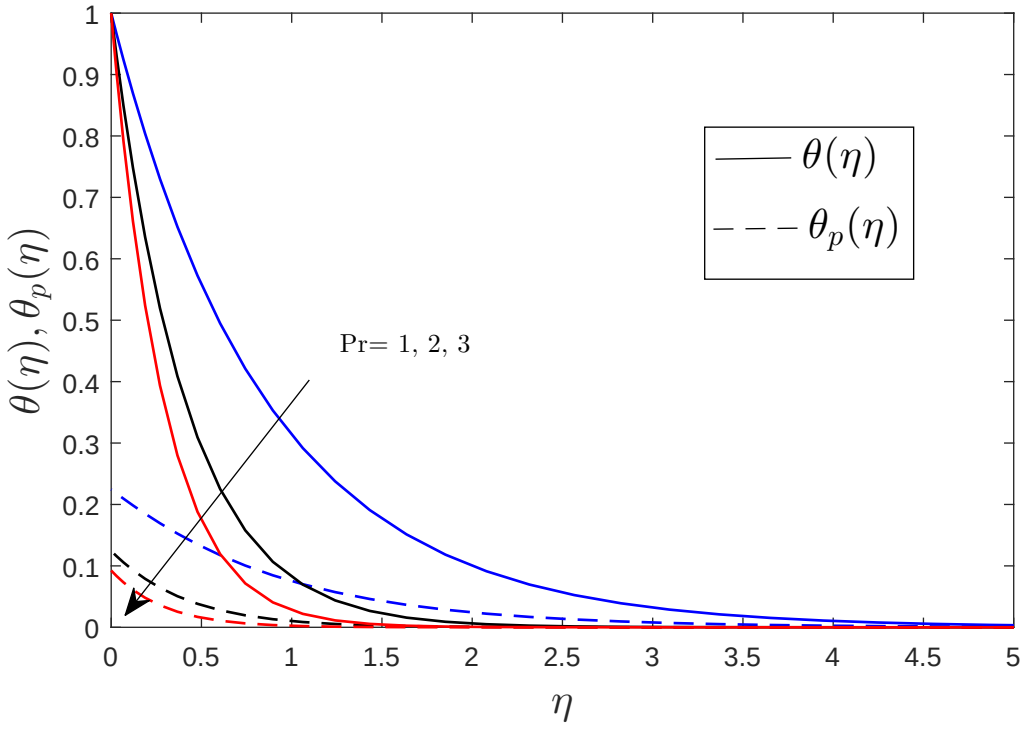

FIGURE 4.15: Profiles of $\theta(\eta)$ and $\theta_p(\eta)$, varying values of Pr when $\alpha = 0.01$, $f_0 = 1$, $l = 1$, $M = 3$, $S = 0.01$, $A^* = 0.3$, $B^* = 0.3$, $\beta_T = 0.5$, $Ec = 0.2$, $\gamma = 0.1$, $\beta = 1$

TABLE 4.2: The values of $C_{fx}Re_x^{1/2}$ and $Re_x^{-1/2}Nu_x$r for varying values of parameters.

α	β	f_0	l	M	S	A^*	B^*	β_T	Ec	γ	Pr	$-C_{fx}Re_x^{1/2}$	$Re_x^{-1/2}Nu_x$
0.01	1	1	1	3	0.01	0.3	0.3	0.5	0.2	0.1	1	2.78983158	1.16540568
0.09												2.80269929	1.25754416
0.2												2.82035563	1.36961684
	1											2.78983158	1.16540568
	7											3.18339809	1.06604539
	15											3.32171011	1.04261028
		1										2.78983158	1.16540568
		2										3.47220351	1.99999271
		3										4.22524619	2.85402081
			1									2.78983158	1.16540568
			7									3.77005440	1.04358974
			15									4.82187298	0.97596093
				1								2.26310856	1.28931028
				3								2.78983158	1.16540568
				5								3.22220440	1.07059158
					0.01							2.78983158	1.16540568
					0.05							2.89230394	1.20591393
					0.1							2.97859116	1.23728270
						-0.1						2.78983194	1.30446474
						0.3						2.78983158	1.16540568
						1.5						2.78983185	0.74822848
							-0.1					2.78983155	1.43420088
							0.3					2.78983158	1.16540568
							0.5					2.78983187	0.88711877
								0.5				2.78983158	1.16540568
								3.5				-2.78983176	1.22879162
								6.5				2.78983194	1.24641086
									0.2			2.78983158	1.16540568
									0.6			2.78983169	0.60702615
									1			2.78983198	0.04864661
										0.1		2.78983158	1.16540568
										0.4		2.78983147	1.25784228
										0.7		2.78983158	1.33888901
											1	2.78983158	1.16540568
											2	2.78983177	2.41235727
											3	2.78983185	3.45613420

To study the effect of varying values of non-dimensional parameters on the significant physical quantities such as the skin-friction coefficient and local Nusselt number, the numerical values of Cf_x and Nu_x are presented in numerical form in Table 4.2. It is worthy to note that the skin-friction coefficient C_{f_x} is mainly influenced by α (the unsteadiness parameter), β (interaction parameter), f_0 (suction parameter), l (concentration of dust particles), M (magnetic parameter), and S (the couple-stress parameter). It is found that the skin-friction coefficient gets increased with increasing values of all these parameters, which implies that the shear stress at the surface of the porous sheet is enhanced with these parameters. All the other flow parameters have almost no influence on the skin-friction coefficient as the variation only appears after the six decimal digits with respect to these parameters. On the other hand, the heat transfer coefficient is significantly influenced by all the physical quantities for which variations are shown in Table 4.2. It is to be noted that with the rising values of suction, the momentum of the fluid and dust phases from the surface increases also causing the thermal energy reduction with the removal of the fluid from the system. This causes the fluid velocity as well as temperature to decrease within the boundary layer. The decrease in the temperature is due to the removal of thermal energy from the porous sheet causing an increase in rate of heat transfer. The unsteadiness parameter, couple-stress parameter, the fluid-interaction parameter for temperature (β_T), specific heat parameter (γ), and the Prandtl number (Pr) has increasing influence on the coefficient of heat transfer from the surface. It follows from these results that the unsteadiness, the fluid couple-stress, temperature fluid interaction, specific heat, and momentum diffusivity tend to increase the heat transfer rate from the surface. The coefficient of heat transfer $Re_x^{-1/2}Nu_x$ is inversely affected by the applied magnetic field, concentration of dust particles, interaction of fluid and dust particles, space and temperature-dependent heat generation/absorption, and the dissipation caused due to viscous frictional forces.

4.6 Conclusions

The combined effects of several factors such as the non-uniform heat source/sink, viscous dissipation, magnetic field, and suction velocity at the surface are investigated successfully for the unsteady two-phase flow of a dusty couple-stress fluid along a stretching surface using the SQLM numerical scheme. The significant findings of the study are

1. Temperature distributions for both liquid and dust phases are enhanced by the magnetic field effect. The coefficient of skin-friction in the x direction falls with an increment in the values of the magnetic field parameter. The magnetic field tends to reduce the heat transfer rate at the surface.

2. Fluid velocities in both the phases decrease with increased values of the suction parameter f_0. The skin-friction in the x direction decreases with increased values of the suction parameter. The rate of heat transfer at the surface tends to become higher with the higher value of the suction parameter. The skin-friction coefficient is also increased with increasing the unsteadiness in the flow-field, interaction between the fluid and dust particles, concentration of dust particles, and the couple-stress of the fluid.

3. An increment in the value of Pr decreases the thermal diffusivity. Due to this, there is a fall in temperature distributions and thermal boundary layer thickness. The unsteadiness, fluid-suction through the wall of the sheet, the fluid couples-stress, temperature fluid interaction, and specific heat tend to increase the rate of heat transfer from the surface whereas the applied magnetic field, concentration of dust particles, interaction of fluid and dust particles, space and temperature dependent heat generation/absorption, and the dissipation caused due to viscous frictional forces show reverse influence on this.

Chapter 5

Entropy Generation Analysis of Magnetohydrodynamic Stagnation Point Flow of a Casson Fluid with Radiative and Dissipative Heat Transfer and Hall Effects

5.1 Introduction

The phenomenon of heat transfer is prevalent in the industrial area due to its vast range of applications. However, in all the earlier studies, the discussion of heat transfer problems is limited to the analysis of the first law of thermodynamics only, which deals with energy conservation. It is just restricted to the quantity of energy, not to the quality of energy. From the first law of thermodynamics, there is no difference between the work (high-grade energy) and the heat (low-grade energy). A measurement of the degree of randomness of energy in a system is known as entropy. It is unavailable for doing useful

Contents of this chapter has been communicated to Journal of Applied Fluid Mechanics [Prashu, R. Nandkeolyar, V. Sangwan, Entropy Generation and Regression Analysis of Magnetohydrodynamic Stagnation Point Flow of a Casson Fluid with Radiative and Dissipative Heat Transfer and Hall Effects, Journal of Applied Fluid Mechanics (Communicated)]

work because work takes place only from ordered molecular motion. Even though many boundary layer models exist in the literature to examine the flow and heat transfer of various fluids along a stretching surface, they have not yet been used at their maximum ability. The main motive of the current research is to discuss entropy generation or its minimization during heat transfer. It was Bejan [90, 91] who initially discussed the phenomena of entropy generation in applied thermal engineering. Rashidi et al. [92] examined the entropy generation analysis for a stagnation point flow over a porous stretching surface considering the existence of heat generation/absorption effects. The entropy generation and minimization analysis of a viscous incompressible fluid along a stretching surface with the frictional and Joule heating terms were investigated by Khan et al. [93]. Aziz and Afify [94] formulated a mathematical model for the entropy generation of Casson fluid over a stretching surface considering the Hall and magnetic field effects. They concluded that a large value of the magnetic parameter enhances the entropy generation; on the other hand, the Hall current parameter reduces it. Some literature relevant to entropy generation is reported in the articles ([115], [95], [96],[97]).

In the current chapter, we present an entropy generation analysis for the transient three-dimensional hydromagnetic stagnation point flow of a Casson fluid over a stretching sheet in the presence of Hall current, viscous dissipation, and nonlinear radiative heat transfer. The mathematical model of the problem is presented as a set of nonlinear PDEs subjected to similarity transformations to convert into a set of ODEs. An efficient numerical method, namely SQLM, is used to obtain the mathematical model's approximate solutions. The expressions of Bejan number, volumetric entropy generation rate, skin-friction, and Nusselt number are also derived. A parametric study involving the emerging physical variables is performed to analyze the effects of relevant flow parameters on the fluid velocity, fluid temperature, Bejan number, entropy generation number, skin-friction, and heat transfer coefficients.

5.2 Mathematical Formulation

Consider the transient three-dimensional hydromagnetic flow of Casson fluid along a stretching sheet near a stagnation point. It is assumed that the surface is placed in the $y = 0$ plane. The sheet-surface is stretched with velocity $u = u_w(x,t) = \frac{bx}{1-\gamma t}$ in x - direction, whereas the free-stream velocity along x - direction is $u_e = \frac{ax}{1-\gamma t}$. A time-dependent magnetic field $B(t) = B_0(1-\gamma t)^{-1/2}$ is applied in a direction normal to the plane of the sheet-surface. It is assumed that the fluid has a considerably small magnetic Reynolds number so that the induced magnetic field is negligible in comparison

the applied magnetic field, see Fig. 5.1. Hall current, viscous dissipation and the thermal radiation are assumed to be affecting the flow and heat transfer.

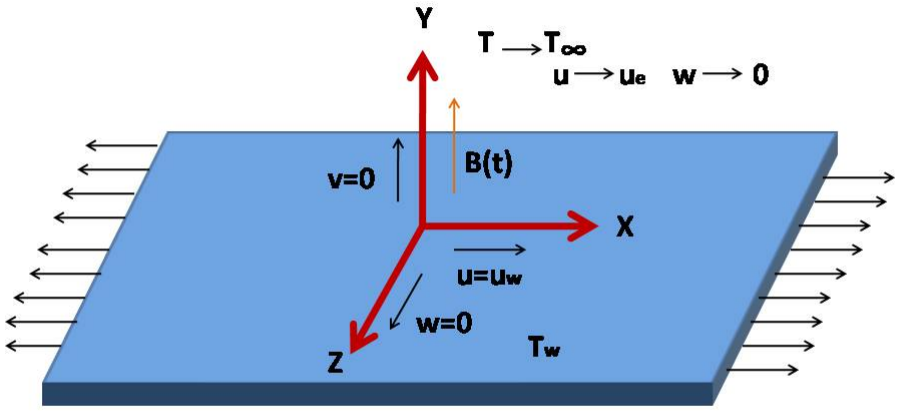

FIGURE 5.1: Physical sketch of the problem

Taking into account these assumptions, the conservation of mass and conservation of momentum equations, governing the fluid flow phenomenon, given by

$$\frac{\partial u}{\partial x}+\frac{\partial v}{\partial y}+\frac{\partial w}{\partial z}=0, \tag{5.1}$$

$$\frac{\partial u}{\partial t}+u\frac{\partial u}{\partial x}+v\frac{\partial u}{\partial y}+w\frac{\partial u}{\partial z}=-\frac{1}{\rho}\frac{\partial P}{\partial x}+\nu\left(1+\frac{1}{\beta}\right)\frac{\partial^2 u}{\partial y^2}-\frac{\sigma B^2(t)}{\rho(1+m^2)}(u+mw), \tag{5.2}$$

$$\frac{\partial w}{\partial t}+u\frac{\partial w}{\partial x}+v\frac{\partial w}{\partial y}+w\frac{\partial w}{\partial z}=-\frac{1}{\rho}\frac{\partial P}{\partial z}+\nu\left(1+\frac{1}{\beta}\right)\frac{\partial^2 w}{\partial y^2}+\frac{\sigma B^2(t)}{\rho(1+m^2)}(mu-w), \tag{5.3}$$

where u, v, w are the velocity components in x, y and z directions, t is time, $\nu=\mu/\rho$ is kinematic viscosity, μ is coefficient of viscosity, ρ is density, m is Hall current parameter, and β is Casson fluid parameter.

Since, the inviscid flow velocity is $u=u_e=\frac{ax}{1-\gamma t}$, where a and γ are constants, the pressure gradient terms in (5.2) and (5.3) are eliminated using the boundary layer approximation, as

$$-\frac{1}{\rho}\frac{\partial P}{\partial x} = \frac{\partial u_e}{\partial t} + u_e\frac{\partial u_e}{\partial x} + \frac{\sigma B^2(t)}{\rho(1+m^2)}u_e, \tag{5.4}$$

$$-\frac{1}{\rho}\frac{\partial P}{\partial z} = -\frac{m\sigma B^2(t)}{\rho(1+m^2)}u_e. \tag{5.5}$$

The heat transfer phenomenon governed by the energy equation, given by

$$\frac{\partial T}{\partial t} + u\frac{\partial T}{\partial x} + v\frac{\partial T}{\partial y} + w\frac{\partial T}{\partial z} = \alpha_m\frac{\partial^2 T}{\partial y^2} - \frac{1}{\rho c_P}\frac{\partial q_r}{\partial y} + \frac{\nu}{c_p}\left(1+\frac{1}{\beta}\right)\left(\left(\frac{\partial u}{\partial y}\right)^2 + \left(\frac{\partial w}{\partial y}\right)^2\right), \tag{5.6}$$

In Eq. (5.6), $\alpha_m = \frac{k}{\rho c_p}$ denotes the fluid's thermal diffusivity. c_p is specific heat capacitance at constant pressure, σ is electric conductivity and T is the temperature within the boundary layer. q_r is the radiative heat flux. Using Rosseland approximation for thermal radiation, the radiative heat flux is simplified as follows:

$$q_r = \frac{-4\sigma^*}{3k^*}\frac{\partial T^4}{\partial y} = \frac{-16\sigma^*}{3k^*}T^3\frac{\partial T}{\partial y}, \tag{5.7}$$

where σ^* and k^* are the Stefan-Boltzmann constant and coefficient of Rosseland mean absorption, respectively.
With the help of (5.7), energy equation (5.6), can be written as

$$\frac{\partial T}{\partial t} + u\frac{\partial T}{\partial x} + v\frac{\partial T}{\partial y} + w\frac{\partial T}{\partial z} = \alpha_m\frac{\partial^2 T}{\partial y^2} + \frac{16\sigma^*}{3k^*\rho c_P}\frac{\partial}{\partial y}\left(T^3\frac{\partial T}{\partial y}\right) + \frac{\nu}{c_p}\left(1+\frac{1}{\beta}\right)\left(\left(\frac{\partial u}{\partial y}\right)^2 + \left(\frac{\partial w}{\partial y}\right)^2\right). \tag{5.8}$$

As per the physical description of the problem, the appropriate boundary conditions are

$$\text{at } y = 0: \ u = u_w = \frac{bx}{1-\gamma t}, \ v = 0, \ w = 0, \ T = T_w \ ; \tag{5.9}$$

$$\text{as } y \to \infty: \ u \to u_e = \frac{ax}{1-\gamma t}, \ w \to 0, \ T \to T_\infty. \tag{5.10}$$

We now choose a similarity transformation:

$$u = \frac{ax}{(1-\gamma t)} f'(\eta),\ v = -\sqrt{\frac{a\nu}{(1-\gamma t)}} f(\eta),\ w = \frac{ax}{(1-\gamma t)} g(\eta), \tag{5.11}$$

$$\theta(\eta) = \frac{T - T_\infty}{T_w - T_\infty},\ \eta = y\sqrt{\frac{a}{\nu(1-\gamma t)}}, \tag{5.12}$$

so that the equation of continuity (5.1) is automatically satisfied, and the Eqs. (5.2, 5.3, 5.8) are transformed to

$$\left(1+\frac{1}{\beta}\right) f''' + ff'' - (f')^2 - A\left(f' + \frac{\eta}{2} f''\right) - \frac{M}{(1+m^2)}\left(f' + mg\right) + \left(A + \frac{M}{1+m^2} + 1\right) = 0, \tag{5.13}$$

$$\left(1+\frac{1}{\beta}\right) g'' - gf' + fg' - A\left(g + \frac{\eta}{2} g'\right) + \frac{M}{(1+m^2)}\left(-m + mf' - g\right) = 0, \tag{5.14}$$

$$\left(1 + \frac{4}{3N_r}\left(1 + (\theta_w - 1)\,\theta\right)^3\right)\theta'' + Prf\theta' + \frac{4}{N_r}\left(\theta_w - 1\right)\left(1 + (\theta_w - 1)\,\theta\right)^2 \theta'^2 + EcPr\left(1+\frac{1}{\beta}\right)\left(\left(f''\right)^2 + \left(g'\right)^2\right) - 2Prf'\theta - 2APr\theta - PrA\frac{\eta}{2}\theta' = 0, \tag{5.15}$$

The boundary conditions (5.9) and (5.10) reduces to

$$\text{at } \eta = 0:\ f' = \frac{b}{a} = s, f = 0,\ g = 0,\ \theta = 1\ ; \tag{5.16}$$

$$\text{as } \eta \to \infty:\ f' \to 1,\ g \to 0,\ \theta \to 0, \tag{5.17}$$

where $A = \frac{\gamma}{a}$ is the unsteadiness parameter, $Ec = \frac{u_e^2}{c_p(T_w - T_\infty)}$ and $Pr = \frac{\nu}{\alpha_m}$ are Eckert and Prandtl numbers, respectively. $\theta_w = \frac{T_w}{T_\infty}$ and $s = \frac{b}{a}$ represent temperature and stretching ratio parameters, respectively. $M = \frac{\sigma B_0^2}{\rho a}$, $N_r = \frac{kk^*}{4\sigma^* T_\infty^3}$ stands for magnetic parameter and radiation parameter respectively.

The other essential physical quantities are the friction coefficients along x and z directions, and the local Nusselt number. These are denoted as C_{fx}, C_{fz}, and Nu_x, respectively, and are defined as

$$C_{fx} = \frac{\tau_{wx}}{\rho u_e^2},\quad C_{fz} = \frac{\tau_{wz}}{\rho u_e^2},\quad Nu_x = \frac{xq_w}{k(T_w - T_\infty)}, \tag{5.18}$$

where

$$\tau_{wx} = \mu\left(1+\frac{1}{\beta}\right)\left(\frac{\partial u}{\partial y}\right)_{y=0},\quad \tau_{wz} = \mu\left(1+\frac{1}{\beta}\right)\left(\frac{\partial w}{\partial y}\right)_{y=0},\quad q_w = \left(-k\left(\frac{\partial T}{\partial y}\right) + q_r\right)_{y=0}. \tag{5.19}$$

Therefore the values of C_{fx}, C_{fz}, and Nu_x are given by

$$C_{fx}Re_x^{1/2} = \left(1+\frac{1}{\beta}\right) f''(0)\,,\ C_{fz}Re_x^{1/2} = \left(1+\frac{1}{\beta}\right) g'(0)\,; \tag{5.20}$$

$$Re_x^{-1/2}Nu_x = -\left[1+\frac{4}{3N_r}\left(1+(\theta_w-1)\,\theta(0)\right)^3\right]\theta'(0)\,, \tag{5.21}$$

where $Re_x = \frac{xu_e}{\nu}$ is the local Reynolds number.

5.3 Entropy generation analysis

The local volumetric rate of entropy generation (S_g) for an incompressible viscous Casson fluid in the presence of Hall current, magnetic field, viscous dissipation and nonlinear radiation along the stretching sheet is defined as

$$\begin{aligned} S_g = {} & \frac{k}{T_\infty^2}\left[\left((T_y)^2+(T_x)^2\right)+\frac{16\sigma^* T^3}{3kk*}\left((T_y)^2+(T_x)^2\right)\right] \\ & +\frac{\mu}{T_\infty}\left(1+\frac{1}{\beta}\right)\left[(u_y)^2+(w_y)^2\right]+\frac{1}{T_\infty}\frac{\sigma B^2}{1+m^2}\left(u^2+w^2\right) \end{aligned} \tag{5.22}$$

There are three sources, which are the reasons of entropy generation (EG) in our formulated model. In the above equation, the first term concerns with the EG due to heat transfer; the second one refers to the EG caused due to fluid friction, and the last one deals with the EG caused due to the magnetic field and Hall current. The dimensionless number N_s representing the rate of entropy generation, can be calculated by dividing S_g with rate of characteristic generation S_{g0}, is defined as

$$S_{g0} = \frac{k(T_w-T_\infty)^2}{L^2 T_{\infty^2}}, \tag{5.23}$$

where L is the characteristic length. Thus, the entropy generation number $N_s = \frac{S_g}{S_{g0}}$ is given by

$$\begin{aligned} N_s \;=\; & Re_L\left(1+\frac{4}{3N_r}(1+\Pi\theta)^3\right)\left(\theta'^2+\frac{4\theta^2}{\chi^2 Re_L}\right)+\frac{Re_L B_r}{\Pi^2}\left(1+\frac{1}{\beta}\right)(f''^2+g'^2) \\ & +\frac{Re_L B_r}{\Pi^2}\frac{M}{1+m^2}(f'^2+g^2), \end{aligned} \tag{5.24}$$

where $Re_L = \frac{u_L L}{\nu}$ denotes the Renyolds number depending on the characteristic length L, $\chi = \frac{x}{L}$ is the non-dimensional surface length, $B_r = \frac{\mu u_e^2}{kT_\infty}$ is the Brinkman number, and $\Pi = (\theta_w - 1)$ is the dimensionless temperature difference.

The dimensionless entropy generation number N_s defined by (5.24) can be further described as

$$N_s = N_H + N_f + N_m = N_H + N_F, \tag{5.25}$$

where $N_H,\ N_m,\ N_f$ are the sources of entropy generation due to the heat transfer, magnetic field, and fluid friction, respectively. We can now define an irreversibility distribution ratio, denoted by ϕ as follows

$$\phi = \frac{N_F}{N_H} = \frac{entropy\ generation\ due\ to\ fluid\ friction\ and\ magnetic\ field}{entropy\ generation\ due\ to\ heat\ transfer}. \tag{5.26}$$

When $0 < \phi < 1$, the heat transfer source will have a dominant impact on the entropy generation process, while when $\phi > 1$, the irreversibility effects due to viscous dissipation and magnetic field are dominant. Also, for $\phi = 1$, both $N_H,$ and N_F have equal contribution.

Also, another essential irreversibility distribution parameter, namely Bejan number Be, can be written as follow

$$Be = \frac{N_H}{N_s} = \frac{1}{1+\phi} \tag{5.27}$$

It is obvious that the Bejan number Be lies in [0,1]. When Be is more than 0.5, the contribution of the heat transfer source in entropy generation is dominant, whereas when $Be < 0.5$ the contribution of flow friction and magnetic field sources are dominant in the entropy generation. For $Be = 0.5$ both will have an equal contribution in the entropy generation.

5.4 Numerical Solution

The solution of governing non-dimensionalized nonlinear equations (5.13)-(5.15) is obtained using spectral quasi-linearization method (SQLM). SQLM follows the idea of linearizing the nonlinear differential terms of the equations using linear Taylor series approximation. Following the algorithm of SQLM, the linearized iteration scheme is obtained as

$$\hat{a}_{11}^{(3)} f_{r+1}''' + \hat{a}_{11}^{(2)} f_{r+1}'' + \hat{a}_{11}^{(1)} f_{r+1}' + \hat{a}_{11}^{(0)} f_{r+1} + \hat{a}_{12}^{(0)} g_{r+1} = \hat{R}_1, \tag{5.28}$$

$$\hat{a}_{22}^{(2)} g_{r+1}'' + \hat{a}_{22}^{(1)} g_{r+1}' + \hat{a}_{22}^{(0)} g_{r+1} + \hat{a}_{21}^{(1)} f_{r+1}' + \hat{a}_{21}^{(0)} f_{r+1} = \hat{R}_2, \tag{5.29}$$

$$\hat{a}_{33}^{(2)} \theta_{r+1}'' + \hat{a}_{33}^{(1)} \theta_{r+1}' + \hat{a}_{33}^{(0)} \theta_{r+1} + \hat{a}_{31}^{(2)} f_{r+1}'' + \hat{a}_{31}^{(1)} f_{r+1}' + \hat{a}_{31}^{(0)} f_{r+1} + \hat{a}_{32}^{(1)} g_{r+1}' = \hat{R}_3, \tag{5.30}$$

where

$$\hat{a}_{11}^{(3)} = \left(1 + \frac{1}{\beta}\right);\ \hat{a}_{11}^{(2)} = f_r - A\frac{\eta}{2};\ \hat{a}_{11}^{(1)} = -2f_r' - A - \frac{M}{1+m^2};\ \hat{a}_{11}^{(0)} = f_r'';\ \hat{a}_{12}^{(0)} = -\frac{Mm}{1+m^2};$$

$$\hat{R}_1 = -A - 1 - \frac{M}{1+m^2} + f_r f_r'' - (f_r')^2;\ \hat{a}_{22}^{(2)} = (1 + \frac{1}{\beta});\ \hat{a}_{22}^{(1)} = f_r - A\frac{\eta}{2};$$

$$\hat{a}_{22}^{(0)} = -f_r' - A - \frac{M}{1+m^2};\ \hat{a}_{21}^{(1)} = -g_r + \frac{Mm}{1+m^2};$$

$$\hat{a}_{21}^{(0)} = g_r';\ \check{R}_2 = -g_r f_r' + g_r' f_r + \frac{Mm}{1+m^2};\ \hat{a}_{33}^{(2)} = \frac{4}{3N_r}\left(1 + (\theta_w - 1)\,\theta_r\right)^3 + 1;$$

$$\hat{a}_{33}^{(1)} = -APr\frac{\eta}{2} + Prf_r + \frac{8\,(\theta_w - 1)}{N_r}\left(1 + (\theta_w - 1)\,\theta_r\right)^2 \theta_r';$$

$$\hat{a}_{33}^{(0)} = \frac{4\,(tr-1)}{N_r}\left(1 + (tr-1)\,\theta_r\right)^2 \theta_r'' + \frac{8\,(tr-1)^2}{N_r}\left(1 + (tr-1)\,\theta_r\right)\left(\theta_r'\right)^2 - 2AP_r - 2P_r f_r';$$

$$\hat{a}_{31}^{2} = 2\left(1 + \frac{1}{\beta}\right) EcP_r f_r'';\ \hat{a}_{31}^{1} = -2P_r\theta_r;\ \hat{a}_{31}^{0} = P_r\theta_r';\ \hat{a}_{32}^{1} = 2\left(1 + \frac{1}{\beta}\right) EcP_r g_r';$$

$$\begin{aligned}\hat{R}_3 = \left(\frac{1}{\beta N_r}\right)\Big(&\beta E_c N_r Pr\left(f_r''\right)^2 + \beta E_c N_r Pr\left(g_r'\right)^2 - \\ &2\beta\theta_r\left(N_r P_r f_r' - 2\left(\theta_w - 1\right)\left(4\left(\theta_w - 1\right)\left(\theta_r'\right)^2 + \theta_r''\right)\right) + \beta N_r P_r f_r \theta_r' + 4\beta\left(\theta_w - 1\right)^3 \theta_r^3 \theta_r'' \\ &+ 4\beta\theta_w\left(\theta_r'\right)^2 + 4\beta\left(\theta_w - 1\right)^2\theta^2\left(3\left(\theta_w - 1\right)\left(\theta_r'\right)^2 + 2\theta_r''\right) - 4\beta\left(\theta_r'\right)^2 + EcN_r P_r\left(f_r''\right)^2 \\ &+ EcN_r P_r\left(g_r'\right)^2\Big);\end{aligned}$$

The boundary conditions for the iteration scheme can be written as follows

$$\text{at } \eta = 0:\ f_{r+1}' = s;\ f_{r+1} = 0;\ g_{r+1} = 0;\ \theta_{r+1} = 1, \tag{5.31}$$

$$\text{as } \eta \to \infty:\ f_{r+1}' \to 1;\ g_{r+1} \to 0;\ \theta_{r+1} \to 0. \tag{5.32}$$

The initial guess required to begin the iterative scheme, is taken as

$$f_0 = (1-s)e^{-\eta} + (s-1) + \eta;\ h_0 = 0;\ \theta_0 = e^{-\eta}.$$

The linearized equations (5.28)-(5.30) are subsequently dealt with Chebyshev pseudo-spectral collocation method. The domain of the physical problem $[0,\ \infty)$ is approximated with $[0, \hat{L}]$, where $\hat{L}$ is chosen to approximate ∞. The computational domain $[0,\ \hat{L}]$ is transformed to $[-1,\ 1]$ using mapping $\eta = \hat{L}\frac{(\hat{\xi}+1)}{2}$ so that the Gauss-Lobatto points can

be used. The values of the functions' derivatives, at the nodes are approximated using the Chebyshev differentiation matrix. The application of the Chebyshev pseudo-spectral collocation method finally yield us

$$\begin{pmatrix} \hat{A}_{11} & \hat{A}_{12} & \hat{A}_{13} \\ \hat{A}_{21} & \hat{A}_{22} & \hat{A}_{23} \\ \hat{A}_{31} & \hat{A}_{32} & \hat{A}_{33} \end{pmatrix} \begin{pmatrix} f_{r+1} \\ g_{r+1} \\ \theta_{r+1} \end{pmatrix} = \begin{pmatrix} \hat{R}_1 \\ \hat{R}_2 \\ \hat{R}_3 \end{pmatrix},$$

where each $\hat{A}_{ij}$ is a square matrix of size $(\hat{N}+1)\times(\hat{N}+1)$, $f_{r+1}, g_{r+1}, \theta_{r+1}, \hat{R}_1, \hat{R}_2$, and $\hat{R}_3$, are each of size $(\hat{N}+1)\times 1$.

5.5 Error Analysis and Discussion of Results

An entropy generation analysis for the transient three-dimensional hydromagnetic stagnation point flow of a Casson fluid along a stretching sheet in the presence of Hall current, viscous dissipation, and nonlinear thermal radiation is carried out in this chapter. The Eqs. (5.13)-(5.15) are coupled highly nonlinear equations. Therefore, it is essential to validate the outcomes in order to trust the obtained numerical solutions. The solutions which the SQLM calculates are verified using a residual analysis of the Eqs. (5.28)-(5.30). The residuals of the primary velocity, secondary velocity, and temperature distribution are presented in Figure 5.2 using 180 collocation points and 20 iterations. It resembles from Fig. 5.2 that the residuals are reduced to $< 10^{-5}$ in just about 20 iterations. Thus, the approximate solutions derived using the SQLM are trustworthy and usable.

Behavior of different physical quantities, such as primary and secondary velocities ($f'(\eta)$ and $g(\eta)$), temperature ($\theta(\eta)$), the dimensionless entropy generation number (N_s), Bejan number (Be), and the skin-friction and heat transfer coefficients are analysed for varying values of the pertinent flow parameters, and the effects are presented through figures and tables. For performing the numerical computations, the default values of the non-dimensional parameters are taken to be $A = 1.5,\ \theta_w = 1.5,\ \beta = 0.4,\ N_r = 1,\ Pr = 15,\ Ec = 1.5,\ m = 0.5,\ M = 4,\ s = 2\ \chi = 0.5,\ Re_L = 0.3$, and $B_r = 3$.

The influence of the Hall current parameter m and magnetic parameter M on the profiles of primary and secondary velocities and the temperature is shown graphically in Fig. 5.3. It is found that on increasing the magnetic parameter M, there is a decrease in $f'(\eta)$ profile. An enhancement in the value of the magnetic parameter corresponds to an increase in the force resisting the flow in the primary direction; however, the influence of the Hall current parameter m results in an acceleration of the primary fluid velocity $f'(\eta)$. The magnetic field and Hall current both have the tendency to accelerate the

secondary flow field, except for the region away from the sheet, where the strength of the induced Lorentz force weakens, and the secondary flow profiles show different behavior. The temperature of the fluid $\theta(\eta)$ rises as the magnetic field parameter M increases. Hall current parameter m results in reducing the fluid temperature. It is concluded from Fig. 5.3 that the momentum boundary layer for both the direction gets thicker with the rising influence of Hall current. The resistive Lorentz force tends to reduce the boundary layer thickness in the primary flow direction. The thermal boundary layer gets thinner with increasing Hall current and gets thicker with Lorentz force.

The effects of unsteadiness parameter A and Casson parameter β on the profiles of primary velocity, secondary velocity, and the temperature are shown graphically in Fig. 5.4. It is found that the increase in both A and β causes retardation in the primary flow-field $f'(\eta)$. Closer to the surface, the profile of $g(\eta)$ increases for the larger Casson parameter β, whereas away from the surface, it changes its characteristics, and the secondary velocity decreases with rising values of Casson parameter β. At the same time, the secondary velocity profile behaves oppositely for unsteadiness parameter A. Profiles of $\theta(\eta)$ fall with the rising values of β and A. From Fig. 5.5, it is visible that for the larger values of stretching ratio parameter s, the profiles of f', g and θ are rising. On increasing the values of the stretching ratio parameter ($s > 1$), the relative velocity of the surface is increased, which is the main reason for the acceleration in the flow field and enhancement in the temperature of the fluid.

Fig. 5.6 represents the profiles of temperature field for several values of N_r and Pr. The parameter Nr is reciprocal to the thermal radiation influence, and the Prandtl number is the ratio of the viscous diffusivity to thermal diffusivity, indicating that the increase in the value of Nr means a decrease in the thermal radiation and an increase in Pr implies a decrease in the thermal diffusivity. This figure shows that there is a fall in the fluid temperature with increasing values of the Nr and Pr, meaning that the radiative heat transfer and thermal diffusivity tend to enhance the fluid temperature within the boundary layer. Fig. 5.7 represents the distribution of temperature field for varying values of the Eckert number Ec. The parameter Ec measures the effect of viscous dissipation in the heat transfer process, and it implies that the increase in viscous dissipation causes a rise in the fluid temperature.

The behavior of N_S and Be for various values of m and M is visible through Fig. 5.8. The entropy generation N_S rises with increasing M. The increase in entropy generation with rising magnetic field reports deceleration of the fluid velocity in the x direction. The entropy generation number decreases with rising values of m. Also, the values of Be get decreased with an increasing value of M. Physically, when we increase M, magnetic field sources' contribution becomes dominant compared to the heat transfer sources in

the entropy generation process. The Be values increase for rising values of m. Figs. 5.9 and 5.10 depict that both N_S and Be decrease for increasing values of β, A and Nr while, both the quantities behave contrarily for the rising values of θ_w.

The impact of Pr and χ on N_S and Be is depicted through Fig. 5.11. Closer to the surface N_S enhances for rising values of Pr. However, away from the surface, it starts diminishing. The reason behind this is that the temperature profiles decrease for large values of Pr, which leads to a sharp decrease in the entropy generation of the flow system. It is evident from Fig. 5.11 that the Bejan number decrease for both Pr and χ.The profiles of N_S and Be, for distinct values of Re_L and B_r, is shown in Fig. 5.12. Raising the Reynolds number also raises entropy generation. The reason behind this is that the larger Reynolds number flows have more disturbances in the flow field. Also, it is noticed that an increment in B_r causes more entropy in the flow field. The Bejan number (Be) decreases for rising values of N_S and Be.

To study the influence of pertinent non-dimensional parameters on the different physical quantities, such as the skin-friction coefficients Cf_x, Cf_z, and the Nusselt number Nu_x, values of these quantities are shown in Table 5.1. It is clearly visible that the skin-friction coefficient Cf_x decreases with the increase in β and m, whereas it gets increased s, A, and M. The skin-friction coefficient Cf_z decreases with rising A and β while it increases with increasing s, M, and m. This shows that the wall shear-stress along the primary direction enhances with the stretching of the velocity of the sheet, unsteadiness, and the strength of the magnetic field, and it decreases with the Casson parameter and Hall current. The wall shear-stress in the secondary flow direction is directly proportional to the stretching velocity, magnetic field, and Hall current, whereas it is inversely proportional to the unsteadiness and Casson parameter. The heat transfer coefficient, i.e., the Nusselt number Nu_x enhances with rising values of θ_w, Pr, and Nr. The other parameters Ec, s, A, β, M, and m has reducing influence on the Nusselt number. Therefore, the heat transfer coefficient rises with the rising temperature of the sheet and viscous diffusion, whereas it is reversely influenced by thermal diffusivity, viscous dissipation, unsteadiness, Casson parameter, magnetic field, and the Hall current.

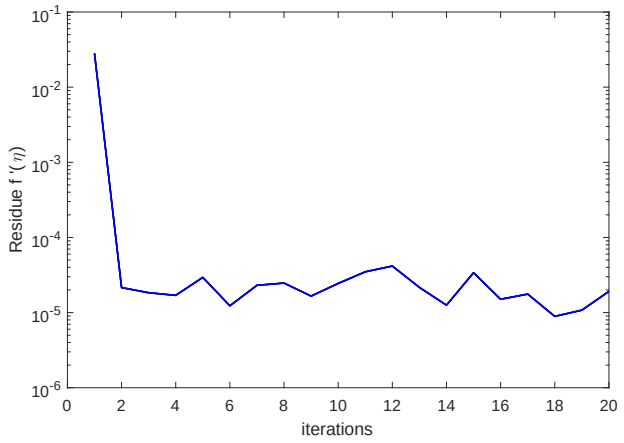

(a)

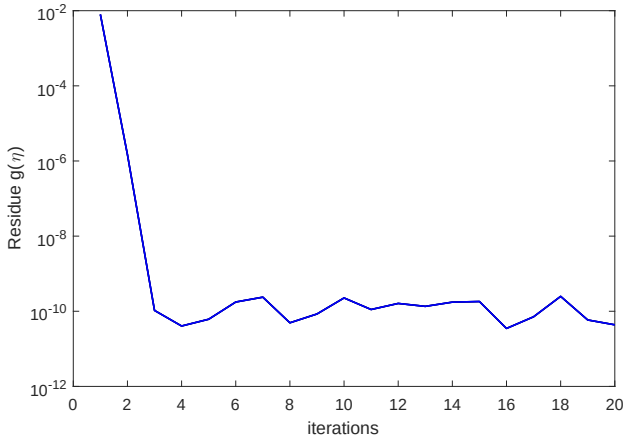

(b)

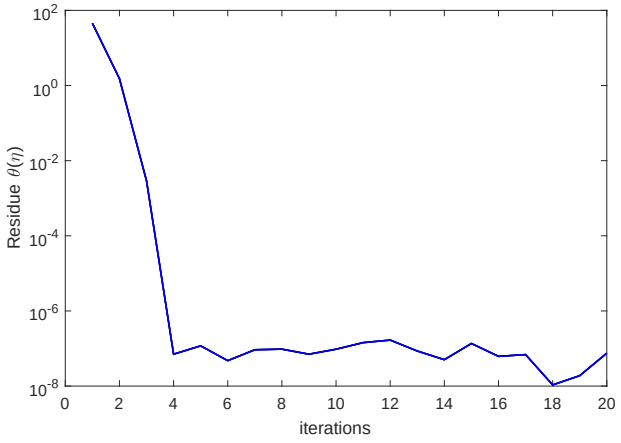

(c)

FIGURE 5.2: Error in $f'(\eta)$, $g(\eta)$, $\theta(\eta)$

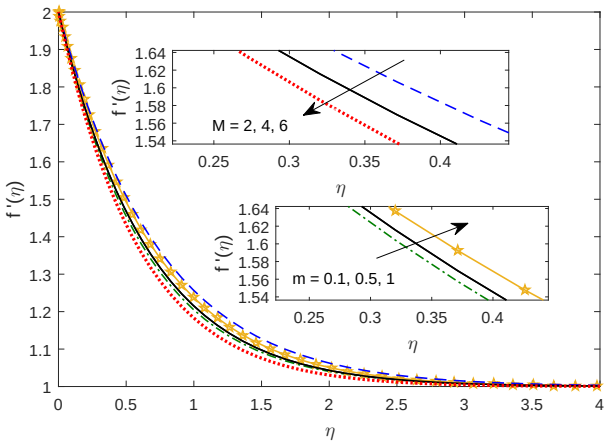

(a)

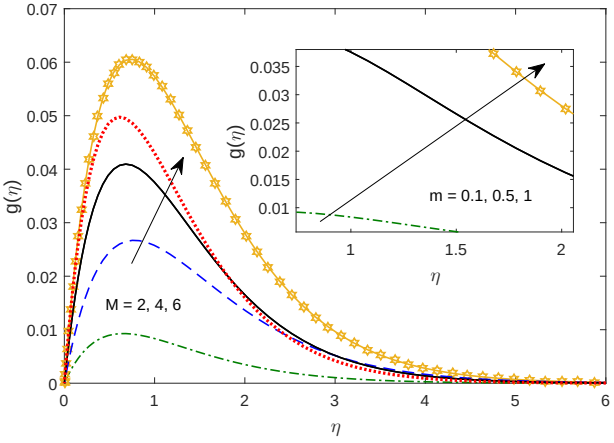

(b)

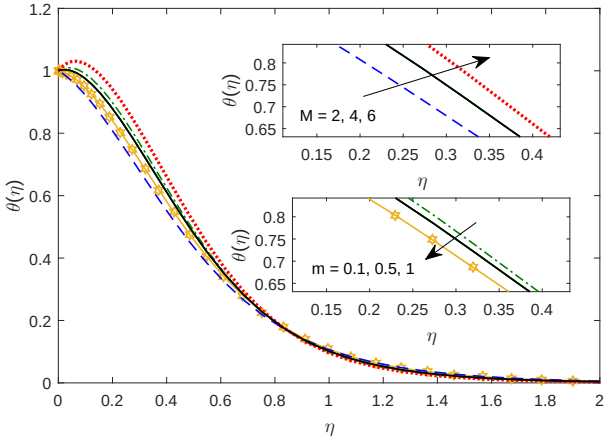

(c)

FIGURE 5.3: Influence of M and m on (a) $f'(\eta)$, (b) $g(\eta)$, and (c) $\theta(\eta)$ when $A = 1.5$, $\theta_w = 1.5$, $\beta = 0.4$, $N_r = 1$, $Pr = 15$, $Ec = 1.5$, $s = 2$ $\chi = 0.5$, $Re_L = 0.3$, $B_r = 3$

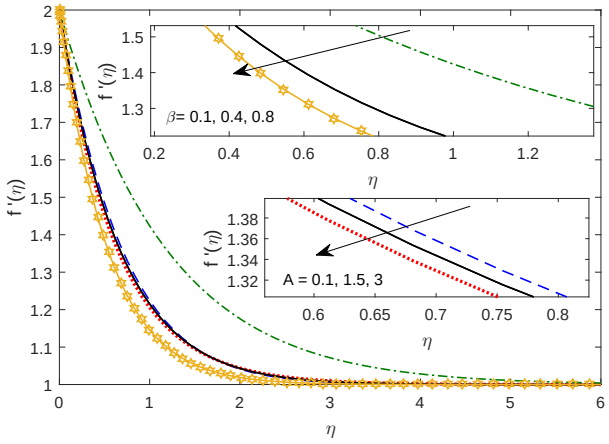

(a)

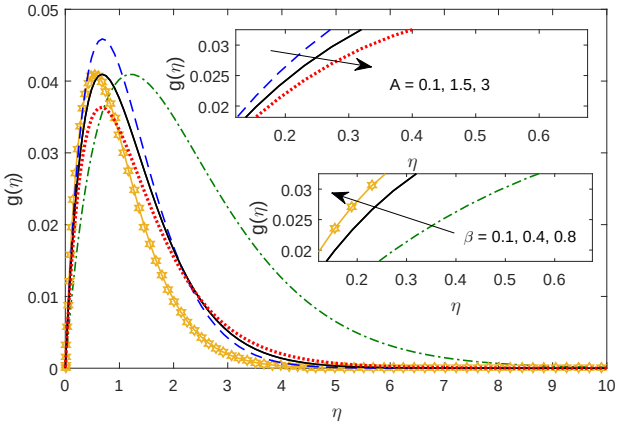

(b)

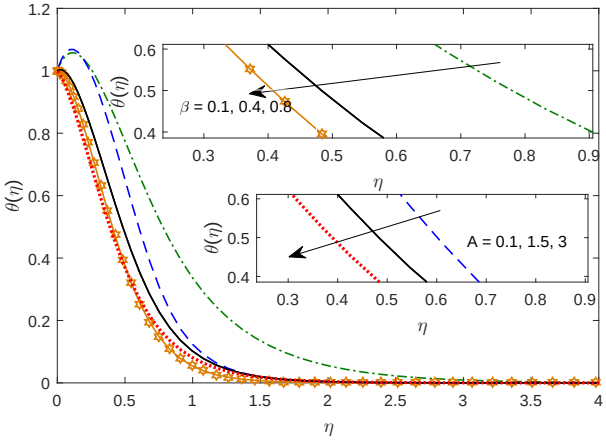

(c)

FIGURE 5.4: Influence of β and A on (a) $f'(\eta)$, (b) $g(\eta)$, and (c) $\theta(\eta)$ when $\theta_w = 1.5,\ N_r = 1,\ Pr = 15,\ Ec = 1.5,\ m = 0.5,\ M = 4,\ s = 2\ \chi = 0.5,\ Re_L = 0.3,\ B_r = 3$

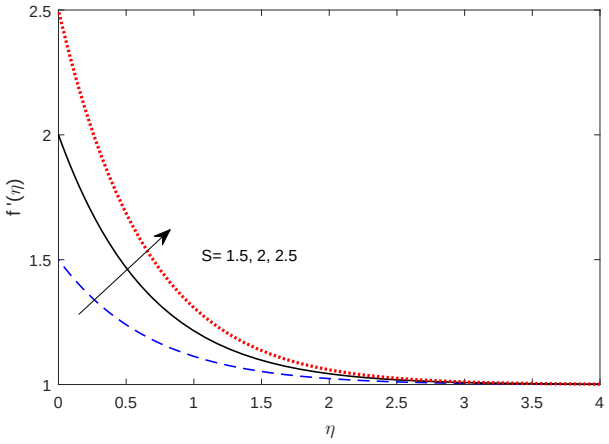

(a)

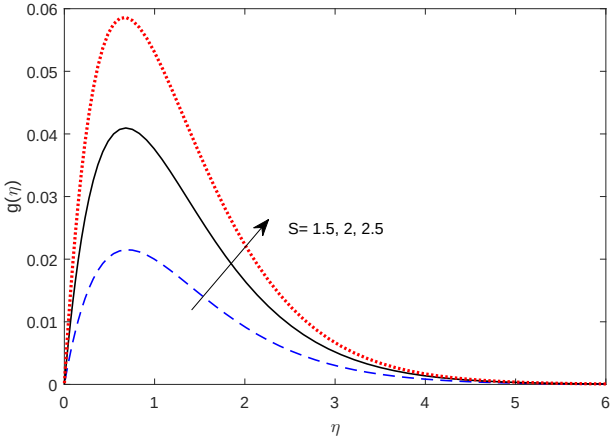

(b)

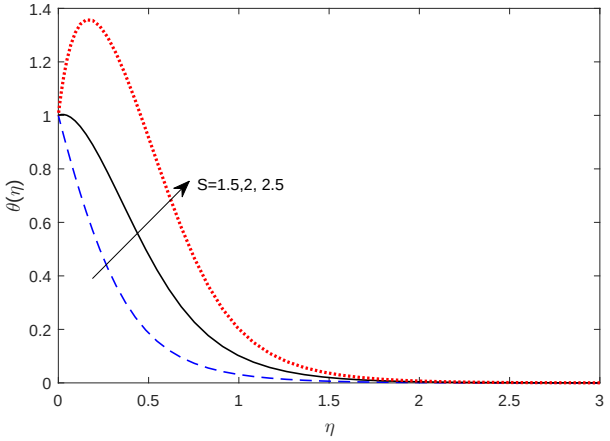

(c)

FIGURE 5.5: Influence of s on (a) $f'(\eta)$, (b) $g(\eta)$, and (c) $\theta(\eta)$ when $A = 1.5$, $\theta_w = 1.5$, $\beta = 0.4$, $N_r = 1$, $Pr = 15$, $Ec = 1.5$, $m = 0.5$, $M = 4$, $\chi = 0.5$, $Re_L = 0.3$, $B_r = 3$

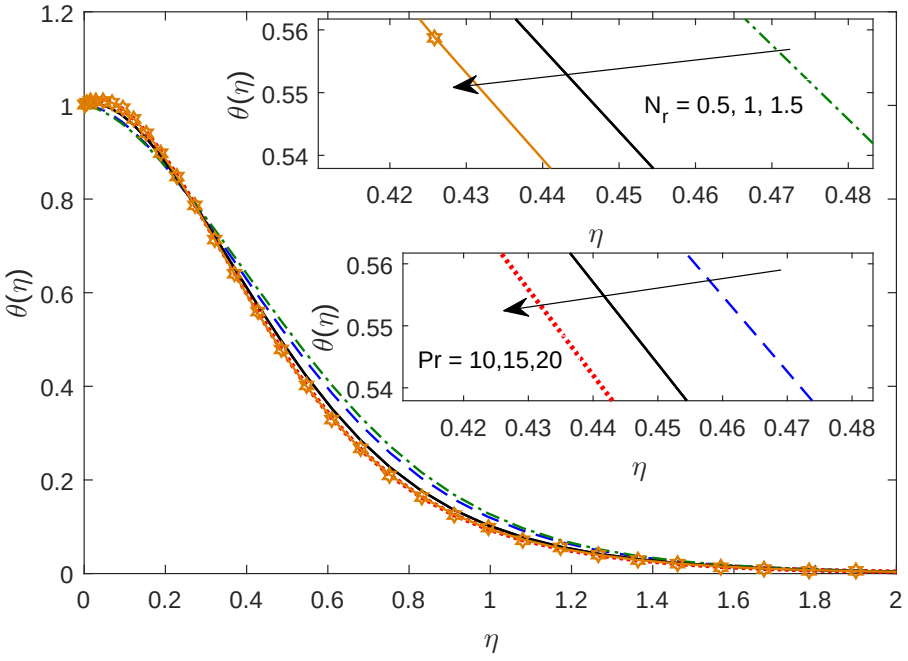

FIGURE 5.6: Influence of N_r and Pr on $\theta(\eta)$ when $A = 1.5,\ \theta_w = 1.5,\ \beta = 0.4,\ Ec = 1.5,\ m = 0.5,\ M = 4,\ s = 2\ \chi = 0.5,\ Re_L = 0.3,\ B_r = 3$

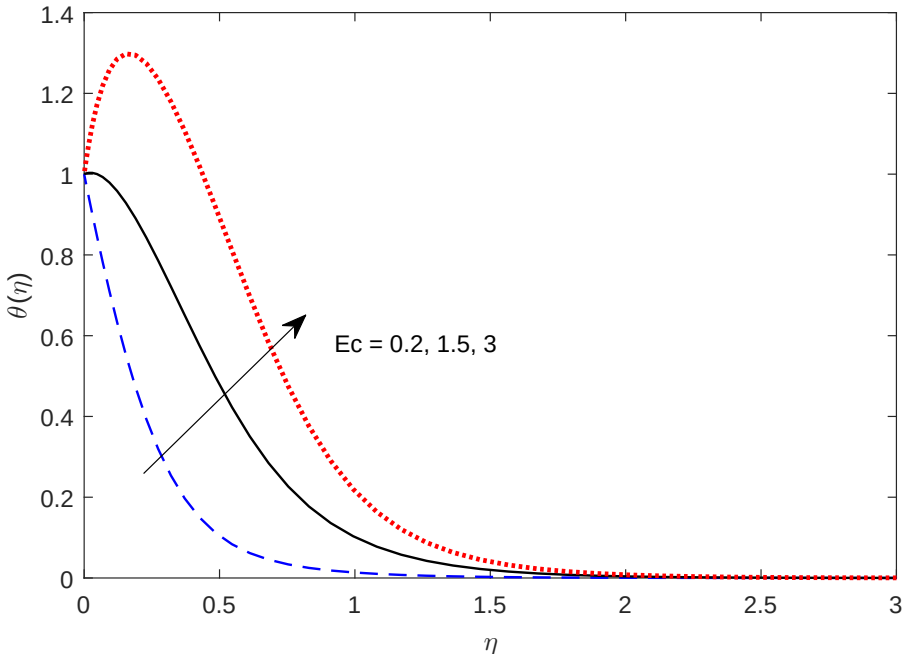

FIGURE 5.7: Influence of Ec on $\theta(\eta)$ when $A = 1.5,\ \theta_w = 1.5,\ \beta = 0.4,\ N_r = 1,\ Pr = 15,\ m = 0.5,\ M = 4,\ s = 2\ \chi = 0.5,\ Re_L = 0.3,\ B_r = 3$

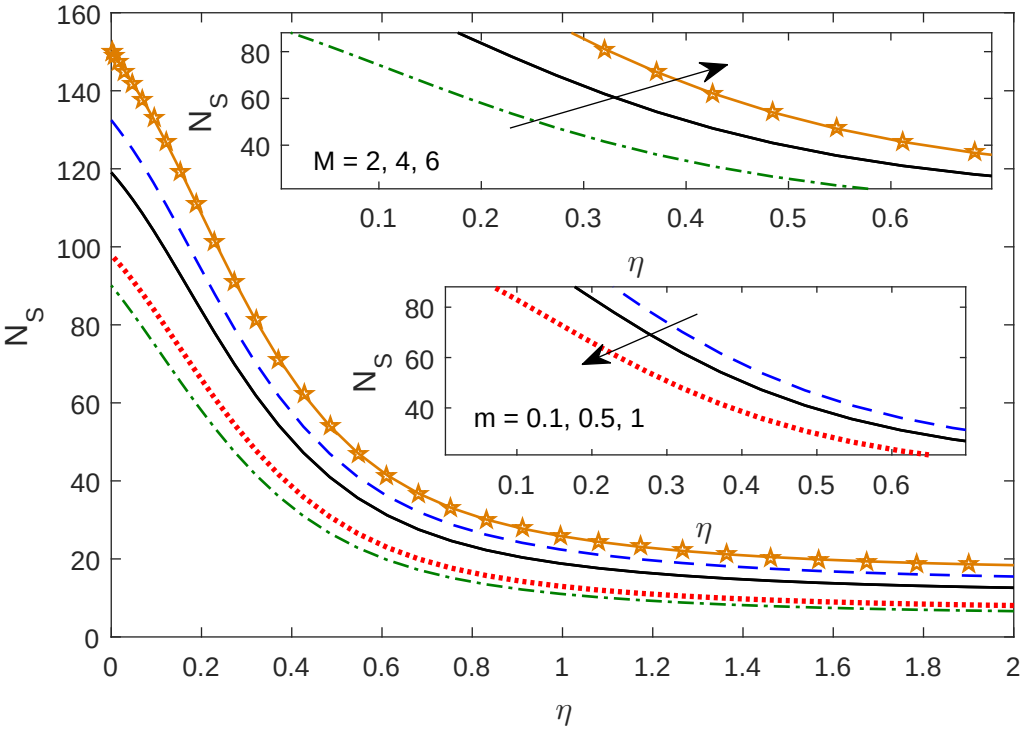

(a)

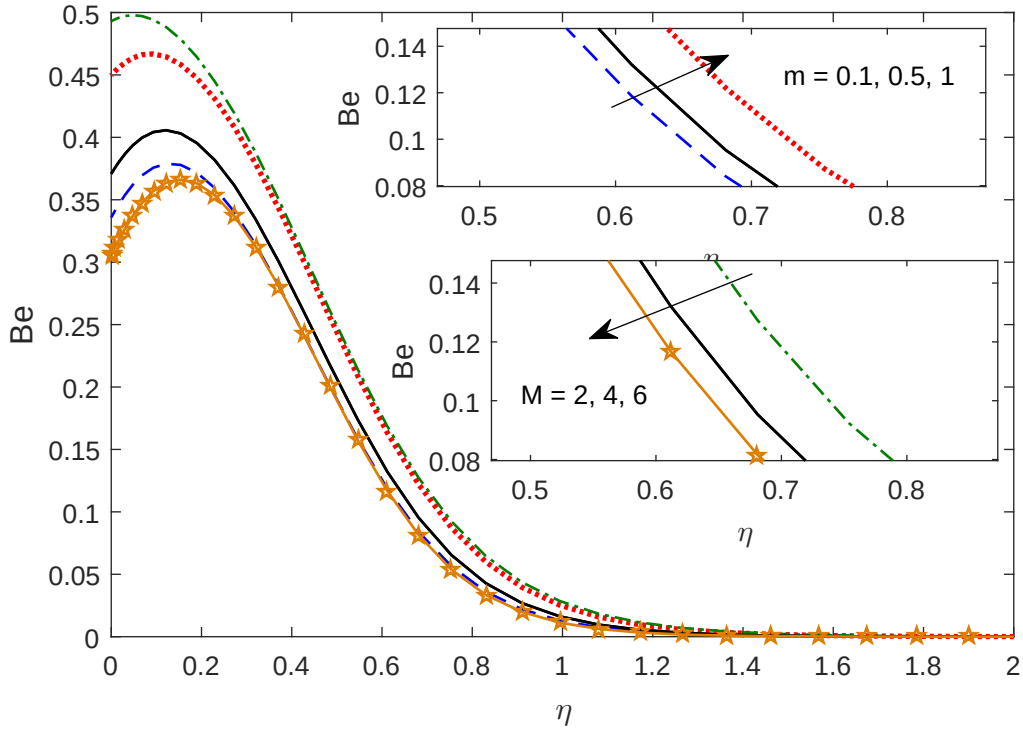

(b)

FIGURE 5.8: Effect of m and M on (a) N_S, (b) Be, when $A = 1.5$, $\theta_w = 1.5$, $\beta = 0.4$, $N_r = 1$, $Pr = 15$, $Ec = 1.5$, $s = 2$ $\chi = 0.5$, $Re_L = 0.3$, $B_r = 3$

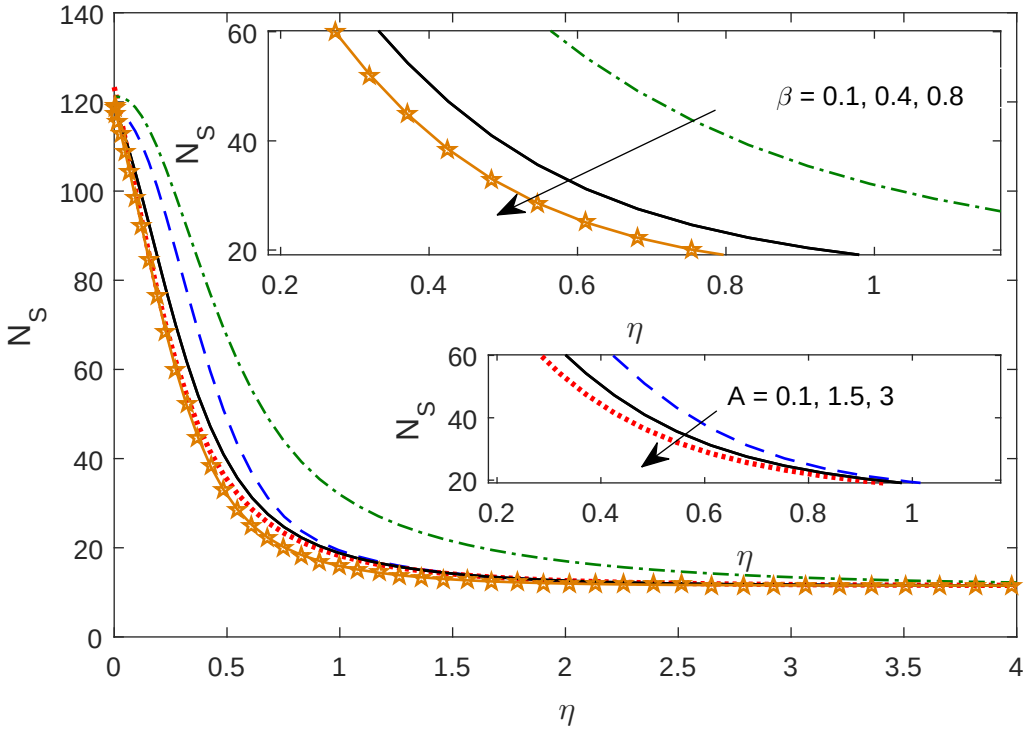

(a)

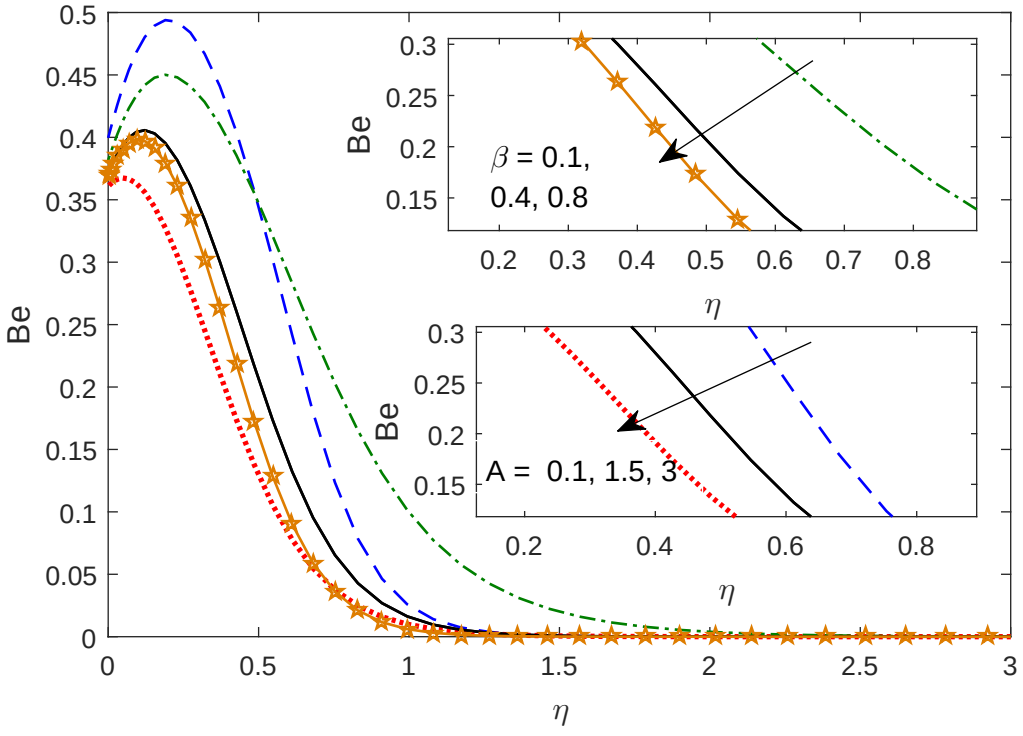

(b)

FIGURE 5.9: Effect of β and A on (a) N_S, (b) Be, when $\theta_w = 1.5$, $N_r = 1$, $Pr = 15$, $Ec = 1.5$, $m = 0.5$, $M = 4$, $s = 2$ $\chi = 0.5$, $Re_L = 0.3$, $B_r = 3$

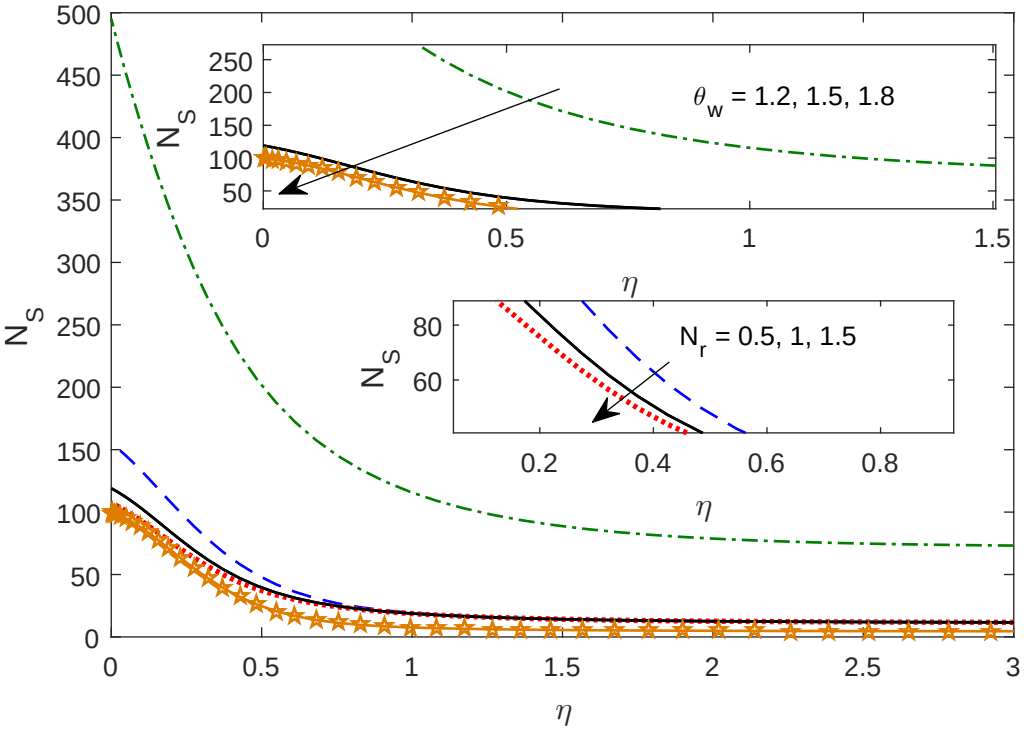

(a)

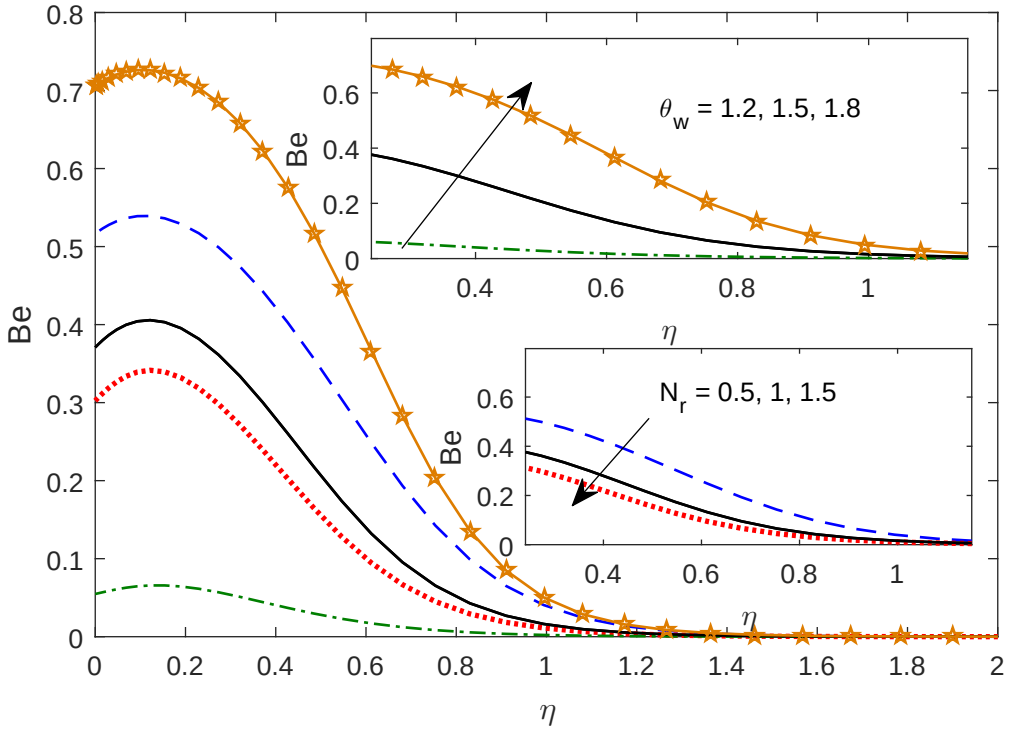

(b)

FIGURE 5.10: Effect of N_r and θ_w on (a) N_S, (b) Be, when $A = 1.5$, $\beta = 0.4$, $Pr = 15$, $Ec = 1.5$, $m = 0.5$, $M = 4$, $s = 2$ $\chi = 0.5$, $Re_L = 0.3$, $B_r = 3$

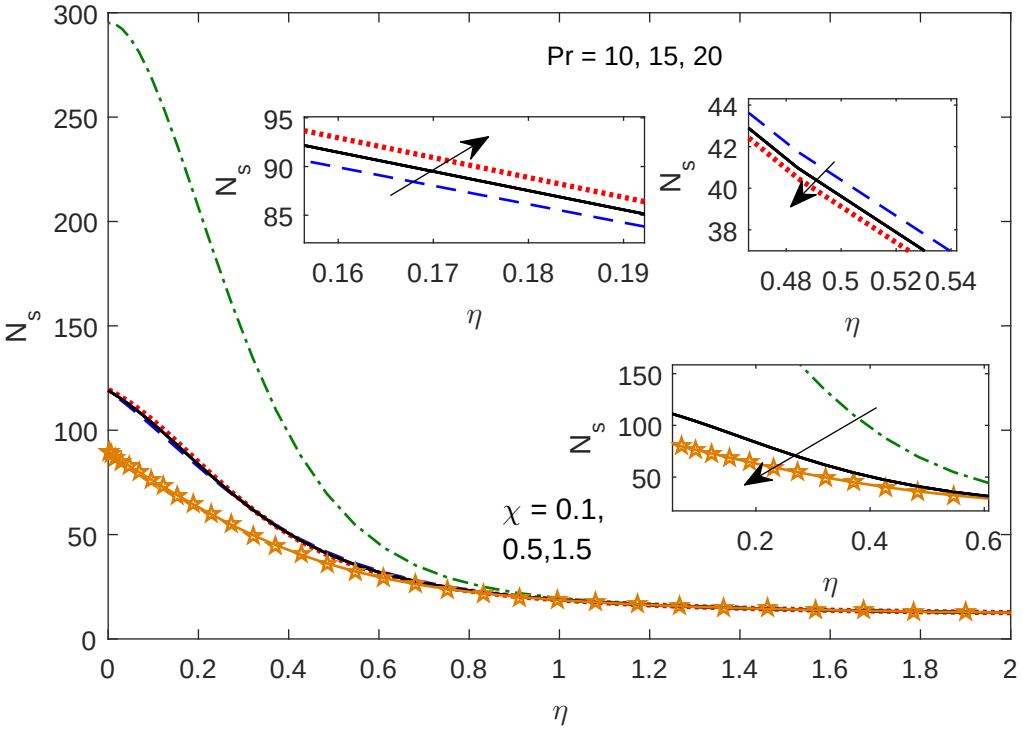

(a)

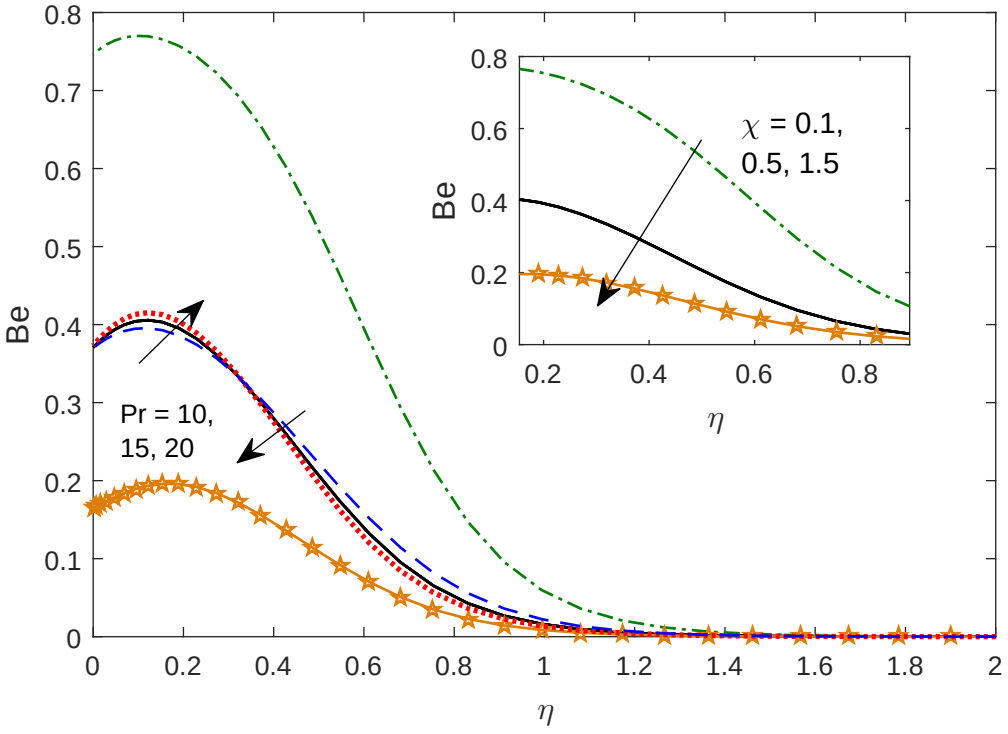

(b)

FIGURE 5.11: Effect of Pr and χ on (a) N_S, (b) Be, when $A = 1.5$, $\theta_w = 1.5$, $\beta = 0.4$, $N_r = 1$, $Ec = 1.5$, $m = 0.5$, $M = 4$, $s = 2$ $Re_L = 0.3$, $B_r = 3$

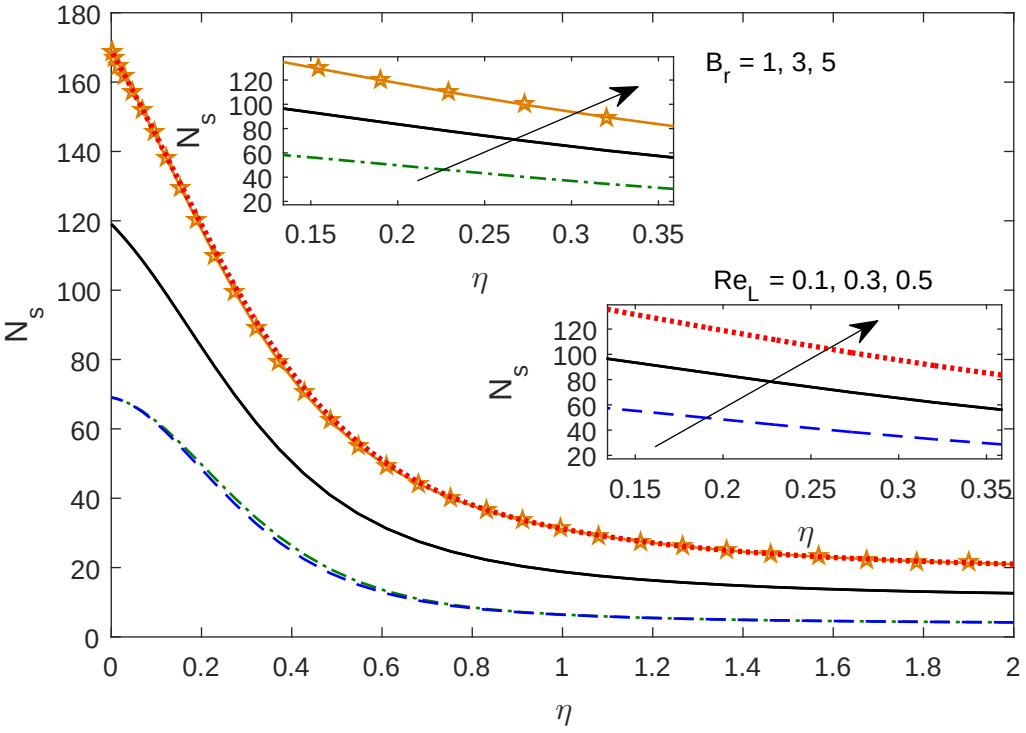

(a)

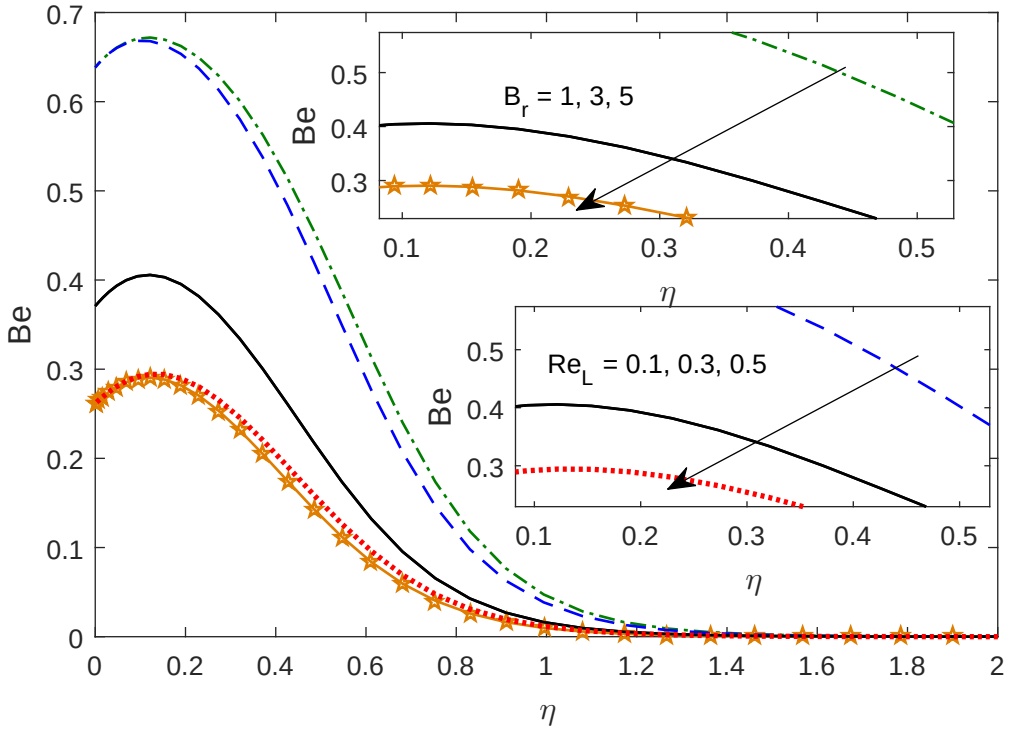

(b)

FIGURE 5.12: Effect of Re_L and B_r on (a) N_S, (b) Be, when $A = 1.5$, $\theta_w = 1.5$, $\beta = 0.4$, $N_r = 1$, $Pr = 15$, $Ec = 1.5$, $m = 0.5$, $M = 4$, $s = 2$ $\chi = 0.5$

TABLE 5.1: Table for the numeric values of skin-friction coefficients and Nusselt number.

θ_w	P_r	Ec	s	A	β	N_r	M	m	$-C_{fx}Re_x^{1/2}$	$C_{fz}Re_x^{1/2}$	$Re_x^{-1/2}Nu_x$
1.5	15	1.5	2	1.5	0.4	1	4	0.5	5.26519402	0.56298252	-1.62841988
1.2									5.26519402	0.56298252	-2.76249691
1.8									5.26519402	0.56298252	0.06573688
	10								5.26519407	0.56298252	0.12859466
	15								5.26519402	0.56298252	-1.62841988
	20								5.26519400	0.56298252	-3.32418037
		0.2							5.26519401	0.56298252	18.58422083
		1.5							5.26519402	0.56298252	-1.62841988
		3							5.26519399	0.56298252	-26.96847674
			1.5						2.54857232	0.28817149	14.35809371
			2						5.26519402	0.56298252	-1.62841988
			2.5						8.14215593	0.82582006	-32.81831748
				0.1					4.91756440	0.60554672	-7.98716429
				1.5					5.26519402	0.56298252	-1.62841988
				3					5.62129381	0.52366485	2.99710756
					0.1				9.33419133	0.99806133	-6.43356255
					0.4				5.26519402	0.56298252	-1.62841988
					0.8				4.22154688	0.45139022	0.31825050
						0.5			5.26519404	0.56298252	1.21024253
						1			5.26519402	0.56298252	-1.62841988
						1.5			5.26519400	0.56298252	-2.52785432
							2		4.68081715	0.32201699	2.76113552
							4		5.26519402	0.56298252	-1.62841988
							6		5.79495372	0.75914345	-5.88055429
								0.1	5.48443303	0.13314107	-3.00463589
								0.5	5.26519402	0.56298252	-1.62841988
								1	4.87871223	0.76736087	0.92385836

5.6 Regression analysis

In this section, the statistical analysis of the skin friction coefficients, and the Nusselt number is performed using a quadratic regression model. For this, $C_{fx}Re_x^{1/2}$ is estimated for the fixed values of s, and a set of 100 values of M and β are arbitrarily chosen from [1.5, 6.5] and [0.05, 0.9], respectively. Likewise, to evaluate $C_{fz}Re_x^{1/2}$ for fixed values

of θ_w, a set of 100 values of A and m are picked arbitrarily from [0, 4], and [0.05, 1.1], respectively. Further, $Re_x^{-1/2}Nu_x$ is figured for fixed values of Nr, and a set of 100 values of Pr, and m are randomly picked from [9, 21], and [0.05, 1.1], respectively. The approximate quadratic regression models of $C_{fx}Re_x^{1/2}$, $C_{fz}Re_x^{1/2}$, and $Re_x^{-1/2}Nu_x$ are given below

$$C_{fx_{est}} = C_{fx} + a_1M + a_2\beta + a_3M^2 + a_4\beta^2 + a_5M\beta, \tag{5.33}$$

$$C_{fz_{est}} = C_{fz} + b_1A + b_2m + b_3A^2 + b_4m^2 + b_5Am, \tag{5.34}$$

$$Nu_{est} = Nu + c_1Pr + c_2m + c_3Pr^2 + c_4m^2 + c_5Prm, \tag{5.35}$$

where a_1, a_2, a_3, a_4, a_5, and b_1, b_2, b_3, b_4, b_5, and c_1, c_2, c_3, c_4, c_5 are the coefficients corresponding to the parameters, which are given in equations (5.33)-(5.35). The maximum relative error $\varepsilon_{C_{fx}}$, $\varepsilon_{C_{fz}}$ and ε_{Nu} are estimated by

$$\left.\begin{aligned} \varepsilon_{C_{fx}} &= \frac{|C_{fx_{est}} - C_{fx}|}{C_{fx}}, \\ \varepsilon_{C_{fz}} &= \frac{|C_{fz_{est}} - C_{fz}|}{C_{fz}}, \\ \varepsilon_{Nu} &= \frac{|Nu_{est} - Nu|}{Nu}. \end{aligned}\right\} \tag{5.36}$$

Table 5.2 expresses that on enhancing values of s, the coefficient of the Casson parameter is larger than that of the magnetic parameter in magnitude, which shows that the influence of β on C_{fx} is dominant as compared to M. From Table 5.3, it is noted that C_{fz}, and the coefficients of A are negative, whereas the coefficient of m are positive with a minor variation in θ_w. Thus, it is elucidated from the equation (5.34) that C_{fz} is positively impacted by the parameter A, however the Hall current parameter has adverse impact on it. Also, Table 5.3 shows that the coefficient of the Hall current is greater than that of the unsteadiness parameter in magnitude for raising the temperature ratio parameter, which indicates that the skin-friction coefficient in z- direction is considerably effected by the Hall current parameter in comparison to the unsteadiness parameter. From the Table 5.4, it is observed that on enhancing the radiative parameter, the coefficient of m is larger than the coefficients of Pr in magnitude, it means that a slight change in the Hall current parameter leads to a significant change in the rate of transfer of mass as compared to the Prandtl number. It is concluded that the estimated accuracy of the skin-friction coefficient in z is larger than that of the skin-friction coefficient in x-direction, and the Nusselt number.

TABLE 5.2: Quadratic regression coefficients and error bound for estimated $C_{fx}Re_x^{1/2}$.

s	C_{fx}	a_1	a_2	a_3	a_4	a_5	$\varepsilon_{C_{fx}}$
1.5	-0.0717	-0.1300	-0.8552	0.0130	0.4866	-0.0502	0.0011
2.0	-0.5177	-0.0520	-2.1739	0.0007	1.3535	-0.0830	0.00056396
2.5	-0.8699	-0.0385	-3.3345	0.0026	2.3296	-0.2294	0.0027

TABLE 5.3: Quadratic regression coefficients and error bound for estimated $C_{fz}Re_x^{1/2}$.

θ_w	C_{fz}	b_1	b_2	b_3	b_4	b_5	$\varepsilon_{C_{fz}}$
1.2	-0.0024	-0.0036	0.6736	0.0005	-0.3219	-0.0181	0.000064305
1.5	-0.0026	-0.0046	0.6805	0.0060	-0.3349	-0.0166	0.0080
1.8	-0.0049	-0.0022	0.6832	0.0003	-0.3333	-0.0201	0.00095353

TABLE 5.4: Quadratic regression coefficients and error bound for estimated $Re_x^{-1/2}Nu_x$.

Nr	Nu	c_1	c_2	c_3	c_4	c_5	ε_{Nu}
0.5	-0.4715	0.0255	0.0606	0.0007	-0.1247	-0.0282	0.0179
1.1	-0.9311	0.1246	0.4316	-0.0012	-0.5779	-0.0478	0.0142
1.5	-1.3647	0.1698	0.8062	-0.0009	-0.3300	-0.0944	0.0061

5.7 Conclusions

An entropy generation analysis for the transient three-dimensional hydromagnetic stagnation point flow of a Casson fluid is performed successfully along a stretching surface in the presence of Hall current, viscous dissipation, and nonlinear radiation. The main findings of the study are

1. Velocity distribution along the x direction is diminished by the magnetic effect. Besides, it is enhanced by the Hall effect. However, The magnetic field and Hall current both tend to accelerate the velocity distribution in the z direction, except for the region away from the sheet, where the strength of the induced Lorentz force weakens, and the secondary flow profiles show different behavior. The fluid temperature increases due to the magnetic effect and gets reduced under the Hall effect.

2. The coefficients of skin friction in x and z directions decrease with increased values of Casson fluid parameter. In comparison, it has a reducing influence on the Nusselt

number. Unsteadiness parameter has the tendency to diminish the skin friction coefficient in z direction and the Nusselt number and to increase the skin-friction coefficient in x direction.

3. Entropy generation is increased by the presence of a magnetic effect. However, the Bejan number diminishes with an increment in the magnetic effect; since the increase in the influence of the magnetic field causes the contribution of magnetic field sources to become dominant compared to the heat transfer sources in the entropy generation process. The increments in the values of Casson, radiation, and unsteadiness parameters decrease the Bejan number and entropy generation.

4. The influence of the Casson fluid parameter is dominant on the skin friction coefficient in x direction, as compared to the magnetic effect. Also, the skin-friction coefficient in the z direction is positively impacted by the unsteadiness parameter. However, the Hall current has an adverse impact on it. The estimated accuracy of the skin-friction coefficient in z is greater than that of the skin-friction coefficient in x direction and the Nusselt number.

Chapter 6

Radiative Heat Transfer Analysis of the Unsteady MHD Darcy-Forchhiemer Flow along a Curved Sheet

6.1 Introduction

In all the earlier studies of the present thesis, the fluid is taken to be flowing along flat stretching surfaces only, and the flow configuration is described with the help of the Cartesian coordinate system. However, the choice of a curved geometry surface is essential for practical purposes. Flow due to a curved stretching surface has applications in a stretch-forming machine with curving jaws. This essentially generalizes the flow configuration, and one need not stick with a particular flow geometry. Sajid et al. [99] were the first who introduced a curvature in the surface and presented the fluid flow model in the curvilinear coordinate system. The flow of a micropolar fluid along a curved stretching surface was examined by Sajid et al. [100]. They concluded that the pressure is not negligible in the fluid flow along a curved surface. Also, the boundary layer thickness is more significant, and the drag force is less in the case of curved surfaces than the flat surface. Abbas et al. [101] analyzed the fluid flow and heat transfer along

Contents of this chapter has been communicated to Pramana [Prashu, R. Nandkeolyar, V. Sangwan, Radiative Heat Transfer Analysis of the Unsteady MHD Darcy-Forchhiemer Flow along a Curved Sheet, Pramana (Communicated)]

a curved stretching surface in the existence of a magnetic field. The transient boundary layer fluid flow along a porous curved stretching surface was investigated by Rosca and Pop [102]. The combined impact of heat source/sink and radiation effects on the flow of a nanofluid along a curved surface was studied by Abbas et al. [103]. Sufficient number of literature on this topic can be seen through ([104], [105], [106], [107], [108]).

Studying the fluid flow through porous media is beneficial in several applications of engineering interests such as drying of wood, catalytic reactors, heat exchanger design, groundwater system, petroleum resources. The classical Darcy's law is not sufficient for non-uniform porosity and high-velocity conditions. It is applicable only when the inertia and boundary features are considered at a low flow rate. Forchheimer [109] modified the classical Darcy's law incorporating a square velocity term in the momentum equation. Muskat [110] recognized this term as the Forchheimer term. The relevant studies regarding fluid flow in Darcy-Forchheimer porous medium can be seen through ([111], [112], [113], [114], [115]).

The present work aims to examine the unsteady two-dimensional hydromagnetic boundary layer flow of fluid towards a curved stretching sheet in a Darcy-Forchheimer porous medium, considering the impact of thermal radiation. The fluid flow model comprises highly nonlinear PDEs with suitable boundary conditions. The curvilinear coordinate system (r, s) is utilized to carry out the study. Similarity transformations are used to convert the PDEs of the mathematical model to ordinary differential equations, which are then solved using the bvp4c routine in the Matlab software. The influences of various parameters are analyzed on the velocity, temperature profiles, skin-friction coefficient, and Nusselt number through figures and tables.

6.2 Mathematical Modeling

The time-dependent two-dimensional MHD boundary layer flow of a viscous fluid in a non-Darcy porous medium along a curved stretching sheet coiled in a circle of radius R is considered. For developing the mathematical model, a curvilinear coordinate system (r, s) is taken, where s denotes the arc length coordinate towards the direction of fluid flow and r is normal to tangent vector at any point on the sheet, see Fig. 6.1. The radius of the curved sheet is taken to be $R(t) = R_0\sqrt{(1-\alpha t)}$, where R_0 is a positive constant. The shape of the curved sheet is actually depends on the distance R of the sheet from the origin, i.e., for a large value of R, the surface tends to become flat. The sheet is stretched with velocity $u = u_w = \frac{as}{1-\alpha t}$ in s direction inducing the fluid motion. A time dependent magnetic field $B(t) = B_0(1-\alpha t)^{-\frac{1}{2}}$ is taken to be acting along the r direction. The

flow through the porous medium is characterized by the Darcy-Forchheimer relation the heat transfer phenomena is taken to be affected by thermal radiation.

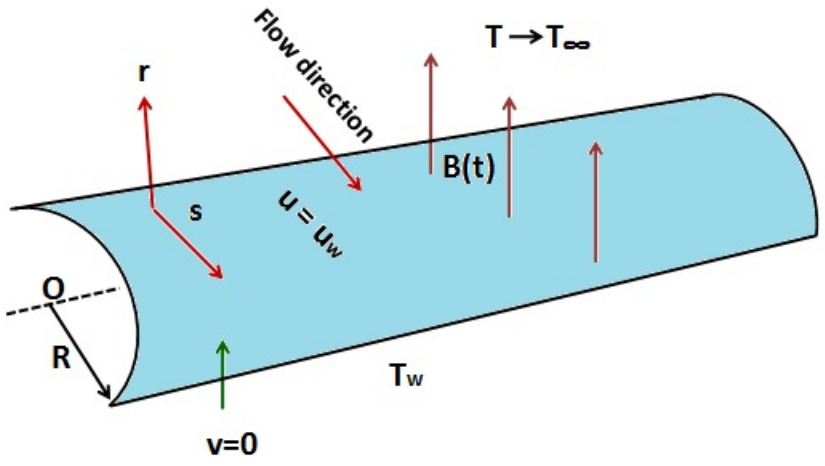

FIGURE 6.1: Model of the problemm

Following the above assumptions, mathematical model governing the flow and heat transfer phenomena is given by

$$\frac{\partial}{\partial r}\{((r+R)v)\} + R\frac{\partial u}{\partial s} = 0, \tag{6.1}$$

$$\frac{u^2}{r+R} = \frac{1}{\rho}\frac{\partial p}{\partial r}, \tag{6.2}$$

$$\frac{\partial u}{\partial t} + v\frac{\partial u}{\partial r} + \frac{Ru}{r+R}\frac{\partial u}{\partial s} + \frac{uv}{r+R} = \frac{-1}{\rho}\frac{R}{r+R}\frac{\partial p}{\partial s} + \nu\left(\frac{\partial^2 u}{\partial r^2} + \frac{1}{r+R}\frac{\partial u}{\partial r} - \frac{u}{(r+R)^2}\right) - \frac{\sigma B^2(t)}{\rho}u - F_1 u^2 - \frac{\nu}{k_2}u, \tag{6.3}$$

$$\rho c_p\left(\frac{\partial T}{\partial t} + v\frac{\partial T}{\partial r} + \frac{Ru}{r+R}\frac{\partial T}{\partial s}\right) = k_1\left(\frac{\partial^2 T}{\partial r^2} + \frac{1}{r+R}\frac{\partial T}{\partial r}\right) - \frac{1}{r+R}\frac{\partial}{\partial r}\left((r+R)q_r\right). \tag{6.4}$$

where (v, u) represents the velocity components in (r, s) directions, respectively. T is the temperature, ρ is density of the fluid and p is pressure. The thermal and electrical conductivities are denoted by k_1 and σ, respectively, ν is fluid's kinematics viscosity, c_p is specific heat at constant pressure, $F_1 = \frac{C_p}{s\sqrt{k_2}}$ is the non-uniform inertia coefficient of porous medium. C_p, k_2 represent the drag coefficient and permeability of porous medium, respectively.

The governing boundary conditions are

$$\text{at } r = 0: \ u = u_w, \ v = 0, \ T = T_w; \tag{6.5}$$

$$\text{as } r \to \infty: \ u \to 0, \ \frac{\partial u}{\partial r} \to 0, \ T \to T_\infty. \tag{6.6}$$

As did earlier, the radiative heat flux is simplified as

$$q_r = \frac{-4\sigma^*}{3k^*}\frac{\partial T^4}{\partial r} = \frac{-16\sigma^* T^3}{3k^*}\frac{\partial T}{\partial r}$$

In view of the definition of the radiative heat flux q_r, the energy equation is modified as

$$\rho c_p\left(\frac{\partial T}{\partial t} + v\frac{\partial T}{\partial r} + \frac{Ru}{r+R}\frac{\partial T}{\partial s}\right) = k_1\left(\frac{\partial^2 T}{\partial r^2} + \frac{1}{r+R}\frac{\partial T}{\partial r}\right) - \frac{1}{r+R}\frac{\partial}{\partial r}\left((r+R)\left(\frac{-16\sigma^* T^3}{3k^*}\frac{\partial T}{\partial r}\right)\right). \tag{6.7}$$

In order to convert the mathematical model involving PDEs into a mathematical model in similarity form, we introduce

$$u = \frac{as}{(1-\alpha t)}f'(\eta), \ v = -\frac{R}{r+R}\sqrt{\frac{a\nu}{(1-\alpha t)}}f(\eta), \ p = \frac{\rho a^2 s^2}{(1-\alpha t)^2}P(\eta),$$
$$\theta(\eta) = \frac{T-T_\infty}{T_w - T_\infty}; \ \theta_w = \frac{T_w}{T_\infty}; \ k = R_0\sqrt{\frac{a}{\nu}}; \ \eta = r\sqrt{\frac{a}{\nu(1-\alpha t)}}. \tag{6.8}$$

Using the above transformations Eq. (6.1) is satisfied trivially, and Eqs. (6.2), (6.3), (6.7) are transformed to

$$P'(\eta) = \frac{f'^2}{(\eta+k)}, \tag{6.9}$$

$$\frac{2k}{(\eta+k)}P(\eta) = f''' + \frac{1}{(\eta+k)}f'' - \frac{1}{(\eta+k)^2}f' + \frac{k}{(\eta+k)}ff'' - \frac{k}{(\eta+k)}(f')^2 + \frac{k}{(\eta+k)^2}ff' - M^2 f' - F_r(f')^2 - \lambda f' - \beta(f' + \frac{\eta}{2}f''), \tag{6.10}$$

$$\left(Nr + \frac{4}{3}(1+(\theta_w-1)\theta)^3\right)\left(\theta'' + \frac{\theta'}{\eta+k}\right) + PrNr\frac{k}{(\eta+k)}f\theta' - PrNr\beta\frac{\eta}{2}\theta' + 4(\theta_w-1)(\theta')^2(1+(\theta_w-1)\theta)^2 = 0. \tag{6.11}$$

On eliminating the pressure term from Eqs. (6.9) and (6.10), we obtain

$$f'''' + \frac{2}{(\eta+k)}f''' - \frac{f''}{(\eta+k)^2} + \frac{f'}{(\eta+k)^3} - \frac{k}{(\eta+k)}\left(f'f'' - ff'''\right) - \frac{k}{(\eta+k)^2}((f')^2 - ff'') - \frac{k}{(\eta+k)^3}ff' - M^2f'' - M^2\frac{f'}{(\eta+k)} - \frac{\beta}{(\eta+k)}\left(\frac{\eta}{2}f'' + f'\right) - \beta\left(\frac{\eta}{2}f''' + \frac{3}{2}f''\right) - F_r\left(2f'f'' + \frac{(f')^2}{(\eta+k)}\right) - \lambda(f'' + \frac{f'}{(\eta+k)}\Big) = 0 \tag{6.12}$$

the transformed boundary conditions are

$$\text{at } \eta = 0: \ f' = 1, \ f = 0, \ \theta = 1; \tag{6.13}$$

$$\text{as } \eta \to \infty: \ f' \to 0, \ f'' \to 0, \ \theta \to 0, \tag{6.14}$$

where k, $F_r = \frac{C_p}{\sqrt{k_2}}$, $\lambda = \frac{\nu(1-\alpha t)}{k_2 a}$, $Pr = \frac{\mu c_p}{k}$, $N_r = \frac{k_1 k*}{4\sigma^* T_\infty^3}$, β, $M^2 = \frac{\sigma B_0^2}{\rho a}$, $\theta_w = \frac{T_w}{T_\infty}$ stand for dimensionless curvature parameter, inertia coefficient (or F_r the Forchheimer number), porosity parameter, Prandtl number, radiation parameter, unsteady parameter, magnetic field parameter and temperature ratio parameter, respectively.

The essential physical quantities of engineering interest such as coefficient of skin friction and Nusselt number are denoted as C_f and Nu_s are defined as

$$C_f = \frac{\tau_{rs}}{\rho u_w^2}, \quad Nu_s = \frac{sq_w}{k_1(T_w - T_\infty)}, \tag{6.15}$$

where

$$\tau_{rs} = \mu\left(\frac{\partial u}{\partial r} - \frac{u}{r+R}\right)_{r=0}, \quad q_w = \left(-k_1\left(\frac{\partial T}{\partial r}\right) + q_r\right)_{r=0}. \tag{6.16}$$

Using (6.16) in (6.15) , the values of C_f, and Nu_s, respectively, are given by

$$C_f Re_s^{1/2} = \left(f''(0) - \frac{f'(0)}{k}\right) = f''(0) - \frac{1}{k}, \tag{6.17}$$

$$Re_s^{-1/2} Nu_s = -\left[1 + \frac{4}{3N_r}(1 + (\theta_w - 1)\theta(0))^3\right]\theta'(0). \tag{6.18}$$

Here $Re_s = \frac{su_w}{\nu}$ is the local Reynolds number.

6.3 Solution Methodology

The transformed mathematical model involving ODEs (6.11), (6.12) with suitable boundary conditions (6.13) and (6.14), are solved by the well-known in-built MATLAB solver bvp4c. The first, for using the solver, is to covert the higher order Eqs. (6.11) and (6.12) a the set of first order ODEs. For this, we make the following substitutions

$$f = y_1,\ f' = y_2,\ f'' = y_3,\ f''' = y_4,\ f'''' = yy_1,\ \theta = y_5,\ \theta' = y_6,\ \theta'' = yy_2. \tag{6.19}$$

Using the above substitutions in Eqs. (6.11) and (6.12), we obtain

$$\begin{aligned} yy_1 = &-\frac{2}{(\eta+k)}y_4 + \frac{y_3}{(\eta+k)^2} - \frac{y_2}{(\eta+k)^3} + \frac{k}{(\eta+k)}(y_2y_3 - y_1y_4) + \frac{k}{(\eta+k)^2}(y_2^2 - y_1y_3) \\ &+ \frac{k}{(\eta+k)^3}y_1y_2 + M^2y_3 + M^2\frac{y_2}{(\eta+k)} + \frac{\beta}{(\eta+k)}\left(\frac{\eta}{2}y_3 + y_2\right) + \beta\left(\frac{\eta}{2}y_4 + \frac{3}{2}y_3\right) \\ &+ F_r\left(2y_2y_3 + \frac{(y_2)^2}{(\eta+k)}\right) + \lambda\left(y_3 + \frac{y_2}{(\eta+k)}\right), \end{aligned} \tag{6.20}$$

$$yy_2 = \frac{-\left(PrNr\frac{k}{(\eta+k)}y_1y_6 - PrNr\beta\frac{\eta}{2}y_6 + 4(\theta_w-1)(y_6)^2(1+(\theta_w-1)y_5)^2\right)}{\left(Nr + \frac{4}{3}(1+(\theta_w-1)y_5)^3\right)} - \frac{y_6}{\eta+k}. \tag{6.21}$$

The above system is to be solved subject to the boundary condition, given as

$$\begin{aligned} &y_1(0) = 0,\ y_2(0) = 1,\ y_5(0) = 0, \\ &y_2(\infty) = 0,\ y_3(\infty) = 0,\ y_5(\infty) = 0. \end{aligned}$$

The above boundary value problem is implemented in bvp4c taking suitable initial guess for $y_3(0)$, $y_4(0)$, and, $y_6(0)$ and $\eta = 5$. For the chosen parameter values, the residuals are found to be less than 10^{-6} and hence obtained results are trustworthy.

6.4 Results and Discussion

We now proceed to analyze the behavior of velocity and temperature profiles through Figures 6.2-6.13 for the distinct values of various emerging parameters such as magnetic field parameter (M), dimensionless radius of curvature parameter (k), porosity parameter (λ), Forchheimer parameter (F_r), unsteadiness parameter (β), radiation parameter (N_r) and temperature ratio parameter (θ_w). Tables 6.1 and 6.2 show the numerical values of the skin-friction coefficient and Nusselt number for the distinct parameter values.

The values of these parameters are taken as $\beta = 0.2,\ k = 0.8,\ Pr = 6.2,\ N_r = 1.5,\ \lambda = 0.1,\ F_r = 0.1,\ M = 0.2$ and $\theta_w = 1.1$.

The impact of magnetic field parameter M on the profiles of velocity $f'(\eta)$ and temperature $\theta(\eta)$ is visible through Fig. 6.2 and Fig. 6.3, respectively. It is observed that with increasing values of M, there is a deceleration in the flow field. The reason behind this effect is the rising resistive force with increasing strength of the magnetic field. Also, the temperature profiles $\theta(\eta)$ rise for increasing values of M. The generated Lorentz force offers more resistance to the fluid flow, and hence the kinetic energy gets converted into thermal energy of the system, which raises the temperature of the fluid.

The change in the behaviour of velocity profile $f'(\eta)$ and temperature profile $\theta(\eta)$ for varying values of dimensionless radius of curvature parameter K can be interpreted through Fig. 6.4 and Fig. 6.5. Both the quantities, the velocity $f'(\eta)$ and the temperature $\theta(\eta)$, are enhanced with the rising values of k. Therefore, it is inferred that the velocity and temperature are higher for the flow over high curvature surfaces, and the thickness of associated boundary layers increases with increasing curvature of the surface.

Figures 6.6-6.9, depict the behavior of velocity and temperature profiles for distinct values of porosity parameter λ and Forchheimer factor F_r. The velocity curves $f'(n)$ fall with rising values of both λ and F_r. The parameter λ is inversely proportional to the permeability influence of the medium, and hence it is concluded that with the increase in porosity of the medium, the fluid velocity increases. The said effect arises due to a decrease in the resistance of the medium. Moreover, the inertia coefficient F_r is directly proportional to the porosity of the medium and drag coefficient. Thus, for a higher value of F_r, both the porosity of the medium and drag coefficient enhances. Hence, the resistive force is enhanced for the fluid, which diminishes the fluid velocity. With a rise in the porosity parameter, the resistance observed by the fluid particles is also increased, which causes some part of the kinetic energy to get transformed to thermal energy; consequently, the fluid temperature increases. The same behavior can be seen for Forchheimer factor F_r in temperature profile $\theta(\eta)$. It is clear from the figures 6.6-6.9 that the influence of the Forchheimer factor is minimal on the fluid velocity and temperature compared to that of the porosity of the medium.

The influences of unsteadiness parameter β on the velocity and temperature curves are visible in Figs. 6.10 and 6.11. When the value of β is enhanced, the velocity field is found to be decelerating; on the other hand, the temperature of the fluid enhances by raising the values of β. Hence, the influence of the unsteadiness parameter β reduces the thickness of the momentum boundary layer and increases the thickness of the thermal boundary layer.

Figures 6.12 and 6.13 show the effects of radiation parameter (N_r) and the temperature ratio parameter (θ_w) on the temperature profiles ($\theta(\eta)$). The radiation parameter is inversely related to the thermal radiation effect, and the increase in Nr implies a fall in the thermal radiation. Also, the rise in the value of (θ_w) corresponds to a rise in the surface temperature. It is visible that the fluid temperature falls for the higher values of N_r, whereas fluid temperature rises for increasing values of θ_w. Thus, it follows that the thermal radiation and the surface temperature have enhancing influence on the fluid temperature. It may be because the fluid temperature is higher than the ambient temperature for a large value of θ_w, which raises the fluid's thermal state.

The numerically computed values of coefficient of skin-friction, and coefficient of heat transfer at the surface, known as the Nusselt number, are tabulated in Tables6.1 and 6.2, respectively. It is noticed from Table 6.1 that the implication of the increase in the applied magnetic field (measured with a variation in M) is to increase the coefficient of skin-friction, whereas the impact of curvature parameter k is to decrease the coefficient of skin-friction. It is also noted from Table 6.2 that the effect of the magnetic field M, radiation N_r, and unsteadiness β is to decrease the coefficient of heat transfer. As the parameter N_r is inversely proportional to the radiation effect, it is inferred that the heat transfer rate enhances with an increase in radiative heat transfer. Also, the heat transfer at the surface increases for rising values of θ_w. The skin-friction coefficient also increases with the increase in the porosity parameter and Forchheimer number. Therefore, it follows that the porosity of the medium reduces the skin-friction coefficient. Forchheimer factor being directly proportional to drag force increases the skin-friction coefficient.

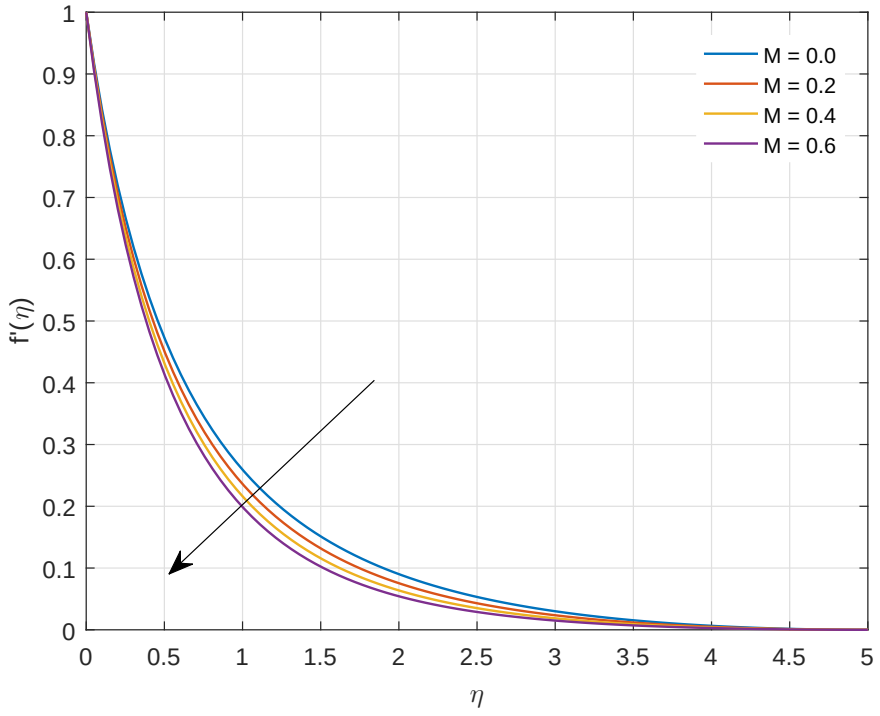

FIGURE 6.2: Graph of $f'(\eta)$ against M.

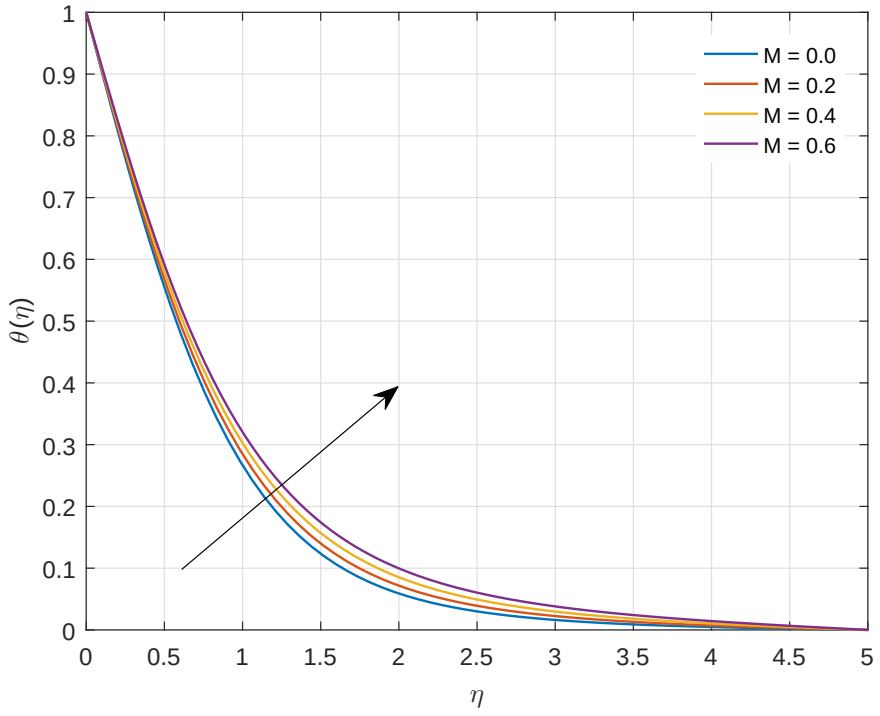

FIGURE 6.3: Graph of $\theta(\eta)$ against M.

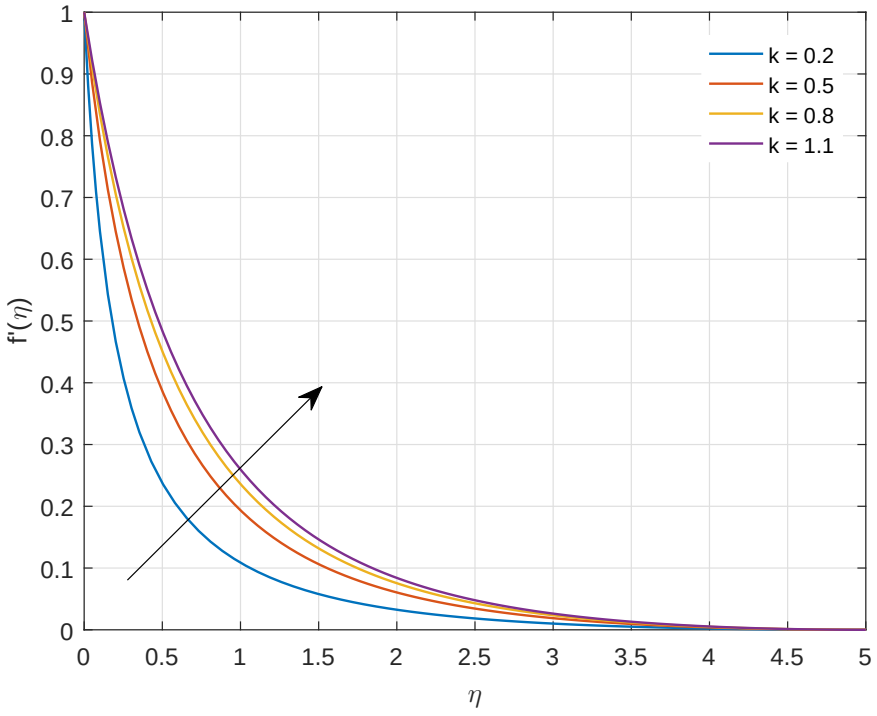

FIGURE 6.4: Graph of $f'(\eta)$ against k.

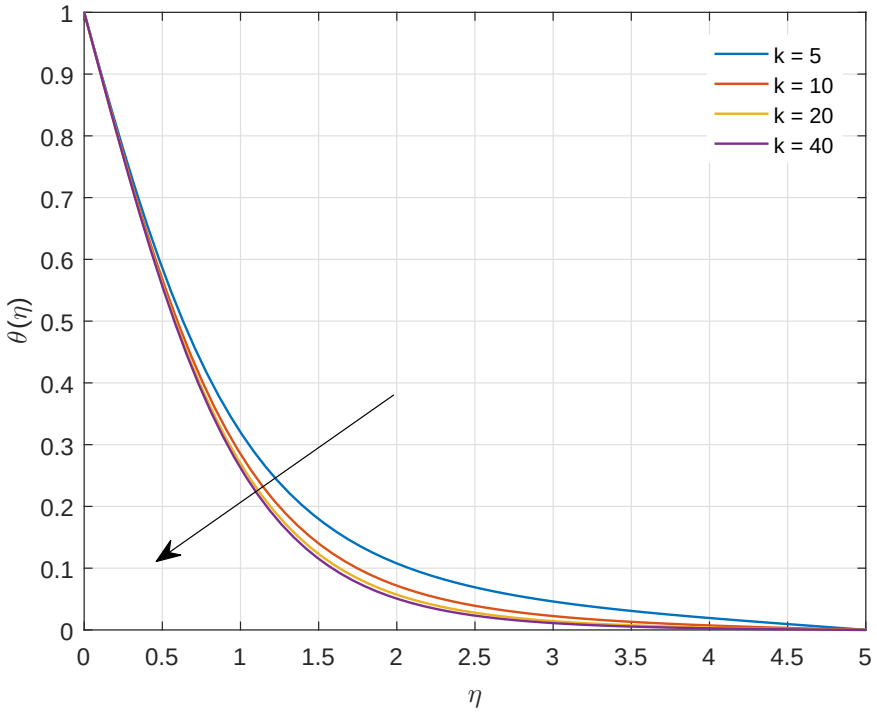

FIGURE 6.5: Graph of $\theta(\eta)$ against k.

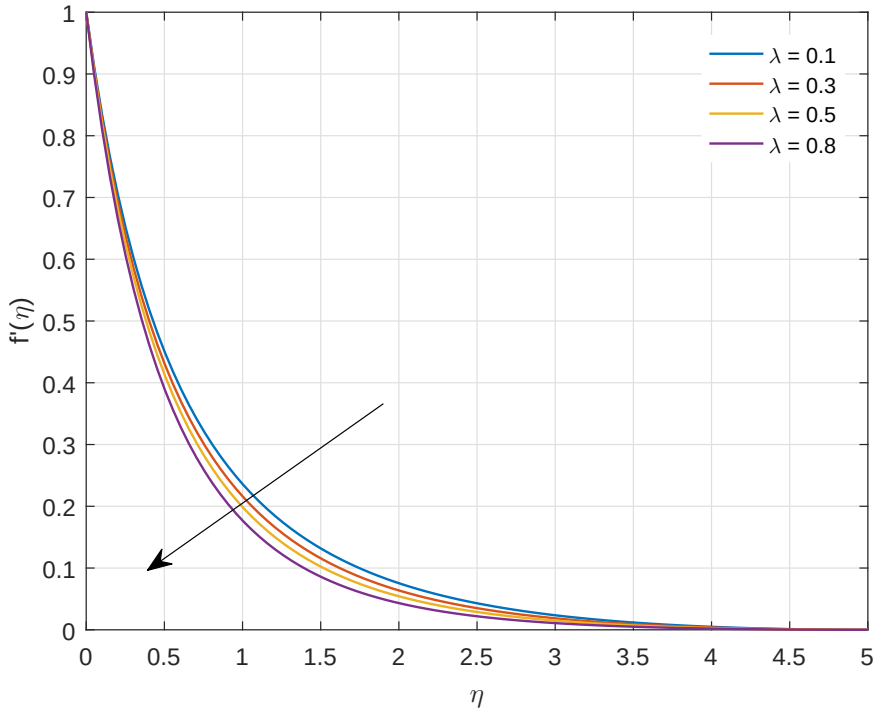

FIGURE 6.6: Graph of $f'(\eta)$ against λ.

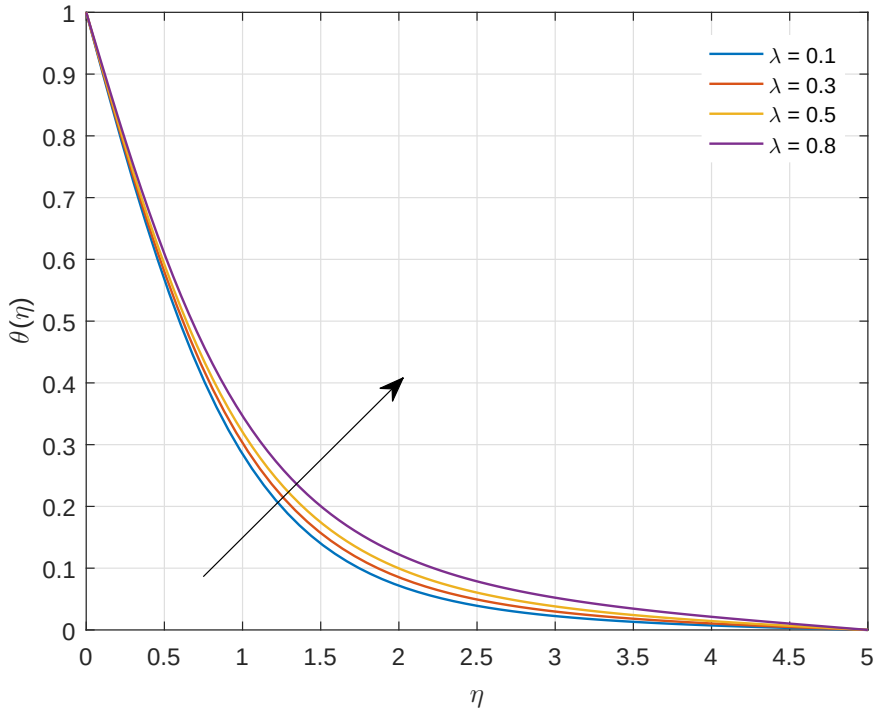

FIGURE 6.7: Graph of $\theta(\eta)$ against λ.

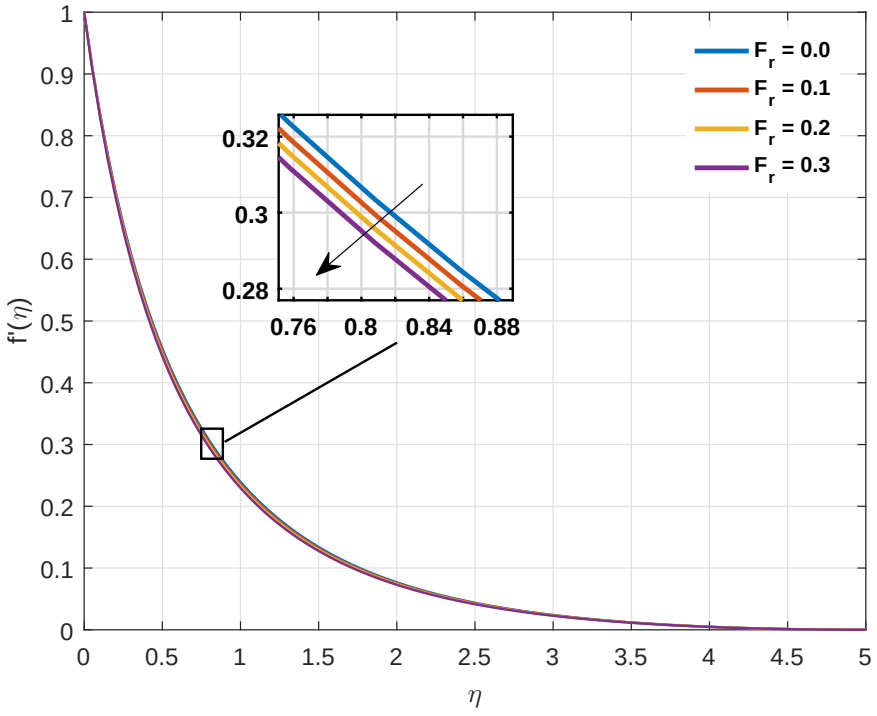

FIGURE 6.8: Graph of $f'(\eta)$ against F_r.

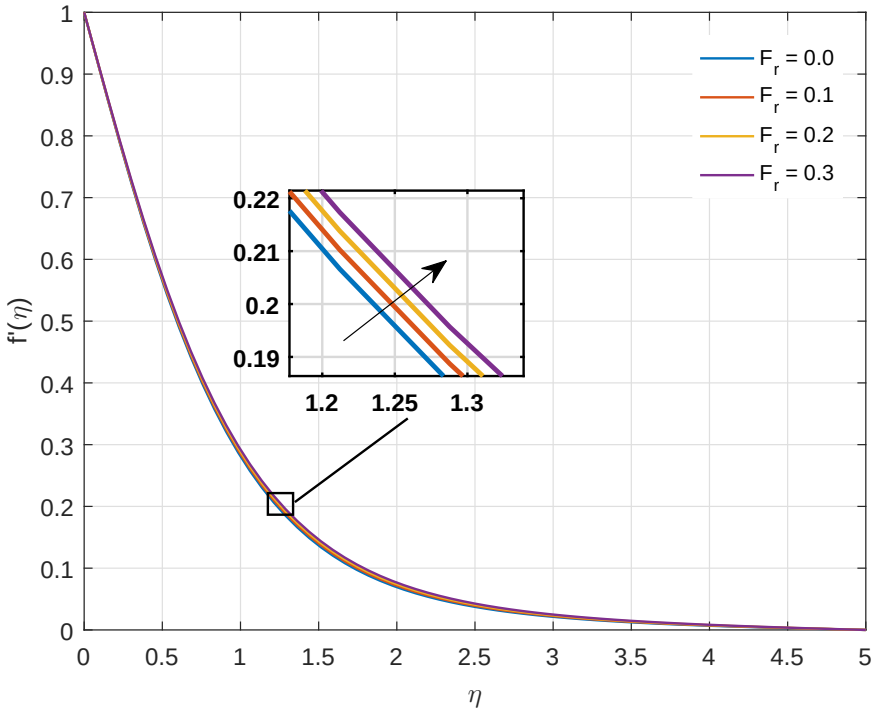

FIGURE 6.9: Graph of $\theta(\eta)$ against F_r.

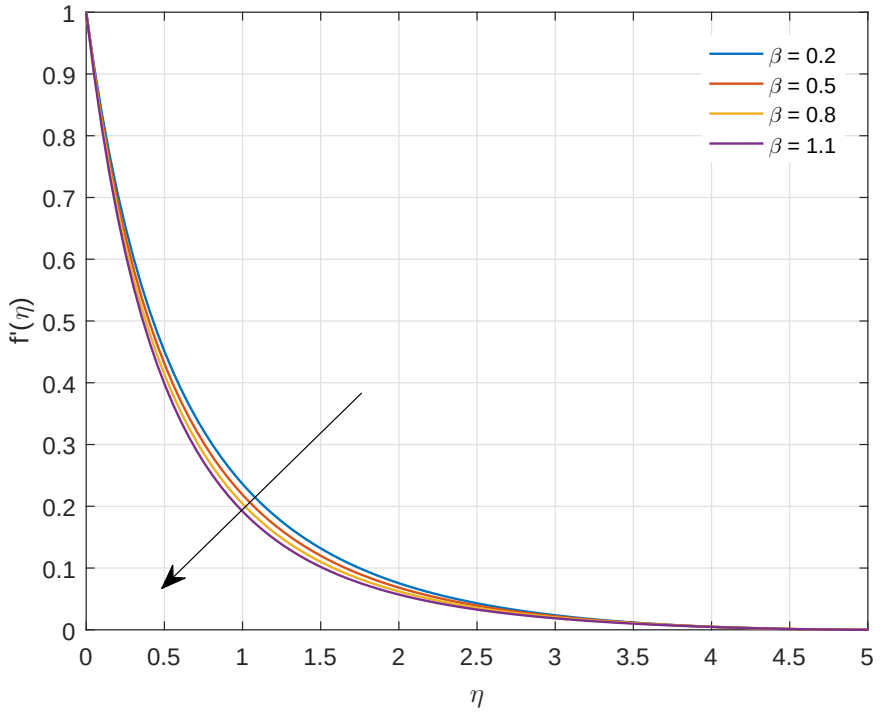

FIGURE 6.10: Graph of $f'(\eta)$ against β.

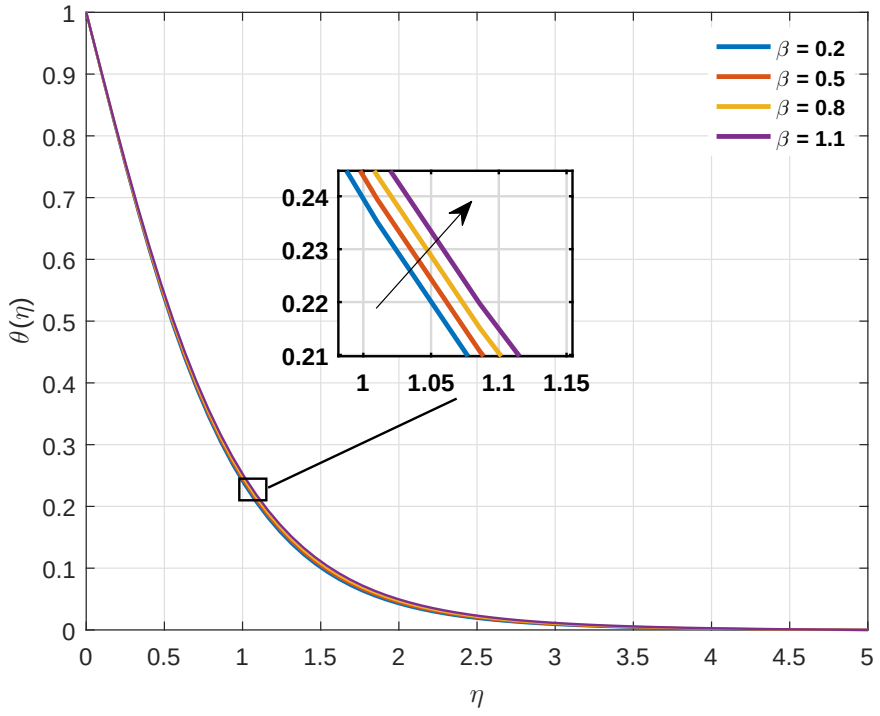

FIGURE 6.11: Graph of $\theta(\eta)$ against β.

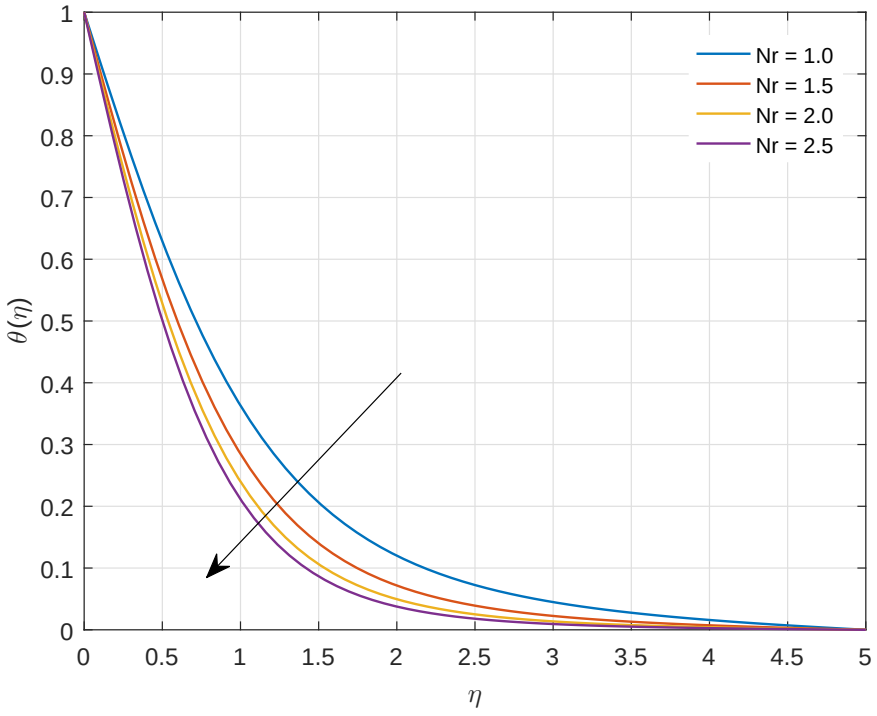

FIGURE 6.12: Graph of $\theta(\eta)$ against Nr.

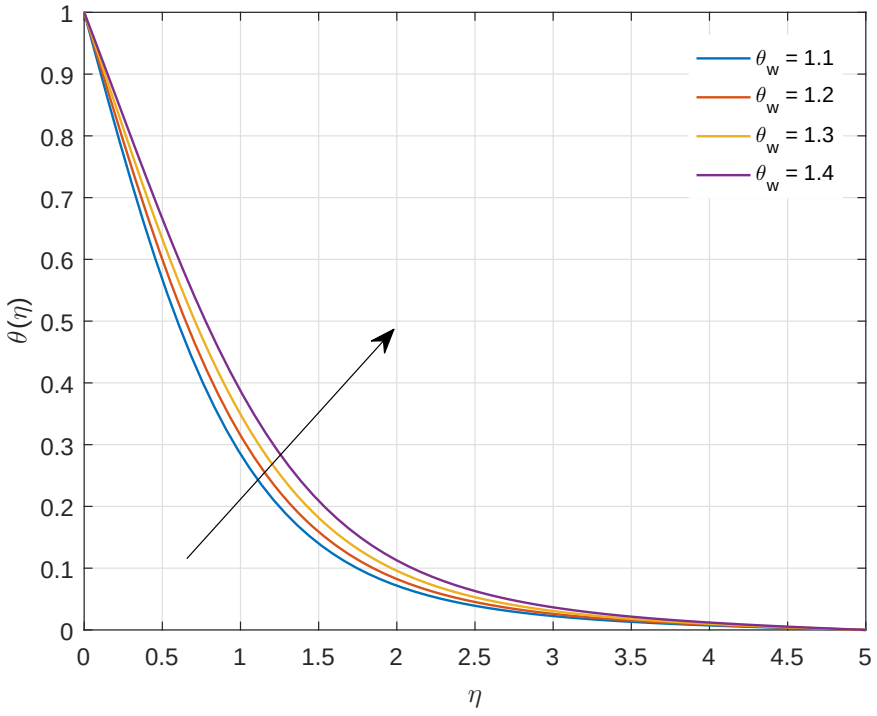

FIGURE 6.13: Graph of $\theta(\eta)$ against θ_w.

TABLE 6.1: Numerical values of skin friction coefficient for various parameter.

Fr	k	M	λ	$-C_f Re_s^{1/2}$
0.1	0.8	0.2	0.1	3.1084
0.2				3.1348
0.3				3.1606
	0.5			4.4734
	0.8			3.1084
	1.1			2.5226
		0.2		3.1084
		0.4		3.1954
		0.6		3.2771
			0.1	3.1084
			0.3	3.1954
			0.5	3.2771

TABLE 6.2: Numerical values of Nusselt number for various parameter.

M	Nr	θ_w	β	$Re_s^{-1/2} Nu_s$
0.2	1.5	1.1	0.2	1.5332
0.4				1.4639
0.6				1.4044
	0.5			2.8922
	1.0			1.8849
	1.5			1.5332
		1.1		1.5332
		1.2		1.8159
		1.3		2.1127
			0.2	1.5332
			0.3	0.6681
			0.4	0.2049

6.5 Conclusions

The unsteady boundary layer hydromagnetic flow of a viscous fluid towards a curved stretching sheet in a Darcy-Forchheimer porous medium considering the influence of nonlinear radiation is investigated numerically using the bvp4c routine. The significant findings of the investigation are as under:

1. The temperature of the fluid rises with enhancement in strength of the magnetic field, unsteadiness, thermal radiation, surface temperature, and the Forchheimer factor, while it falls with the increase in curvature of the sheet and permeability of the medium.

2. Increasing the radius of curvature of the sheet and permeability of the medium lead to the acceleration of the flow velocity. In contrast, the flow velocity gets retarded with increasing strength of the magnetic field, Forchheimer factor, and unsteadiness.

3. The coefficient of skin-friction reduces with increment in the curvature of the sheet and permeability of the medium, whereas it enhances with Forchheimer number and magnetic field.

4. The magnetic field and unsteadiness tend to diminish the heat transfer rate at the surface, whereas the thermal radiation and temperature ratio have the opposite effect.

Chapter 7

Summary, Conclusions, and Scope for Future Work

This chapter summarizes the significant contributions of the work presented in the thesis and the scope of its possible extensions. The present thesis aims to carry out a theoretical study of the magnetohydrodynamic boundary layer flow of a viscous incompressible electrically conducting fluid along a stretching surface under the existence of different conditions and configurations. The heat transfer analysis is also carried out together with the discussion of the skin-friction and Nusselt number. The goal has been achieved through five main chapters (Chapter-2 to Chapter-6). The summary and significant findings of these chapters are discussed as follows:

Chapter-1 is an introductory chapter that contains a brief background of magnetohydrodynamics, its applications, basic definitions, fundamental laws and equations, heat transfer process, relevant literature, objectives, and a brief discussion on numerical schemes, which are used in further chapters. This chapter is an attempt to make this thesis as self-contained as possible. In **Chapter-2**, a flow configuration is proposed to study the transient hydromagnetic three dimensional boundary layer radiative flow of a viscous Casson fluid towards a stretching surface considering the influences of Hall current. The governing model is presented as a set of time-dependent PDEs which are nonlinear and coupled. Similarity transformations are used to obtain ODEs in similarity form which are solved by a numerical method, namely the spectral quasilinearization method. The obtained numerical results are validated using residual analysis. A detailed study is carried out to examine the influences of significant parameters on the velocity field and temperature field profiles. The behavior of emerging quantities of engineering interest, such as skin-friction coefficient and the Nusselt number, is also studied. The

fluid flow model presented in this chapter finds applications in silicon suspensions, blood flow, polymer engineering, and the printing industry.

Chapter-3 presents a numerical analysis of the time-dependent three-dimensional hydromagnetic Casson fluid flow along a stretching surface through a porous medium considering the effects of Hall current and nonlinear radiation. The flow model formulated in **Chapter-2** is extended to include the existence of Darcy porous medium and convective heat transfer at the surface. The mathematical model of the problem is presented in a set of nonlinear partial differential equations and suitable boundary conditions. These equations are transformed to a set of nonlinear ordinary differential equations using suitable similarity transformations, which are later dealt with by the efficient Spectral quasi-linearization method (SQLM) to obtain the numerical solution. A parametric study involving the emerging physical parameters is performed to analyze the effects of relevant flow parameters on the fluid velocity, fluid temperature, and the coefficients of skin-friction and heat transfer at the surface. **Chapter-4** deals with the study of time-dependent MHD flow of a couple-stress two-phase dusty fluid flowing over a stretching surface under the influence of suction, heat generation/absorption, and viscous dissipation effects. The physical model is presented as a set of highly nonlinear partial differential equations that are further transformed into nonlinear ordinary differential equations using similarity transformations. These nonlinear ODEs are subsequently dealt with the efficient numerical technique SQLM to obtain the approximate solutions. Also, in order to validate the results, a comparison between the current results and the results existing in literature is carried out. Also, a residual analysis is performed, showing the efficiency of the technique. Moreover, a detailed study of the behavior of significant physical quantities such as skin friction coefficient and Nusselt number for distinct parameters is presented. **Chapter-5** presents an entropy generation analysis for the transient three-dimensional stagnation point flow of a hydromagnetic Casson fluid along a stretching sheet in the presence of Hall current, viscous dissipation, and nonlinear radiation. The physical model of the problem is described in terms of nonlinear PDEs with suitable boundary conditions. These PDEs are transformed into ODEs with the help of similarity transformations. The spectral quasi-linearization method (SQLM) is used to solve this model. A statistical analysis of the skin friction coefficients and the Nusselt number is performed using quadratic regression. The expressions of Bejan number and volumetric entropy generation rate are also computed. A parametric study involving the emerging physical parameters is performed to analyze the influences of relevant flow parameters on the fluid velocity, fluid temperature, Bejan number, entropy generation number, and the coefficients of skin-friction and heat transfer at the surface. **Chapter-6** presents a study of time-dependent hydromagnetic two-dimensional boundary layer flow of a viscous electrically conducting fluid in Darcy-Forchheimer porous

medium along a curved stretching sheet in the existence of nonlinear radiation. The flow model is presented in the form of partial differential equations using the curvilinear coordinate system (r, s). Similarity transformations are used to convert the partial differential equations into ordinary differential equations and solved by using the bvp4c routine. The influences of various parameters are analyzed on velocity and temperature profiles through figures and tables. Also, the essential physical quantities such as the coefficient of skin-friction and Nusselt number are discussed.

The work presented in **Chapter-2** reveals that the momentum boundary layer in x direction gets thinner with increasing effects of the magnetic field, yield stress, and unsteadiness in the flow-field, whereas the Hall effect increases it. Secondary velocity distribution is increased near the sheet's surface, and then it decreases away from the surface for the higher values of yield stress and magnetic field. The momentum boundary layer in the z direction gets thicker with the increasing effects of Hall current, whereas it gets thinner with the unsteadiness in the flow field. The effects of thermal radiation, magnetic field, unsteadiness, yield stress all have increasing effects on thermal boundary layer thickness, whereas it is diminished by Prandtl number and Hall current parameter. The effect of the applied magnetic field is to increase the coefficients of skin-friction in x and z-directions, whereas the impact of yield stress is to decrease shear-stress in both directions. The shear-stress in x-direction decreases while the shear-stress in z-direction increases due to the existence of Hall effects into the flow-field. Hall current, Prandtl number, and temperature ratio parameter increase the rate of heat transfer from the surface, whereas the effects of the magnetic field, unsteadiness in the flow-field, and Casson parameter are to reduce the rate of heat transfer at the surface. Analysis of **Chapter-3** demonstrates that the effects of the magnetic field, Hall current have the same tendency as **Chapter-2** towards the momentum boundary layers in both the directions and on the thermal boundary layer. Velocity profiles in both directions are enhanced with the higher permeability of the medium. The skin friction in the x direction is diminished with the increasing value of permeability of the medium, whereas skin friction in z direction gets higher with the increment in the permeability. The rate of heat transfer at the surface is lower in mediums with lower permeability. This decrease in the rate of heat transfer contributes to reducing the fluid temperature. The convective heating from the surface and thermal radiation tends to increase the fluid temperature within the boundary layer region, and as a result, an increment in the heat transfer rate may also be observed. An increment in the value of Pr decreases the thermal diffusivity. Due to this, there is a fall in temperature distributions and thermal boundary layer thickness. From the results of **Chapter-4**, it may be concluded that the velocity profiles for both fluid and dust phases get decelerated with the increasing effect of the suction in the flow field. The suction parameter tends to decrease the shear-stress

and increases the rate of heat transfer at the surface. Shear stress is increased for the increasing values of unsteadiness, the interaction between the fluid and dust particles, the couple-stress in the flow field. The unsteadiness, fluid-suction through the wall of the sheet, the fluid couples-stress, temperature fluid interaction, and specific heat tend to increase the rate of heat transfer from the surface, whereas the applied magnetic field, concentration of dust particles, interaction of fluid and dust particles, space and temperature-dependent heat generation/absorption, and the dissipation caused due to viscous frictional forces show reverse influence on it. It is found from **Chapter-5** that the Hall effect enhances the thickness of the momentum boundary layer in x direction, while it reduces the thickness of the thermal boundary layer, whereas an opposite behavior is observed for the effect of the magnetic field. The magnetic field and Hall current tend to accelerate the velocity distribution in z direction near the surface, while in the region away from the surface, where the strength of the induced Lorentz force weakens, the secondary flow profile behaves oppositely. There is a rise in entropy generation due to the high magnetic field, whereas the Bejan number gets reduced under the high magnetic field effect, which resolves that the contribution of magnetic field sources is dominant compared to the heat transfer sources in the entropy generation process. The effects of yield stress and unsteadiness increase the Bejan number and entropy generation in the flow field. Also, the impacts of yield stress are dominant on skin friction coefficient in x direction, compared to the magnetic effect. The estimated accuracy of the skin-friction coefficient in z is greater than that of the skin-friction coefficient in x. The work presented in **Chapter-6** reveals that the effect of the magnetic field remains similar to the previous chapters on the velocity and temperature profiles. The velocity of the fluid is decreased with increasing values of the Forchheimer factor and porosity parameter. The radius of curvature, Forchheimer factor, and porosity parameter tend to increase the temperature of the fluid. The influence of the radiation parameter is to reduce the rate of heat transfer from the surface. Hence there is a fall in the fluid temperature profile and thermal boundary layer thickness. In contrast, skin friction at the surface is increased by the magnetic field.

In the future, all the problems presented in the thesis may be extended, taking the sheet's rotational motion, further inducing a velocity field in the secondary flow direction. One may also be interested in studying the entropy generation for the problems presented in Chapter-2, Chapter-3, Chapter-4, and Chapter-6. The problem considered in Chapter-6 may further be investigated considering the presence of dust particles in the flow-field. The impacts of the induced magnetic field may be analyzed on all the problems of the thesis.

Bibliography

[1] B. C. Sakiadis. Boundary-layer behaviour on continuous solid surface:i, boundary-layer equations for two-dimensional and axisymmetric flow. *American Inst. Chemical Eng. J.*, 7(1):26–29, 1961.

[2] L. J. Crane. Flow past a stretching plate. *Z. Angew. Math. Phys.*, 21:645–647, 1970.

[3] L. E. Erickson, L. T. Fan, and V. G. Fox. Heat and mass transfer on a moving continuous at plate with suction or injection. *Ind. Eng. Chem. Fund.*, 5:19–25, 1966.

[4] B. K. Dutta, P. Roy, and A. S. Gupta. Temperature field in the flow over a stretching sheet with uniform heat flux. *Int. Commun. Heat Mass Transf.*, 12: 89–94, 1985.

[5] P. M. Patil, S. Roy, and Ali J. Chamkha. Mixed convection flow over a vertical power-law stretching sheet. *Int. J. Numer. Method. H.*, 20(4):445–458, 2010.

[6] H. Maleki, M. R. Safaei, H. Togun, and M. Dahari. Heat transfer and fluid flow of pseudo-plastic nanofluid over a moving permeable plate with viscous dissipation and heat absorption/generation. *J. Therm. Anal. Calorim*, 135(3):1643–1654, 2019.

[7] M. K. A. Mohamed, M. Z. Salleh, and A. Ishak. Effects of viscous dissipation on mixed convection boundary layer flow past a vertical moving plate in a nanofluid. *J. Adv. Res. Fluid Mech. Therm. Sci.*, 69:1–18, 2021.

[8] N. A. Kelson and A. Desseaux. Effect of surface conditions on flow of a micropolar fluid driven by a porous stretching sheet. *Int. J. Eng. Sci.*, 39:1881–1897, 2001.

[9] S. R Mishra, P. Mathur, and H. M. Ali. Analysis of homogeneous-heterogeneous reactions in a micropolar nanofluid past a nonlinear stretching surface: semi-analytical approach. *J. Them. Anal. Calorim.*, 144:2247–2257, 2021.

[10] R. Bhargava, L. Kumar, and H. S. Takhar. Finite element solution of mixed convection micropolar flow driven by a porous stretching sheet. *Int. J. Eng. Sci.*, 41:2161–2178, 2003.

[11] M. M. Janjua, N. U. Khan, W. A. Khan, W. S. Khan, and H. M. Ali. Numerical study of forced convection heat transfer across a cylinder with various cross sections. *J. Therm. Anal. Calorim.*, 143:2039–2052, 2021.

[12] S. Nadeem, R. Ul Haq, and Z. H. Khan. Heat transfer analysis of water-based nano fluid over an exponentially stretching sheet. *Alex. Eng. J.*, 53:219–224, 2014.

[13] M. Mustafa, A. Mushtaq, T. Hayat, and B. Ahmad. Nonlinear radiation heat transfer effects in the natural convective boundary layer flow of nano fluid past a vertical plate: A numerical study. *Plos One*, 9, 2014. ISSN 9. doi: 10.1371/journal.pone.0103946.

[14] O. D. Makinde and A. Aziz. Boundary layer flow of a nanofluid past a stretching sheet with a convective boundary condition. *Int. J. Therm. Sci.*, 50:1326–1332, 2011.

[15] A. Kumar, R. Tripathi, R. Singh, and M. A. Sheremet. Entropy generation on double diffusive MHD Casson nanofluid flow with convective heat transfer and activation energy. *Indian J. Phys.*, 95:1423–1436, 2021.

[16] J. Hartmann. Hg-dynamics. part-i, kgl. danske videnskad. *Mat. Fus. Medd*, 6:15, 1937.

[17] F. Lazarus J. Hartmann. Hg-dynamics. part-ii kgl. danske videnskad. *Mat. Fus. Medd.*, 6:15, 1937.

[18] H. Alfven. Existence of electromagnetic-hydrodynamic waves. *Nature*, 150:405–406, 1942. ISSN 3805.

[19] K. B. Pavlov. Magnetohydrodynamic flow of an incompressible viscous fluid caused by deformation of a surface. *Magn. Gidrodin.*, 4:146–147., 1974.

[20] V. Kumaran, A. K. Banerjee, A. Vanav Kumar, and K. Vajravelu. MHD flow past a stretching permeable sheet. *Appl. Math. Comput.*, 210:26–32, 2009.

[21] B. Mahanthesh, B. J. Gireesha, R. S. Reddy Gorla, F. M. Abbasi, and S. A. Shehzad. Numerical solutions for magnetohydrodynamic flow of nanofluid over a bidirectional non-linear stretching surface with prescribed surface heat flux boundary. *J. Magn. Mang. Mater.*, 417:189–196, 2016.

[22] R. Jusoh, R. Nazar, and I. Pop. Magnetohydrodynamic boundary layer flow and heat transfer of nanofluids past a bidirectional exponential permeable stretching/shrinking sheet with viscous dissipation effect. *J. Heat Trans.*, 141(1):012406, 2018.

[23] B. J. Gireesha, M. Umeshaiah, B. C. Prasannakumara, N. S. Shashikumar, and M. Archana. Impact of nonlinear thermal radiation on magnetohydrodynamic three dimensional boundary layer flow of jeffrey nanofluid over a nonlinearly permeable stretching sheet. *Physica A*, 124051, 2020. doi: 10.1016/j.physa.2019.124051.

[24] M. A. Kumar, Y. D. Reddy, V. S. Rao, and B. S Goud. Thermal radiation impact on MHD heat transfer natural convective nano fluid flow over an impulsively started vertical plate. *Case Stud. Therm. Eng.*, 24, 2021. doi: 10.1016/j.csite.2020.100826.

[25] A. Tassaddiq. Impact of cattaneo-christov heat fux model on MHD hybrid nanomicropolar fuid fow and heat transfer with viscous and joule dissipation efects. *Scientific Reports*, 2021. doi: 10.1038/s41598-020-77419-x.

[26] S. Nadeem, S. Akhtar, and N. Abbas. Heat transfer of Maxwell base fluid flow of nanomaterial with MHD over a vertical moving surface. *Alex. Eng. J.*, 59: 1847–1856, 2020.

[27] A. M. Megahed and M. G. Reddy. Numerical treatment for MHD viscoelastic fluid flow with variable fluid properties and viscous dissipation. *Indian J. Phys.*, 95: 673–679, 2021. ISSN 4.

[28] P. K. Kameswaran, M. Narayana, P. Sibanda, and P. V. S. N. Murthy. Hydromagnetic nanofluid flow due to a stretching or shrinking sheet with viscous dissipation and chemical reaction effects. *Int. J. Heat Mass Tran.*, 55:7587–7595, 2012.

[29] E. H. Hall. On a new action of the magnet on electric currents. *Am. J. Math*, 2: 287–292, 1879.

[30] A. S. Gupta. Hydromagnetic flow past a porous flat plate with Hall effects. *Acta Mech.*, 22:281–287, 1975.

[31] T. Hayat, Z. Abbas, and S. Asghar. Effects of Hall current and heat transfer on rotating flow of a second grade fluid through a porous medium. *Commun. Nonlinear Sci. Numer. Simul.*, 13:2177–2192, 2008.

[32] A. M. Saleem and M. A. E. Aziz. Effect of Hall currents and chemical reaction on hydromagnetic flow of a stretching vertical surface with internal heat generation/absorption. *Appl. Math. Model*, 32:1236–1254, 2008.

[33] S. S. Motsa and S. Shateyi. The effects of chemical reaction, Hall, and ion-slip currents on MHD micropolar fluid flow with thermal diffusivity using a novel numerical technique. *J. Applied Math.*, 2012:1–30, 2012.

[34] Ali. J. Chamkha. MHD-free convection from a vertical plate embedded in a thermally stratified porous medium with hall effects. *Appl. Math. Model*, 21:603–609, 1997. ISSN 10.

[35] M. A. Seddeek. Effects of Hall and ion-slip currents on magneto-micropolar fluid and heat transfer over a non-isothermal stretching sheet with suction and blowing. *Proc. R. Soc. Lond. A*, 457:3039–3050, 2001.

[36] A. S. Sabu, A. Mathew, T. S. Neethu, and K. Anil George. Statistical analysis of MHD convective ferro-nanofluid flow through an inclined channel with Hall current, heat source and soret effect. *Therm. Sci. Eng. Prog.*, 100816, 2020. doi: 1016/j.tsep.2020.100816.

[37] D. Kumar, A. K. Singh, K. Bhattacharyya, and A. Banerjee. Effects of Hall current on MHD natural convection in between two vertical flat walls with induced magnetic field and heat source/sink. *Int. J. Ambient Energy*, 2021. doi: 1080/01430750.2021.1874516.

[38] M. Fiza, A. Alsubie, H. Ullah, N. N. Hamadneh, S. Islam, and I. Khan. Three-dimensional rotating flow of MHD jeffrey fluid flow between two parallel plates with impact of Hall current. *Math. Probl. Eng.*, 2021, 2021. doi: 1155/2021/6626411.

[39] N. Riley. Siam rev. *Unsteady laminar boundary layers*, 17:274–297, 1975.

[40] W.J. McCroskey. Some current research in unsteady fluid dynamics. *J. Fluid Eng.-T. ASME*, 99:8–39, 1977.

[41] D. P. Telionis. Review- unsteady boundary layers separated and attached. *J. Fluids Eng.-T. ASME*, 101:29–43, 1979.

[42] T. Cebeci. Unsteady boundary layers with an intelligent numerical scheme. *J. Fluids Mech.*, 163:129–140, 1986.

[43] J. Coustex. Three-dimensional and unsteady boundary layer computions. *Annu. Rev. Fluid Mech.*, 18:173–196, 1986.

[44] E. M. A. Elbashbeshy. Heat transfer over a stretching surface with variable surface heat flux. *J. Phys. D: Appl. Phys.*, 31:1951–1954, 1998.

[45] T. R. Mahapatra and A. S. Gupta. Heat transfer in stagnation-point flow towards a stretching sheet. *Heat Mass Transfer*, 38:517–521, 2002.

[46] C. Y. Wang. Liquid film on an unsteady stretching surface. *Q. Appl. Math.*, 48: 1234–1237, 1990.

[47] E. M. A. Elbashbeshy and M. A. A. Bazid. Heat transfer over an unsteady stretching surface. *Heat Mass Transfer*, 41:1–4, 2004.

[48] A. Ishak, R. Nazar, and I. Pop. Boundary layer flow and heat transfer over an unsteady stretching vertical surface. *Meccanica*, 44:369–375, 2009.

[49] M. A. E. Aziz. Radiation effect on the flow and heat transfer over an unsteady stretching sheet. *Int. Commun. Heat Mass*, 36:521–524, 2009.

[50] D. Pal. Hall current and MHD effects on heat transfer over an unsteady stretching permeable surface with thermal radiation. *Comput. Math. Appl.*, 66:1161–1180, 2013.

[51] A. M. Megahed, M. G. Reddy, and W.Abbas. Modeling of MHD fluid flow over an unsteady stretching sheet with thermal radiation, variable fluid properties and heat flux. *Math. Comput. Simulat.*, 185:583–593, 2021.

[52] S. Matta, BalaSidduluMalga, L. Appidi, and P. P. Kumar. Radiation and chemical reaction effects on unsteady MHD free convention mass transfer fluid flow in a porous plate. *Indian J. Sci. Technol.*, 14:707–717, 2021.

[53] M. N. Khan, N. Ullah, and S. Nadeem. Transient flow of Maxwell nanofluid over a shrinking surface: Numerical solutions and stability analysis. *Surf. Interfaces*, 22:100829, 2021. doi: 016/j.surfin.2020.100829.

[54] A. Bhandari. Numerical study of time-dependent ferrofuid fow past a cylinder in the presence of stationary magnetic feld. *SN Applied Sciences*, 2021.

[55] R. Vemula, M. Kavitha, and M. A. Sheremet. Effects of internal heat generation and Lorentz force on unsteady hybrid nanoliquid flow and heat transfer along a moving plate with nonuniform temperature. *Heat Transfer*, 50:2975–2996, 2021.

[56] N. T. M. Eldabe and M. G. E. Salwa. Heat transfer of MHD non-newtonian Casson fluid flow between two rotating cylinders. *J. Phys. Soc. Jpn.*, 64:41–64, 1995.

[57] S. A. Shehzad, T. Hayat, M. Qasim, and S. Asghar. Effects of mass transfer on MHD flow of a Casson fluid with chemical reaction and suction. *Braz. J. Chem. Eng.*, 30:187–195, 2013.

[58] M. N. Tufail, A. S. Butt, and A. Ali. Heat source/sink effects on non-newtonian MHD fluid flow and heat transfer over a permeable stretching surface: Lie group analysis. *Indian J. Phys.*, 88:75–82, 2013. doi: 10.1007/s12648-013-0376-3.

[59] S. K. Nandy. Analytical solution of MHD stagnation-point flow and heat transfer of Casson fluid over a stretching sheet with partial slip. *ISRN. Thermodynamics*, 2013:Article ID 108264, 2013. doi: 10.1155/2013/108264.

[60] S. Mukhopadhyay. Casson fluid flow and heat transfer over a nonlinearly stretching surface. *Chinese Phys.*, 27:074701–074705, 2013.

[61] K. Vajravelu, S. Mukhopadhyay, and R. A. V. Gorder. Casson fluid flow and heat transfer at an exponentially stretching permeable surface. *J. Appl. Mech.*, 80: 054502–054509, 2013.

[62] S. Mukhophadhyay and K. Vajravelu. Diffusion of chemically reactive species in Casson fluid flow over an unsteady permeable stretching surface. *J. Hydrodyn.*, 25:591–598, 2013.

[63] A. S. Butt, M. N. Tufaila, and Asif Alia. Three-dimensinal flow of a magneto-hydrodynamic Casson fluid over an unsteady stretching sheet embedded into a porous medium. *J. App. Mech. Tech. Phys.*, 57:283–292, 2016.

[64] M. I. Khan, M. Waqas, T. Hayat, and A. Alsaedi. A comparative study of Casson fluid with homogeneous-heterogeneous reactions. *J. Coll. Int. Sci.*, 498:85–90, 2017.

[65] M. B. Ashraf, T. Hayat, and A. Alsaedi. Mixed convection flow of Casson fluid over a stretching sheet with convective boundary conditions and Hall effect. *Boundary Value Problems*, 2017:137, 2017.

[66] M. Hamid, M. Usman, Z. H. Khan, R. Ahmad, and W. Wang. Dual solutions and stability analysis of flow and heat transfer of Casson fluid over the stretching sheet. *Phys. Lett. A*, 383:2400–2408, 2019.

[67] M. Awais, M. A. Z. Raja, S. E. Awan, M. Shoaib, and H. M. Ali. Heat and mass transfer phenomenon for the dynamics of Casson fluid through porous medium over shrinking wall subject to Lorentz force and heat source/sink. *Alex. Eng. J.*, 60:1355–1363, 2021.

[68] T. Salahuddin, M. Arshad, N. Siddique, A. S. Alqahtani, and M.Y. Malik. Thermophyical properties and internal energy change in Casson fluid flow along with activation energy. *Ain Shams Eng. J.*, 11:1355–1365, 2020.

[69] A. S. Mittal and H. R. Patel. Influence of thermophoresis and Brownian motion on mixed convection two dimensional MHD Casson fluid flow with non-linear radiation and heat generation. *Physica A*, 537:122710, 2020. doi: 10.1016/j.physa.2019.122710.

[70] V. K. Stokes. Couple stresses in fluids. *Phys. Fluids*, 9:1709–1715, 1966.

[71] T. Hayata, M. Awaisa, A. Safdara, and A. A. Hendib. Unsteady three dimensional flow of couple stress fluid over a stretching surface with chemical reaction. *Nonlinear Anal. - Model.*, 17(1):47–59, 2012.

[72] M. Ramzan, M. Farooq, A. Alsaedi, and T. Hayat. MHD three-dimensional flow of couple stress fluid with Newtonian heating. *Eur. Phys. J. Plus*, 128(49), 2013. doi: 10.1140/epjp/i2013-13049-5.

[73] M. Kumar, G. J. Reddy, N. N. Kumar, and O. A. Beg. Computational study of unsteady couple stress magnetic nanofluid flow from a stretching sheet with Ohmic dissipation. *Proc. Inst. Mech. Eng.-Part N: J. Nanoeng. Nanomater. Nanosyst.*, 233:49–63, 2019. doi: 10.1177/2397791419843730.

[74] P. V. S. Narayana, N. Tarakaramu, and D. H. Babu. Influence of chemical reaction on MHD couple stress nanoliquid flow over a bidirectional stretched sheet. *Int. J. Ambient Energy*, 2021. doi: 10.1080/01430750.2021.1923569.

[75] S. Aziz, I. Ahmad, N. Ali, and S. U. Khan. Magnetohydrodynamic mixed convection 3-D simulations for chemically reactive couple stress nanofuid over periodically moving surface with thermal radiation. *J. Therm. Anal. Calorim.*, 2020. doi: 10.1007/s10973-020-09962-8.

[76] R. Ali, A. Farooq, A. Shahzad, A. C. Benim, A. Iqbal, and M. Razzaq. Computational approach on three-dimensional flow of couple-stress fluid with convective boundary conditions. *Physica A*, 553:124056, 2020. doi: 10.1016/j.physa.2019.124056.

[77] P. V. S. Narayana, N. Tarakaramu, G. Sarojamma, and I. L. Animasaun. Numerical simulation of nonlinear thermal radiation on the 3D flow of a couple stress Casson nanofluid due to a stretching sheet. *J. Thermal Sci. Eng. Appl*, 13:021028, 2021. doi: 10.1115/1.4049425.

[78] P.G. Saffman. The stability of laminar flow of a dusty gas. *J. Fluid Mech.*, 13: 120–128, 1962.

[79] K. Vajravelu and J. Nayfeh. Hydromagnetic flow of a dusty fluid over a stretching sheet. *Int. J. Nonlinear Mechanics*, 27(6):937–945, 1992.

[80] B. J. Gireesha, G. K. Ramesh, M. S. Abel, and C. S. Bagewadi. Boundary layer flow and heat transfer of a dusty fluid flow over a stretching sheet with non-uniform heat source/sink. *Int. J. Multiphase Flow*, 37(8):977–982, 2011.

[81] M. Turkyilmazoglu. Magnetohydrodynamic two-phase dusty fluid flow and heat model over deforming isothermal surfaces. *Phys. Fluids*, 29(1):013302–013309, 2017.

[82] K. Ganesh Kumar, B. J. Gireesha, and R. S. R. Gorla. Flow and heat transfer of dusty hyperbolic tangent fluid over a stretching sheet in the presence of thermal radiation and magnetic field. *Int. J. Mech. Mater. Eng.*, 13, 2018. doi: 10.1186/s40712-018-0088-8.

[83] Z. Abbas, J. Hasnain, and M. Sajid. Effects of slip on MHD flow of a dusty fluid over a stretching sheet through porous space. *J. Engin. Thermophys.*, 28(1): 84–102, 2019.

[84] M. Bibi, A. Zeeshan, M. Y. Malik, and K. U. Rehman. Numerical investigation of the unsteady solid-particle flow of a tangent hyperbolic fluid with variable thermal conductivity and convective boundary. *Eur. Phys. J. Plus*, 134, 2019. doi: 10.1140/epjp/i2019-12651-9.

[85] M. A. Ali, A. M. Ismail, and S. Vaithyasubramanian. Dusty fluid flow - unsteady MHD with two parallel plates with heat and mass source. *J. Phys.: Conf. Ser.*, 1710:012046, 2021. doi: 10.1088/1742-6596/1770/1/012046.

[86] B. Mahanthesh, J. Mackolil, M.Radhika, W. Al-Kouz, and Siddabasappa. Significance of quadratic thermal radiation and quadratic convection on boundary layer two-phase flow of a dusty nanoliquid past a vertical plate. *Int. Commun. Heat Mass*, 120:105029, 2021. doi: 10.1016/j.icheatmasstransfer.2020.105029.

[87] M. Bilal, S. Khan, F. Ali, M. Arif, I. Khan, and K. S. Nisar. Couette flow of viscoelastic dusty fluid in a rotating frame along with the heat transfer. *Sci. Rep.*, 11, 2021. doi: 10.1038/s41598-020-79795-w.

[88] B.J. Gireesha, B. M. Shankaralingappa, B.C. Prasannakumar, and B. Nagaraja. MHD flow and melting heat transfer of dusty Casson fluid over a stretching sheet with Cattaneo Christov heat flux model. *Int. J. Ambient Energy*, 2020. doi: 10.1080/01430750.2020.1785938.

[89] I. Waini, A. Ishak, I. Pop, and R. Nazar. Dusty hybrid nanofluid flow over a shrinking sheet with magnetic field effects. *Int. J. Numer. Method H.*, 2021. doi: 10.1108/HFF-01-2021-0081.

[90] A. Bejan. A study of entropy generation in fundamental convective heat transfer. *ASME. J. Heat Transfer*, 101(4):718–725, 1979.

[91] A. Bejan. Second law analysis in heat transfer and thermal design. *Adv. Heat Transfer*, 15:1–58, 1982.

[92] M. M. Rashidi, F. Mohammadi, S. Abbasbandy, and M. S. Alhuthali. Entropy generation analysis for stagnation point flow in a porous medium over a permeable stretching surface. *J. Appl. Fluid Mech.*, 8:753–765, 2014.

[93] S. U. Khan, S. A. Shehzad, A. Rauf, and N. Ali. Mixed convection flow of couple stress nanofluid over oscillatory stretching sheet with heat absorption/generation effects. *Results Phys.*, 8:1223–1231, 2018.

[94] M. Abd El-Aziz and A. A. Afify. MHD Casson fluid flow over a stretching sheet with entropy generation analysis and Hall influence. *Entropy*, 21(6), 2019. doi: 10.3390/e21060592.

[95] A. R. Hassan. The entropy generation analysis of a reactive hydromagnetic couple stress fluid flow through a saturated porous channel. *Appl. Math. Comput.*, 369: 124843, 2020.

[96] A. Alsaedi, T. Hayat, S. Qayyumb, and R. Yaqoobb. Eyring-powell nanofluid flow with nonlinear mixed convection: Entropy generation minimization. *Comput. Meth. Prog. Bio.*, 186:105183, 2020.

[97] A. Zaib, R. U. Haq, M. Sheikholeslami, A. J. Chamkha, and M. M. Rashidi. Impact of non-darcy medium on mixed convective flow towards a plate containing micropolar water-based tio2 nanomaterial with entropy generation. *J. Porous Media*, 23:11–26, 2020.

[98] C. Siddabasappa, P. G. Siddheshwar, and O. D. Makinde. A study on entropy generation and heat transfer in a magnetohydrodynamic flow of a couple-stress fluid through a thermal nonequilibrium vertical porous channel. *Heat Transfer*, 50:6377–6400, 2021.

[99] M. Sajid, N. Ali, T. Javed, and Z. Abbas. Stretching a curved surface in a viscous fluid. *Chin. Phys. Lett.*, 27:024703, 2010.

[100] M. Sajid, N. Ali, T. Javed, and Z. Abbas. Flow of a micropolar fluid over a curved stretching surface. *J. Eng. Phys. Thermophys.*, 84:798–804, 2011.

[101] Z. Abbas, M. Naveed, and M. Sajid. Heat transfer analysis for stretching flow over a curved surface with magnetic field. *J. Eng. Thermophys.*, 22:337–345, 2013.

[102] N.C. Rosca and I. Pop. Unsteady boundary layer flow over a permeable curved stretching/shrinking surface. *Eur. J. Mech. B. Fluids*, 51:61–67, 2015.

[103] Z. Abbas, M. Naveed, and M. Sajid. Hydromagnetic slip flow of nanofluid over a curved stretching surface with heat generation and thermal radiation. *J. Mol. Liq.*, 215:756–762, 2016.

[104] T. Hayat, M. Rashid, M. Imtiaz, and A. Alsaedi. MHD convective flow due to a curved surface with thermal radiation and chemical reaction. *J. Mol. Liq.*, 225: 482–489, 2017.

[105] M. Imtiaz, T. Hayat, and A. Alsaedi. Convective flow of ferrofluid due to a curved stretching surface with homogeneous-heterogeneous reactions. *Powder Technol.*, 310:154–162, 2017.

[106] T. Shabbir, M. Mushtaq, M. I. Khan, and T. Hayat. Modeling and numerical simulation of micropolar fluid over a curved surface: Keller box method. *Comput. Meth. Prog. Bio.*, 187:105220, 2020.

[107] R. S. Saif, T. Muhammad, H. Sadia, and R. Ellahi. Boundary layer flow due to a nonlinear stretching curved surface with convective boundary condition and homogeneous and heterogeneous reactions. *Physica A*, 551:123996, 2020.

[108] S. Nadeem, N. Abbas, and M. Y. Malik. Inspection of hybrid based nanofluid flow over a curved surface. *Comput. Meth. Prog. Bio.*, 189:105193, 2020.

[109] P. Forchheimer. Wasserbewegung durch boden. *Z. Ver. Dtsch, Ing.*, 45:1782–1788, 1901.

[110] M. Muskat. The flow of homogeneous fluids through porous media. *MI: Edwards*, 1946.

[111] M. A. Seddeek. Influence of viscous dissipation and thermophoresis on Darcy-Forchheimer mixed convection in a fluid saturated porous media. *J. Colloid Interf. Sci.*, 293:137–142, 2006.

[112] T. Hayat, T. Muhammad, S. Al-Mezal, and S. J. Liao. Darcy-Forchheimer flow with variable thermal conductivity and Cattaneo-Christov heat flux. *Int. J. Numer. Method. H.*, 26:2355–2369, 2016.

[113] T. Muhammad, A. Alsaedi, T. Hayat, and S. A. Shehzad. A revised model for Darcy-Forchheimer three-dimensional flow of nanofluid subject to convective boundary condition. *Results Phys.*, 7:2791–2797, 2017.

[114] Y. Do, G. Ramesh, G. Roopa, and M. Sankar. Naviers slip condition on time dependent Darcy-forchheimer nanofluid using spectral relaxation method. *J. Cent. South Univ.*, 26:2000–2010, 2019.

[115] T. Hayat, S. Qayyum, A. Alsaedi, and B. Ahmad. Entropy generation minimization: Darcy-forchheimer nanofluid flow due to curved stretching sheet with partial slip. *Int. Commun. Heat Mass*, 111:104445, 2020.

[116] F. B. Tadesse, O. D. Makinde, and L. G. Enyadene. Hydromagnetic stagnation point flow of a magnetite ferrofluid past a convectively heated permeable stretching/shrinking sheet in a Darcy-forchheimer porous medium. *Sadhana*, 46, 2021. doi: 10.1007/s12046-021-01643-y.

[117] S. Nadeem, M. Ijaz, and M. Ayub. DarcyForchheimer fow under rotating disk and entropy generation with thermal radiation and heat source/sink. *J. Therm. Anal. Calorim.*, 143:2313–2328, 2021.

[118] S. A. Khan, T. Hayat, and A. Alsaedi. Irreversibility analysis in Darcy-Forchheimer flow of viscous fluid with Dufour and Soret effects via finite difference method. *Case Stud. Therm. Eng.*, 101065, 2021. doi: 10.1016/j.csite.2021.101065.

[119] B. M. Shankaralingappa, B. J. Gireesha, B. C. Prasannakumara, and B. Nagaraja. Darcy-Forchheimer flow of dusty tangent hyperbolic fluid over a stretching sheet with Cattaneo-Christov heat flux. *Wave. Random. Complex.*, 2021. doi: 10.1080/17455030.2021.1889711.

[120] F. Haider, T. Hayat, and A. Alsaedi. Flow of hybrid nanofluid through Darcy-Forchheimer porous space with variable characteristics. *Alex. Eng. J.*, 60:3047–3056, 2021.

[121] A. Saeed, W. Alghamdi, S. Mukhtar, S. I. A. Shah, P. Kumam, T. Gul, S. Nasir, and W. Kumam. Darcy-Forchheimer hybrid nanofluid flow over a stretching curved surface with heat and mass transfer. *Plos One*, 2021. doi: 10.1371/journal.pone.0249434.

[122] K. Loganathan, N. Alessa, K. Tamilvanan, and F. S. Alshammari. Significances of Darcy-Forchheimer porous medium in third-grade nanofluid flow with entropy features. *Eur. Phys. J. Spec. Top*, 2021. doi: 10.1140/epjs/s11734-021-00056-6.

[123] M. I. Khan and F. Alzahrani. Dynamics of activation energy and nonlinear mixed convection in Darcy-Forchheimer radiated flow of carreau nanofluid near stagnation point region. *J. Thermal Sci. Eng. Appl.*, 13, 2021. doi: 10.1115/1.4049434.

[124] A. Shafiq, G. Rasool, H. Alotaibi, H. M. Aljohani, A. Wakif, I. Khan, and S. Akram. Thermally enhanced Darcy-Forchheimer Casson-water/glycerine rotating nanofluid flow with uniform magnetic field. *Micromachines*, 12, 2021. doi: 10.3390/mi12060605.

[125] M. Z. Ullah, T. Muhammad, and F. Mallawi. On model for Darcy-Forchheimer 3-D nanofluid flow subject to heat flux boundary condition. *J. Therm. Anal. Calorim.*, 143:2411–2418, 2021.

[126] L. A. Lund, Z. Omar, and I. Khan. Darcy-Forchheimer porous medium effect on rotating hybrid nanofluid on a linear shrinking/stretching sheet. *Int J. Numer. Method. H.*, 2021. doi: 10.1108/HFF-11-2020-0716.

[127] H. S. Takhar, Ali J. Chamkha, and G. Nath. Flow and heat transfer on a stretching surface in a rotating fluid with a magnetic field. *Int. J. Therm. Sci.*, 42(1):23–31, 2003.

[128] Ali Al-Mudhaf and Ali J. Chamkha. Similarity solutions for MHD thermosolutal Marangoni convection over a flat surface in the presence of heat generation or absorption effects. *Heat Mass Transfer*, 42(2):112–121, 2005.

[129] E. Magyari and A. J. Chamkha. Exact analytical results for the thermosolutal MHD marangoni boundary layers. *Int. J. Therm. Sci.*, 47:848–857, 2008.

[130] M. M. Rashidi, S. Abelman, and N. Freidooni Mehr. Entropy generation in steady MHD flow due to a rotating porous disk in a nanofluid. *Int. J. Heat Mass Transf.*, 62:515–525, 2013.

[131] M. Sheikholeslami, K. Vajravelu, and M. M. Rashidi. Forced convection heat transfer in a semi annulus under the influence of a variable magnetic field. *Int. J. Heat Mass Transf.*, 92:339–348, 2016.

[132] Ali J. Chamkha and Abdul-Rahim A. Khaled. Similarity solutions for hydromagnetic mixed convection heat and mass transfer for Hiemenz flow through porous media. *Int. J. Num. Meth. Heat Fluid Flow*, 10(1):94–115, 2000.

[133] M. E. M. Khedr, Ali J. Chamkha, and M. Bayomi. MHD flow of a micropolar fluid past a stretched permeable with heat generation or absorption. *Nonlinear Anal.: Modell. Control*, 14(1):27–40, 2009.

[134] Ali J. Chamkha, A. M. Aly, and H. F. Ali-Mudhaf. Laminar MHD mixed convection flow of a nanofluid along a stretching permeable surface in the presence of heat generation or absorption effects. *Int. J. Micro. Nano. Thermal Fluid Trans. Phen.*, 2(1):51–70, 2011.

[135] H. S. Takhar, A. J. Chamkha, and G. Nath. Unsteady flow and heat transfer on a semi-infinite flat plate with an aligned magnetic field. *Int. J. Engng. Sci.*, 37(13): 1723–1736, 1999.

[136] H. S. Takhar, Ali J. Chamkha, and G. Nath. Unsteady mixed convection flow from a rotating vertical cone with a magnetic field. *Heat Mass Transfer*, 39(4): 297–304, 2003.

[137] Ali J. Chamkha and Ali Al-Mudhaf. Unsteady heat and mass transfer from a rotating vertical cone with a magnetic field and heat generation or absorption effects. *Int. J. Therm. Sci.*, 44(3):267–276, 2005.

[138] Ali J. Chamkha and S. E. Ahmed. Similarity solution for unsteady MHD flow near a stagnation point of a three-dimensional porous body with heat and mass transfer, heat generation/absorption and chemical reaction. *J. Appl. Fluid Mech.*, 4(2):87–94, 2011.

[139] Ali J. Chamkha. Coupled heat and mass transfer by natural convection about a truncated cone in the presence of magnetic field and radiation effects. *Numerical Heat Transf. A*, 39:511–530, 2001.

[140] M. M. Rashidi, S. A. M. Pour, and S. Abbasbandy. Analytic approximate solutions for heat transfer of a micropolar fluid through a porous medium with radiation. *Comm. Nonlin. Sci. Num. Simul.*, 16(4):1874–1889, 2011.

[141] Ali J. Chamkha, R. A. Mohamed, and S. E. Ahmed. Unsteady MHD natural convection from a heated vertical porous plate in a micropolar fluid with Joule heating, chemical reaction and radiation effects. *Meccanica*, 46:399–411, 2011.

[142] G. S. Seth, S. M. Hussain, and S. Sarkar. Hydromagnetic natural convection flow with radiative heat transfer past an accelerated moving vertical plate with ramped temperature through a porous medium. *J. Porous Med.*, 17:67–79, 2014.

[143] M. M. Rashidi, N. V. Ganesh, A. K. A. Hakeem, and B. Ganga. Buoyancy effect on MHD flow of nanofluid over a stretching sheet in the presence of thermal radiation. *J. Molecular liquids*, 198:234–238, 2014.

[144] G. S. Seth, R. Sharma, B. Kumbhakar, and Ali J. Chamkha. Hydromagnetic flow of heat absorbing and radiating fluid over exponentially stretching sheet with partial slip and viscous and joule dissipation. *Engineering Computations*, 33(3): 907–925, 2016.

[145] M. M. Bhatti and M. M. Rashidi. Effects of thermo-diffusion and thermal radiation on Williamson nanofluid over a porous shrinking/stretching sheet. *J. Molecular liquids*, 221:567–573, 2016.

[146] G. S. Seth and M. K. Mishra. Analysis of transient flow of MHD nanofluid past a non-linear stretching sheet considering naviers slip boundary condition. *Adv. Powder Tech.*, 28(2):375–384, 2017.

[147] H. S. Takhar, Ali J. Chamkha, and G. Nath. MHD flow over a moving plate in a rotating fluid with magnetic field, Hall currents and free stream velocity. *Int. J. Engng. Sci.*, 40(13):1511–1527, 2002.

[148] G. S. Seth, R. Sharma, and S. Sarkar. Natural convection heat and mass transfer flow with Hall current, rotation, radiation and heat absorption past an accelerated moving vertical plate with ramped temperature. *J. Appl. Fluid Mech.*, 8(1):7–20, 2015.

[149] G. S. Seth, R. Tripathi, and R. Sharma. An analysis of MHD natural convection heat and mass transfer flow with Hall effects of a heat absorbing, radiating and rotating fluid over an exponentially accelerated moving vertical plate with ramped temperature. *Bul. Chem. Comm.*, 48(4):770–778, 2016.

[150] S. M. Hussain, J. Jain, G. S. Seth, and M. M. Rashidi. Free convective heat transfer with Hall effects, heat absorption and chemical reaction over an accelerated moving plate in a rotating system. *J. Magn. Magn. Mater.*, 422:112–123, 2017.

[151] M. H. Abolbashari, N. Freidoonimehr, and M. M. Rashidi. Analytical modeling of entropy generation for Casson nano-fluid flow induced by a stretching surface. *Adv. Powder Tech.*, 26(2):542–552, 2015.

[152] G. S. Seth, R. Tripathi, and M. K. Mishra. Hydromagnetic thin film flow of a Casson fluid in a non-Darcy porous medium with Joule dissipation and Naviers partial slip. *Appl. Math. Mech.*, 38(11):1613–1626, 2017.

[153] I. L. Animasaun, E. A. Adebile, and A. I. Fagbade. Casson fluid flow with variable thermo-physical property along exponentially stretching sheet with suction and exponentially decaying internal heat generation using the homotopy analysis method. *J. Nigerian Math. Soc.*, 35:1–17, 2016.

[154] G. K. Ramesh, B. C. Prasannakumara, B. J.Gireesha, and M. M. Rashidi. Casson fluid flow near the stagnation point over a stretching sheet with variable thickness and radiation. *J. A. F. M.*, 9:1115–1122, 2016.

[155] K. Bhattacharyya. MHD stagnation-point flow of Casson fluid and heat transfer over a stretching sheet with thermal radiation. *J. Thermodyn.*, 2013:1–9, 2013.

[156] S. Pramanik. Casson fluid flow and heat transfer past an exponentially porous stretching surface in presence of thermal radiation. *Ain Shams Eng. J.*, 5:205–212, 2014.

[157] Ch. Krishna Sagar and G. Srinivas. Computational solutions for mixed convective radiating Casson fluid flow past an inclined flat plate in presence of Hall current. *Int. J. Appl. Eng. Res.*, 9:2212–2227, 2014.

[158] A. Pantokratoras and T. Fang. Blasius flow with non-linear rosseland thermal radiation,. *Meccanica*, 49:1539–1545, 2014. ISSN 6.

[159] R. Cortell. Fluid flow and radiative nonlinear heat transfer over a stretching sheet. *J. King Saud University - Sci.*, 26:161–167, 2014.

[160] M. A. El-Aziz. Flow and heat transfer over an unsteady stretching surface with Hall effect. *Meccanica*, 45:97–109, 2010.

[161] S. Shateyi and S. S. Motsa. Variable viscosity on Magnetohydrodynamic fluid flow and heat transfer over an unsteady stretching surface with Hall effect. *Boundary Value Problems*, 2010, 2010. doi: 10.1155/2010/257568.

[162] R. Nandkeolyar, S. S. Motsa, and P. Sibanda. Viscous and joule heating in the stagnation point nanofluid flow through a stretching sheet with homogenous-heterogeneous reactions and nonlinear convection. *J. Nanotechnol. Eng. Med.*, 4 (4):041002, 2013.

[163] R. Nandkeolyar, P. K. Kameswaran, S. Shaw, and P. Sibanda. Heat transfer on nanofluid flow with homogeneous-heterogeneous reactions and internal heat generation. *J. Heat Transfer*, 136(12):122001, 2014.

[164] N. B. Reddy and D. Bathaiah. Hall effects on MHD flow through a porous straight channel. *Def. Sci. J.*, 32(4):312–326, 1982.

[165] G. S. Seth, R. Nandkeolyar, and Md. S. Ansari. Hartmann flow in a rotating system in the presence of inclined magnetic field with Hall effects. *Tamkang J. Sci. Eng.*, 13(3):243–252, 2010.

[166] B. C. Sarkar, S. Das, and R. N. Jana. Hall effects on MHD flow in a rotating channel in the presence of an inclined magnetic field. *Tamkang J. Sci. Eng.*, 17 (3):243–252, 2014.

[167] K. V. Prasad, K. Vajravelu, and H. Vaidya. Hall effect on MHD flow and heat transfer over a stretching sheet with variable thickness. *Int. J. Comp. Meth. Eng. Sci. Mech.*, 17(4):288–297, 2016.

[168] P. Ram, A. Singh, and H. Singh. Effect of porosity on unsteady MHD flow past a semi-infinite moving vertical plate with time dependent suction. *Ind. J. Pure Appl. Phys.*, 51:461–470, 2013.

[169] P. Ram, H. Singh, R. Kumar, V. Kumar, and V. K. Joshi. Free convective boundary layer flow of radiating and reacting MHD fluid past a cosinusoidally fluctuating heated plate. *Int. J. Appl. Comp. Math.*, 3:261–294, 2017.

[170] H. Singh, P. Ram, and V. Kumar. Unsteady MHD free convection fluctuating flow past an impulsively started isothermal vertical plate with radiation and viscous dissipation. *Fluid Dyn. Mat. Proc.*, 10(4):1–30, 2014.

[171] A. M. Rashad, S. E. Ahmed, and M. A. Mansour. Effects of chemical reaction and thermal radiation on unsteady double diffusive convection. *Int. J. Num. Meth. Heat Fluid Flow*, 24(5):1124–1140, 2014.

[172] S. M. M. EL-Kabeir, M. Modather, and A. M. Rashad. Effect of thermal radiation on mixed convection flow of a nanofluid about a solid sphere in a saturated porous medium under convective boundary condition. *J. Porous Media*, 18(6):569–584, 2015.

[173] H. A. Nabwey, S. M. M. EL-Kabeir, and A. M. Rashad. Lie group analysis of effects of radiation and chemical reaction on heat and mass transfer by unsteady slip flow from a non-isothermal stretching sheet immersed in a porous medium. *J. Comput. Theor. Nanosci.*, 12:4056–4062, 2015.

[174] B. Mallikarjuna, A. M. Rashad, A. K. Hussein, and S. H. Raju. Transpiration and thermophoresis effects on non-Darcy convective flow past a rotating cone with thermal radiation. *Arab. J. Sci. Eng.*, 41:4691–4700, 2016.

[175] V. K. Joshi, P. Ram, R. K. Sharma, and D. Tripathi. Porosity effect on boundary layer Bodewadt flow of magnetic nanofluid in presence of geothermal viscosity. *Eur. Phy. J. Plus*, 132:254, 2017.

[176] V. K. Joshi, P. Ram, D. Tripathi, and K. Sharma. Numerical investigation of magnetic nanofluids flow over rotating disk embedded in a porous medium. *Thermal Sci.*, 2017. doi: 10.2298/TSCI170323139J.

[177] O. D. Makinde, Z. H. Khan, R. Ahmad, and W. A. Khan. Numerical study of unsteady hydromagnetic radiating fluid flow past a slippery stretching sheet embedded in a porous medium. *Phys. Fluids*, 30:083601, 2018.

[178] K. R. Sekhar, G. V. Reddy, C. S. K. Raju, S. M. Ibrahim, and O. D. Makinde. Multiple slip effects on magnetohydrodynamic boundary layer flow over a stretching sheet embedded in a porous medium with radiation and Joule heating. *Special Topics & Reviews in Porous Media: An International Journal*, 9(2):117–132, 2018.

[179] M. Sheikholeslami and S. Abelman. Numerical study of the effect of magnetic field on Fe_3O_4-water ferrofluid convection with thermal radiation. *Eng. Computations*, 35(5):1855–1872, 2018.

[180] S. M. M. EL-Kabeir, E. R. EL-Zahar, and A. M. Rashad. Effect of chemical reaction on heat and mass transfer by mixed convection flow of Casson fluid about a sphere with partial slip. *J. Comput. Theor. Nanosci.*, 13(8):5218–5226, 2016.

[181] S. M. Mousavi, M. N. Rostami, M. Yousefi, S. Dinarvand, I. Pop, and M. A. Sheremet. Dual solutions for Casson hybrid nanofluid flow due to a stretching/shrinking sheet: A new combination of theoretical and experimental models. *Chinese J. Phys.*, 71:574–588, 2021.

List of Publications

Following research papers have been published/accepted/communicated from the present thesis:

1. Prashu, R. Nandkeolyar, A numerical treatment of unsteady three-dimensional hydromagnetic flow of a Casson fluid with Hall and radiation effects, Published in ***Results in Physics***, Vol. 11, pp. 966-974, 2018.

2. Prashu, R. Nandkeolyar, Ali J. Chamkha, A numerical investigation of Hall and radiation effects on MHD three-dimensional Casson fluid flow in a porous medium, Published in ***Journal of Porous Media***, Vol. 24, pp. 15-30, 2021.

3. Prashu, R. Nandkeolyar, V. Sangwan, Numerical Simulation of Non-uniform Heat Generation and Dissipation Effects on the Unsteady MHD Flow of a Couple -Stress Dusty Fluid, Accepted for publication in ***AIP Conference Proceedings***.

4. Prashu, R. Nandkeolyar, V. Sangwan, Entropy Generation and Regression Analysis of Magnetohydrodynamic Stagnation Point Flow of a Casson Fluid with Radiative and Dissipative Heat Transfer and Hall Effects, Communicated to ***Journal of Applied Fluid Mechanics***.

5. Prashu, R. Nandkeolyar, V. Sangwan, Radiative Heat Transfer Analysis of the Unsteady MHD Darcy-Forchhiemer Flow along a Curved Sheet, Communicated to ***Pramana***.